2010

NANOSCALE FUNCTIONALIZATION AND CHARACTERIZATION OF SURFACES WITH HYDROGEL PATTERNS AND BIOMOLECULES

Hariharasudhan Chirra Dinakar
University of Kentucky, harih2s@gmail.com

ABSTRACT OF DISSERTATION

Hariharasudhan Chirra Dinakar

The Graduate School

University of Kentucky

2010

NANOSCALE FUNCTIONALIZATION AND CHARACTERIZATION OF SURFACES WITH HYDROGEL PATTERNS AND BIOMOLECULES

ABSTRACT OF DISSERTATION

A dissertation submitted in partial fulfillment of the requirements for the degree of Doctor of Philosophy in the College of Engineering at the University of Kentucky

By

Hariharasudhan Chirra Dinakar

Lexington, Kentucky

Director: Dr. James Zachary Hilt, Associate Professor of Chemical Engineering

Lexington, Kentucky

2010

ABSTRACT OF DISSERTATION

NANOSCALE FUNCTIONALIZATION AND CHARACTERIZATION OF SURFACES WITH HYDROGEL PATTERNS AND BIOMOLECULES

The advent of numerous tools, ease of techniques, and concepts related to nanotechnology, in combination with functionalization via simple chemistry has made gold important for various biomedical applications. In this dissertation, the development and characterization of planar gold surfaces with responsive hydrogel patterns for rapid point of care sensing and the functionalization of gold nanoparticles for drug delivery are highlighted.

Biomedical micro- and nanoscale devices that are spatially functionalized with intelligent hydrogels are typically fabricated using conventional UV-lithography. Herein, precise 3-D hydrogel patterns made up of temperature responsive crosslinked poly(N-isopropylacrylamide) over gold were synthesized. The XY control of the hydrogel was achieved using microcontact printing, while thickness control was achieved using atom transfer radical polymerization (ATRP). Atomic force microscopy analysis showed that to the ATRP reaction time governed the pattern growth. The temperature dependent swelling ratio was tailored by tuning the mesh size of the hydrogel. While nanopatterns exhibited a broad lower critical solution temperature (LCST) transition, surface roughness showed a sharp LCST transition. Quartz crystal microbalance with dissipation showed rapid response behavior of the thin films, which makes them applicable as functional components in biomedical devices.

The easy synthesis, relative biocompatibility, inertness, and easy functionalization of gold nanoparticles (GNPs) have made them useful for various biomedical applications. Although ATRP can be successfully carried out over GNPs, the yield of stable solution based GNPs for biomedical applications prove to be low. As an alternative approach, a novel method of ISOlating, FUnctionalizing, and REleasing nanoparticles (ISOFURE) was proposed. Biodegradable poly(β-amino ester) hydrogels were used to synthesize ISOFURE-GNP composites. ATRP was performed inside the composite, and the final hydrogel coated GNPs were released via matrix degradation. Response analysis

confirmed that the ISOFURE method led to the increased stability and yield of the hydrogel coated ISOFURE-GNPs. The ISOFURE protocol was also utilized in functionalizing GNPs with enzyme catalase in the absence of a stabilizing reagent. Biotin-streptavidin affinity was used as the bioconjugation method. Activity analysis of the conjugated enzyme showed that the ISOFURE-GNPs showed enhanced biomolecular loading relative to solution based stabilizing reagent passivated GNPs.

KEYWORDS: Hydrogel, Gold nanoparticle, ISOFURE, Atom transfer radical polymerization, Microcontact printing

Hariharasudhan Chirra Dinakar

NANOSCALE FUNCTIONALIZATION AND CHARACTERIZATION OF SURFACES WITH HYDROGEL PATTERNS AND BIOMOLECULES

By

Hariharasudhan Chirra Dinakar

Dr. J. Zach Hilt
Director of Dissertation

Dr. Stephen Rankin
Director of Graduate Studies

RULES FOR THE USE OF DISSERTATIONS

Unpublished dissertations submitted for the Doctor's degree and deposited in the University of Kentucky Library are as a rule open for inspection, but are to be used only with due regard to the rights of the authors. Bibliographical references may be noted, but quotations or summaries of parts may be published only with the permission of the author, and with the usual scholarly acknowledgments.

Extensive copying or publication of the dissertation in whole or in part also requires the consent of the Dean of the Graduate School of the University of Kentucky.

A library that borrows this dissertation for use by its patrons is expected to secure the signature of each user.

Name	Date

DISSERTATION

Hariharasudhan Chirra Dinakar

The Graduate School

University of Kentucky

2010

NANOSCALE FUNCTIONALIZATION AND CHARACTERIZATION OF SURFACES WITH HYDROGEL PATTERNS AND BIOMOLECULES

DISSERTATION

A dissertation submitted in partial fulfillment of the
requirements for the degree of Doctor of Philosophy in the
College of Engineering at the University of Kentucky

By

Hariharasudhan Chirra Dinakar

Lexington, Kentucky

Director: Dr. James Zachary Hilt, Associate Professor of Chemical Engineering

Lexington, Kentucky

2010

Dedicated to the few dreams that turned into mere lies……

ACKNOWLEDGEMENTS

It would be unfair to say that the duration of getting a Ph.D. is around five years, since without the guidance, teachings, sacrifices, inputs, and the motivation of many people over the pre-Ph.D. years, this would have been an indomitable task to even think about. Chronologically saying, I owe a lot to the efforts of my mother who planted the initial seeds of curiosity towards education. Next in line would be my dad who strategically pushed me into the ranks of toppers by bribing me with gifts, in exchange to my academic efforts. Also, I am grateful to the many eventful childhood days spent with my brother, which molded me into a better competitive person. I sincerely thank all my school and undergrad teachers, mentors, and friends who taught me the various fundamentals of science and life. Special acknowledgements go to my high school mentor Mr. Manivannan, friends Sreema, Geetha, Lukes, Prakash, undergrad mentor Dr. Renganathan, members of S.M.I.L.E, late Guli, and best friends – Abhikoo, Avi and Kitcha.

More than the invaluable support and guidance that an advisor usually provides, it was the added patience of Dr. Zach Hilt, and his beliefs in my skills that made me perform in one of the most testing periods of my lifetime. I am extremely grateful for this and many other professional skills I learnt from him. Also, I thank him for teaching me and the members of the lab the little humane rules in life that make us a better person (e.g. the importance of the word “please” to a waitress, and the impact of the phrase “works *with* me” rather than “works *for* me”). I also thank my Ph.D. committee

members: Drs. Kimberly Anderson, Stephen Rankin, Yuguang Cai, and my collaborator-cum-external examiner, Dr. Louis Hersh for their time and resourceful inputs that have helped me shape this work. Special gratitude goes to all the other faculties and staff at University of Kentucky whose support in various capacities ensured the completion of my studies.

Special thanks go to a great friend and colleague, Colonel (Dr. Reynolds Frimpong) for showing me the nuances of extracting fun in a competitive lab. Also, my sincere gratitude goes to Bhabhi (Dr. Dipti Biswal) and Sheldon (Paritosh Whattamwar), who answered most of my technical queries and helped in planning my experiments. And then, I am grateful to have great friends, Nintendo (Dr. Nitin Satarkar) and Dr. Abhay Ladhe in the form of colleagues, without whom I would have been in a ton of strangled situations. I would also like to thank my fun-filled yet hard working undergrads - Mr. Midas (David Spencer), Kruti Patel, and Lee Hundley who 'worked *with* me' and contributed significantly towards a better interesting dissertation. More acknowledgements go to the other members - Rob Wydra, Ashley Hawkins, Sam (Dr. Samantha Meenach), David Kryscio, and Stew Frasier for supporting my work.

My special thanks to the God sent best friends Potiga (Anand Varahala) and Ramsey (Ramu Vangari) who unequivocally shouldered my personal burdens, patiently listened to my professional frustrations, and goofed around to extreme limits to make me smile. A great deal of an acknowledgement goes to my little nephew 'J' (Lewis Jayanth), who showed me the wonders of a happy balanced life from sleeping to bed time stories of

Nature and Langmuir papers to arguing that the material in his diapers were made of plastics and not halogels (hydrogels). Sincere gratitude also goes to the many members of the university cricket club, especially Teddy Bear (Akshay Vummanagari), Chotu (Russel Viego), K2 (Ketu Vagdiya), and his family (delayed ruby Tuesday - little Niva and big momma Kshiti) who helped me gain focus and the spirit to succeed from weekend cricket. I would also like to thank Anthu (Dr. Anantharaman), Pam (Dr. Padhma), my adopted brother Nick (Nishant), great roommates Tesa (Prasanna Padmanaban) and Bhai (Anand Ramakrishnan), Capi (Dinesh Puppala), CID (Vetrivel Kanagasabai), Arul, Bubbles (Sharanya Desikan), Burrito (Sarita Hardas), and Jivan Yewle for their immense support. My heartfelt gratitude goes to a distant friend Beta (Vivek Vichare) for encouraging and keeping me on track during the tough third and fourth year of Ph.D.

And finally, I would like to thank a great friend with whom later I unknowingly, eventually, and relentlessly fell in love with – Choco. Without her, reality would have never been this enticing and dreams may never seem more challenging.

TABLE OF CONTENTS

LIST OF TABLES

LIST OF FIGURES

CHAPTER 1

Introduction

The age of nanoscience and nanotechnology has exerted a greater influence than custom macroscopic technology on how researchers understand and design analytical nanomaterials to unravel the mysteries of systems biology, thereby delivering novel devices for various biomedical applications. Nanomaterials can be simply defined as all objects encompassing components with at least one feature at the nanoscale dimension (10^{-9} m) [1, 2]. At this scale, quantum mechanical effects begin to emerge, more often leading to the invalidation of the governing rules of the macroscopic level, which provides various physico-chemical material properties. In addition, the high surface to volume ratio that come with size reduction has given rise to increased catalytic, electronic, optical, mechanical, and magnetic properties [3-8]. These properties have been harnessed to find applications in medicine, semiconductors and opto-electronics, aerospace and sports materials, ceramics, consumer products, and environmental remediation [9-12].

The transition of semiconductor nanotechnology into producing micro-electro-mechanical systems (MEMS) and microfluidic lab-on-chip biomedical systems has enabled the field of point-of-care medicine to grow leaps and bounds. These biomaterials have been used for molecular sensing, diagnostics, sieving, controlled drug release, and biomarker guided targeted therapeutics [13-16]. For use of these biomaterial surfaces as implantable biomedical devices, their interactions with cells are critical. Both the

topography and the chemical composition of the surface at the nanoscale greatly influence cell adhesion, mobility, and differentiation [17]. In several instances, either polymeric networks or biomolecules have been used to tailor the surface features of a biomaterial implant. One common polymeric network system used for biomaterial coating is hydrogels. Novel hydrogels, whose polymeric backbones have been tailored to provide swelling response behavior to different environmental cues, find interests as components of various micro-/nanodevices such as micropumps, microvalves, microfluidic channels, microcantilever sensor platforms, etc [18-23]. While the coating of surfaces with hydrogels has been well established by methods of conventional lithography, precise patterning of hydrogels into three-dimensional structures is at its relative inception. Some techniques that have been developed to achieve a fine level of control for patterning surfaces include e-beam and ion-beam lithography, nano-imprint lithography, dip pen nanolithography, and other novel soft lithographic techniques [24].

Highly sensitive biosensors that detect molecular biomarkers at extremely low concentration levels or recognize environmental changes arising from biological processes are crucial for the early detection of diseases and prognosis. Also, the need to provide a controlled release of the appropriate drug from implanted biomaterials is critical for self-regulated therapeutic applications. In the case of hydrogel micro-/nanodevices, the sensitive and controlled response behavior of the polymer matrix is mostly governed by the diffusion of molecules into and out of the polymer matrix. Nanoscale thin hydrogel films provide means to accelerate the diffusion process, thereby defining the effectiveness of a micro/nanodevice for rapid point of care diagnosis and

therapeutics [25]. Synthesis of thin polymer layers covalently bound to a material surface is achieved by either ‘grafting to’ or ‘grafting from’ chemistries [26]. While ‘grafting to’ approach is most preferred in the case of biomolecules, ‘grafting from’ approach associated with the ease of monomer accessibility at reactive sites, provides higher grafting densities [27, 28]. Both the spatial control and the thickness of the hydrogel coating involved in the fabrication of hydrogel nanostructures plays a critical role in the development of micro- and nanodevices for their prospective applications in the biomedical field.

While the focus of research on using polymeric biomaterials as implantable devices offer improvements to existing or traditional biomedical techniques, novel multifunctional inorganic nanoparticles are used to overcome some of the inherent limitations and issues associated with traditional diagnostic and therapeutic agents. Nanotechnology enables a various approaches towards nanoparticle surface modifications such as targeting moieties, contrast agents, stealth polymers, and drug cargos. These have provided some advantages such as alternative routes of drug administration, improved solubility of poorly water-soluble drugs, targeted drug delivery that reduced systemic side effects, enhanced *in vivo* half-life of drugs with reduced immunogenic response, increased sensitivity and specificity during magnetic resonance and ultrasound imaging, and the release of drugs at a sustained rate or in response to an environmental stimuli [29-33]. Also, nanoparticles have been used in the realm of tissue engineering for the delivery of molecules, drugs, growth factors, and DNA [34]. They are not only used as delivery systems, but also exploited as mechanical reinforcements of polymeric scaffolds [35].

While, these polymer-nanoparticle composites prove as scaffolds for constructive tissue development, the utilization of the inherent property of certain nanoparticles to heat remotely paves way for thermoablative treatment [36]. Although, the synthesis of biomolecule and other short molecule protected nanoparticle is well established, polymer coated particles are currently receiving considerable attention because the polymers are capable of effectively stabilizing nanoparticles by steric effects, controlling the particle shell size and monodispersity, thereby providing good stability and uniform properties for biomedical applications. Therefore, 'grafting from' approach of introducing polymer networks over nanoparticle surfaces similar to above described implantable devices is of great interest.

1.1. Dissertation Overview

The overall objective of this research was to develop innovative methods for the integration of a wide variety of polymer networks, in particular intelligent hydrogel systems, and biomolecules over gold surfaces. These novel materials have great promise for application as biomedical point of care micro- and nanodevices. The specific research objectives of this dissertation can be summarized as

- Acquire spatial control (XY control) over planar gold surface by employing a suitable soft lithographic technique;
- Use a surface initiated polymerization technique to achieve thickness control (Z control) over the growth of intelligent hydrogel systems over planar gold surface;
- Characterize the growth and response behavior of the novel intelligent hydrogel patterns using various nano-analytical tools;

- Develop an innovative strategy to synthesize stable intelligent hydrogel coated gold nanoparticles using surface initiated polymerization and the properties of degradable hydrogel nanocomposites;
- Extend the novel ISOFURE strategy of isolating the nanoparticles in a polymer matrix, functionalizing them, and finally releasing them via degradation of the polymer matrix into producing stable functionalized bioactive gold nanoparticles; and
- Demonstrate the use of hydrogels as functional components of biomedical micro- and nanodevices.

Chapter 2 discusses the background on the functionalization of surfaces, in particular gold, with biomolecules and polymer networks. Some of the methods of patterning and functionalization of surfaces such as 'grafting to' and 'grafting from' are highlighted. Atom transfer radical polymerization (ATRP), the surface initiated polymerization method employed in this research, is emphasized. Chapter 3 focuses on the background of hydrogel systems. Additionally, applications of responsive intelligent hydrogels in micro- and nanodevices for biosensing, actuation, and drug delivery are summarized. The patterning techniques associated with these devices are also highlighted, with more focus given to microcontact printing (μCP).

In chapter 4, the viability of achieving precise spatial XY control of patterns on gold using μCP and tunable thickness (Z control) of hydrogel structures using ATRP is demonstrated. Poly(N-isopropyl acrylamide) (PNIPAAm) hydrogels crosslinked with

poly(ethylene glycol) n dimethacrylate (PEGnDMA) hydrogels were synthesized as the model hydrogel platform for this experimental chapter. Characterization of the hydrogel's chemical composition and its structure via patterning and ATRP was carried out using optical microscopy, Fourier transform infrared (FTIR) spectroscopy, and atomic force microscopy (AFM). Chapter 5 details the effect of crosslinking parameters on equilibrium response kinetics of the hydrogel structures at the nanoscale. For this study, temperature response behavior of PEGnDMA crosslinked PNIPAAm hydrogels were studied using AFM and quartz crystal microbalance with dissipation (QCM-D).

Chapter 6 describes the transition of controlled hydrogel growth into gold nanoparticle (GNP) systems, wherein issues associated with agglomeration with hydrogel formation is highlighted. A novel strategy called the ISOFURE methodology of ISOlating nanoparticles using a degradable hydrogel matrix, followed by FUnctionalization of their surface with a surface initiated polymerized hydrogel shell, and subsequent RElease of the stable functionalized nanoparticles is discussed in detail. Two methods of synthesizing the GNP-degradable hydrogel nanocomposites: one by pre-synthesizing GNPs and then adding to hydrogel prepolymer solution and the other involving in-situ precipitation of GNPs inside the polymerized degradable hydrogel matrix is also introduced for comparison purposes. This methodology of isolation of GNPs, functionalization, followed by release of stable nanoparticles is extended for biofunctionalization reactions in chapter 7. A model biofunctionalization reaction of protein immobilization over GNPs is used to study the effectiveness of this strategy in enhancing the functional loading of a nanoparticle surface. Both the stability and the

activity of the protein tethered to the surface of the nanoparticle is characterized using biomolecular assays and compared to that of solution based protein attached nanoparticles (synthesized without the use of the degradable entrapping hydrogel matrix). The conclusions and potential future work related to this dissertation are presented in Chapter 8.

1.2. References:

1. The United States National Nanotechnology Initiative website. Retrieved on September 1, 2010. "Nanotechnology - Big things from a tiny world" document. http://www.nano.gov.
2. Theis T, Parr D, Binks P, Ying J, Drexler KE, Schepers E, Mullis K, Bai C, Boland JJ, nan'o.tech.nol'o.gy n. *Nat. Nanotech.* **2006**, 1, 8-10.
3. Schmid, G, Baumle M, Geerkens M, Heim, I, Osemann C, Sawitowski T. Current and future applications of nanoclusters. *Chem. Soc. Rev.* **1999,** 28, 179-185.
4. Weller H. Colloidal semiconductor Q- particles: chemistry in the transition region between solid state and molecules. *Angew. Chem. Int. Ed.* **1993,** 32, 41-53.
5. Zhang X, Jenekhe SA, Perlstein J. Nanoscale Size Effects on Photoconductivity of Semiconducting Polymer Thin Films. *Chem. Mater.* **1996,** 8, 1571–1574.
6. Jenekhe SA, Zhang X, Chen XL, Choong V-E, Gao Y, Hsieh BR. Finite Size Effects on Electroluminescence of Nanoscale Semiconducting Polymer Heterojunctions. *Chem. Mater.* **1997**, 9, 409–412.
7. Manandhar P, Jang J, Schatz GC, Ratner MA, Hong S. Anomalous Surface Diffusion in Nanoscale Direct Deposition Processes. *Phys. Rev. Let.* **2003**, 90, 115505-115507.

8. Clark LA, Ye GT, Snurr RQ. Molecular Traffic Control in a Nanoscale System. *Phys. Rev. Let.* **2000,** 84, 2893-2895.
9. Son SJ, Bai X, Lee SB. Inorganic hollow nanoparticles and nanotubes in nanomedicine part 2: imaging, diagnostic and therapeutic applications. *Drug. Discov. Today*. **2007,** 12, 657-663.
10. Zhao QQ, Boxmann A, Chowdhry U. Nanotechnology in the chemical industry – opportunities and challenges. *J. Nanoparticle Res.* **2003,** 5, 567-572.
11. Zhan J, Bando Y, Hu J, Liu Z, Yin L, Goldberg D. Fabrication of metal-semiconductor nanowire heterojunctions. *Angew. Chem. Int. Ed.* **2005,** 44, 2140-2144.
12. Yean S, Cong L, Yavuz CT, Mayo JT, Yu WW, Kan AT, Colvin VL, Tomson MB. Effect of magnetite particle size on adsorption and desorption of arsenite and arsenate. *J. Mater. Res.* **2005** 20, 3255-3264.
13. Santini JT, Richards AC, Scheidt R, Cima MJ, Langer R. Microchips as controlled drug-delivery devices. *Angew. Chem. Int. Ed.* **2000**, 39, 2396–2407.
14. Whitesides GM, Ostuni E, Takayama S, Jiang XY, Ingber DE. Soft lithography in biology and biochemistry. *Ann. Rev. Biomed. Eng.* **2001**, 3, 335–373.
15. LaVan DA, McGuire T, Langer R. Small-scale systems for in vivo drug delivery. *Nat. Biotech.* **2003**, 21, 1184–1191.
16. Orosco MM, Pacholski C, Sailor MJ. Real-time monitoring of enzyme activity in a mesoporous silicon double layer. *Nat. Nanotech.* **2009**, 4, 255–258.
17. Chun YW, Webster TJ. The role of nanomedicine in growing tissues. *Ann. Biomed. Eng.* **2009**, 37, 2034–2047.

18. Peppas NA, Hilt JZ, Khademhosseini A, Langer R. Hydrogels in biology and medicine: from fundamentals to bionanotechnolgoy. *Adv. Mater.* **2006,** 18, 1345-1350.

19. Beebe DJ, Moore JS, Bauer JM, Yu Q, Liu RH, Devadoss C, Jo B. Functional hydrogel structures for autonomous flow control. *Nature* **2000,** 404, 588-590.

20. Sershen S, Mensing G, Beebe D, West J. Independent optical control of microfluidic valves formed from optomechanically responsive nanocomoposite hydrogels. *Adv. Mater.* **2005,** 17, 1366-1372.

21. Low LM, Seetharaman S, Madou MJ. Microactuators towards microvalves for responsive controlled drug delivery. *Sens. Actuators B,* **2000,** 67, 149-160.

22. Hilt JZ, Gupta AK, Bashir R, Peppas NA. Ultrasensitive bioMEMs sensors based on microcantilevers patterned with environmentally responsive hydrogels. *Biomed. Microdev.* **2003**, 5, 177-184.

23. Baldi A, Lei M, Gu Y, Siegel RA, Ziaie B. Microstructured silicon membrane with entrapped environmentally sensitive hydrogel for smart flow control. *Sens. Actuators B,* **2006,** 114, 9-18.

24. Truskett VN, Watts MPC. Trends in imprint lithography for biological applications. *Trends Biotech.* **2006**, 24, 312-317.

25. Ritger PL, Peppas NA. A simple equation for description of solute release: Fickian and non Fickian release. *J. Control. Rel.* **1987**, 5, 23-30.

26. Odian G. Principles of Polymerization, Wiley Intersceince, 4th ed., **2004**.

27. Prucker O, Ruhe J. Synthesis of Poly(styrene) Monolayers Attached to High Surface Area Silica Gels through Self-Assembled Monolayers of Azo Initiators, *Macromolecules,* **1998,** 31, 592-597.
28. Tu H, Heitzman CE, Braun PV. Patterned Poly(N-isopropylacrylamide) Brushes on Silica Sufaces by Microcontact Printing Followed by Surface-Initiated Polymerization, *Langmuir* **2004,** 20, 8313-8320.
29. Zhang L, Gu FX, Chan JM, Wang AZ, Langer R, Farokhzad OC. Nanoparticles in medicine: therapeutic, applications and developments. *Clini. Pharmaco. Thera.* **2008,** 83, 761-769.
30. Veiseh O, Sun C, Gunn J, Kohler N, Gabikian P, Lee D, Bhattarai N, Ellenbogen R, Sze R, Hallahan A, Olson J, Zhang M. Optical and MRI multifunctional nanoprobe for targeting gliomas. *Nano Letters* **2005,** 5, 1003-1008.
31. Wang YX, Hussain SM, Krestin GP. Superparamagnetic iron oxide contrast agents: physicochemical characteristics and applications in MR imaging. *Eur. Radiol*. **2001**, 11, 2319–2331.
32. Cai QY, Kim SH, Choi KS, Kim SY, Byun SJ, Kim KW. Colloidal gold nanoparticles as a blood-pool contrast agent for X-ray computed tomography in mice. *Invest. Radiol.* **2007**, 42, 797–806.
33. Lindner JR. Contrast ultrasound molecular imaging: harnessing the power of bubbles. *Cardiovasc. Res.* **2009**, 83, 615–616.
34. Engel E, Michiardi A, Navarro M, Lacroix D, Planell JA. Nanotechnology in regenerative medicine: the materials side. *Trends. Biotechnol.* **2008**, 26, 39–47.

35. Place ES, George JH, Williams CK, Stevens MM. Synthetic polymer scaffolds for tissue engineering. *Chem. Soc. Rev.* **2009**, 38, 1139–1151.

36. Meenach SA, Hilt JZ, Anderson KW, Poly(ethylene glycol) based magnetic hydrogel nanocomposites for hyperthermia cancer therapy. *Acta Biomaterialia* **2010**, 6, 1039-1046.

CHAPTER 2

Background on the functionalization of gold with biomolecules and polymeric networks

This chapter is based in part on

- Book chapter published as:

  H.D. Chirra, D. Biswal, J.Z. Hilt, "Gold Nanoparticles and Surfaces: Nanodevices for Diagnostics and Therapeutics", in Nanoparticulate Drug Delivery Systems (NPDDS) II: Formulation and Characterization, Y. Pathak, D. Thassu, eds., Informa Healthcare USA Inc., 2009, 90-114.

2.1. Introduction

Gold has received much interest in the field of biomedical engineering. The use of gold as a key component in diagnostics and therapeutics field has emerged primarily over a period of three decades. During the 19^{th} century, the pure form of gold called activated gold, due to its inert behavior to harsh environments, was prominently employed for catalysis [1]. With the advent of numerous tools, techniques, and concepts related to nanotechnology, in combination with the inherent property of gold to form functionalized bioconjugates via simple chemistry, gold has found importance in various diagnostic and therapeutic applications [2-6]. The unique chemical and physical properties of gold render it as effective sensing and delivery systems for pharmaceutical applications [7]. Gold is mostly considered inert and non-toxic, and although gold can be directly used for biomedical applications, unique applications of this inert metal require functionalization

with other biomolecules or biocompatible polymeric systems. Herein, we detail the progress made in the functionalization of gold surfaces, both planar and particulates, at the nanoscale for diagnostic and therapeutic applications.

Functionalization of gold surfaces, both planar and spherical can be achieved by using either 'grafting to' or 'grafting from' methods [8]. Figure 2.1 shows the schematic representation of functionalizing gold surfaces with polymeric materials. The 'grafting to' method involves the reaction of end functionalized polymers with appropriate surface sites. Initially grafted polymer layers over these active sites however, hinder the further attachment of polymer chains because of limited availability of more active sites, thus limiting film thickness and brush density. In the 'grafting from' approach, a reactive unit on the surface initiates the polymerization, and consequently, the polymer chains grow from the surface. Most 'grafting from' polymerization reactions utilize controlled radical polymerization mechanisms. Since monomers diffuse more easily to reactive sites than macromolecules, this approach generally leads to higher grafting densities. A variety of functionalization techniques over gold surface are described in the following.

2.2. Conventional *'grafting to'* method with biomolecules and assembled monolayers

The various properties of gold nanoparticles (GNP) are mostly size dependant and surface characterized, and therefore, the controlled synthesis of GNP is important for applications in bionanotechnology. Monodispersed gold nanoparticles (GNPs) are relatively easy to form with core sizes ranging from 1 nm to 150 nm. Gold nanoparticles with varying core sizes are usually prepared by the reduction of gold salts in aqueous,

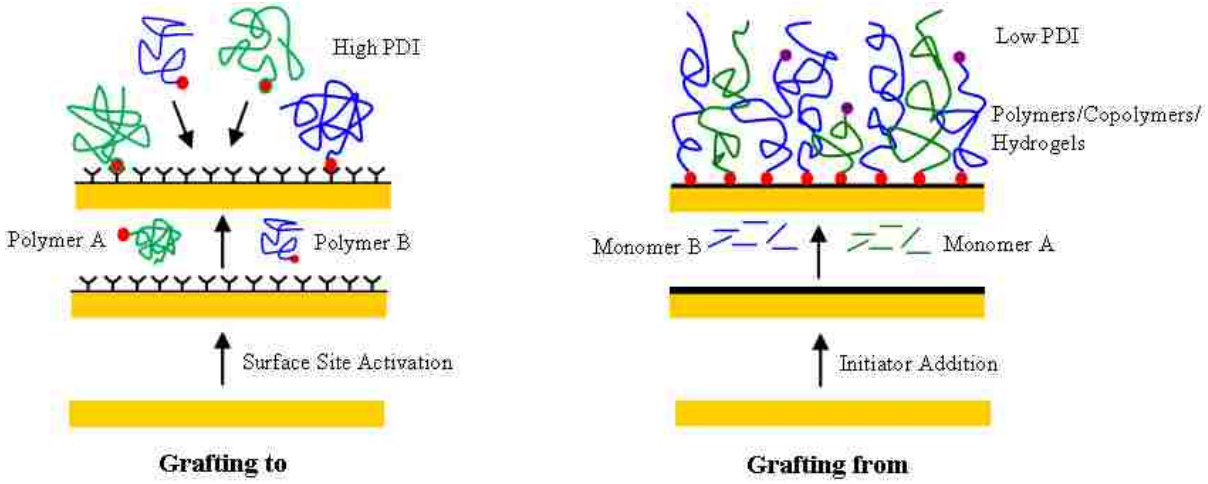

Figure 2.1. Scheme explaining the difference between grafting to and grafting from surface functionalization methods. The polydispersity index of the polymer over the surface is high for the 'grafting to' method and low for the 'grafting from' technique respectively.

organic phase, or two phases [9, 10]. However, the high surface energy of GNPs makes them highly reactive, and as a result, they undergo aggregation. The presence of an appropriate stabilizing agent prevents particle agglomeration by binding to the particle surface to impart high stability and also rich linking chemistry if it acts as a functional group for bioconjugation [11, 12].

Surface modification of gold particles with stabilizing agents can be achieved by many methods. The thiol gold chemistry is used as the key mechanism for grafting small biomolecules and short chain end functionalized polymeric stabilizers to gold. The 'grafting to' fabrication of sensor and/or delivery systems based on gold nanoparticles bearing functional moieties has been made easy by using the one-pot protocol developed by Schriffin et al. in 1994 [10]. These monolayer protected clusters of 1.5 nm – 6 nm are prepared by the reduction of $HAuCl_4$ by sodium borohydride in the presence of alkanethiol capping agents. Murray and his coworkers extended Schriffin's method to diversify the functionality of monolayer protected clusters to mixed monolayer protected clusters using a place-exchange reaction between the thiols [13]. Table 2.1 gives a list of 'grafting to' surface modified particles, as synthesized by various researchers for bio-related diagnostic and therapeutic applications. For further information, the reader is directed to the respective references of the table for the attachment/reaction chemistry.

Although, the synthesis of biomolecule and other short molecule protected GNP is easy, polymer coated GNP are currently receiving considerable attention because the polymers are capable of effectively stabilizing nanoparticles by steric effects and the controlled

Table 2.1. Different types of functionalization methods used for the preparation of modified bio-diagnostic and therapeutic gold nanoparticles.

Type of GNP	Functional Group Attached	References
Biomolecule protected	Peptide	108, 109
	Phospholipids	110, 111
	Synthetic lipids	112-115
	Microorganism	114, 116
	Viruses	117, 118
Natural and degradable	Ionic liquids	119-122
	Polysaccharides - chitosan	123-126
	Polysaccharides - sucrose	127
Polymer (dendrimers)	Poly(amidoamine) based	128-131
	Other dendrimers	132-136
Polymer (others)	Linear polymer	137, 138
	Hyperbranched polymer	139-141
	Amphiphilic polymer	142, 143
	Environmentally responsive	144, 145
	PEG functionalized	146-149
	Bioconjugated PEG	150-152

growth of the polymers provide a control over the particle size thereby providing good stability for biomedical applications. 'Grafting to' approaches for the synthesis of such monodispersed particles is not viable. This is due to the effect of steric hindrance on the non uniform attachment of polymer chains to the gold surface. To overcome this problem, the 'grafting from' approach is often preferred.

2.3. Surface initiated *'grafting from'* methods with polymeric networks

In the 'grafting from' approach, a reactive unit on the surface initiates the polymerization, and consequently, the polymer chains grow from the surface (Figure 2.1). This one monomer at a time attachment to the surface of interest leads to a much denser and more uniform polymer coated surface when compared to 'grafting to' techniques. While a wide combination of polymeric networks can be obtained via 'grafting from' techniques, the same is not viable by using 'grafting to' techniques. Surface modification with polymer brushes had been widely used to tailor various surface properties of gold [14, 15]. Most 'grafting from' or surface initiated polymerization (SIP) reactions, work on the principle of controlled radical polymerizations [16]. A general mechanism of how controlled radical polymerization renders a uniform polymer coated surface is shown in Figure 2.2. Briefly an initiator and/or a ligand transforms into a surface attached radical (R•), that thereby undergoes polymer propagation in a controlled manner, while the ligand complex radical (in this case Z• or ZY•) participates in controlling the polymerization reaction and finally undergoes termination with the remaining free radicals. A few key elements of the reaction molecules are mentioned in Figure 2.2.

Living Radical Polymerization:

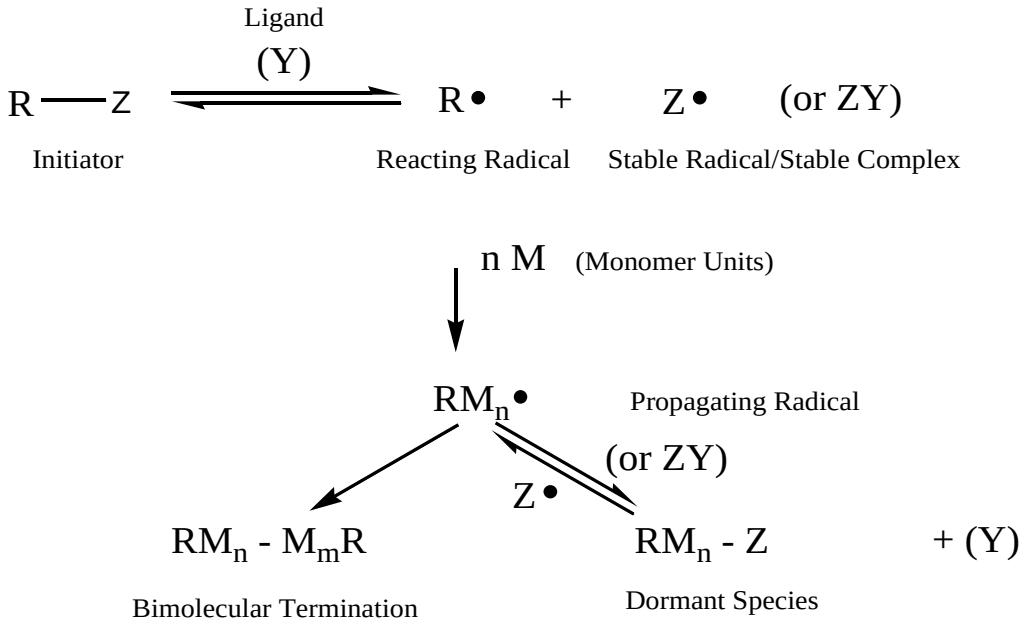

	Z	**Y**	**ZY**
ATRP	Br	CuBr	$CuBr_2$
RAFT	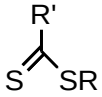	-	-

Living Ionic (Cationic) Polymerization:

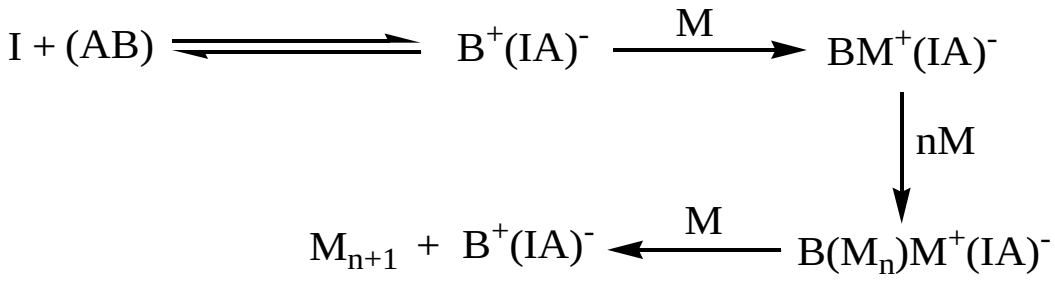

Figure 2.2. Mechanisms of polymerization in living radical and ionic polymerization.

There are different types of surface initiated polymerization (SIP) mechanisms utilized on both planar and particulate gold surfaces. The many types of polymerization mechanism include, free radical, cationic, anionic, ring opening metathesis polymerization (ROMP), atom transfer radical polymerization (ATRP), and polymerization using 2, 2, 6, 6,- tetramethyl-1-piperidyloxy (TEMPO) [8]. Though, bioconjugation with modified thiols is the most common method for addressing bio-applied gold surfaces, polymerization via 'grafting from' techniques affords controlled polymer grafting density and composition. This control is vital in the development of various biosensors and drug delivery therapeutic systems for precise bio-diagnostic and therapeutic applications. A few of these 'grafting from' methods are addressed as follows.

2.3.1. Free radical polymerization

Surface initiated free radical polymerization (FRP) is used for the polymerization of a large variety of monomers [17, 18]. For example, Duner et al. reported the synthesis of acrylamide/acrylate polymer brushes from the Au surface using thermal FRP which were initially coated with polystyrene-type thin films, derivatized from photolabile groups [19]. These acrylamide and acrylate brushes, in general, are sensitive to environmental stimuli such as temperature and pH. By encompassing biomolecules which lead to a change in the environmental conditions, these materials on gold surface can be effectively used as biosensors. Though, FRP can be used over a variety of polymers, it is often not preferred due to uncontrolled polymer growth leading to coating of varying thickness. The surface initiated polymerization in conjunction with a living

radical polymerization (LRP) technique is among the most useful synthetic routes to precisely design and functionalize the surface of various materials. Surface initiated LRP is particularly promising due to its simplicity and versatility.

2.3.2. Living ionic polymerization

The use of multiple functionalities on material surfaces enables multiplex usage for various biomedical applications. A control over the polymer thickness, the type of polymer formed (e.g. block copolymer systems), can be controlled via ionic polymerization. Briefly, in this technique, the coinitiator I in Figure 2.2 combines with a Lewis acid or Lewis base (considered also as the initiator), to generate the ionic radical complex $B^{+}(IA)^{-}$ which adds up monomer units (M) in propagation steps to produce the polymer. The Advincula group reported the living anionic surface initiated polymerization of styrene and diene homopolymers as well as diblock copolymer brushes on gold surfaces [20, 21]. They used 1,1-diphenylethylene self assembled monolayer as the immobilized precursor initiator from which anionic polymerization of monomer was carried out. Other groups have also reported work related to anionic polymerization on gold surfaces [22]. Recently, Ohno et al. synthesized gold nanoparticles coated with well defined high density polymer brushes via anionic polymerization [23]. Jordan and coworkers have carried out surface initiated living cationic polymerization over planar gold substrates and functionalized gold nanoparticles [24, 25]. Using these polymerization techniques, dense polymer brushes were prepared in a “one-pot multi-step” reaction.

2.3.3. Reversible addition fragmentation chain transfer polymerization

Reversible addition fragmentation chain transfer polymerization (RAFT) is a versatile, controlled free radical polymerization technique that operates via a degenerative transfer mechanism in which a thiocarbonylthio compound acts as a chain transfer agent (Figure 2.2) [26]. An advantage of the RAFT polymerization is the synthesis of wide range of polymers with narrow polydispersity (PDI, which is defined as the ratio of weight average molecular weight to number average molecular weight) and controlled end groups. Poly(N-isopropylacrylamide) monolayer protected clusters on GNPs were synthesized using RAFT, where a dithiobenzoate was used as the chain transfer reagent [27]. Li et al. synthesized poly(styrene-b-n-isopropylacrylamide) with dithiobenzoate terminal group which was later converted to thiol terminal group using sodium borohydride ($NaBH_4$), resulting in a thiol-terminated polymer (PSt-b-PNIPAAm-SH). After PSt-b-PNIPAM-SH re-assembled into core-shell micelles in an aqueous solution, gold nanoparticles were surface-linked onto the micelles in situ through the reduction of gold precursor anions with $NaBH_4$. Thus, temperature responsive core/shell micelles of PSt-b-PNIPAM surface-linked with gold nanoparticles (PSt-b-PNIPAM-GNP) were obtained [28].

2.3.4. Atom transfer radical polymerization

Among the various controlled radical polymerization methods, atom transfer radical polymerization (ATRP) has received high interest, because of its versatility in producing controlled polymers with low polydispersity and its compatibility with a variety of functionalized monomers [29]. ATRP is relatively tolerant to the presence of

water and oxygen, and with the correct choice of catalyst, ATRP can be performed at relatively low temperatures [14]. The halogen atom undergoes reversible switching between the oxidation states of the transition metal complexes, thereby reducing the initial radical concentration and also suppresses the bimolecular termination step. This in addition to the suitable catalyst increases the control over the polymer growth in ATRP. It has been successfully employed on various surfaces such as gold, silicon, glass, etc. by researchers. It has been used to amplify patterned monolayers of assembled initiators formed using various lithography techniques, into polymeric brushes [30-33]. For example, Huck and co-workers prepared poly(N-isopropyl acrylamide) (PNIPAAm) micropatterned domains from mixed SAMs on gold substrates [33, 34]. Recently, ATRP has been successfully employed for the synthesis of pH sensitive brushes over gold surfaces [35, 36]. The combined synthetic route of microcontact printing and ATRP has been effectively used in multicomponent polymeric brush patterning by Huck et al. [37]. In this case, various brushes of different monomer systems have been patterned over gold surface using repeated microcontact printing followed by ATRP. In addition to these surface initiated polymerization techniques, a wide variety of 'grafting from' techniques are available. The reader is directed to books compiled by Odian and Matyjaszewski et al. [11, 38].

2.4. Diagnostic applications of functionalized gold nanoparticles

Over the past decade, nanotechnology for biomolecular detection has made enormous advancements. Nanoparticles, in particular, have been developed for accurate, sensitive, and selective biosensing devices due to their unique size-related, ease of

functionalization, and unique physical properties (electrical, optical, electrochemical, and magnetic) [39]. Gold nanoparticles are mostly used in biomedical field as labels for biomolecular detection in the place of conventional molecular fluorophores, where their unique size-tuned optical properties are exploited [40]. Some of the biosensing applications of GNPs are detailed in the following.

2.4.1. Gold nanoparticles as optical biosensors

In 1996, Mirkin et al. reported the combined optical and melting properties of GNP-oligonucleotide aggregates, which paved way for the development of a plethora of biomolecular optical detection strategies [41]. The immediate follow up work done by researchers using the colorimetric system, worked on the principle of color change observed when a polymer network of nanoparticles was formed specific to the length of the oligonucleotide that aggregated to the biomolecule of interest [5, 42]. In addition to the color change, the modified GNP-DNA detection probes also exhibited a sharp melting transition at the detection limit, which was used to distinguish complementary target sequences for one-base-mismatch sequences [43, 44]. While selectivity was achieved with the melting property, the sensitivity was improved 100 times compared to conventional fluorophores, by carrying out catalytic silver (Ag) deposition on GNP labels [45]. Bio-barcode amplification, which is an extension of scanometric nucleotide detection of labeling oligonucleotide targets with GNPs and studying their melting profiles on an array substrate, employs magnetic microparticles with capture probes along with GNPs with both receptor probes and numerous barcode oligonucleotides [46]. The presence of a target molecule that matches both the capture and reporter probes forms a

magnetic microparticle-GNP sandwich. The scanometric detection of the barcode nucleotides via Ag amplification, gives a detection limit of both DNA and proteins as low as 500 zM.

The surface-enhanced Raman scattering (SERS) of Raman dye conjugated nanoparticles, along with the narrow spectral characteristics of Raman dyes, was used with GNPs for multiplexed detection of proteins and nucleic acids [47, 48]. In both instances, Raman dyes and detection probes are first attached to the GNPs and then were hybridized with the captured targets. A silver coating on the GNP promotes SERS of the dye, and the amplified signal is captured by spectroscopy for fM level detection. On a similar principle, GNP coupled surface plasmon resonance effect has been reported for nucleic acid and protein detection [49-51]. A real-time bioaffinity monitoring system based on an angular-ratiometric approach to plasmon resonance light scattering was recently developed by Asian and colleagues [52]. The process depends on the basic principle that, as the bioaffinity reaction proceeds with the size increase of GNPs, they deviate from Rayleigh theory and thereby scatter more light in a forward direction relative to the incident geometry. An innovative technique involving a GNP-detector-fluorophore was employed by Maxwell and coworkers for the optical detection of nucleic acids [53]. In this strategy, the target molecule induces a conformational change of the detector-fluorophore chain, from arch to stretched form and vice versa, thereby either restoring or quenching the fluorophore for optical detection.

2.4.2. Biomolecule conjugated gold nanoparticle electrochemical biosensors

Though direct electrical detection is the simplest method for biosensing, a large fraction of the GNP based sensing research involves electrochemical detection for bioaffinity, specificity, and improved sensitivity reasons [54]. A summary of the recent approaches in the construction of electrochemical biosensors utilizing the various binding and electro-enhancing properties of GNPs is best reviewed by Pingarron et al. [55]. Research involving GNPs for electrochemical biosensing is largely focused on enzyme conjugated electrodes. One of the first electrochemical GNP biosensor was a simple enzymatic glucose biosensor that had the glucose oxidase (GOx), covalently attached to a GNP-modified Au electrode. A modification of the GOx sensor for increased sensitivity and lifetime was then designed by Mena et al. [56]. They used a configuration involving colloidal gold, bound to cystamine self assembled monolayer on a gold electrode for blood glucose sensing. GNP modified with 4-aminothiophenol, conjugated with Hepatitis B antibody was used to detect Hepatitis B virus surface antigen via electrochemical impedance spectroscopy (EIS) [57].

Electrochemical DNA biosensors provide useful analytical tools for the diagnosis of sequence-specific DNA strands. The redox property of GNPs forms the key element for their widespread use as electrochemical labels for nucleic acid detection, thereby assisting in gene analysis, detection of genetic disorders, tissue matching and forensics. By measuring the oxide wave current generated from a complementary probe-GNP hybridized to an immobilized target DNA on an electrode, Ozsos and coworkers detected nucleic acid sequences [58]. In another modified configuration, GNP labels are attached

to a single stranded DNA binding protein [59]. When these capture probes are hybridized to matching targets, the binding of the labeled proteins is hindered and is indicated by the decrease in the Au redox signal. The Au oxide wave technique was modified to a greater level by Kerman and coworkers to not only detect the presence of a single-nucleotide polymorphism (SNP), but also identify the bases involved in the nucleotide using GNP attached monobase nucleotide labels [60]. Particular base-particles attach only in the presence of DNA polymerase to its counterpart in the nucleotide strand. This in turn establishes a unique gold oxidation wave which is the potential developed at the gold oxidation for specific nucleotide, which is detected using the electrode.

2.4.3. Gold nanoparticle composite biosensors

Electrodes made of composite matrices, encompassing nanoparticles, provide improved enzymatic biosensing and better analytical performances. These devices have an added advantage of low background currents depending on the type of electrode used [55]. A reagentless glucose biosensor, based on the direct electron transfer of GOx has been constructed [61]. While immobilization of the enzyme onto the electrode was done by mixing colloidal gold with the carbon paste components, a layer-by-layer (LBL) technique was used to prepare a GOx amperometric biosensor with a relatively high sensitivity [62]. A film, made up of alternating layers of dendrimer modified GNP and poly(vinylsulfonic acid), was used as the substrate for immobilizing GOx in the presence of bovine serum albumin and glutaraldehyde cross-linker. This was successfully applied as a biosensor for the amperometric detection of glucose at 0.0 V.

α-Fetoprotein, (AFP) is an oncofetal glycoprotein that is widely employed as a tumor marker for the diagnosis of germ cell carcinoma and hepatocellular cancer in patients. An immunosensor for AFP detection was prepared by entrapping thionine into Nafion matrix into a membrane, which at the amine interface assemble GNP layer for the immobilization of AFP antibody. The detection is identified by the linear drop in current across the membrane with increasing concentrations of AFP protein [63]. A similar matrix was used by Tang and coworkers for the detection of carcinoma antigen 125 as represented in various tumors [64].

Other composite materials, such as GNP conjugated carbon nanotube (CNT) composite electrodes, has attracted much interest due to their synergistic properties. While hybridized GNPs possess properties related to bioaffinity and inertness, CNTs improve the electrocatalytic ability of the electrode. The electrocatalytic ability towards the electrooxidation of NADH or H_2O_2 has been utilitzed for the fabrication of a colloidal gold-CNT composite electrode. Significant H_2O_2 response was observed by Manso et al. who then incorporated GOx into the composite matrix for the preparation of a mediatorless glucose biosensor with remarkable sensitivity [65].

2.4.4. Polymer hybridized gold nanoparticle biosensors

The widely used method for the synthesis of immobilized matrices of biomolecules is via electropolymerization. GNPs incorporated in the conductive polymer matrix provide enhanced electrochemical activity and conductivity. Further, rapid diffusion of biomolecular substrate and product, using small amount of enzyme is

achieved in the presence of GNPs [55]. The main advantage of incorporating GNPs is that the enzyme degrading electrodeposition process is substituted with a chemical polymerization technique. A simple substitution reaction was used for the synthesis of GNP-polymer hybrids for glucose biosening and H_2O_2 detection [66, 67]. Tang and coworkers developed GNP-polymer based biosensing electrodes, for the detection of Hepatitis B and diphtheria infection. They immobilized the respective antigens on colloidal GNPs, associated with polyvinyl butyral polymer on a Nafion-gelatin coated platinum electrode by using a modified self-assembling and opposite-charge adsorption technique [68, 69].

Chitosan, a natural polymer exhibiting excellent film forming and adhesion ability, together with susceptibility to chemical modification have led to the immobilization of various enzymes over conductive electrodes. Self-assembled GNP adsorbed chitosan hydrogels, coated on Au electrodes were used as GOx and horse radish peroxidase (HRP) biosensors [70, 71]. Zhao et al. carried out layer by layer (LBL) assembly of multilayer films composed of chitosan, GNPs and GOx over Pt electrodes for amperometric glucose detection [72]. Sol-gel technology a conventional technique is used for the preparation of three dimensional networks of hybrid biosensors made up of encapsulated biomolecules and GNPs. GNPs immobilized by silica gel act as highly sensitive nanostructure electrochemical biosensor and had been used for the construction of various polymer based hybrid biosensors [73].

2.5. Therapeutic applications of functionalized gold nanoparticles

The inert and non-toxic property of gold along with the ready addition of biological molecules and antibodies capitalizing on the thiol-gold chemistry has rendered gold applicable in a variety of therapeutic systems ranging from drug and biomolecular delivery, hyperthermia, and active and passive targeting (Figure 2.3). GNPs have recently emerged as an attractive platform for the delivery of small drug molecules and large biomolecules to specific targets [74]. The release of these therapeutic agents can be triggered by cellular chemical (e.g. glutathione GSH) or pH or external (e.g. light) stimuli [75-77]. Further, the external stimuli via light can be controlled, by exploiting the plasmon resonance effect of GNPs (10-100 nm) for precise drug delivery applications and hyperthermia [78, 79]. The various biomedical therapeutic applications of gold nanoparticles are detailed in the following.

2.5.1. Gold nanoparticles for active and passive *in vivo* targeting

The disadvantage of conventional drug administration is that the drug typically does not localize to the target site but is systemically distributed. Nanoparticles, on the other hand, can aid in the targeted accumulation of drugs. The success of any *in vivo* medical application depends on the ability of a nanocarrier to arrive at the targeted tissues after administration into the circulatory system. While passive targeting can be used for certain applications (e.g., extravasation through leaky vasculature in tumors), active targeting employs the use of ligands on the carrier surface for specific recognition by the cell surface receptors [80]. GNPs offer excellent drug delivery systems for *in vivo* applications due to their tunable size and versatile surface functionalization properties.

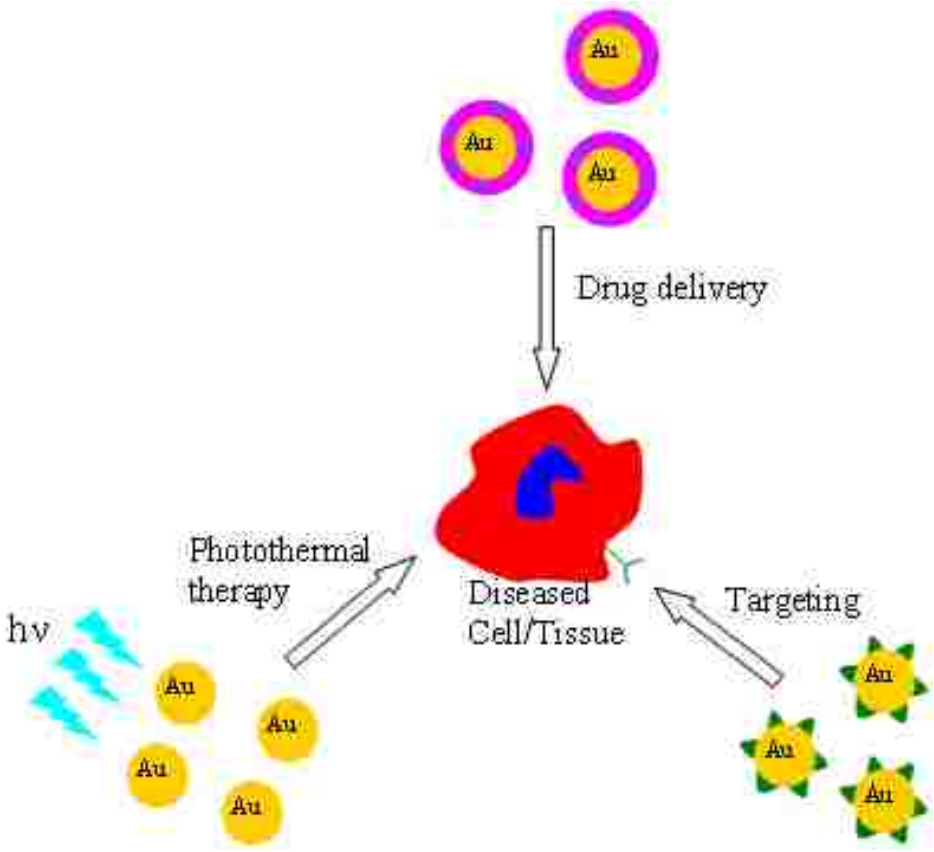

Figure 2.3. Various therapeutic applications of gold nanoparticles

GNPs can be designed to be big enough to be retained in the liver and spleen, but small enough to pass through other organs. Passive targeting with these particles along with radiotherapy has been used, for the treatment of liver cancer, where the sinus endothelium of liver has openings of 150 nm in diameter. O'Neal et al. used the fact that tumor vasculature is more permeable than healthy tissues to concentrate gold nanoshells with diameters of 130 nm for photoablative therapy in mice [81].

Active targeting which employs a ligand or antibody functionalized particle, has been successfully used by many researchers to treat certain diseases. Though these ligands are specific to target receptors, the presence of the particle in the circulatory system provides possibility of normal host immune response. In order to overcome this issue, poly(ethylene glycol) PEG-coated stealth particles are widely employed [3]. Pun et al. injected PEGylated nanoparticles (PEG-NP), unmodified NP, and galactose attached NP of varying sizes to explain the effect of size and functionalization over gold for active targeting [82]. They discovered that PEGylation increased blood circulation life time of the particles, while galactose coated particles actively targeted liver cells and so had higher filtration inside the liver.

More specific active targeting for treatment was shown by Andrews et al. They recently employed folic acid (FA) conjugated GNPs (10 nm) with PEG spacer for the cellular uptake of tumor cells that exhibit folate receptors [83]. Wu and coworkers extended this method by using methotrexate (MTX), another tumor-folate-receptor ligand and an anticancer drug for inhibition of lung tumor growth in mice [84]. Once the MTX

conjugated particles got bound to the tumor cells, methotrexate was activated via cellular uptake and caused programmed cell death. Active targeting using PEGylated gold colloids were studied by Paciotti et al, where tumor necrosis factor, TNF was conjugated to colloidal Au-PEG. An extended application of this work was also done with the help of grafted Paclitaxel, an anticancer drug, onto colloidal Au-PEG-TNF, for the treatment of colon carcinoma tumors [74].

2.5.2. Delivery of drug molecules by gold nanoparticles

One of the main advantages of using gold particles at the nanoscale is its surface to volume ratio. Gold nanoparticles can be loaded on their surface to form drug delivery systems. These systems can be used for chemotherapeutic delivery to tumor cells. The enhanced permeation and retention effect as provided by passive targeting has been used for treating carcinogenic tumors. The surface to volume ratio was utilized to prepare passive targeting GNPs conjugated with chemotherapeutic Paclitaxel and diatomic cytotoxic singlet oxygen ($^1O_2$), and nitric oxide (NO) GNP reservoirs [85-87]. Triggered release of NO was shown by Schoenfisch et al. NO was released from water-soluble nanocontainers when a pH stimulus (pH=3) was given to these drug delivery systems [76]. Since tumor tissues have mild acidic environment of pH, NO carrying gold nanoparticles can be potentially used effectively to treat cancer. While external stimuli such as pH and temperature prove effective in triggered release, internal cellular signals/chemicals can provide an enhanced control on drug release. Glutathione (GSH), an antioxidant that protects the cell from toxins such as free radicals, in its reduced form has been used to mediate activated release of prodrugs from gold nanoparticles. The

release is caused by a simple difference in the molar concentration of GSH inside the cell and that of thiols of glutathione in the blood plasma/outside the cell [88, 89].

2.5.3. Gold nanoparticle based gene delivery

Gold nanoparticles are easy to tune in terms of size and functionality, and thereby contribute as a useful platform for efficient recognition and delivery of biomolecules. Their success in delivering peptides, proteins, or nucleic acids (DNA and RNA) is introduced in the following. Gene therapy is the treatment of genetic as well as acquired diseases by the insertion of genes into the cell or tissues. Although an Adenovirus vector vehicle for gene delivery has been successfully used for gene therapy, safety issues concerned with unpredictable viral cytotoxicity and immune responses has minimized viability of gene therapy [90, 91]. Synthetic DNA delivery vehicles have to be effective in protecting the nucleic acid from degradation, efficiently enter the cell, and release the functional nucleic acid to the cell nucleus. Small GNPs with high surface to volume ratio prove to be successful candidates for gene therapy. Along with maximized payload/carrier ratio, GNPs can be functionalized to behave non toxic and hydrophobic for efficient transfection. Rotello and coworkers used functionalized GNPs with cationic quaternary ammonium groups to show the effective binding of plasmid DNA to the cell, protection of DNA from enzymatic digestion, release of bound DNA by GSH treatment in cuvettes, and in gene delivery in mammalian 293T cells [92-95]. The increase in hydrophobicity of the GNPs enhances its transfection efficiency, thereby contributing to better cellular internalization. Klibanov et al, prepared hybrid GNP-polymer transfection vectors using branched polyethyleimine (PEI, 2 kDa) and showed that the increase in

hydrophobicity increased the potency of the conjugate in monkey kidney (Cos-7) cells, by approximately twelve folds than the polymer itself [96]. Recently, Liu et al, fabricated β-cyclodextrin end capped oligo(ethylenediamino)-modified GNPs to deliver plasmid DNA into breast cancer cells (MCF-7) [97].

Polycationic materials are famous for condensing and transporting DNA inside the cell. A recent breakthrough by Mirkin et al, however, showed that DNA loaded GNPs carrying a large negative surface potential was successfully internalized for cellular uptake and were stable against enzymatic digestion [98]. RNA interference (RNAi) mechanism that inhibits gene expressions at the translation or transcription of specific genes has revolutionized gene therapy strategy with the help of thiolated nucleic acids. RNA-modified GNPs were coated with poly(ethylene glycol)-block-poly(2-(N,N-dimethylamino)ethyl methacrylate) copolymer for cellular delivery in HuH-7 cells [99]. In addition to nucleic acids, GNPs is also used directly as nanocarriers for peptides and proteins. Electrostatic interaction between an anionic protein and cationic tetra alkyl ammonium functionalized GNPs has been utilized effectively for protein delivery [100, 101].

2.5.4. Gold nanoparticles for hyperthermia treatment

Hyperthermia is the process of using heat in a controlled manner for therapeutic treatment at elevated temperatures. Plasmon resonance effect of GNPs with light, whereby the electrons of gold resonate with that of the incoming radiation causing them to both absorb and scatter light, has been used to generate heating. By varying the relative

thickness of the core and shell layers, the plasmon resonance effect of the nanoshell can be shifted dramatically towards the IR region for introducing plasmon resonance assisted heating. This physical property of GNPs to locally heat, when irradiated with light in the therapeutic window (800-1200 nm) can be potentially harnessed to either destroy local tissue or release payload therapeutics. The plasmon resonance for GNPs is at around 520 nm, whereas for complex shapes such as nanorods, this can be shifted from visible spectrum to near infrared (NIR). This is advantageous because body tissue is semi transparent to NIR light and thereby be used for implantable therapeutics [81]. Halas, West, and coworkers have utilized the photothermal effect of GNPs for hyperthermia treatment [102, 103]. They used PEG-sheathed gold-on-silica nanoshells for passive targeting and were able to destroy breast cancer cells via NIR irradiation. El-Sayed et al. used citrate-stabilized GNPs of size 30 nm, for photoablative therapy [104]. The EGFR (epidermal growth factor receptor) coated particles targeted HSC3 cancer cells (human oral squamous cell carcinoma) thereby increasing the viability of the particles available for heating the cancer cells.

Photo-activated drug release by plasmonically active particles was performed by Caruso and coworkers [105, 106]. Microcapsules (polymer gel matrix) encapsulating fluorescein-labeled dextrans and lysozyme, were doped with near infra red light responsive gold nanospheres (gold-on-gold-sulfide core-shell particles). When a laser of wavelength 1064 nm was applied to these microcapsules, the gold nanoparticles heated up and released the fluorescein-labeled dextran and lysozyme via rupture of the shells to destroy the bacterium *Micrococcus lysodeikticus*. Skirtach et al. extended this strategy for

cancer treatment via a laser induced release of encapsulated drug inside living cells [78]. A remote controlled drug delivery strategy based on nanocomposite hydrogels was developed by West and colleagues [107]. Copolymers of NIPAAm and acrylamide (AAm) exhibit a lower critical solution temperature (LCST) that is slightly above body temperature. As the temperature exceeds LCST, the polymer collapses, which can be used to release components soluble in the imbibed water. Gold nanoshells were incorporated in such a poly(NIPAAm-co-AAm) matrix and were then loaded with proteins of varying molecular weight in which, the triggered release of the proteins was done by using a laser of wavelength 1064 nm.

2.6. Conclusions

It is clear that gold has been an important material in medical applications and that it continues to find new and unique applications, especially at the nanoscale. For most applications, it is critical that the gold surfaces are functionalized in a controlled manner. Here, methods for the functionalization of gold surfaces were highlighted, with a focus on 'grafting from' methodologies built around surface initiated polymerizations. In addition, recent research activities in applying gold structures (specifically, nanoparticles) in diagnostic and therapeutic applications were presented. Gold has a long history of applications at the nanoscale, but only recently applications in medical fields has grown exponentially in part due to the development of novel methods for functionalization. The history is long, but only the surface of potential applications in nanomedicine has been scratched.

2.7. References

1. Ware M. Photographic Printing in Colloidal Gold. *The Journal of Photographic Science* **1994**, 42, 157-161.

2. Daniel MC, Astruc D. Gold Nanoparticles: Assembly, Supramolecular Chemistry, Quantum-Size-Related Properties, and Applications toward Biology, Catalysis, and Nanotechnology. *Chem Rev* **2004**, 104, 293-346.

3. Love JC, Estroff LA, Whitesides GM, et al. Self-Assembled Monolayers of Thiolates on Metals as a Form of Nanotechnology. *Chem Rev* **2005**, 105, 1103-1170.

4. Cortie MB. The Weird World of Nanoscale Gold. *Gold Bulletin* **2004**, 37, 12-19.

5. Elghanian R, Storhoff JJ, Mirkin CA, et al. Selective Colorimetric Detection of Polynucleotides Based on the Distance-Dependent Optical Properties of Gold Nanoparticles. *Science* **1997**, 277, 1078-1081.

6. Bendayan M. Worth Its Weight in Gold. *Science* **2001**, 291, 1363-1365.

7. Pekka P. Theoretical Chemistry of Gold. *Angewandte Chemie International Edition* **2004**, 43, 4412-4456.

8. Odian G. Principles of Polymerization. Fourth ed. New Jersey, John Wiley & Sons, 2004, 198-349.

9. Turkevich J, Stevenson PC, Hillier J. A study of the nucleation and growth processes in the synthesis of colloidal gold. *Discussions of the Faraday Society* **1951**, 11, 55-75.

10. Brust M, Walker M, Schriffin DJ, et al. Synthesis of thiol-derivatised gold nanoparticles in a two-phase Liquid-Liquid system. *J Chem Soc Commun* **1994**, 801-802.

11. Frens G. Controlled nucleation for the regulation of the particle size in monodisperse gold suspensions. *Nature (London) Physical Science* **1973**, 241, 20.

12. Schmid G. Large Clusters and Colloids. Metals in Embryotic State. *Chem Rev* **1992**, 92, 1709-1727.

13. Templeton AC, Wuelfing WP, Murray RW. Monolayer-Protected Cluster Molecules. *Acc Chem Res* **2000**, 33, 27-36.

14. Advincula RC. Surface Initiated Polymerization from Nanoparticle Surfaces. *Journal of Dispersion Science and Technology* **2003**, 24, 343 - 361.

15. Edmondson S, Osborne VL, Huck WTS. Polymer brushes via surface-initiated polymerizations. *Chemical Society Reviews* **2004**, 33, 14-22.

16. Prucker O, Ruhe J. Synthesis of Poly(styrene) Monolayers Attached to High Surface Area Silica Gels through Self-Assembled Monolayers of Azo Initiators. *Macromolecules* **1998**, 31, 592-601.

17. Huang W, Baker GL, Bruening ML, et al. Surface-Initiated Thermal Radical Polymerization on Gold. *Langmuir* **2001**, 17, 1731-1736.

18. Schmidt R, Zhao T, Green JB, et al. Photoinitiated Polymerization of Styrene from Self-Assembled Monolayers on Gold. *Langmuir* **2002**, 18, 1281-1287.

19. Dune X, Henrik A, Teodor A, et al. Surface-Confined Photopolymerization of pH-Responsive Acrylamide/Acrylate Brushes on Polymer Thin Films. *Langmuir* **2008**, 24, 7559-7564.

20. Advincula R, Zhou Q, Park M, et al. Polymer Brushes by Living Anionic Surface Initiated Polymerization on Flat Silicon (SiOx) and Gold Surfaces: Homopolymers and Block Copolymers. *Langmuir* **2002**, 18, 8672-8684.

21. Sakellariou G, Advincula R, Mays J, et al. Homopolymer and block copolymer brushes on gold by living anionic surface-initiated polymerization in a polar solvent. *Journal of Polymer Science Part A: Polymer Chemistry* **2006**, 44, 769-782.

22. Jordan R, Ulman A, Kang JF, et al. Surface-Initiated Anionic Polymerization of Styrene by Means of Self-Assembled Monolayers. *J Am Chem Soc* **1999**, 121, 1016-1022.

23. Ohno K, Koh Km, Tsujii Y, et al. Synthesis of Gold Nanoparticles Coated with Well-Defined, High-Density Polymer Brushes by Surface-Initiated Living Radical Polymerization. *Macromolecules* **2002**, 35, 8989-8993.

24. Jordan R, Ulman A. Surface Initiated Living Cationic Polymerization of 2-Oxazolines. *J Am Chem Soc* **1998**, 120, 243-247.

25. Jordan R, West N, Ulman A, et al. Nanocomposites by Surface-Initiated Living Cationic Polymerization of 2-Oxazolines on Functionalized Gold Nanoparticles. *Macromolecules* **2001**, 34, 1606-1611.

26. Mayadunne RTA, Rizzardo E, Chiefari J, et al. Living Radical Polymerization with Reversible Addition-Fragmentation Chain Transfer (RAFT Polymerization) Using Dithiocarbamates as Chain Transfer Agents. *Macromolecules* **1999**, 32, 6977-6980.

27. Shan J, Nuopponen M, Jiang H, et al. Preparation of Poly(N-isopropylacrylamide)-Monolayer-Protected Gold Clusters: Synthesis Methods, Core Size, and Thickness of Monolayer. *Macromolecules* **2003**, 36, 4526-4533.

28. Jian Li, He W, Sun X. Preparation of poly(styrene-co-N-isopropylacrylamide) micelles surface-linked with gold nanoparticles and thermo-responsive ultraviolet-visible

absorbance. *Journal of Polymer Science Part A: Polymer Chemistry* **2007**, 45, 5156-5163.

29. Matyjaszewski K, Miller PJ, Shukla N, et al. Polymers at Interfaces: Using Atom Transfer Radical Polymerization in the Controlled Growth of Homopolymers and Block Copolymers from Silicon Surfaces in the Absence of Untethered Sacrificial Initiator. *Macromolecules* **1999**, 32, 8716-8724.

30. Matyjaszewski K, Dong H, Jakubowski W, et al. Grafting from Surfaces for "Everyone": ARGET ATRP in the Presence of Air. *Langmuir* **2007**, 23, 4528-4531.

31. Kim JB, Bruening ML, Baker GL. Surface-Initiated Atom Transfer Radical Polymerization on Gold at Ambient Temperature. *J Am Chem Soc* **2000**, 122, 7616-7617.

32. Takei YG, Aoki T, Sanui K, et al, Okano T. Dynamic Contact Angle Measurement of Temperature-Responsive Surface Properties for Poly(N-isopropylacrylamide) Grafted Surfaces. *Macromolecules* **1994**, 27, 6163-6166.

33. He Q, Kuller A, Grunze M, et al. Fabrication of Thermosensitive Polymer Nanopatterns through Chemical Lithography and Atom Transfer Radical Polymerization. *Langmuir* **2007**, 23, 3981-3987.

34. Jones DM, Huck WTS. Controlled Surface-Initiated Polymerizations in Aqueous Media. *Advanced Materials* **2001**, 13, 1256-1259.

35. Treat ND, Ayres N, Boyes SG, et al. A Facile Route to Poly(acrylic acid) Brushes Using Atom Transfer Radical Polymerization. *Macromolecules* **2006**, 39, 26-29.

36. Tugulu S, Barbey R, Harms M, et al. Synthesis of Poly(methacrylic acid) Brushes via Surface-Initiated Atom Transfer Radical Polymerization of Sodium Methacrylate and

Their Use as Substrates for the Mineralization of Calcium Carbonate. *Macromolecules* **2007**, 40, 168-177.

37. Zhou F, Zheng Z, Huck WTS, et al. Multicomponent Polymer Brushes. *J Am Chem Soc* **2006**, 128, 16253-16258.

38. Matyjasewski K, Davis TP. Handbook of Radical Polymerization. First ed. Hoboken: John Wiley & Sons; **2002,** 28-143.

39. Fortina P, Kricka LJ, Surrey S, et al. Nanobiotechnology: the promise and reality of new approaches to molecular recognition. *Trends in Biotechnology* **2005**, 23, 168-173.

40. Tansil NC, Gao Z. Nanoparticles in biomolecular detection. Nano Today 2006, 1, 28-37.

41. Mirkin CA, Letsinger RL, Mucic RC, et al. A DNA-based method for rationally assembling nanoparticles into macroscopic materials. *Nature* **1996**, 382, 607-609.

42. Storhoff JJ, Elghanian R, Mirkin CA, et al. One-Pot Colorimetric Differentiation of Polynucleotides with Single Base Imperfections Using Gold Nanoparticle Probes. *J Am Chem Soc* **1998**, 120, 1959-1964.

43. Taton TA, Mucic RC, Mirkin CA, et al. The DNA-Mediated Formation of Supramolecular Mono- and Multilayered Nanoparticle Structures. *J Am Chem Soc* **2000**, 122, 6305-636.

44. Jin R, Wu G, Mirkin CA, et al. What Controls the Melting Properties of DNA-Linked Gold Nanoparticle Assemblies? *J Am Chem Soc* **2003**, 125, 1643-1654.

45. Taton TA, Mirkin CA, Letsinger RL. Scanometric DNA Array Detection with Nanoparticle Probes. *Science* **2000**, 289, 1757-1760.

46. Nam JM, Stoeva SI, Mirkin CA. Bio-Bar-Code-Based DNA Detection with PCR-like Sensitivity. *J Am Chem Soc* **2004**, 126, 5932-5933.

47. Mulvaney SP, Musick MD, Keating CD, et al. Glass-Coated, Analyte-Tagged Nanoparticles: A New Tagging System Based on Detection with Surface-Enhanced Raman Scattering. *Langmuir* **2003**, 19, 4784-4790.

48. Cao YC, Jin R, Mirkin CA. Nanoparticles with Raman Spectroscopic Fingerprints for DNA and RNA Detection. *Science* **2002**, 297, 1536-1540.

49. He L, Musick MD, Nicewarner SR, et al. Colloidal Au-Enhanced Surface Plasmon Resonance for Ultrasensitive Detection of DNA Hybridization. *J Am Chem Soc* **2000**, 122, 9071-9077.

50. Lyon LA, Musick MD, Natan MJ. Colloidal Au-Enhanced Surface Plasmon Resonance Immunosensing. *Anal Chem* **1998**, 70, 5177-5183.

51. Hsu H-Y, Huang Y-Y. RCA combined nanoparticle-based optical detection technique for protein microarray: a novel approach. *Biosensors and Bioelectronics* **2004**, 20, 123-126.

52. Aslan K, Holley P, Davies L, et al. Angular-Ratiometric Plasmon-Resonance Based Light Scattering for Bioaffinity Sensing. *J Am Chem Soc* **2005**, 127, 12115-12121.

53. Maxwell DJ, Taylor JR, Nie S. Self-Assembled Nanoparticle Probes for Recognition and Detection of Biomolecules. *J Am Chem Soc* **2002**, 124, 9606-9612.

54. Park S-J, Taton TA, Mirkin CA. Array-Based Electrical Detection of DNA with Nanoparticle Probes. *Science* **2002**, 295, 1503-1506.

55. Pingarrón JM, Yáñez-Sedeño P, González-Cortés A. Gold nanoparticle-based electrochemical biosensors. *Electrochimica Acta* **2008**, 53, 5848-5466.

56. Mena ML, Yáñez-Sedeño P, Pingarrón JM. A comparison of different strategies for the construction of amperometric enzyme biosensors using gold nanoparticle-modified electrodes. *Analytical Biochemistry* **2005**, 336, 20-27.

57. Wang M, Wang L, Wang G, et al. Application of impedance spectroscopy for monitoring colloid Au-enhanced antibody immobilization and antibody-antigen reactions. *Biosensors and Bioelectronics* **2004**, 19, 575-582.

58. Ozsoz M, Erdem A, Kerman K, et al. Electrochemical Genosensor Based on Colloidal Gold Nanoparticles for the Detection of Factor V Leiden Mutation Using Disposable Pencil Graphite Electrodes. *Anal Chem* **2003**, 75, 2181-2187.

59. Kerman K, Morita Y, Takamura Y, et al. Modification of Escherichia coli single-stranded DNA binding protein with gold nanoparticles for electrochemical detection of DNA hybridization. *Analytica Chimica Acta* **2004**, 510, 169-174.

60. Kerman K, Saito M, Morita Y, et al. Electrochemical Coding of Single-Nucleotide Polymorphisms By Monobase-Modified Gold Nanoparticles. *Anal Chem* **2004**, 76, 1877-1884.

61. Liu S, Ju H. Reagentless glucose biosensor based on direct electron transfer of glucose oxidase immobilized on colloidal gold modified carbon paste electrode. *Biosensors and Bioelectronics* **2003**, 19, 177-183.

62. Crespilho FN, Emilia Ghica M, Florescu M, et al. A strategy for enzyme immobilization on layer-by-layer dendrimer-gold nanoparticle electrocatalytic membrane incorporating redox mediator. *Electrochemistry Communications* **2006**, 8, 1665-1670.

63. Zhuo Y, Yuan R, Chai Y, et al. A reagentless amperometric immunosensor based on gold nanoparticles/thionine/Nafion-membrane-modified gold electrode for determination of [alpha]-1-fetoprotein. *Electrochemistry Communications* **2005**, 7, 355-360.

64. Tang D, Yuan R, Chai Y. Electrochemical immuno-bioanalysis for carcinoma antigen 125 based on thionine and gold nanoparticles-modified carbon paste interface. *Analytica Chimica Acta* **2006**, 564, 158-165.

65. Manso J, Mena ML, Pingarrón J, et al. Electrochemical biosensors based on colloidal gold-carbon nanotubes composite electrodes. *Journal of Electroanalytical Chemistry* **2007**, 603, 1-7.

66. Xian Y, Hu Y, Liu F, et al. Glucose biosensor based on Au nanoparticles-conductive polyaniline nanocomposite. *Biosensors and Bioelectronics* **2006**, 21, 1996-2000.

67. Gao F, Yuan R, Chai Y, et al. Amperometric hydrogen peroxide biosensor based on the immobilization of HRP on nano-Au/Thi/poly (p-aminobenzene sulfonic acid)-modified glassy carbon electrode. *Journal of Biochemical and Biophysical Methods* **2007**, 70, 407-413.

68. Tang DP, Yuan R, Chai YQ, et al. Novel potentiometric immunosensor for hepatitis B surface antigen using a gold nanoparticle-based biomolecular immobilization method. *Analytical Biochemistry* **2004**, 333, 345-350.

69. Tang D, Yuan R, Chai Y, et al. Preparation and application on a kind of immobilization method of anti-diphtheria for potentiometric immunosensor modified colloidal Au and polyvinyl butyral as matrixes. *Sensors and Actuators B: Chemical* **2005**, 104, 199-206.

70. Luo X-L, Xu J-J, et al. A glucose biosensor based on chitosan-glucose oxidase-gold nanoparticles biocomposite formed by one-step electrodeposition. *Analytical Biochemistry* **2004**, 334, 284-289.

71. Luo X-L, Xu J-J, Zhang Q, et al. Electrochemically deposited chitosan hydrogel for horseradish peroxidase immobilization through gold nanoparticles self-assembly. *Biosensors and Bioelectronics* **2005**, 21, 190-196.

72. Wu B-Y, Hou S-H, Yin F, et al. Amperometric glucose biosensor based on layer-by-layer assembly of multilayer films composed of chitosan, gold nanoparticles and glucose oxidase modified Pt electrode. *Biosensors and Bioelectronics* **2007**, 22, 838-844.

73. Jena BK, Raj CR. Electrochemical Biosensor Based on Integrated Assembly of Dehydrogenase Enzymes and Gold Nanoparticles. *Anal Chem* **2006**, 78, 6332-6339.

74. Paciotti GF, David GI, Tamarkin KL, et al. Colloidal gold nanoparticles: a novel nanoparticle platform for developing multifunctional tumor-targeted drug delivery vectors. *Drug Development Research* **2006**, 67, 47-54.

75. Hong R, Forbes NS, Rotello VM, et al. Glutathione-Mediated Delivery and Release Using Monolayer Protected Nanoparticle Carriers. *J Am Chem Soc* **2006**, 128, 1078-1079.

76. Polizzi MA, Stasko NA, Schoenfisch MH. Water-Soluble Nitric Oxide-Releasing Gold Nanoparticles. *Langmuir* **2007**, 23, 4938-4943.

77. Gang Han, You C-C, Rotello VM, et al. Light-Regulated Release of DNA and Its Delivery to Nuclei by Means of Photolabile Gold Nanoparticles13. *Angewandte Chemie International Edition* **2006**, 45, 3165-3169.

78. Skirtach AG, Oliver J, Karen K, et al. Laser-Induced Release of Encapsulated Materials inside Living Cells. *Angewandte Chemie International Edition* **2006**, 45, 4612-4617.

79. Loo C, Lin A, Hirsch L, et al. Nanoshell-Enabled Photonics Based Imaging and Therapy of Cancer. *Technology in Cancer Research and Treatment* **2004**, 3, 33-40.

80. Moghimi SM, Hunter AC, Murray JC. Nanomedicine: current status and future prospects. *FASEB J* **2005**, 19, 311-330.

81. O'Neal DP, Hirsch LR, West JL, et al. Photo-thermal tumor ablation in mice using near infrared-absorbing nanoparticles. *Cancer Letters* **2004**, 209, 171-176.

82. Bergen JM, Archana P, Pun H, et al. Gold Nanoparticles as a Versatile Platform for Optimizing Physicochemical Parameters for Targeted Drug Delivery. *Macromolecular Bioscience* **2006**, 6, 506-516.

83. Dixit V, Bossche J, Sherman DM, et al. Synthesis and Grafting of Thioctic Acid-PEG-Folate Conjugates onto Au Nanoparticles for Selective Targeting of Folate Receptor-Positive Tumor Cells. *Bioconjugate Chem* **2006**, 17, 603-609.

84. Chen Y-H, Tsai C-Y, Huang P-Y, et al. Methotrexate Conjugated to Gold Nanoparticles Inhibits Tumor Growth in a Syngeneic Lung Tumor Model. *Mol Pharmaceutics* **2007**, 4, 713-22.

85. Gibson JD, Khanal BP, Zubarev ER. Paclitaxel-Functionalized Gold Nanoparticles. *J Am Chem Soc* **2007**, 129, 11653-11661.

86. Hone DC, Walker PI, Evans-Gowing R, et al. Generation of Cytotoxic Singlet Oxygen via Phthalocyanine-Stabilized Gold Nanoparticles: A Potential Delivery Vehicle for Photodynamic Therapy. *Langmuir* **2002**, 18, 2985-2987.

87. Mocellin S, Bronte V, Nitti D, et al. Nitric oxide, a double edged sword in cancer biology: Searching for therapeutic opportunities. *Medicinal Research Reviews* **2007**, 27, 317-352.

88. Saito G, Swanson JA, Lee K-D. Drug delivery strategy utilizing conjugation via reversible disulfide linkages: role and site of cellular reducing activities. *Advanced Drug Delivery Reviews* **2003**, 55, 199-215.

89. Sapsford KE, Berti L, Mendintz IL, et al. Materials for Fluorescence Resonance Energy Transfer Analysis: Beyond Traditional Donor-Acceptor Combinations. *Angewandte Chemie International Edition* **2006**, 45, 4562-4589.

90. Yeh P, Perricaudet M. Advances in adenoviral vectors: from genetic engineering to their biology. *FASEB J* **1997**, 11, 615-623.

91. Check E. Gene therapy: A tragic setback. *Nature* **2002**, 420, 116-118.

92. McIntosh CM, Martin CT, Rotello VM, et al. Inhibition of DNA Transcription Using Cationic Mixed Monolayer Protected Gold Clusters. *J Am Chem Soc* **2001**, 123, 7626-7629.

93. Han G, Martin CT, Rotello VM, et al. Stability of Gold Nanoparticle-Bound DNA toward Biological, Physical, and Chemical Agents. *Chemical Biology & Drug Design* **2006**, 67, 78-82.

94. Han G, Chari NS, Rotello VM, et al. Controlled Recovery of the Transcription of Nanoparticle-Bound DNA by Intracellular Concentrations of Glutathione. *Bioconjugate Chem* **2005**, 16, 1356-1359.

95. Sandhu KK, McIntosh CM, Rotello VM, et al. Gold Nanoparticle-Mediated Transfection of Mammalian Cells. *Bioconjugate Chem* **2002**, 13, 3-6.

96. Thomas M, Klibanov AM. Conjugation to gold nanoparticles enhances polyethylenimine's transfer of plasmid DNA into mammalian cells. *Proceedings of the National Academy of Sciences of the United States of America* **2003**, 100, 9138-9143.

97. Wang H, Chen Y, Li XY, et al. Synthesis of Oligo(ethylenediamino)-β-Cyclodextrin Modified Gold Nanoparticle as a DNA Concentrator. *Mol Pharmaceutics* **2007**, 4, 189-198.

98. Rosi NL, Giljohann DA, Thaxton CS, et al. Oligonucleotide-Modified Gold Nanoparticles for Intracellular Gene Regulation. *Science* **2006**, 312, 1027-1030.

99. Oishi M, Nakaogami J, Ishii T, et al. Smart PEGylated Gold Nanoparticles for the Cytoplasmic Delivery of siRNA to Induce Enhanced Gene Silencing. *Chemistry Letters* **2006**, 35, 1046-1047.

100. Verma A, Simard JM, Rotello VM, et al. Tunable Reactivation of Nanoparticle-Inhibited β-Galactosidase by Glutathione at Intracellular Concentrations. *J Am Chem Soc* **2004**, 126, 13987-1399.

101. Bhumkar D, Joshi H, Sastry M, et al. Chitosan Reduced Gold Nanoparticles as Novel Carriers for Transmucosal Delivery of Insulin. *Pharmaceutical Research* **2007**, 24, 1415-1426.

102. Hirsch LR, Stafford RJ, Bankson JA, et al. Nanoshell-mediated near-infrared thermal therapy of tumors under magnetic resonance guidance. *Proceedings of the National Academy of Sciences of the United States of America* **2003**, 100, 13549-13554.

103. Hirsch LR, Halas NJ, West JL, et al. A Whole Blood Immunoassay Using Gold Nanoshells. *Anal Chem* **2003**, 75, 2377-2381.

104. Huang X, Qian W, El-Sayed IH, et al. The potential use of the enhanced nonlinear properties of gold nanospheres in photothermal cancer therapy. *Lasers in Surgery and Medicine* **2007**, 39, 747-753.

105. Radt B, Smith A, Caruso F. Optically Addressable Nanostructured Capsules. *Advanced Materials* **2004**, 16, 2184-2189.

106. Angelatos AS, Radt B, Caruso F. Light-Responsive Polyelectrolyte/Gold Nanoparticle Microcapsules. *J Phys Chem B* **2005**, 109, 3071-3076.

107. West JL, Halas NJ. Applications of nanotechnology to biotechnology: Commentary. *Current Opinion in Biotechnology* **2000**, 11, 215-217.

108. Aili D, Enander K, Rydberg J, et al. Aggregation-Induced Folding of a De Novo Designed Polypeptide Immobilized on Gold Nanoparticles. *J Am Chem Soc* **2006**, 128, 2194-2195.

109. Slocik JM, Morley OS, Rajesh RN. Synthesis of Gold Nanoparticles Using Multifunctional Peptides13. *Small* **2005**, 1, 1048-1052.

110. He P, Urban MW. Phospholipid-Stabilized Au-Nanoparticles. *Biomacromolecules* **2005**, 6, 1224-1225.

111. He P, Zhu X. Phospholipid-assisted synthesis of size-controlled gold nanoparticles. *Materials Research Bulletin* **2007**, 42, 1310-1315.

112. Zhang L, Sun X, Song Y, et al. Didodecyldimethylammonium Bromide Lipid Bilayer-Protected Gold Nanoparticles: Synthesis, Characterization, and Self-Assembly. *Langmuir* **2006**, 22, 2838-2843.

113. Cheng W, Dong S, Wang E. Synthesis and Self-Assembly of Cetyltrimethylammonium Bromide-Capped Gold Nanoparticles. *Langmuir* **2003**, 19, 9434-9439.

114. Isaacs SR, Cutler EC, Park JS, et al. Synthesis of Tetraoctylammonium-Protected Gold Nanoparticles with Improved Stability. *Langmuir* **2005**, 21, 5689-5692.

115. Cheng W, Wang E. Size-Dependent Phase Transfer of Gold Nanoparticles from Water into Toluene by Tetraoctylammonium Cations: A Wholly Electrostatic Interaction. *J Phys Chem B* **2004**, 108, 24-26.

116. Du L, Jiang H, Liu X, et al. Biosynthesis of gold nanoparticles assisted by Escherichia coli DH5[α] and its application on direct electrochemistry of hemoglobin. *Electrochemistry Communications* **2007**, 9, 1165-1170.

117. Loo L, Guenther RH, Basnayake VR, et al. Controlled Encapsidation of Gold Nanoparticles by a Viral Protein Shell. *J Am Chem Soc* **2006**, 128, 4502-4503.

118. Slocik JM, Naik RR, Stone MO, et al. Viral templates for gold nanoparticle synthesis. *Journal of Materials Chemistry* **2005**, 15, 749-753.

119. Scheeren CW, Machado G, Dupont J, et al. Nanoscale Pt(0) Particles Prepared in Imidazolium Room Temperature Ionic Liquids: Synthesis from an Organometallic Precursor, Characterization, and Catalytic Properties in Hydrogenation Reactions. *Inorg Chem* **2003**, 42, 4738-4742.

120. Dupont J, Fonseca GS, Umpierre AP, et al. Transition-Metal Nanoparticles in Imidazolium Ionic Liquids: Recycable Catalysts for Biphasic Hydrogenation Reactions. *J Am Chem Soc* **2002**, 124, 4228-4229.

121. Itoh H, Naka K, Chujo Y. Synthesis of Gold Nanoparticles Modified with Ionic Liquid Based on the Imidazolium Cation. *J Am Chem Soc* **2004**, 126, 3026-3027.

122. Kim KS, Demberelnyamba D, Lee H. Size-Selective Synthesis of Gold and Platinum Nanoparticles Using Novel Thiol-Functionalized Ionic Liquids. *Langmuir* **2004**, 20, 556-560.

123. Huang H, Yang X. Synthesis of Chitosan-Stabilized Gold Nanoparticles in the Absence/Presence of Tripolyphosphate. *Biomacromolecules* **2004**, 5, 2340-2346.

124. Wang B, Chen K, Jiang S, et al. Chitosan-Mediated Synthesis of Gold Nanoparticles on Patterned Poly(dimethylsiloxane) Surfaces. *Biomacromolecules* **2006,** 7, 1203-1209.

125. DosSantos DS, Goulet PJG, Pieczonka NPW, et al. Gold Nanoparticle Embedded, Self-Sustained Chitosan Films as Substrates for Surface-Enhanced Raman Scattering. *Langmuir* **2004**, 20, 10273-10277.

126. Miyama T, Yonezawa Y. Aggregation of Photolytic Gold Nanoparticles at the Surface of Chitosan Films. *Langmuir* **2004**, 20, 5918-5923.

127. Qi Z, Zhou H, Matsuda N, et al. Characterization of Gold Nanoparticles Synthesized Using Sucrose by Seeding Formation in the Solid Phase and Seeding Growth in Aqueous Solution. *J Phys Chem B* **2004**, 108, 7006-7011.

128. Garcia ME, Baker LA, Crooks RM. Preparation and Characterization of Dendrimer-Gold Colloid Nanocomposites. *Anal Chem* **1999**, 71, 256-258.

129. Esumi K, Hosoya T, Suzuki A, et al. Spontaneous Formation of Gold Nanoparticles in Aqueous Solution of Sugar-Persubstituted Poly(amidoamine)dendrimers. *Langmuir* **2000**, 16, 2978-2980.

130. Kim YG, Oh SK, Crooks RM. Preparation and Characterization of 1-2 nm Dendrimer-Encapsulated Gold Nanoparticles Having Very Narrow Size Distributions. *Chem Mater* **2004**, 16, 167-172.

131. Haba Y, Kojima C, Harada A, et al. Preparation of Poly(ethylene glycol)-Modified Poly(amido amine) Dendrimers Encapsulating Gold Nanoparticles and Their Heat-Generating Ability. *Langmuir* **2007,** 23, 5243-5246.

132. Xuping Sun. One-Step Synthesis and Size Control of Dendrimer-Protected Gold Nanoparticles: A Heat-Treatment-Based Strategy. *Macromolecular Rapid Communications* **2003**, 24, 1024-1028.

133. Brusatin G, Abbotto A, Innocenzi SP, et al. Poled Sol-Gel Materials With Heterocycle Push-Pull Chromophores that Confer Enhanced Second-Order Optical Nonlinearity. *Advanced Functional Materials* **2004**, 14, 1160-1166.

134. Wang R, Yang J, Seraphin S, et al. Dendron-Controlled Nucleation and Growth of Gold Nanoparticles. *Angewandte Chemie International Edition* **2001**, 40, 549-552.

135. Nakao S, Torigoe K, Kon-No K, et al. Self-Assembled One-Dimensional Arrays of Gold-Dendron Nanocomposites. *J Phys Chem B* **2002**, 106, 12097-12100.

136. Kim M-K, Jeon Y-M, Jeon WS, et al. Novel dendron-stabilized gold nanoparticles with high stability and narrow size distribution. *Chemical Communications* **2001**, 667-668.

137. Hussain I, Graham S, Wang Z, et al. Size-Controlled Synthesis of Near-Monodisperse Gold Nanoparticles in the 1-4 nm Range Using Polymeric Stabilizers. *J Am Chem Soc* **2005**, 127, 16398-16399.

138. Teranishi T, Kiyokawa I, Miyake M. Synthesis of Monodisperse Gold Nanoparticles Using Linear Polymers as Protective Agents. *Advanced Materials* **1998**, 10, 596-599.

139. Wan D, Fu Q, Huan J. Synthesis of amphiphilic hyperbranched polyglycerol polymers and their application as template for size control of gold nanoparticles. *Journal of Applied Polymer Science* **2006**, 101, 509-514.

140. Perignon N, Marty JD, Mingotaud AF, et al. Hyperbranched Polymers Analogous to PAMAM Dendrimers for the Formation and Stabilization of Gold Nanoparticles. *Macromolecules* **2007**, 40, 3034-3041.

141. Duan H, Nie S. Etching Colloidal Gold Nanocrystals with Hyperbranched and Multivalent Polymers: A New Route to Fluorescent and Water-Soluble Atomic Clusters. *J Am Chem So*c **2007**, 129, 2412-2413.

142. Kang Y, Taton TA. Core/Shell Gold Nanoparticles by Self-Assembly and Crosslinking of Micellar, Block-Copolymer Shells. *Angewandte Chemie International Edition* **2005**, 44, 409-412.

143. Zubarev ER, Xu J, Sayyad A, et al. Amphiphilic Gold Nanoparticles with V-Shaped Arms. *J Am Chem Soc* **2006**, 128, 4958-4959.

144. Kim JH, Lee TR. Thermo- and pH-Responsive Hydrogel-Coated Gold Nanoparticles. *Chem Mater* **2004**, 16, 3647-3651.

145. Zheng P, Jiang X, Zhang X, et al. Formation of Gold at Polymer Core-Shell Particles and Gold Particle Clusters on a Template of Thermoresponsive and pH-Responsive Coordination Triblock Copolymer. *Langmuir* **2006**, 22, 9393-9396.

146. Wuelfing WP, Gross SM, Murray RW, et al. Nanometer Gold Clusters Protected by Surface-Bound Monolayers of Thiolated Poly(ethylene glycol) Polymer Electrolyte. *J Am Chem Soc* **1998**, 120, 12696-12697.

147. Otsuka H, Akiyama Y, Nagasaki Y, et al. Quantitative and Reversible Lectin-Induced Association of Gold Nanoparticles Modified with α-Lactosyl-ω-mercapto-poly(ethylene glycol). *J Am Chem Soc* **2001**, 123, 8226-8230.

148. Otsuka H, Nagasaki Y, Kataoka K. PEGylated nanoparticles for biological and pharmaceutical applications. *Advanced Drug Delivery Reviews* **2003**, 55, 403-419.

149. Shimmin RG, Schoch AB, Braun PV. Polymer Size and Concentration Effects on the Size of Gold Nanoparticles Capped by Polymeric Thiols. *Langmuir* **2004**, 20, 5613-5620.

150. Takae S, Akiyama Y, Otsuka H, et al. Ligand Density Effect on Biorecognition by PEGylated Gold Nanoparticles: Regulated Interaction of RCA Lectin with Lactose Installed to the Distal End of Tethered PEG Strands on Gold Surface. *Biomacromolecules* **2005**, 6, 818-824.

151. Ishii T, Otsuka H, Kataoka K, et al. Preparation of Functionally PEGylated Gold Nanoparticles with Narrow Distribution through Autoreduction of Auric Cation by α-Biotinyl-PEG-block-[poly(2-(N,N-dimethylamino)ethyl methacrylate)]. *Langmuir* **2004**, 20, 561-564.

152. Olivier J-C, Huertas R, Lee HJ, et al. Synthesis of Pegylated Immunonanoparticles. *Pharmaceutical Research* **2002**, 19, 1137-1143.

153. Oldenburg SJ, Averitt RD, Westcott SL, et al. Nanoengineering of optical resonances. *Chemical Physics Letters* **1998**, 288, 243-247.

CHAPTER 3

Background on hydrogels and their small scale applications

3.1. Hydrogels: Definition and applications

Hydrogels are crosslinked, hydrophilic, insoluble, polymeric networks that have the unique property of swelling to a high degree when placed in an aqueous or biological medium [1, 2]. Their elastic swelling behavior is because of their high affinity for water, and they are insoluble due to the presence of chemical or physical crosslinks. They exhibit an elastic nature once they absorb water and therefore resemble a variety of natural living tissues. The various hydrogel materials that are in close resemblance to that of natural living tissues are widely employed in various biomedical applications [3, 4]. By tailoring the various functional groups along the polymer backbone, hydrogels can be designed to be sensitive when subjected to changes in the surrounding ambient conditions such as temperature, pH, electric field, or ionic strength. Their unique swelling and shrinking capabilities that constitute an actuation process makes them attractive for many aqueous applications. In addition, their biocompatibility has promoted their use in biomaterials such as contact lenses, sutures, implants, and controlled drug delivery systems, etc. [5, 6].

Hydrogels are used as carriers in pharmaceutical formulations for self-regulated pulsatile delivery and when functionalized with biospecific molecules they are used for site specific delivery. In the field of tissue engineering, they are applied as matrices and scaffolds for the repair and regeneration of cells and tissues [7]. They have also been used

as absorbers in diapers, as separation media in ion-exchange and size exclusion chromatography, in microfluidic devices, in biosensors, and as actuators [8-11]. In medical applications, hydrogels find importance as one of the most common material to be used. For example, IONSYS™ system uses hydrogels for controlled delivery of an opioid agonist for transdermal delivery. Cervidil® is a vaginal insert commonly used for the induction of labor among pregnant women. Vantas® is a transdermal hydrogel implant used for the systemic delivery of histrelin acetate for prostate cancer control. NanoDOX™ and Avogel hydrogels are used for treating burn wounds and scars. ProGEL™ is used as a sealant for lung surgical pleural leaks.

3.2. Classification of environmentally responsive hydrogels

Hydrogels are usually classified as either physical or chemical systems based on the kind of crosslinks within the network. Non-covalent forces such as molecular entanglements and secondary forces (hydrogen bonding, ionic/hydrophobic interactions, etc.) hold together the network of physically crosslinked hydrogels. Since the molecular entanglements and secondary forces can be localized, these systems are typically heterogeneous in nature. The interactions of physical gels with other compounds can be reversible and are easily affected by conditions such as temperature, pH, and ionic strength. In the case of the chemically crosslinked hydrogels, the polymeric network is held together by crosslinks that are formed via covalent bonds. The crosslink density, which is controlled by the amount of crosslinker and the type of crosslinker used, defines the equilibrium swelling of the chemical hydrogels [4]. Hydrogels are also classified

based on the nature of the side groups in their polymer backbone, which could be either neutral or ionic [3].

By tailoring the various functional groups of the monomer – crosslinker system and crosslinking ratio, hydrogels can be designed to respond to specific environmental stimuli to varying degrees. The environmental stimuli could be pH, temperature, ionic strength, light, magnetic field, or even biological cues [12]. The response to stimuli is characterized by a dynamic and reversible change to some physico-chemical property of the system defined by the various parameters as mentioned above. Also, the behavior of the polymer in the immersed solvent is related to the balance between solvent-solvent, solvent-polymer, and polymer-polymer interactions which are modulated by the various forces such as ionic interactions, hydrophobic-hydrophilic interactions, hydrogen-bonding, and van der Waals forces. These interactions dictate the hydrogel volume swelling response [13]. Some examples of environmentally responsive hydrogels are poly(hydroxyethyl methacrylate) and poly(ethylene glycol) (neutral), poly(acrylic acid) and poly(methacrylic acid) (ionic/pH-sensitive), and poly(N-isopropylacrylamide) and poly(N,N-diethylacrylamide) (temperature responsive).

3.2.1. pH-Responsive hydrogels

Ionic hydrogels are pH responsive and swell or shrink in response to changes in pH. Properties such as ionic content, nature of counter ions, ionization equilibrium considerations, and polymer composition and crosslinking ratio affect the swelling behavior of these gels. Faster swelling and higher equilibrium swelling ratio is governed

by the increase in the ionic content of the gel and a lower crosslinking ratio. The pK_a and pK_b values in the case of anionic and cationic gels control their swelling behaviors, respectively [14]. In the case of anionic gels, ionization of the acid groups that constitute the gel occurs when the pH of the medium is above the pK_a value of the acid group. Deprotonation occurs, and increased charge on the chain results in an electrostatic repulsion between the various parts of the chain and thereby an increased hydrophilicity of the gel. The difference in the charges that exist between the interior of the gel caused by protonation or deprotonation and the outside swelling medium results in an osmotic effect which induces water absorption thereby swelling the gel.

3.2.2. Temperature sensitive hydrogels

Temperature sensitive hydrogels exhibit significant volume-phase transition around their lower critical solution temperature (LCST) or upper critical solution temperatures (UCST). At these critical temperatures, the hydrogel undergoes its reversible transition from a swollen state to a collapsed state and vice versa. Similar to that of pH responsive hydrogel, the swelling behavior of these gels depends on the components of the gel and the crosslinking ratios. At the critical solution temperatures, the hydrogel undergoes a reversible transition that changes the hydrophilic/hydrophobic balance of the system. Also, researchers have shown that hydrophilic/hydrophobic co-monomers and crosslinkers used can modify the critical solution temperature significantly [15].

A positive temperature sensitive hydrogel is one that has an UCST and expands when its temperature is raised above the transition temperature, resulting in more

swelling. On the other hand, negative temperature sensitive hydrogels tend to shrink or collapse as temperature is increased above the LCST and swells upon lowering the temperature below the LCST. This reversible swelling response for both the systems is shown in Figure 3.1. Poly(N-isopropyl acrylamide (PNIPAAm) is a negative temperature sensitive polymer which exhibits phase transition aroun 32 ^{o}C [16]. Due to this property, crosslinked PNIPAAm hydrogels find applications in the fields of drug delivery and tissue engineering [17]. PNIPAAm behaves more hydrophilic below LCST thereby swelling at temperatures below the LCST and behaves hydrophobic at temperatures above LCST causing the collapse of the gel. This can be better explained by comparing the isobaric phase diagram (Figure 3.2., adapted from [18]) between uncrosslinked PNIPAAm polymer chain and crosslinked PNIPAAm hydrogel in an aqueous medium/water. PNIPAAm polymer chain exhibits a LCST at around 32 ^{o}C, below which the polymer chain and water/aqueous medium are completely miscible forming a polymer solution. As the temperature is raised, the polymer chain and water are only partially miscible leading to the formation of a two phase region made up of water rich phase and polymer rich phase. Now in the case of the crosslinked PNIPAAm hydrogel, the phase behavior above ~ 32 ^{o}C is similar to that of the uncrosslinked PNIPAAm chain, except that herein, the water rich phase is composed of only pure water. This is because the hydrogel cannot partially mix due to the presence of chemical crosslinks that inhibit them from dissolving into the water phase. The hydrogel below its gel transition temperature/volume phase transition temperature exists either as a homogenous hydrogel phase or a swollen hydrogel in equilibrium with excess surrounding water. Below the LCST, hydrogen bonding occurs between the amide moieties (–NH and C=O) of the

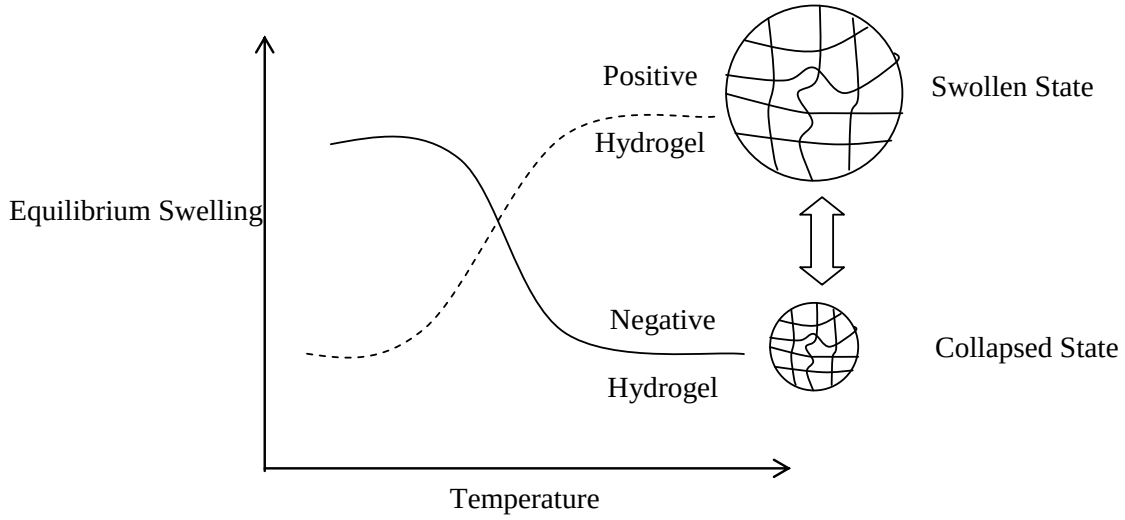

Figure 3.1. Equilibrium swelling of temperature sensitive hydrogels versus temperature

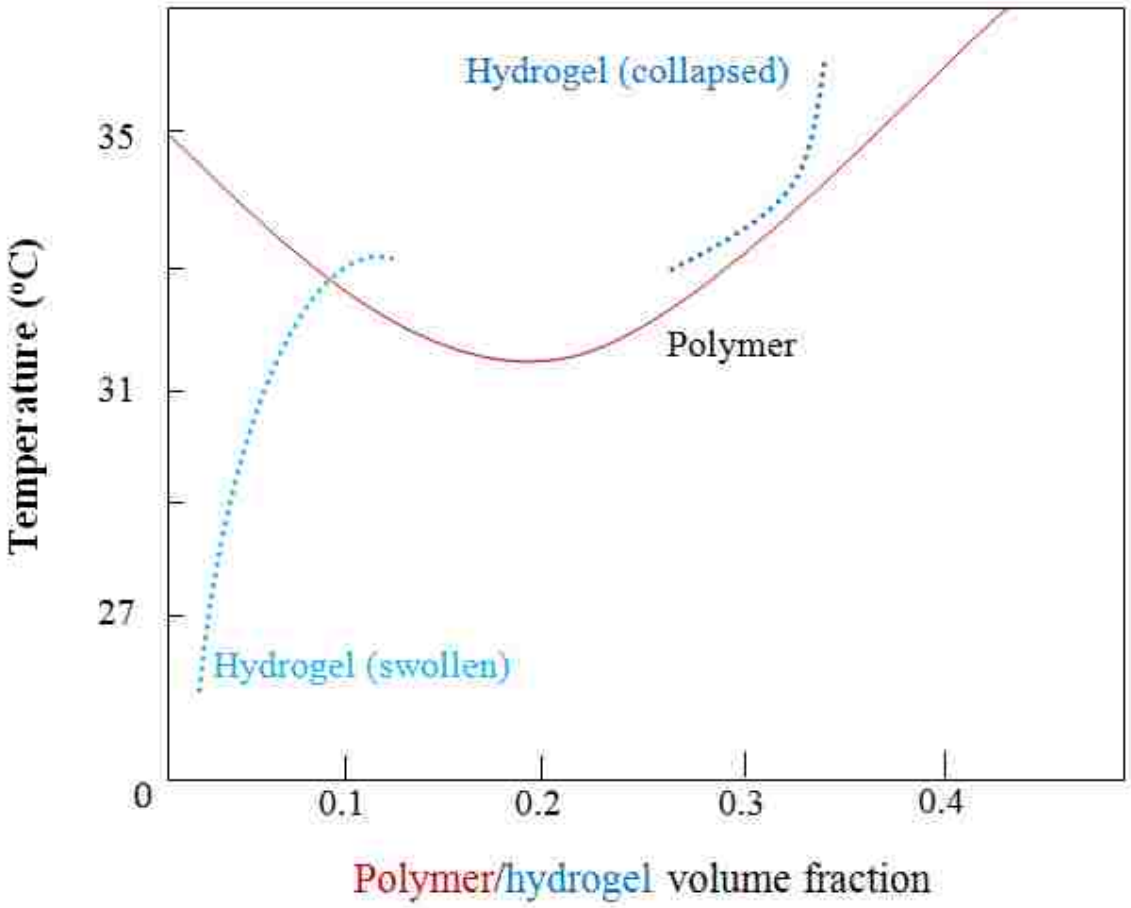

Figure 3.2. A typical phase diagram for uncrosslinked PNIPAAm polymer chain and crosslinked PNPAAm hydrogel.

PINPAAm backbone and the surrounding water causing the hydrogel to swell. Above the LCST, the hydrogen bonds break and polymer-polymer interactions occur via the hydrophobicity between the isopropyl acrylamide moieties leading to the collapse of the hydrogel, thereby expelling water out of the hydrogel matrix [19].

3.3. Biodegradable Hydrogels

Biodegradable polymeric systems have been frequently used in the development of advanced drug delivery systems and tissue engineering scaffolds. Their use in the design of drug delivering implants and tissue scaffolds is mainly due to the various advantages associated with the degradation of their polymeric matrix. The degradation of the drug delivering hydrogel matrix avoids the removal of the device from the body by surgery or other means when the device is no longer needed. Also, they provide flexibility in the design of delivery systems for large molecular weight drugs, such as peptides and proteins, which are not suitable for diffusion-controlled release through nondegrdable hydrogel matrices [20]. Further, the ability to tailor the balance of the hydrophilicity and hydrophobicity of the hydrogel allows the release of different types of drugs [21]. Their polymeric backbone can be modified to suit pH or temperature response behavior, thereby using them for self regulative sensing, drug delivery, and subsequent biodegradation [22]. Their degradation kinetics and mechanical properties can be tuned for systemic delivery of various drugs for a wide variety of biomedical applications.

One class of biodegradable hydrogels is the poly(β-amino ester) (PBAE) polymeric systems developed by Anderson and coworkers [23]. PBAE macromers are

synthesized usually by the reaction of a primary or secondary amine with an acrylate as found in the combinatorial library of biodegradable crosslinkable biomaterials [23]. These polyester systems can be degraded into innocuous by-products via hydrolytic degradation. The various advantages of using PBAE systems over other conventional biodegradable polymeric systems is that the monomer reagents used for their synthesis are commercially available and inexpensive, the macromer synthesis can be completed without additional protection/deprotection reagents since the amine readily reacts with the acrylate, and no significant by-products are generated resulting in no additional purification steps. Also, the library of amines and acrylates can be combined as per need to generate PBAE macromers that can be utilized to generate biodegradable hydrogels with tuned mechanical strength and degradation kinetics [24].

3.4. Hydrogels as functional components of micro-/nanodevices

Novel, intelligent hydrogels are of high interest and have found numerous applications in a wide variety of fields. In particular, hydrogels have received high interests as components of micro/nanodevices. For example, microactuators were fabricated by Beebe [25] and Zhao et al. [26]. In these cases, the responsive hydrogels act as the actuator in a microfluidic system where it senses changes in environmental conditions and therefore actuates in response. The posts in the microchannel of the device were jacketed with a pH responsive hydrogel. The swelling and shrinking characteristic of the pH sensitive hydrogel around the posts was used for actuating the fluid flow through microchannel. Responsive hydrogel systems were used for controlled pulsatile drug delivery in a microdevice. They were used as microactuators for controlled drug

delivery applications by Madou and group [27]. They used the artificial muscle concept for opening and closing holes in a drug reservoir and designed drug delivery devices of sphincter, plunger, and tube configuration. Baldi and his group [28] have synthesized micropumps and microvalves using a micro-structured silicon membrane with entrapped temperature sensitive hydrogels for environmentally sensitive fluid gating. The stimuli sensitive hydrogel coated over the microposts inside the orifice was incorporated using thermal polymerization. The valves close when the hydrogel swells and open when the gels collapse. Using this system, pulsatile release of a drug can be achieved.

Hydrogels are also being used in microdevices for biosensor applications. Biosensing electrodes were patterned with gels containing entrapped enzymes and were used for monitoring biospecific analyte-enzyme levels [29]. The concept of dual stimuli sensitive hydrogels for biospecific sensing and subsequent drug delivery was discussed by Miyata et al. [30]. Optical biosensors were fabricated by using pH responsive hydrogels for fluorescence sensing application by Revzin et al. [31]. Peppas and his coworkers [32] have patterned poly(ethylene glycol) hydrogels onto polymer surfaces to create novel surfaces for possible applications as biosensors. Surface modified microcantilevers are widely employed for sensing applications. Hydrogels coated on similar microcantilevers provide a variety of sensing applications. Hilt et al. [9, 33] used UV photolithography to align and pattern environmentally responsive hydrogels onto silicon microcantilevers to develop ultrasensitive microsensors.

3.4.1. Conventional lithography of hydrogels over microdevices

The ability to generate microstructures with ease and in large numbers has brought in various fabrication techniques that have been employed for the development of integrated circuit compenents. Although microfabrication has its foundations in microelectronics, it is being applied in areas outside of microelectronics like microelectromechanical systems (MEMS), microreactors, microanalysis, microsensors, microoptics, and biotechnology. Most of the micro/nanodevices such as the Beebe's microactuator [25], Peppas group's microcantilevers [9, 33], Baldi's micropumps and microvalves [28], and Madou's microactuators [27] for drug delivery applications are fabricated using photolithography. Lithography is the most successful technology in microfabrication. It has been the workhorse of the semiconductor industry. In fact, all integrated circuits that are present in electronic equipments are made by using this technology. MEMS/NEMS, microarrays, microfluidics, lab on a chip, and other micro/nanodevices are currently being widely developed using the principles of photolithography. For example, the process involves the photopolymerization of the monomers and crosslinkers in the presence of a photoinitiator to give the hydrogel in the device. The patterning is usually controlled by the type of photomask involved. Since the scales encountered in the field of biology and medicine lie in the micro- and nanometer range, novel lithographic techniques such as e-beam and ion-beam lithography have been developed to achieve a fine level of control for patterning on surfaces of biomaterials.

Though photolithography is the most successful technology for microfabrication in the electronic era, it has certain disadvantages. As the sizes of the features goes lower

and lower, a better illuminating source with shorter wavelength is required. Other limitations include the use of a high energy illuminating source, cost and difficulty of production, maintenance, and safety considerations. To overcome these problems, the field of soft lithography has been demonstrated for fabricating high quality micro- and nanostructures, without having the continuous need for the laborious photolithography techniques. The most commonly employed soft lithography techniques include microcontact printing (μCP), replica molding (REM), microtransfer molding (μTM), micromolding in capillaries (MIMIC), solvent assisted micromolding (SAMIM), nanoimprint lithography, etc. for fabricating high quality microstructures and nanostructures [34-38].

3.4.2. Soft lithography

In soft lithography, the key element is an elastomeric stamp or mold which transfers the pattern to the substrate. Many such elastomeric stamps can be prepared from a single master stamp which is prefabricated using a single photolithographic step. The same mold can be used multiple times because of their rigidity, and they enable rapid prototyping of similar patterns. Another advantage is that the flexible property of molds enables patterning on surfaces which are non planar [37]. Further the amalgamation of various soft lithography techniques with self assembled monolayers (SAMs) has led to the easy patterning of various functionalities over surfaces with ease [39].

Polydimethylsiloxane (PDMS) is a widely used polymer for stamps in soft lithography. It is usually prepared by replica molding (REM) by casting the liquid

prepolymer of PDMS with curing agent against a master that has a patterned relief structure in its surface. The advantages of using PDMS for soft lithography are that it is chemically inert, does not adhere irreversibly to or react with most surfaces, homogenous, isotropic, and optically transparent down to about 300 nm and thus UV crosslinking of prepolymers that are being molded is possible [38]. Other materials that can be used for stamp making are polyurethanes, polyimides, and crosslinked Novolac resins [40].

Soft lithography has found numerous applications in the field of biology and biochemistry. Most mammalian cells are anchorage dependant and therefore must adhere to and spread on a substrate in order to live and remain functional. Soft lithography is well suited to pattern the composition, topography, and properties of surfaces [38], patterning of hydrophilic or hydrophobic molecules or polymers [41], polysaccharides [42], stimuli sensitive and responsive materials [43], and proteins or growth factors [44] over a wide variety of surfaces. An important application of soft lithography in biology is to generate patterns of proteins or cells which in turn are based on patterning the surfaces into regions that either promote or resist the adhesion of proteins and cells [45]. By using soft lithography, cells were patterned onto specific regions of a surface and their migration, and growth was controlled suitably [46]. Of all the soft lithographic techniques, microcontact printing is widely used for patterning various SAMs for biological applications over various surfaces.

3.4.3. Microcontact printing (μCP)

Microcontact printing is a flexible, non photolithographic method, which is used to pattern SAMs containing regions terminated by different chemical functionalities over various surfaces. The ability of SAMs to form ordered structures rapidly on suitable surfaces is the ultimate factor for the success of μCP [37]. Kumar et al. [40] were the first to report the process of μCP. It involves usually an elastomeric PDMS stamp that is used to pattern a certain chemical agent ("ink") onto the surface of a substrate through direct contact. A second SAM can be backfilled to the regions that are not stamped by washing the surface with suitable solution containing the second SAM molecules. The rapid reaction of the various SAMs on the surface of interest and the 'autophobicity' of the resulting SAMs makes μCP an efficient method to develop microstructures over surfaces [47].

Microcontact printing has been used to pattern SAMs over surfaces which are used as ultrathin resists in selective wet etching, or as templates to control the wetting, dewetting, nucleation, growth, and deposition of other materials [48]. In particular, it is useful for chemists, biologists and material scientists for micro- and nanopatterning in cases, such as patterning over nonplanar surfaces, where optically based lithography simply fails. The process of modifying an underlying surface using μCP has made it possible to study biological processes, such as cell adhesion and migration, as well as to conduct miniaturized and high-throughput assays [38]. Mrksich and coworkers were able to pattern hydrophobic hexadecanethiol onto gold surface that promote the adsorption of proteins whereas the remainder of the surface is covered with an alkanethiol that was

terminated with $(EG)_3OH$ groups which resisted the adsorption of proteins and adhesion of cells. Microcontact printing can also be used to transfer proteins on to the surface of glass, polystyrene, or silicon.

3.5. Hydrogel functionalized surfaces for biomedical devices

Surface modification with thin polymer films or polymer brushes has been a well established method to tailor various surface properties for biosensing applications such as wettability, biocompatibility, corrosion resistance, and friction [49, 50]. Braun et al. [51] used microcontact printing to pattern PNIPAAm brushes over specific regions of oxidized silicon wafers using ATRP as the reaction mechanism. Similar amplification of SAMs to polymeric brushes has been carried out by Hedrick et al. [52].

Environmentally responsive hydrogel patterns have several advantages that make them attractive over polymeric brushes. Unlike polymeric brushes that have an open polymeric structure for free molecular diffusion, the mesh size of a hydrogel matrix, which can be tailored by crosslinker constraints such as type and amount, governs the transport of molecular species into and out of the hydrogel [53]. This control over the hydrogel mesh can be harnessed for cellular entrapment and manipulations and controlled drug delivery applications [54-57]. Further, the network structure increases the mechanical integrity and stability of the hydrogel, making them more robust than brushes made up of the same polymer backbone [58]. These properties of hydrogels along with its response behavior make them attractive as alternatives to polymer brushes for certain applications.

3.6. Need for micro- and nanostructured hydrogels

The unique property of reversible swelling and shrinking of hydrogels makes them attractive for many aqueous actuation applications. The control over the thickness and pattern of the various hydrogels in micro- and nanoscale devices is vital for the effective use in biomedical applications. Since these systems are placed mostly in an aqueous media, the equilibrium swelling process depends on the transport of the fluid through the hydrogel mesh. The response behavior of hydrogels in various devices is typically diffusion limited. The characteristic diffusion time (θ_D) is directly proportional to the square of the length scale of the element under study (L) and inversely proportional to the diffusion coefficient (D_{AB}) [59].

$$\theta_D \propto \frac{L^2}{D_{AB}}$$

Therefore, a reduction of thickness from macro- to micro- to nanoscale can lead to responsive hydrogels that can respond 'instantaneously' to external stimuli. This is key for the application of hydrogels as sensors and actuators. In addition, smaller means portable, handheld, or even implantable devices which have a wider reach in the biomedical and pharmaceutical fields. Although, a wide variety of hydrogel pattern fabrication methods for surface based applications are already available, the methods to prepare hydrogel thin films at the nanoscale for 'instantaneous' stimuli recognition is still at its infancy [60-62].

By amalgamating μCP and ATRP, various hydrogel networks can be patterned over various surfaces. The two key goals for the current work are to attain the spatial

control over the surface (XY control by μCP and Z control by surface initiated polymerization – ATRP). By controlling the spatial patterning of the hydrogels, it is possible to synthesize flexible platforms over the surfaces and using the response behavior, these gels can be employed as functional components of various biomedical micro- and nanodevices. As an example, a temperature sensitive hydrogel pattern platform over gold surface and its demonstration as an ultra-fast responsive sensor is described in the forthcoming chapters.

3.7. References

[1] Lowman AM, Peppas NA. Hydrogels. in: E. Mathiowitz (Ed.), Encyclopedia of Controlled Drug Delivery, Vol. 1, *Wiley*, New York, **1999**, pp. 397-418.

[2] Peppas NA, Hilt JZ, Khademhosseini A, Langer R. Hydrogels in biology and medicine: from molecular principles to bionanotechnology. *Adv. Mater.* **2006**, 18, 1345-1360.

[3] Peppas NA, Bures P, Leobandung W, Ichikawa H. Hydrogels in pharmaceutical formulations. European *J. Pharm Biopharm* **2000**, 50, 27-46.

[4] Hoffman AS. Hydrogels in biomedical applications. *Adv. Drug Deliver. Rev.* **2002**, 43, 3-12.

[5] Langer R, Peppas NA. Advances in Biomaterials, Drug Delivery, and Bionanotechnology. *AICHE J.* **2003,** 49, 2990-3006.

[6] Peppas NA, Huang Y, Torres-Lugo M, Ward JH, Zhang J. Physiochemical foundations and structural design of hydrogels in medicine and biology. *Ann. Revs. Biomed. Eng.* **2000,** 2, 9-29.

[7] Aubin H, Nichol JW, Hutson C, Khademhosseini A. Directed 3D cell alignment and elongation in microengineered hydrogels. *Biomaterials* **2010,** DOI: 10.1016.

[8] Kim SY, Shin HS, Lee YM, Jeong CN. Properties of electroresponsive poly(vinyl) alcohol/poly(acrylic acid) IPN hydrogels under an electric stimulus. *J. App. Polym. Sci.* **1999,** 73, 1675-1683.

[9] Hilt JZ, Gupta AK, Bashir R, Peppas NA. Ultrasensitive biomems sensors based on microcantilevers patterned with environmentally responsive hydrogels. *Biomed. Microdevices* **2003,** 5, 177-184.

[10] Okano T, Yamada N, Sakai H, Sakurai Y. A novel recovery system for cultured cells using plasma-treated polystyrene dishes grafted with poly(N-isopropylacrylamide). *J. Biomed. Mater. Res.* **1993,** 27, 1243-1251.

[11] Ehrick JD, Deo SK, Browning TW, Bachas LG, Madou MJ, Daunert S. Genetically engineered protein in hydrogels tailors stimuli-responsive characteristics. *Nature Materials* **2005,** 4, 298-302.

[12] Hoffman AS. Intelligent polymers. In: Controlled Drug Delivery: Challenges and Strategies, Park, K. (Ed.), *American Chemical Society **1997***, Washington, DC, pp 485-497.

[13] Soppimath KS, Aminabhavi TM, Dave AM, Kumbar SG, Rudzinski WE. Stimulus-responsive "smart" hydrogels as novel drug delivery systems. *Drug Development and Industrial Pharmacy* **2002,** 28, 957-974.

[14] Khare AR, Peppas NA. Release Behavior of Bioactive Agents from pH-Sensitive Hydrogels, *J. Biomat. Sci., Polym. Ed.* **1993,** 4, 275-289.

[15] Lutz JF, Hoth A. Preparation of ideal PEG analogues with a tunable thermosensitivity by controlled radical copolymerization of 2-(2-methoxyethoxy)ethyl methacrylate and oligo(ethylene glycol) methacrylate. *Macromolecules* **2006,** 39, 893-896.

[16] Hirotsu S, Hirokawa Y, Tanaka T, Volume-phase transitions of ionized N-isopropyl acrylamide. *J. Chem Phys* **1987,** 87, 1392-1395.

[17] Jeong B, Kim SW, Bae YH. Thermosensitive sol-gel reversible hydrogels, *Adv. Drug Deliv. Revs.* **2002,** 54, 37-51.

[18] Marchetti M, Prager S, Cussler EL. Thermodynamic predictions of volume changes in temperature-sensitive gels. 1. Theory. *Macromolecules* **1990,** 23, 1760-1765.

[19] Schild HG. Poly(n-isopropylacrylamide): Experiment, theory and application. *Progress in Polymer Science* **1992,** 17, 163-249.

[20] Sanders LM, McRae GI, Vitale KM, Kell BA. Controlled delivery of an LHRH analogue from biodegradable injectable microspheres. *J. Controlled Rel.* **1985,** 2, 187-195.

[21] Guo K, Chu CC. Controlled release of paclitaxel from biodegradable unsaturated poly(ester amide)s/poly(ethylene glycol) diacrylate hydrogels. *J. Biomaterials Sci. Polym. Ed.* **2007**, 18, 489-504.

[22] Casadei MA, Pitarresi G. Biodegradable and pH-sensitive hydrogels for potential colon-specific drug delivery: Characterization and in vitro release studies. *Biomacromolecules* **2008,** 9, 43-49.

[23] Anderson DG, Tweedie CA, Hossain N, Navarro SM, Brey DM, Vliet KJV, Langer R, Burdick JA. A combinatorial library of photocrosslinkable and degradable materials. *Adv. Mater*. **2006,** 18, 2614-2618.

[24] Anderson DG, Akinc A, Langer R. Structure/property studies of polymeric gene delivery using a library of poly(β-amino esters). *Mol. Ther.* **2005,** 26, 4892-4897.

[25] Beebe DJ, Moore JS, Bauer JM, Yu Q, Liu RH, Devadoss C, Jo B. Funtional hydrogel structures for autonomous flow control inside microfluidic channels. *Nature* **2000,** 404, 588-590.

[26] Zhao B, Moore JS. Fast pH and ionic strength responsive hydrogels in microchannels, *Langmuir* **2001,** 17, 4758-4763.

[27] Low LM, Seetharaman S, Madou MJ. Microactuators toward microvalves for responsive controlled drug delivery. *Sens. Actuators. B* **2000,** 67, 149-160.

[28] Baldi A, Lei M, Gu Y, Siegel RA, Ziaie B, A microstructured silicon membrane with entrapped hydrogels for environmentally sensitive fluid gating, *Sens. Actuators B* **2006**, 114, 9-18.

[29] Sirkar K, Pishko MV. Amperometric biosensors based on oxidoredictases immobilized in photopolymerized poly(ethylene glycol) redox polymer hydrogels. *Anal. Chem.* **1998,** 70, 2888-2894.

[30] Miyata T, Uragami T, Nakamae K. Biomolecule-sensitive hydrogels, *Adv. Drug Delivery Revs.* **2002**, 54, 79-98.

[31] Revzin A, Russell RJ, Yadavalli VK, Koh W, Deister C, Hile DD, Mellott MB, Pishko MV, Fabrication of poly(ethylene glycol) hydrogel microstructrues using photolithography. *Langmuir* **2001**, 17, 5440-5447.

[32] Ward JH, Bashir R, Peppas NA. Micropatterning of Biomedical Polymer Surfaces by Novel UV Polymerization Techniques, *J. Biomed. Mater. Res.* **2001**, 56, 351-360.

[33] Bashir R, Hilt JZ, Elibol O, Gupta AK, Peppas NA. Micromechanical cantilever as an ultrasensitive pH microsensor. *App. Phys. Lett.* **2002,** 81, 3091-3093.

[34] Whitesides GM. The right size in nanobiotechnology. *Nat. Biotechnol.* **2003**, 21, 1161-1165.

[35] Truskett VN, Watts MPC. Trends in imprint lithography for biological applications, *Trends Biotech.* **2006**, 24, 312-317.

[36] Willner I, Baron R, Willner B. Integrated nanoparticle–biomolecules systems for biosensing and bioelectronics, *Biosens. Bioelectronics*. **2006**, Paper presented as a plenary lecture at Biosensors 2006, Toronto, Canada.

[37] Xia Y, Whitesides GM. Soft Lithography. *Annu. Rev. Mater. Sci.* **1998,** 28, 153-184.

[38] Xia Y, Whitesides GM. Extending Microcontact Printing as a Microlithographic Technique, *Langmuir* **1997**, 13, 2059-2067.

[39] Whitesides GM, Labinis PE. Wet chemical approaches to the characterization of organic surfaces: self-assembled monolayers, wetting, and the physical-organic chemistry of the solid-liquid interface, *Langmuir* **1990,** 6, 87-96.

[40] Kumar A, Whitesides GM. Features of gold having micrometer to centimeter dimensions can be formed through a combination of stamping with an elastomeric stamp and an alkanethiol "ink" followed by chemical etching, *Appl. Phys. Lett.* **1993,** 63, 2002-2004.

[41] Tan J, Tien J, Chen C. Microcontact printing of proteins on mixed self-assembled monolayers. *Langmuir* **2002,** 18, 519-523.

[42] Bos GW, Scharenborg NM, Engbers GHM. Proliferation of endothelial cells on surface-immobilized albumin-heparin conjugate loaded with basic fibroblast growth factor. *J. Biomed. Mater. Res*. **1999**, 44, 330-340.

[43] Yamato M, Konno C, Utsumi M, Kikichi A. Thermally responsive polymer-grafted surfaces facilitate patterned cell seeding and co-culture. *Biomaterials* **2003,** 23, 561-567.

[44] Blawas AS, Reichert WM. Protein patterning. *Biomaterials* **1998,** 19, 595-609.

[45] Whitesides GM, Ostuni E, Takayama S, Jiang X, Ingber DE. Soft Lithography in Biology and Biochemistry. *Annu. Rev. Biomed. Eng.* **2001,** 3, 335-373.

[46] Weibel DB, Garstecki P, Whitesides GM. Combining microscience and neurobiology, *Current Opinions in Neurobiology* **2005,** 15, 560-567.

[47] Biebuyck HA, Whitesides GM**.** Autophobic Pinning of Drops of Alkanethiols on Gold. *Langmuir* **1994,** 10, 4581-4587.

[48] Hammond P, Whitesides GM. Formation of Polymer Microstructures by selective deposition of Polyion Multilayers Using self-assembled monolayers as a Template, *Macromolecules* **1995**, 28, 7569-7571.

[49] Advincula RC. Surface initiated polymerization from nanoparticle surfaces. *J. Dispersion Sci. Technol.* **2003,** 24, 343-361.

[50] Edmondson S, Osborne VL, Huck WTS. Polymer brushes via surface initiated polymerizations. *Chem. Soc. Rev.* **2004,** 33, 14-22.

[51] Tu H, Heitzman CE, Braun PV. Patterned poly(N-isopropylacrylamide) brushes on silica surfaces by microcontact printing followed by surface-initiated polymerization *Langmuir* **2004,** 20, 8313-8320.

[52] Shah RR, Merreceyes DM, Hedrick JL. Using Atom Transfer Radical Polymerization to Amplify Patterned Monolayers of Initiator into Polymeric Barriers for Wet Chemical Etchants. *Macromolecules* **2000,** 33, 597-605.

[53] Satarkar NS, Hilt JZ. Hydrogel nanocomposites as remote controlled biomaterials. *Acta Biomater.* **2008,** 4, 11-16.

[54] Schmaljohann D, Oswald J, Jorgensen B, Nitschke M, Beyerlein D, Werner C. Thermo responsive PINPAAm-g-PEG films for controlled cell detachment. *Biomacromolecules* **2003,** 4, 1733-1739.

[55] Schneider GB, English A, Abraham M, Zaharias R, Stanford C, Keller J. The effect of charge density on cellular detachment. *Biomaterials* **2004,** 25, 3023-3028.

[56] Cushing MC, Anseth KS. Hydrogel cell cultures. *Science* **2007,** 316, 1133-1134.

[57] Ali M, Horikawa S, Venkatesh S, Saha J, Hong JW, Byrne ME. Zero order therapeutic release from imprinted hydrogel contact lenses within an in vitro physiological ocular tear flow. *J. Controlled Release* **2007,** 124, 154-162.

[58] Yildiz Y, Uyanik N, Erbil C. Compressive elastic moduli of PNIPAAm hydrogels crosslinked with PDMS. *J. Macromolecular Sci. A* **2006,** 43, 1091-1106.

[59] Ritger PL, Peppas NA. A simple equation for description of solute release II. Fickian and anomalous release from swellable devices. *J. Controlled Release* **1987,** 5, 37-42.

[60] Chiellini F, Bizzazrri R, Ober CK, Yu T, Schmaljohann D, Chiellini E. Patterning of polymeric hydrogels for biomedical applications. *Macromol. Rapid Commun.* **2001,** 22, 1284-1287.

[61] Papavasiliou G, Songprawat P, Perez-Luna V, Hammes E, Morris M, Chiu YC, Brey E. Three Dimensional Patterning in Poly(ethylene glycol) Hydrogels Through Surface Initiated Photopolymerization. *Tissue Eng. C* 2008, 14, 129-140.

[62] Zourob M, Gough JE, Ulijn RV. A Micropatterned Hydrogel Platform for Chemical Synthesis and Biological Analysis. *Adv. Mater.* **2006**, 18, 655-659.

CHAPTER 4

Controlled synthesis of responsive hydrogel nanostructures via microcontact printing and ATRP

This chapter is modified from the article published as

Chirra HD, Biswal D, Hilt JZ. *Polym. Adv. Tech.* **2009,** DOI. 10.1002/pat.1576

4.1. Summary

Surfaces that are spatially functionalized with intelligent hydrogels, especially at the micro- and nanoscale, are of high interest in the diagnostic and therapeutic fields. Conventional methods of the semiconductor industry have been successfully employed for the patterning of hydrogels for various applications, but methods for fabricating precise 3-D patterns of hydrogels at the micro- and nanoscale over material surfaces remain limited. Herein, microcontact printing (μCP) followed by atom transfer radical polymerization (ATRP) was applied as a platform to synthesize temperature responsive poly(N-isopropylacrylamide) hydrogels with varied network structure (e.g., different molecular weight crosslinkers) over gold surfaces. The XY control of the hydrogels was achieved using μCP, and the Z (thickness) control was achieved using ATRP. The controlled growth and the responsive behavior of hydrogels to temperature stimuli were characterized using Fourier transform infrared (FTIR) spectroscopy and atomic force microscopy (AFM). The results demonstrate that this platform allows for the controlled growth of hydrogel nanostructures using the controlled ATRP mechanism. It is also shown that the molecular weight of the crosslinker affects the rate of hydrogel growth.

These PNIPAAm based crosslinked hydrogel patterns were also demonstrated to have a temperature dependent swelling response. Using this technique, it is possible to synthesize responsive hydrogel patterns over various surfaces for potential applications in the biomedical field.

4.2. Introduction

Surfaces that are spatially functionalized with hydrogels, especially at the micro- and nanoscale, are increasingly gaining attention in the field of biology and medicine. Over the last several years hydrogels have gained increasing applications as functional components in biomedical micro- and nanodevices. For example, pH responsive hydrogels were applied for autonomous flow control in microfluidic channels by Beebe and coworkers [1]. Additionally, hydrogels have been used as microactuators for controlled drug delivery, on microcantilevers as bioMEMS sensor platforms, and in micropumps and microvalves [2-4]. For these and other similar devices to be fabricated, the ability to integrate hydrogels at the micro- and nanoscale is critical. Here, a simple approach for the controlled synthesis of thin responsive hydrogels on surfaces at the micro- and nanoscale using microcontact printing and atom transfer radical polymerization is introduced.

Hydrogels are a class of crosslinked, hydrophilic polymer systems which possess a high affinity towards water or other physiological fluids and therefore swell to resemble natural living tissue [5]. They find applications as biomaterials in contact lenses, sutures, dental materials, linings for artificial hearts, materials for artificial skin, and tissue

engineering [6, 7]. By tailoring the various functional groups along the hydrophilic polymer backbone, intelligent environmentally responsive hydrogels have been synthesized. They sense and exhibit responsive behavior, when triggered by changes in the surrounding environmental conditions, such as pH, temperature and ionic strength [8]. This unique ability of hydrogels to reversibly swell and shrink to external stimuli makes them attractive for use as a key component of novel biomedical micro- and nanodevices. Though conventional methods of the semiconductor industry, especially UV photolithography, have been employed for the patterning of such networks in devices, methods for fabricating precise 3-D patterns of hydrogels (at the micro- and nanoscale) over material surfaces and devices remain limited. In the last few years, various novel lithography techniques such as electron-beam and ion-beam lithography, nanoimprint lithography, dip pen nanolithography, and a wide variety of soft lithography techniques have been developed to achieve a fine level of control for patterning on surfaces of biomaterials [9]. The introduction of microcontact printing (μCP), a flexible soft lithography technique, has revolutionized the way patterned surfaces can be generated with ease [10]. The rapid preparation of the various self assembled monolayers (SAMs) introduced by μCP on the surface of interest and the functionality of the resulting SAMs make μCP an efficient method for developing micropatterned surfaces and to study biological processes [11, 12].

'Grafting from' or surface initiated polymerization (SIP) reactions are commonly used to modify surfaces with thin polymer films or polymer brushes [13-16]. Among the various controlled radical polymerization methods, atom transfer radical polymerization

(ATRP) gains special interest, because of its versatility in producing controlled polymers with low polydispersity and its compatibility with a variety of monomers [17, 18]. ATRP accepts water as the solvent in many formulations, and with the correct choice of catalyst, ATRP can be performed at relatively low temperatures [19]. ATRP has been successfully employed on various surfaces and to amplify patterned monolayers of SAM formed using various lithography techniques into robust polymeric brushes, temperature sensitive poly(N-isopropyl acrylamide) PNIPAAm brushes, and pH responsive brushes [20-28]. In contrast to the above examples where either a fully coated initiator surface or initiator patterns introduced via expensive lithography techniques were used, easy patterning of responsive brushes from initiator SAMs was obtained via simple μCP and ATRP by Braun et al, and Huck et al [29-31].

Environmentally responsive hydrogel patterns have several advantages that make them attractive over polymeric brushes. Hydrogel coated surfaces are widely used in micro- and nanodevices for microfluidic, sensing, and therapeutic applications [32, 33]. Unlike polymeric brushes that have an open polymeric structure for free molecular diffusion, the mesh size of a hydrogel matrix, which can be tailored by crosslinker constraints such as type and amount, governs the transport of molecular species into and out of the hydrogel [34]. This control over the hydrogel mesh can be harnessed for cellular entrapment and manipulations and controlled drug delivery applications [35-38]. Further, the network structure increases the mechanical integrity and stability of the hydrogel, making them more robust than brushes made up of the same polymer backbone [39]. These properties of hydrogels along make them attractive alternatives to polymer

brushes for certain applications. Further, for diffusion limited processes, the characteristic transport time is directly proportional to the square of the length scale [40]. Therefore, a reduction of thickness from macro- to micro- to nanoscale makes responsive hydrogels respond 'instantaneously' to external stimuli. Although, a wide variety of hydrogel pattern fabrication methods for surface based applications are already available, the methods to prepare hydrogel thin films at the nanoscale for 'instantaneous' stimuli recognition is still at its infancy [41-43]. ATRP, which has been successfully employed for the synthesis of polymeric brushes over surfaces, can be potentially employed to obtain nanoscale thin hydrogel films for 'instantaneous' biosensing and drug delivery applications.

In this chapter, the viability of achieving precise spatial XY control of patterns on gold using μCP and tunable thickness (Z control) of hydrogel structures using ATRP is demonstrated. PNIPAAm has been used as the functional monomer with ethylene glycol dimethacrylate (EGDMA), and poly(ethylene glycol) n dimethacrylate (PEGnDMA; n = 200/400), as the different crosslinkers for preparing hydrogels over gold surfaces. Specifically, PNIPAAm is interesting as a model responsive hydrogel system because it is thermoresponsive exhibiting reversible swelling behavior across its lower critical solution temperature (LCST) near 32 ^{o}C [44-46]. This unique property of being temperature sensitive has enabled PNIPAAm to be used widely for controlled drug delivery applications. EGDMA, PEG200DMA and PEG400DMA, which possesses many unique physical and biochemical properties, such as biocompatibility and miscibility with many solvents were applied as crosslinkers with different molecular weights for the

model hydrogel systems [42]. Characterization of the hydrogel structures was carried out using optical microscopy, AFM, and FTIR spectroscopy. With various temperature, pH, and biomolecule sensitive hydrogels finding an ever-expanding range of biomedical and industrial applications, this modified patterning and controlled growth technique provides a model platform for the incorporation of hydrogel systems into various point of care diagnostic and therapeutic devices.

4.3. Experimental Section

4.3.1. Materials

All chemicals were purchased from Sigma Aldrich and used as received, unless noted otherwise. The thiol used for patterning and initiator for ATRP were 1-octadecanethiol (ODT) and bromoisobutyrate-terminated undecyl disulfide (Br-Ini, Asemblon Inc), respectively. The temperature sensitive monomer was N-isopropylacrylamide (NIPAAm), and the different crosslinkers used to form the various hydrogels were ethylene glycol dimethacrylate (EGDMA), poly(ethylene glycol) 200 dimethacrylate (PEG200DMA), and poly(ethylene glycol) 400 dimethacrylate (PEG400DMA), (Polyscience Inc.). Fluorescein dimethacrylate (Fluor 511) was used for fluorescent tagging of the hydrogel (Polyscience Inc.). Copper (I) bromide (CuBr) was used as the catalyst and 2,2’-dipyridyl was used as the ligand during the ATRP reaction. Dimethyl formamide (DMF) and methanol were used as solvents. Copper powder of size less than 425 microns was also used in the reaction. The gold wafers used in this process were purchased from Platypus Technologies.

4.3.2. Instrumentation

Chemical characterization of the various steps involved in the synthesis of hydrogels over gold surface was performed using a Varian 7000e Fourier transform infrared (FTIR) spectrophotometer. The attenuated total reflectance, ATR-FTIR spectra were collected between 800 and 4000 cm^{-1} for 32 scans at a resolution of 8 cm^{-1}. The hydrophobic effect of the patterned SAMs and the XY control achieved via μCP was analyzed using a Nikon Eclipse ME600 optical microscope. The surface morphology of the patterned thiols, thickness of the hydrogel patterns, and temperature sensitive responsive behavior of the hydrogel patterns were observed using an atomic force microscope (AFM, Agilent Technologies Inc.). The temperature sensitive analysis was performed in liquid cell set up of the AFM using an autotunable temperature controller (Lake Shore).

4.3.3. Microcontact printing (μCP) and assembly of initiator for spatial XY control

The details of the procedure involved in the fabrication of the master chips using UV photolithography and polydimethylsiloxane PDMS by replica molding is given in appendix A [47]. For microscale spatial XY control of the hydrogel patterns over gold surface, μCP was employed. The PDMS stamp with square microstructures (as pits) was initially inked with 1 mM solution ODT in ethanol, air dried for 10 seconds, and then, the stamp was brought in contact with the cleaned gold substrate for 45 seconds (μCP step of schematic in figure 4.1). The gold surface modified with ODT patterns (outside square regions), was subsequently washed with ethanol and finally dried. After the patterning of hydrophobic ODT SAMs on the gold substrate, the hydrophilic bromo disulfide initiator

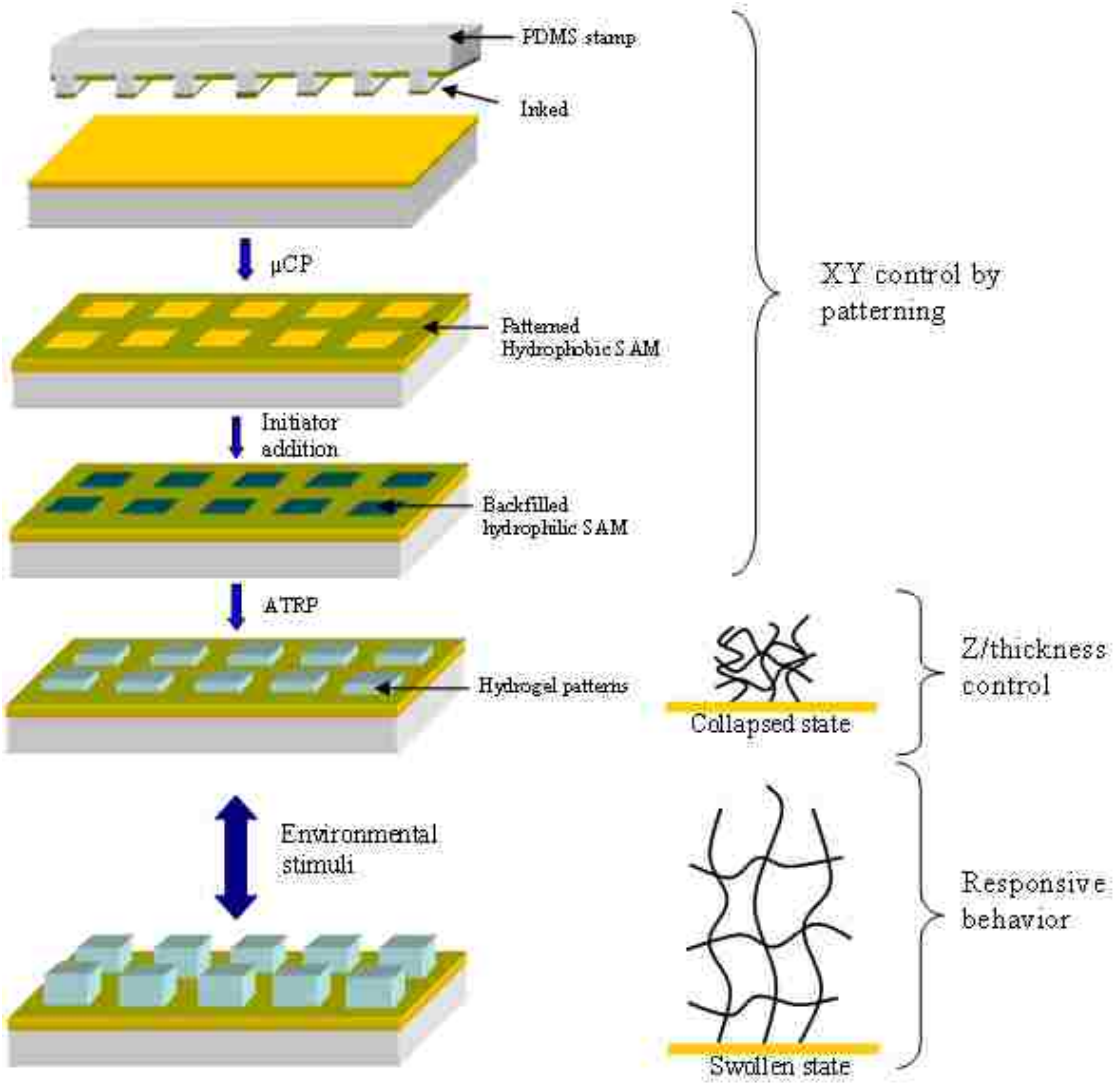

Figure 4.1. Schematic diagram showing the various steps involved in the synthesis of thin hydrogel micropatterns by microcontact printing (μCP) followed by atom transfer radical polymerization (ATRP), and the stimuli sensitive behavior of the patterned hydrogel.

(Br-Ini) SAM was assembled inside the square regions by immersing the substrate in a 2 mM solution of initiator in ethanol for 24 hours (initiator backfill step of schematic in figure 4.1). After 24 hours, the substrates containing precise square patterns of initiator and ODT were washed with ethanol, and were subsequently used for hydrogel pattern formation. In addition to these substrates, half coated and non-patterned fully coated initiator substrates were also prepared for ATR-FTIR characterization needs.

4.3.4. Preparation of temperature sensitive hydrogel patterns using ATRP

Surface-initiated atom transfer radical polymerization (ATRP) was used for the preparation of temperature sensitive hydrogel patterns over the gold substrate (ATRP step of schematic in figure 4.1). First, a solution made up of 0.2 mM CuBr catalyst, and 0.6 mM of the ligand dipyridyl were prepared in solvent DMF. The catalytic cycle involves a reversible switching of the halogen atom between the two oxidation states of the transition metal complex thereby controlling the amount of free radicals available for hydrogel growth. A 90:10 molar ratio of hydrogel ingredients made up of 22.50 mM of the monomer NIPAAm and 2.50 mM of crosslinker EGDMA was added to the above solution. Water (1:10 volume% w.r.t solvent) was also added to the solution. The presence of water is important for rapid ATRP at room temperature [48]. Pure copper powder was also added to the ATRP solution (0.1 wt% with respect to NIPAAm) in order to generate the Cu(I) species, by reducing the deactivator Cu(II) species obtained during the initiation step of the ATRP reaction [49]. For the EGDMA system, 0.01 wt% of Fluor 511 was also added to the system for fluorescent tagging and qualitative observation of the growth. The substrate containing the thiols was immersed in the ATRP solution,

purged with nitrogen, and allowed to react at room temperature for 24 hours. The resultant hydrogel patterned substrate was washed with methanol and dried. The hydrogel patterned substrates were stored in a desiccator until used for the various analyses. In the case of the higher molecular weight PEG200DMA and PEG400DMA crosslinked hydrogel patterns, methanol was used as the solvent. 52.5 mmol of NIPAAm and 22.5 mmol of PEG200DMA or PEG400DMA were used to prepare the 70:30 hydrogel patterns.

Stamped gold substrates with 500, 250, 50, 25, and 10 μm squares were created using μCP. The samples were verified using the optical microscope and AFM imaging. A half patterned gold substrate with ODT and the other half assembled with the Br-Ini thiol was also prepared for stepwise attenuated total reflectance (ATR) FTIR analysis. The ATRP reaction was then carried out on the patterned sample, and it was used as such for characterizing the hydrogel grown over the gold substrate. The presence of monomer NIPAAm and crosslinkers in the hydrogel pattern was analyzed using the ATR-FTIR spectroscopy. In order to compare the hydrogel grown via ATRP, pure NIPAAm brush patterns and pure EGDMA patterned substrates were synthesized using previously published procedures [50, 51]. The controlled growth of the hydrogel via ATRP was identified using non contact AFM analysis in dry state. The swollen state analysis and subsequent temperature sensitive behavior of the hydrogel network was analyzed using the liquid cell setup of AFM with a temperature controller.

4.4. Results and Discussion

4.4.1. Characterization of SAMs for XY control by μCP

Silicon master chips with 500-250 μm and 50-25-10 μm square features were fabricated using UV photolithography and were subsequently used for the synthesis of PDMS stamps with reverse features via replica molding. The detailed results and discussion of the features obtained in the master chips and PDMS stamp were described in our previous publication [52]. Briefly, by using atomic force microscopy (AFM), the thickness of both the master chips and PDMS stamp was found out to be 1.9 μm. Using this PDMS stamp, self assembled monolayers of ODT with square features were successfully patterned over gold surface via μCP. The patterned ODT monolayer was characterized using AFM and the thickness of the thiol was determined to be 2.2 nm.

The patterned gold substrate with hydrophobic ODT was then treated with the initiator, Br-Ini. Since the head moiety of the initiator is comparatively hydrophilic than the linear alkyl hydrophobic chain of ODT, it occupied only the square regions not patterned with hydrophobic thiol. Since ATRP initiates from those sites assembled with bromine initiator, the growth of the hydrogel occurs only in the hydrophilic initiator assembled square regions, which are surrounded by the hydrophobic ODT.

4.4.2. Characterization of hydrogel patterns

ATR-FTIR was used to verify every step of the hydrogel synthesis process via μCP followed by ATRP. Specific characteristic functional groups involved in each layer were identified to confirm the growth of the hydrogel. A half coated ODT sample was

analyzed first. Then it was immersed in Br-Ini to assemble the initiator thiol, and the FTIR spectrum of the initiator attached to the other half of the sample was obtained. The samples were then polymerized via ATRP for 24 hours to produce the various hydrogels, and the characteristic FTIR spectrums of the hydrogels were obtained. Figure 4.2 shows the ATR-FTIR spectra of the thiols, hydrogels, and the pure brushes in the range of 1000-1800 cm^{-1}.

From figure 4.2, it is observed that the characteristic peaks of monomer NIPAAm (brown dashed lines) at 1653 cm^{-1} and 1540 cm^{-1} which corresponds to the –C=O stretching and the –N–H bending, respectively, are observed in the hydrogels. These peaks are characteristic of the amide I and amide II groups, respectively, of PNIPAAm. The characteristic peaks of EGDMA (blue solid lines) at 1733 cm^{-1} (– C=O) and 1144 cm^{-1} (–C–O–C–) are also observed in the hydrogel case. A slight shift in the –C–O–C– peak is noticed in the case of the PEG400DMA crosslinked hydrogel. This shift may be attributed to the increase in the number of ethylene glycol units to nine in comparison to just one for the EGDMA crosslinker, which produced more inter- and intramolecular hydrogen bonding. From the FTIR analysis, it is clear that the hydrogel structures are made up of a network comprising of both NIPAAm and EGDMA or PEG400DMA. Also observed from figure 4.2 are the characteristic –C–H peak of ODT in the finger print region at 1103 cm^{-1} and the characteristic bromine peak of the initiator at 1053 cm^{-1} confirming the monolayer formation of both the thiols over the gold surface. The presence of the residual bromine peak (1053 cm^{-1}) in both the hydrogels is due to the non bimolecular termination of a few chains during ATRP.

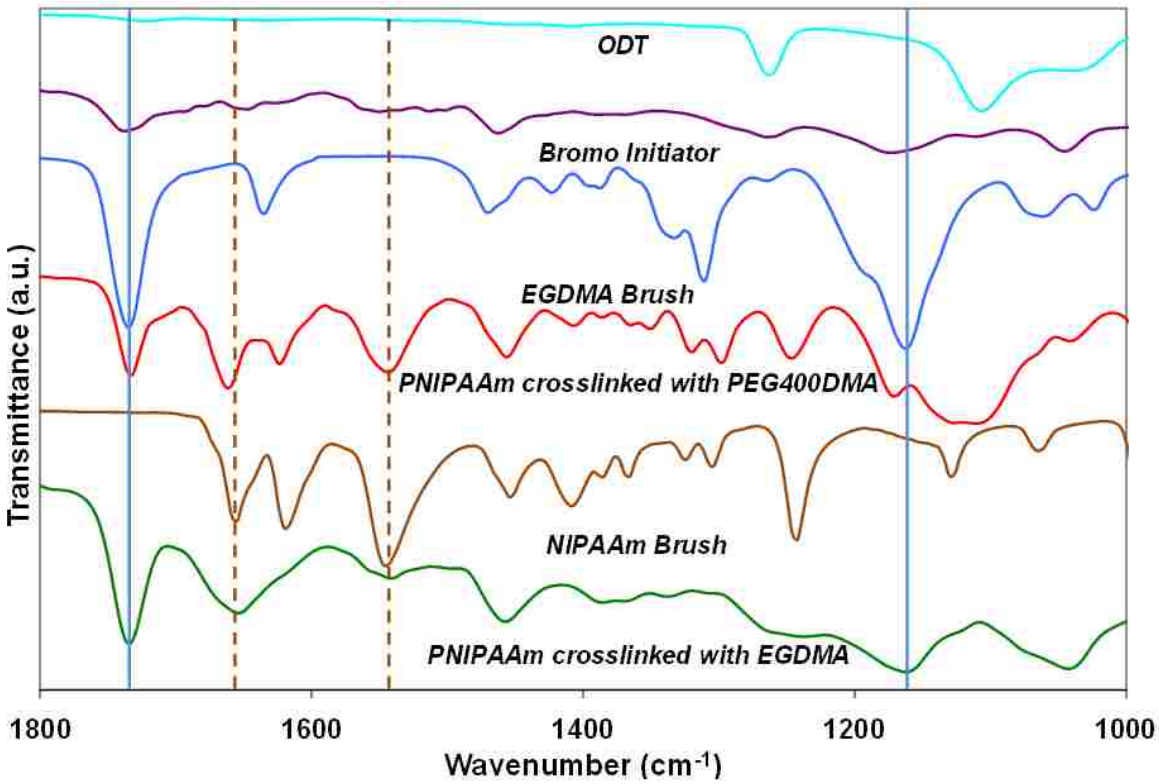

Figure 4.2. An expanded ATR-FTIR profile in the 1800-1000 cm^{-1} range showing the characteristic peaks of NIPAAm (brown dashed lines at 1540 and 1653cm^{-1}) and EGDMA (blue solid lines at 1144 and 1733 cm^{-1}) respectively occurring in the EGDMA and PEG400DMA crosslinked hydrogel profiles.

4.4.3. Controlled Z/thickness growth of the hydrogel via ATRP

The effectiveness of surface initiated ATRP in producing patterned hydrogels over material surfaces was verified by measuring the height of the hydrogel networks grown over the Br-Ini assembled squares using non contact mode AFM imaging. The various heights of the hydrogel samples were measured in dry condition. The drying of the μCP patterned hydrogels was done overnight in a desiccator. Figure 4.3 shows the normalized 3-dimensional images of some of these patterns in dry state. We observed XY control in the hydrogel patterns that were tagged with fluorophore before AFM analysis using optical microscopy and scanning electron microscopy (results not shown). From figure 4.3, we observed that the hydrogels grew only in those regions where the initiator Br-Ini was present confirming the control on the XY plane achieved using μCP. We also observe that the patterned hydrogels grew only in the Z direction as the XY plane was localized by the presence of hydrophobic ODT. To confirm the effectiveness of controlled growth at the nanoscale by using ATRP, different gold patterns were immersed in the same ATRP solution over varying periods of reaction time for the various systems under study. The respective heights measured in dry state using AFM were then plotted as a function of the type of crosslinker used (EGDMA, PEG200DMA, and PEG400DMA) and the crosslinking density employed (10 mol% or 30 mol%) versus reaction time (figures 4.4 and 4.5).

Both figures 4.4 and 4.5 illustrate a well defined and controlled Z/thickness growth of the hydrogel patterns using ATRP in the various systems. The concentrations of the monomer NIPAAm and crosslinkers were kept in excess, so that the growth of the

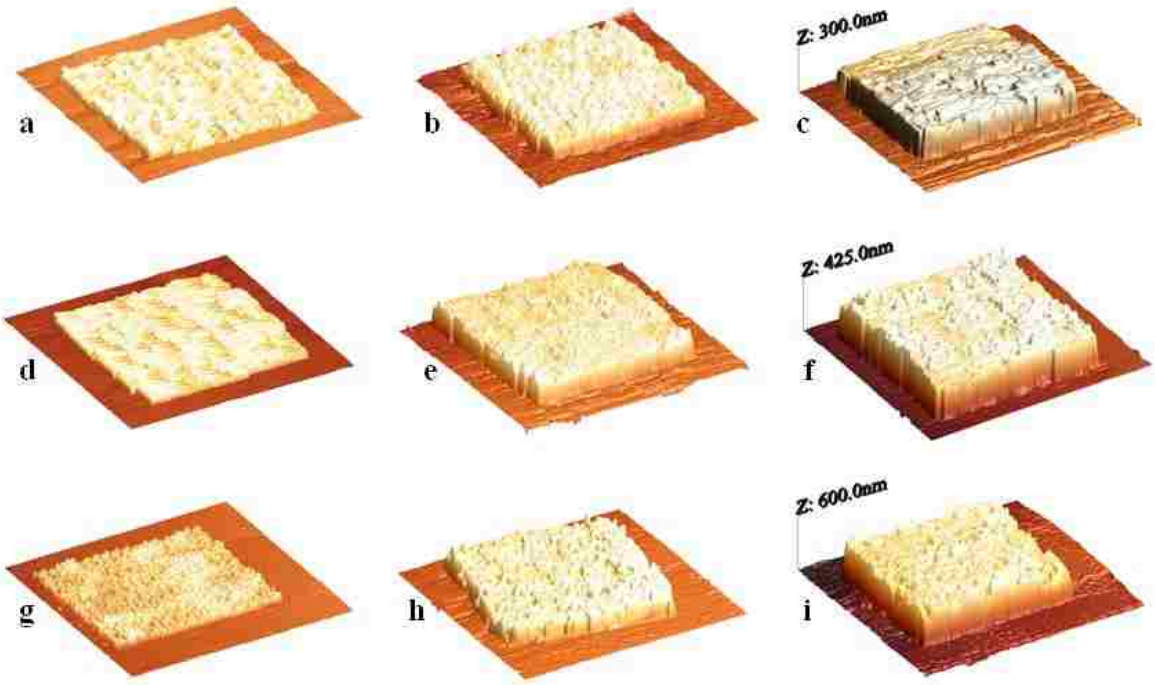

Figure 4.3. Normalized AFM images of patterned 25 µm PNIPAAm crosslinked with EGDMA (90:10 mol%) hydrogels grown for (a) 25, (b) 36, and (c) 48 hours respectively; 50 µm PNIPAAm crosslinked with PEG400DMA (70:30 mol%) hydrogels grown for (d) 5, (e) 16, (f) 20 hours respectively; and 50 µm PNIPAAm crosslinked with PEG400DMA (90:10 mol%) hydrogels for (g) 4.5, (h) 16, and (i) 36 hours respectively.

hydrogel continued over longer reaction periods. The effect of the crosslinker used (constant crosslinking amount at 10 mol%) on the rate of controlled growth can be deduced from figure 4.4. It is observed that the reaction rate or hydrogel growth increased from EGDMA to PEG200DMA and subsequently to PEG400DMA. The crosslinkers PEG400DMA and PEG200DMA is composed of approximately 9 units and 4.5 EG units, respectively, of ethylene glycol (EG), while EGDMA has a single EG unit. This increase in crosslinker molecular weight with EG units resulted in the increased growth rate from EGDMA to PEG400DMA. This increasing reaction rate with increasing EG units in the crosslinking system has been observed in previous studies [53].

The application of ATRP to produce PNIPAAm brushes of high thickness in short reaction periods is well known. Wang et al. produced PNIPAAm brushes of thickness 100 nm in 3 hrs [54], while Kaholek et al. produced PNIPAAm brushes of thickness 250 nm in 1 hr [24]. In the case of EGDMA thin film formation via ATRP, Huang et al showed that it took 37 hrs of ATRP to obtain a 100 nm EGDMA film [48]. Further, a combined ATRP approach to prepare PNIPAAm-co-PEGMA copolymer (1% PEGMA used) gave a thickness of 33 nm in 10 hrs of ATRP reaction [45]. From figure 4.4 we noticed that our EGDMA crosslinked PNIPAAm hydrogel achieved a thickness of 100 nm over a period of 12 hrs, while PNIPAAm crosslinked with PEGxDMA (where, x = 200 or 400) hydrogels required about 5 hrs of reaction time. Considering the results as reported from other ATRP work, it appears that the addition of EGDMA crosslinker decreases the thickness of the hydrogel grown when compared to that of pure linear PNIPAAm brushes. This is because of the formation of the crosslinked mesh network,

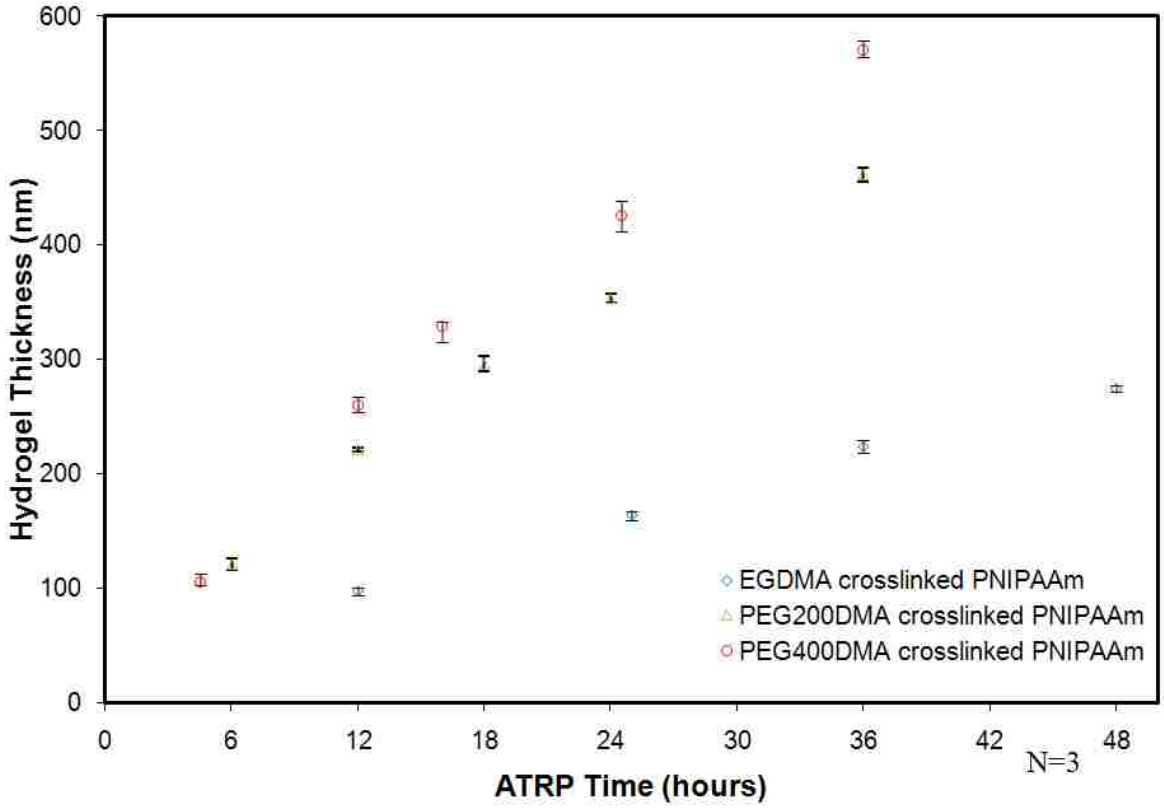

Figure 4.4. Controlled growth of 90:10 mol% crosslinked PNIPAAm hydrogel patterns in nanometer scale with increasing polymerization time, showing the dependence on the type of crosslinker used (dry state).

which is absent in the case of linear grafted PNIPAAm brushes. While pure PNIPAAm brushes grow linearly perpendicular to the surface, crosslinked hydrogels grow in all directions forming links between adjacent growing chains. This compact mesh formation decreases the apparent mobility of growing radical chains and also decreases the availability of free monomer in solution for further thickness growth. As the crosslinker molecular weight/length increases, the mesh size increases providing an improved mobility of the growing radical chains, thereby increasing the thickness of the hydrogel (as observed in figures 4.4 and figure 4.5). Although, the average rate of thickness growth for EGDMA, PEG200DMA and PEG400DMA is in the order of 6.2, 14.1, 17.5 nm/hr, this nanometer level controlled growth achieved using ATRP is critical in fabricating biomedical devices with thin film responsive hydrogels for point of care 'instantaneous' applications.

The effect of the amount of crosslinker on hydrogel growth was studied by using PEG200DMA and PEG400DMA crosslinkers at 10 mol% and 30 mol% crosslinking densities. From figure 4.5 (a), we noticed that only a slight increase in thickness is obtained from the 90:10 crosslinked PEG400DMA hydrogel pattern than the 70:30 crosslinked PEG400DMA system. No significant change in thickness with respect to crosslinking density is noticed in the case of PEG200DMA systems (figure 4.5 (b)). It is to be noted that these thicknesses were measured in dry state. Crosslinking density of a hydrogel plays a significant role in the swelling behavior of a hydrogel [55]. As the crosslinking density of the hydrogel increases, the mesh size of the hydrogel matrix decreases, thereby decreasing the volume swelling ratio of the hydrogel. While our

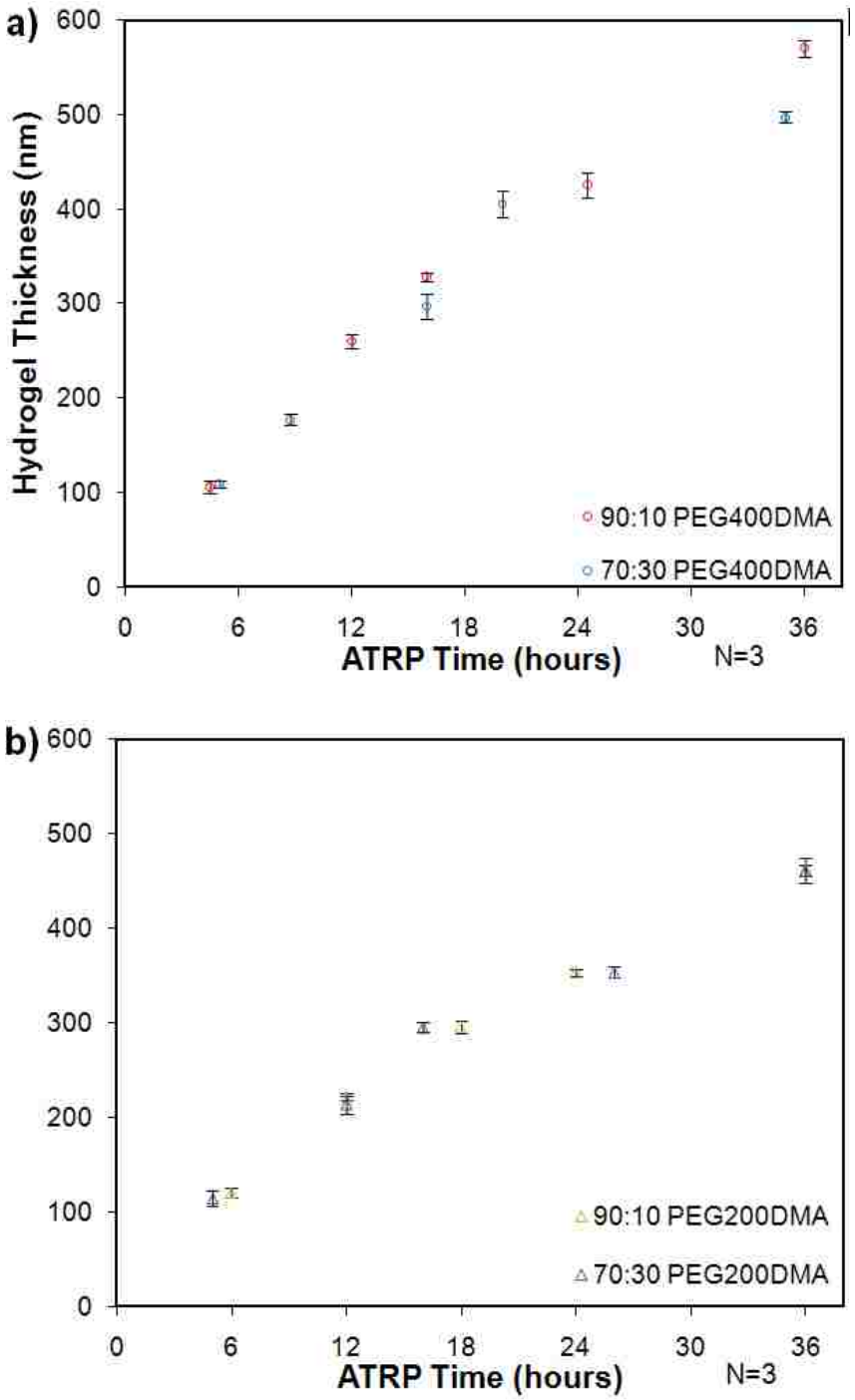

Figure 4.5. Dry state thickness growth of the hydrogels of (a) PNIPAAm crosslinked with PEG400DMA and, (b) PNIPAAm crosslinked with PEG200DMA with polymerization time, showing the effect of crosslinking density (90:10 mol% and 70:30 mol%) used.

current observation on the effect of crosslinking density on controlled growth via ATRP (dry thickness) does not indicate an effect, it is expected that the crosslinking density (e.g., amount of crosslinker used) plays a significant role in the swelling behavior of the hydrogel structure. A detailed study on the effects of crosslinking density on reaction rate and responsive behavior are reported in chapter 5.

4.4.4. Temperature sensitive hydrogel surfaces

The responsive behavior of the temperature sensitive PNIPAAm based hydrogel network was studied using the liquid cell set up mode of the AFM with an autotunable temperature controller. For this work, only the results obtained for the 90:10 mol% PNIPAAm crosslinked with PEG400DMA hydrogel system are highlighted. The temperature of water in the chamber was maintained with a measured deviation of $<\pm 0.05$ ^{o}C. For the temperatures chosen for imaging, the hydrogel pattern was allowed to equilibrate for at least 5 minutes with the water to ensure stability during imaging. Figure 4.6 (a) and (b) show the 3-dimentional topography images of a single 25x25 μm 12 hour ATRP reacted pattern at 25^{o}C (room temperature and below LCST of PNIPAAm brushes) and 40 ^{o}C respectively (above LCST of PNIPAAm brushes), while figure 4.6 (c) shows the thickness profile of the respective hydrogel states.

From figure 4.4, we observed that the average dry thickness of the 10 mol% PEG400DMA crosslinked hydrogel was around 260 nm at room temperature. This gel was then placed at room temperature in the liquid cell set up of the AFM. While the presence of water typically swells the hydrogel in all three dimensions simultaneously

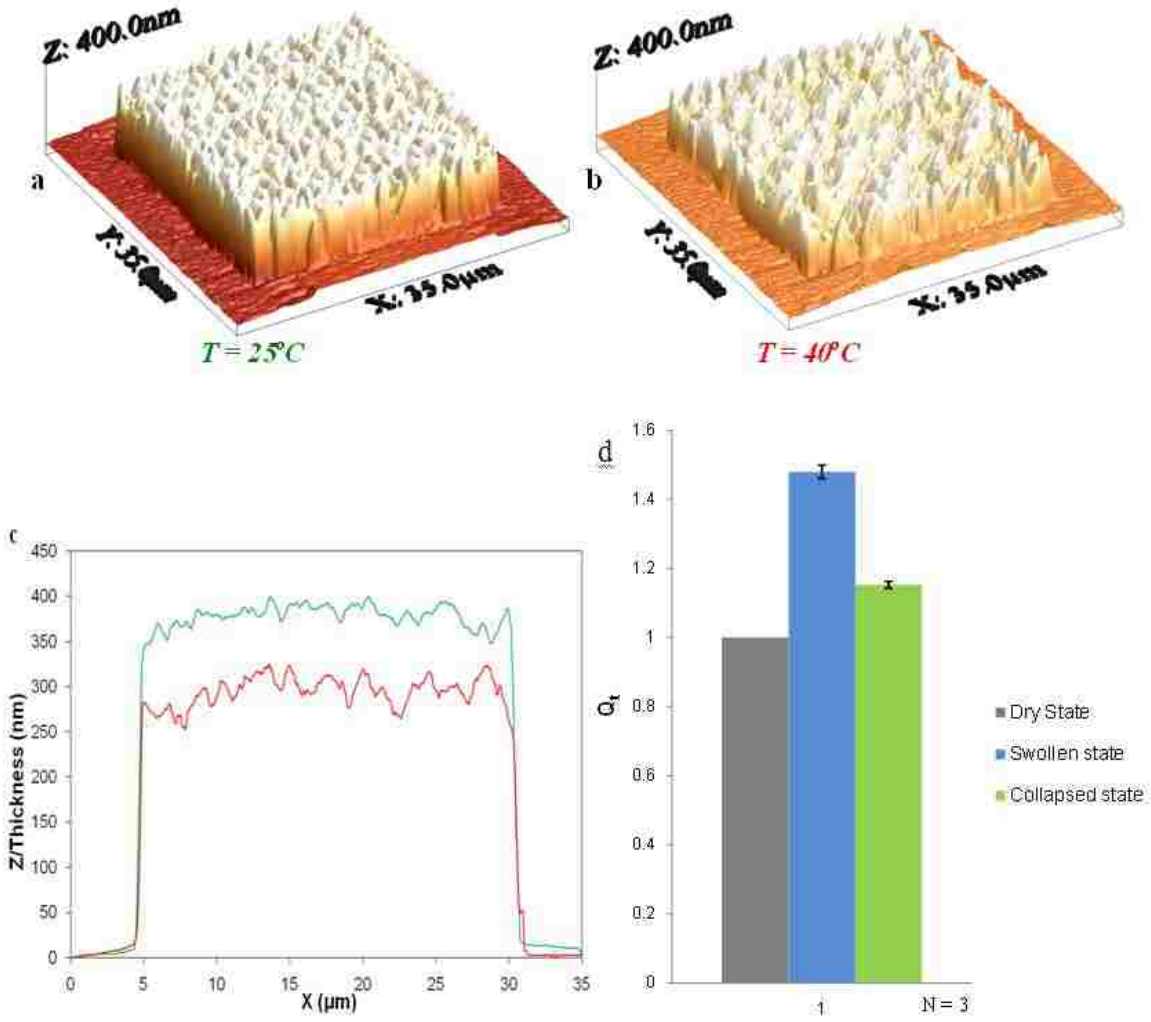

Figure 4.6. Normalized 3-D AFM images showing the temperature sensitive behavior of the 25 μm square made up of 90:10 mol% of NIPAAm crosslinked with PEG400DMA hydrogel at (a) T=25 ^{o}C, and (b) T=40 ^{o}C. The thickness profile depicting the responsive behavior, (c) where the red and green curve represents the thickness at 25 ^{o}C and 40 ^{o}C respectively. (d) Bar graph showing the volume swelling ratio (Q_t) calculated from change in thickness of the responsive hydrogel, at dry state, swollen state in water at 25 ^{o}C, and collapsed state in water at 40 ^{o}C.

[56], the swelling in these surface-tethered hydrogels is spatially confined, and the hydrogel swelling is restricted mainly to the direction perpendicular to the substrate [25, 57]. At equilibrium, the average thickness of the gel was determined to be 385 nm (figure 4.6 (c)). Assuming, hydrogel formation over the entire 25 x 25 μm2 area, the volume swelling ratio (Q_t) measured from the change in thickness with respect to dry state is around 1.48 (figure 4.6(d)). The water medium around the hydrogel pattern was then heated to 40 ^oC, and the thickness of the pattern was again determined after equilibrium. We observed that the hydrogel collapsed in thickness having an average thickness of 299 nm and a volume swelling ratio of 1.15. While PNIPAAm brushes swell with response to changes in temperature, limited control over the swelling behavior is possible. In the case of hydrogel systems, it is well-known that the crosslinking density determines the extent of swelling of the hydrogel [34]. Further, it is well known that the addition of hydrophobic or hydrophilic co-monomers/crosslinkers decreases or increases the transition temperature of PNIPAAm brushes [58]. Therefore by changing the type of crosslinker employed one can tune the transition temperature of PNIPAAm hydrogels for a variety of applications. This tunable responsive behavior along with the controlled growth of the hydrogel at the nanometer scale can be successfully utilized for biomedical diagnostic and therapeutic applications.

4.5. Conclusion

In the present study, the development of a flexible platform for the controlled growth of hydrogel nanostructures on gold surfaces has been presented. Temperature responsive hydrogel systems were synthesized using ethylene glycol based crosslinkers

of various molecular weight. Microcontact printing proved to be a useful soft lithographic tool to provide precise 2-dimensional XY planar control at the microscale. ATRP was used to successfully produce various hydrogel structures with controlled thickness at the nanoscale. A considerable difference in the controlled thickness was observed over the various hydrogels using AFM imaging for variations in the type of crosslinker employed. The addition of EGDMA decreased the thickness rate of the hydrogel achieved via ATRP as compared to pure PNIPAAm brushes. The PNIPAAm based hydrogels were also characterized for its responsive behavior using the liquid cell setup of AFM. The hydrogel was in a collapsed state at higher temperatures and in swollen state at lower temperatures. The synthesis of several tunable intelligent hydrogel platforms at the nanometer scale holds significant promise for sensing and actuation in diagnostic and therapeutic applications, where hydrogel thin film actuators may manipulate the transportation, diffusion, entrapment, reaction, and detection of a multitude of biomolecules.

4.6. References

[1] Beebe DJ, Moore JS, Bauer JM, Yu Q, Liu RH, Devadoss C, Jo B. Funtional hydrogel structures for autonomous flow control inside microfluidic channels. *Nature* **2000,** 404, 588-590.

[2] Low LM, Seetharaman S, Madou MJ. Microactuators toward microvalves for responsive controlled drug delivery. *Sens. Actuators. B* **2000,** 67, 149-160.

[3] Hilt JZ, Gupta AK, Bashir R, Peppas NA. Ultrasensitive biomems sensors based on microcantilevers patterned with environmentally responsive hydrogels. *Biomed. Microdevices* **2003,** 5, 177-184.

[4] Baldi A, Lei M, Gu Y, Siegel RA, Ziaie B, A microstructured silicon membrane with entrapped hydrogels for environmentally sensitive fluid gating, *Sens. Actuators B* **2006**, 114, 9-18.

[5] Peppas NA, Hilt JZ, Khademhosseini A, Langer R. Hydrogels in biology and medicine: from molecular principles to bionanotechnology. *Adv. Mater.* **2006**, 18, 1345-1360.

[6] Peppas NA, Bures P, Leobandung W, Ichikawa H. Hydrogels in pharmaceutical formulations. *European J. Pharm Biopharm* **2000**, 50, 27-46.

[7] Peppas NA, Huang Y, Torres-Lugo M, Ward JH, Zhang J. Physiochemical foundations and structural design of hydrogels in medicine and biology. *Ann. Revs. Biomed. Eng.* **2000,** 2, 9-29.

[8] Peppas NA, Khare AR. Preparation, structure and diffusional behavior of hydrogels in controlled release. *Adv. Drug Delivery Rev.* **1993,** 11, 1-35.

[9] J.Z. Hilt, M.E. Byrne, Tissue Engineering, Therapeutic Devices, and Diagnostic Systems. In *Dekker Encyclopedia of Nanoscience and Nanotechnology* Schwartz J A, Contescu C and Putyera K Eds. Marcel Dekker: New York NY **2004,** pp 247.

[10] Xia Y, Whitesides GM. **Extending Microcontact Printing as a Microlithographic Technique,** *Langmuir* **1997**, 13, 2059-2067.

[11] Biebuyck HA, Whitesides GM. **Autophobic Pinning of Drops of Alkanethiols on Gold.** *Langmuir* **1994,** 10, 4581-4587.

[12] Xia Y, Whitesides GM. Soft Lithography. *Annu. Rev. Mater. Sci.* **1998,** 28, 153-184.

[13] Edmondson S, Osborne VL, Huck WTS. Polymer brushes via surface initiated polymerizations. *Chem. Soc. Rev.* **2004,** 33, 14-22.

[14] Andruzzi L, Hexemer A, Li X, Ober CK, Kramer EJ, Galli G, Chiellini E, Fischer DA. Control of surface properties using fluorinated polymer brushes produced by surface initiated controlled radical polymerization. *Langmuir* **2004,** 20, 10498-10506.

[15] Husseman M, Malmstrom EE, McNamara M, Mate M, Mecerreyes D, Benoit DG, Hedrick JL, Mansky P, Huang E, Russell TP, Hawker CJ. Controlled Synthesis of Polymer Brushes by Living Free Radical Polymerization Techniques. *Macromolecules* **1999 ,** 32, 1424-1431.

[16] Braun M, Brittain WJ. Synthesis of Polymer Brushes on Silicate Substrates via Reversible Addition Fragmentation Chain Transfer Technique. *Macromolecules* **2002,** 35, 610-615.

[17] Prucker O, Ruhe J. Synthesis of Poly(styrene) Monolayers Attached to High Surface Area Silica Gels through Self-Assembled Monolayers of Azo Initiators. *Macromolecules* **1998,** 31, 592-601.

[18] Matyjaszewski K, Miller PJ, Shukla N, Immaraporn B, Gelman A, Luokala BB, Siclovan TM, Kickelbick G, Vallant T, Hoffmann H, Pakula T. Polymers at Interfaces: Using Atom Transfer Radical Polymerization in the Controlled Growth of Homopolymers and Block Copolymers from Silicon Surfaces in the Absence of Untethered Sacrificial Initiator. *Macromolecules* 1999, 32, 8716-8724.

[19] Advincula RC. Surface initiated polymerization from nanoparticle surfaces. *J. Dispersion Sci. Technol.* **2003,** 24, 343-361.

[20] Matyjaszewski K, Dong H, Jakubowski W, et al. Grafting from Surfaces for "Everyone": ARGET ATRP in the Presence of Air. *Langmuir* **2007**, 23, 4528-4531.

[21] Kim JB, M. Bruening M, Baker GL. Surface-Initiated Atom Transfer Radical Polymerization on Gold at Ambient Temperature. *J. Am. Chem. Soc.* **2000,** 122, 7616-7617.

[22] Takei YG, Aoki T, Sanui K, Ogata N, Sakurai Y, Okano T. Dynamic Contact Angle Measurement of Temperature-Responsive Surface Properties for Poly(N-isopropylacrylamide) Grafted Surfaces. *Macromolecules* **1994,** 27, 6163-6166.

[23] He Q, Kuller A, Grunze M, Li J. Fabrication of Thermosensitive Polymer Nanopatterns through Chemical Lithography and Atom Transfer Radical Polymerization. *Langmuir* **2007,** 23, 3981-3987.

[24] Kaholek M, Lee WK, Ahn SJ, Ma H, Caster KC, LaMattina B, Zauscher S. Stimulus-Responsive Poly(*N*-isopropylacrylamide) Brushes and Nanopatterns Prepared by Surface-Initiated Polymerization. *Chem. Mater.* **2004**, 16, 3688-3692.

[25] Kaholek M, Lee WK, LaMattina B, Caster KC, Zauscher S. Fabrication of Stimulus-Responsive Nanopatterned Polymer Brushes by Scanning-Probe Lithography. *Nano Lett.* **2004**, 4, 373-376.

[26] Ashford EJ, Naldi V, O'Dell R, Billingham NC, Armes SP. First example of the atom transfer radical polymerisation of an acidic monomer: direct synthesis of methacrylic acid copolymers in aqueous media. *Chem. Comm.* **1999,** 14, 1285-1286.

[27] Treat ND, Ayres N, Boyes SG, Brittain WJ. A Facile Route to Poly(acrylic acid) Brushes Using Atom Transfer Radical Polymerization. *Macromolecules* **2006,** 39, 26-29.

[28] Tugulu S, Barbey R, Harms M, Fricke M, Volkmer D, Rossi A, Klok H, Synthesis of Poly(methacrylic acid) Brushes via Surface-Initiated Atom Transfer Radical Polymerization of Sodium Methacrylate and Their Use as Substrates for the Mineralization of Calcium Carbonate. *Macromolecules* **2007,** 40, 168-177.

[29] Tu H, Heitzman CE, Braun PV, Patterned Poly(N-isopropylacrylamide) Brushes on Silica Surfaces by Microcontact Printing Followed by Surface-Initiated Polymerization.*Langmuir* **2004,** 20, 83138320.

[30] Jones DM, Huck WTS, Controlled Surface-Initiated Polymerizations in Aqueous Media. *Adv. Mater.* **2001,** 13, 1256-1259.

[31] Zhou F, Zheng Z, Yu B, Liu W, Huck WTS, Multicomponent Polymer Brushes.*J. Am. Chem. Soc.* **2006,** 128, 16253-16258.

[32] Dong L, Jiang H, Autonomous microfluidics with stimuli-responsive hydrogels. *Soft Matter* **2007,** 3, 1223-1239.

[33] Zeng X, Jiang H, Tunable liquid microlens actuated by infrared light-responsive hydrogel. *App. Phys. Lett.* **2008,** 93, 151101.

[34] Satarkar NS, Hilt JZ. Hydrogel nanocomposites as remote controlled biomaterials. *Acta Biomater.* **2008,** 4, 11-16.

[35] Schmaljohann D, Oswald J, Jorgensen B, Nitschke M, Beyerlein D, Werner C, Thermo-Responsive PNiPAAm-*g*-PEG Films for Controlled Cell Detachment. *Biomacromolecules* **2003,** 4, 1733-1739.

[36] Schneider GB, English A, Abraham M, Zaharias R, Stanford C, Kelle Jr, The effect of hydrogel charge density on cell attachment. *Biomaterials* **2004,** 25, 3023.

[37] Cushing MC, Anseth KS, Hydrogel Cell Cultures. *Science* **2007,** 316, 1133-1134.

[38] Ali M, Horikawa S, Venkatesh S, Saha J, Hong JW, Byrne ME, Zero-order therapeutic release from imprinted hydrogel contact lenses within *in vitro* physiological ocular tear flow. *J. Controlled Release* **2007,** 124, 154.

[39] Yildiz Y, Uyanik N, Erbil C. Compressive elastic moduli of PNIPAAm hydrogels crosslinked with PDMS. *J. Macromolecular Sci. A* **2006,** 43, 1091-1106.

[40] Ritger PL, Peppas NA. A simple equation for description of solute release II. Fickian and anomalous release from swellable devices. *J. Controlled Release* **1987,** 5, 37-42.

[41] Chiellini F, Bizzazrri R, Ober CK, Yu T, Schmaljohann D, Chiellini E. Patterning of polymeric hydrogels for biomedical applications. *Macromol. Rapid Commun.* **2001,** 22, 1284-1287.

[42] Papavasiliou G, Songprawat P, Perez-Luna V, Hammes E, Morris M, Chiu YC, Brey E. Three Dimensional Patterning in Poly(ethylene glycol) Hydrogels Through Surface Initiated Photopolymerization. *Tissue Eng. C* 2008, 14, 129-140.

[43] Zourob M, Gough JE, Ulijn RV, A Micropatterned Hydrogel Platform for Chemical Synthesis and Biological Analysis. *Adv. Mater.* **2006,** 18, 655.

[44] Schild HG, Poly(N-isopropylacrylamide): experiment, theory and application. *Progr. Polym. Sci.* **1992,** 17, 163-249.

[45] Xu FJ, Zhong SP, Yung LYL, Kang ET, Neoh KG, Surface-Active and Stimuli-Responsive Polymer-Si(100) Hybrids from Surface-Initiated Atom Transfer Radical Polymerization for Control of Cell Adhesion. *Biomacromolecules* **2004,** 5, 2392-2403.

[46] Nath N, Chilkoti A, Creating "Smart" Surfaces Using Stimuli Responsive Polymers.*Adv. Mater.* **2002,** 14, 1243-1247.

[47] Biswal D, Chirra H, Hilt JZ, Microscale analysis of patterning reactions via FTIR imaging: Application to intelligent hydrogel systems.*Polymer* **2006,** 47, 7355-7360.

[48] Huang W, Baker GL, Bruening ML, Controlled Synthesis of Cross-Linked Ultrathin Polymer Films by Using Surface-Initiated Atom Transfer Radical Polymerization*Angew. Chem. Int. Ed.* **2001,** 40, 1510-1512.

[49] Matyjaszewski K, Beers KL, Woodworth B, Metzner Z, Controlled/Living Radical Polymerization in the Undergraduate Laboratories. 2. Using ATRP in Limited Amounts of Air to Prepare Block and Statistical Copolymers of n-Butyl Acrylate and Styrene. *J. Chem. Edu.* **2001,** 78, 547-550.

[50] Jones DM, Smith JR, Huck WTS, Variable Adhesion of Micropatterned Thermoresponsive Polymer Brushes: AFM Investigations of Poly(N-isopropylacrylamide) Brushes Prepared by Surface-Initiated Polymerizations. *Adv. Mater.* **2002,** 14, 1130-1134.

[51] Huang W, Baker GL, Bruening ML, Controlled Synthesis of Cross-Linked Ultrathin Polymer Films by Using Surface-Initiated Atom Transfer Radical Polymerization. *Angew. Chem. Int. Ed.* **2001,** 40, 1510-1512.

[52] Biswal D, Chirra H, Hilt JZ, Fabrication of hydrogel microstructures using polymerization controlled by microcontact printing (PCμCP). *Biomed. Microdev.* **2008,** 10, 213-222.

[53] Bowman CN, Carver AL, Kennett SL, Williams MM, Peppas NA, Polymers for information storage systems. *Polymer Bulletin* **1988**, 20, 329-333.

[54] Wang W, Zhang C, Wang S, Zhao J, Diffusion of Single Polyelectrolytes on the Surface of Poly(*N*-isopropylacrylamide) Brushes. *Macromolecules* **2007,** 40, 9564.

[55] Hüther A, Maurer M, Swelling of *N*-isopropyl acrylamide hydrogels in aqueous solutions of poly(ethylene glycol). *Fluid Phase Equil.* **2004,** 226, 321.

[56] Shibayama M, Tanaka T, Volume phase transition and related phenomena of polymer gels. In *Responsive Gels: Volume Transitions I* **1993,** pp 1-92.

[57] Dingenouts N, Norhausen C, Ballauff M, Observation of the Volume Transition in Thermosensitive Core−Shell Latex Particles by Small-Angle X-ray Scattering. *Macromolecules* **1998,** 31, 8912-8916.

[58] Yoshida R, Sakai K, Okano T, Sakurai Y, *J. Biomaterial Sci. Polymer Ed.* Comb-type grafted hydrogels with rapid deswelling response to temperature changes. **1995,** 6, 585-591.

CHAPTER 5

Nanoscale characterization of the equilibrium and kinetic response of hydrogel structures

This chapter is modified from the article published as

Chirra HD, Hilt JZ. *Langmuir* **2010,** 26, 11249-11257.

5.1. Summary

The use of hydrogel nanostructured patterns and films in biomedical micro- and nanodevices requires the ability to analyze and understand their response properties at the nanoscale. Herein, the thermo-response behavior of atom transfer radical polymerization (ATRP) grown poly(ethylene glycol) n dimethacrylate (PEGnDMA) crosslinked poly(N-isopropyl acrylamide) (PNIPAAm) hydrogel thin films over gold was studied. By controlling the mesh size of the hydrogel matrix through tuning the crosslinking density (i.e. using different molecular weight crosslinker and/or various amounts of crosslinker), the hydrogel volume swelling ratio was tailored for response applications. Thermo-responsive patterns exhibited a broad lower critical solution temperature (LCST) swelling transition, while RMS roughness analysis of the hydrogel surface showed a sharp LCST transition. Mass and visco-elastic property change were monitored using quartz crystal microbalance with dissipation (QCM-D), and the rapid response behavior of the thin hydrogel films was observed. The tunable response behavior along with the controlled growth of the hydrogel achieved via ATRP at the nanoscale make them applicable as functional components in diagnostic and therapeutic devices.

5.2. Introduction

Hydrogels have gained interest as functional components in biomedical devices such as, microfluidic channels, drug delivery microactuators, biosensing microcantilevers, microlens, and micropumps [1-5]. The key element that influences the use of hydrogels for such applications is their unique ability to respond to environmental stimuli in a pre-programmed, intelligent manner [6]. Poly(N-isopropyl acrylamide) (PNIPAAm), which has a lower critical solution temperature (LCST) of around 32^{o}C, is used as the paradigm polymer for various thermo-response studies [7]. The unique property to swell in response to temperature changes has enabled PNIPAAm to be used widely for controlled drug delivery applications [8, 9]. PNIPAAm and other responsive hydrogels have been patterned at specific locations of device surfaces using conventional yet cumbersome UV photolithography. Recently, for applications related to devices, tethering of PNIPAAm over surfaces has been carried out using soft lithography of an initiator from which PNIPAAm is grown bottom-up via a surface initiated polymerization technique. Using microcontact printing (μCP) and atom transfer radical polymerization (ATRP) several responsive polymeric brushes including PNIPAAm have been successfully amplified from patterned monolayers of initiators [10-15].

The majority of the prior PNIPAAm and other brush studies have focused on the synthesis and the response behavior by elucidating how the brush thickness is dictated by ATRP and the change in structural conformation by the surrounding environment. However, the synthesis of spatially controlled, crosslinked responsive hydrogels over surfaces has been relatively unexplored. Unlike polymeric brushes, the transport

properties of molecular species into and out of the hydrogel mesh network can be tailored by the type, molecular weight, and amount of crosslinker used. Cells can be entrapped inside the hydrogels mesh network and manipulated for therapeutic reasons [16]. In addition to the loading of hydrogels with drug molecules [17], hydrogel nanocomposites can be synthesized by in-situ precipitation of nanoparticles inside their matrix. These advantages, along with the increased mechanical integrity and stability provided by the crosslinked matrix, make responsive hydrogels a better alternative to polymeric brushes for a variety of biomedical diagnostic and therapeutic applications.

We recently reported the synthesis of controlled thin patterns of poly(ethylene glycol) n dimethacrylate (PEGnDMA; n=200/400/600; n denotes the average molecular weight of the PEG chain and corresponding approximately to 4.5, 9, and 13.5 repeating units) crosslinked PNIPAAm hydrogel over gold via microcontact printing (μCP) followed by ATRP [18]. In various studies, researchers have shown that the swelling behavior of a hydrogel can be tuned by varying the crosslinking density used [19, 20]. Therefore, the swelling response of PNIPAAm hydrogel nanopatterns synthesized via ATRP can be tuned by changing the crosslinking density. In figure 5.1, a schematic of the temperature dependant swelling response of a nanoscale hydrogel pattern is shown. This schematic also illustrates the potential for a different response at the surface of the hydrogel as compared to the bulk of the pattern. This phenomenon and the general response properties of hydrogel patterns are discussed in the following. Since the kinetics of hydrogel swelling responses are typically diffusion limited, the size of the hydrogel structure can dramatically impact its response time. It is expected that the response will

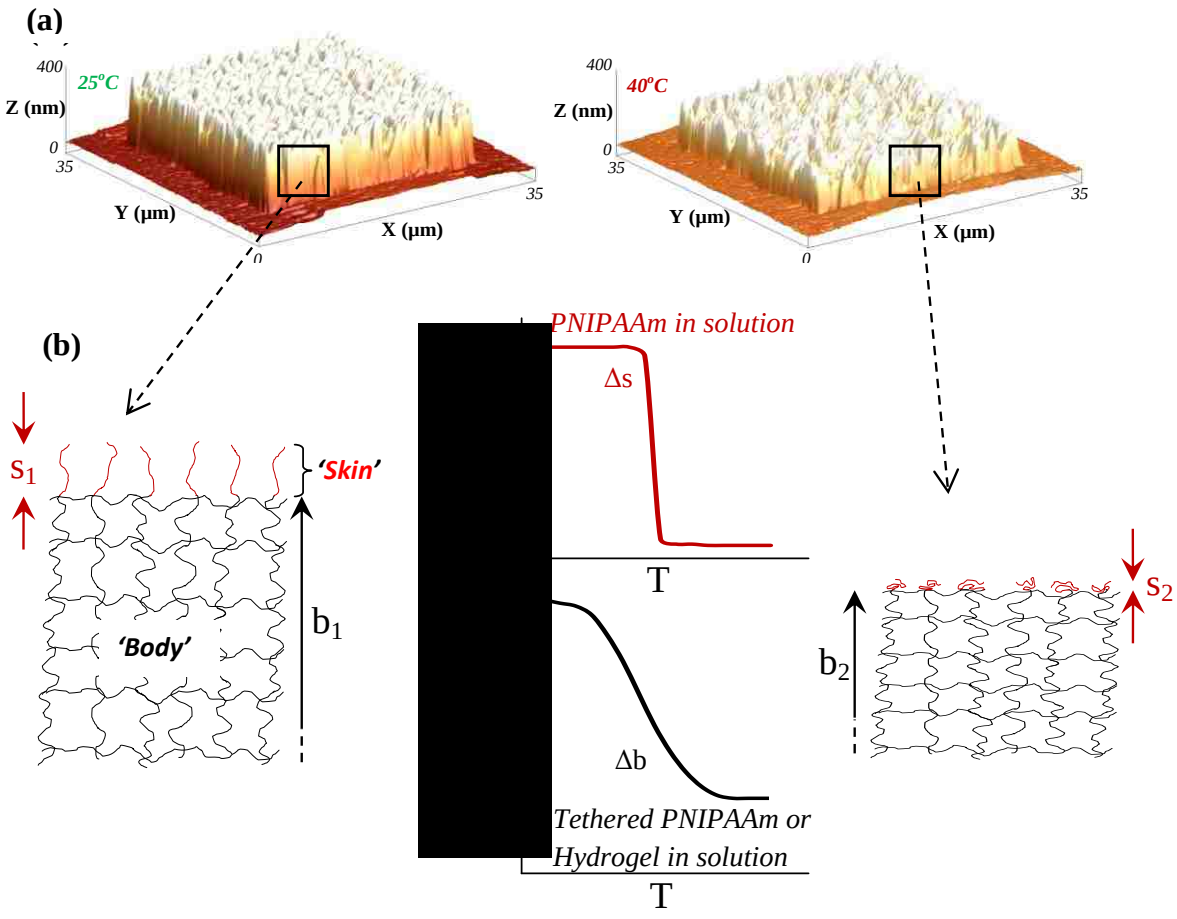

Figure 5.1. (a) AFM images showing the temperature sensitive behavior of a 25µm 10 mol% PEG400DMA crosslinked PNIPAAm square pattern at the 25°C and 40°C, and (b) Zoomed in schematic representation of the differences in the rate of response between the 'bulk' crosslinked matrix (Δx) and tethered free PNIPAAm chains at the surface of the pattern (Δy). Also shown are the response transition profiles of free PNIPAAm chain in solution and hydrogel in solution/tethered PNIPAAm over a surface.

become instantaneous as the size of the hydrogel structures are decreased to the nanoscale due to the direct proportionality between the characteristic diffusion time and the square of the length scale [21]. There have been prior studies investigating the response time of micro- and macro-scale hydrogel structures, but minimal prior experimental work has been done in studying the response properties of nanoscale hydrogel films or patterns [22]. Also, the authors are not aware of any previous studies related to the differences in surface response to that of bulk response.

A detailed understanding of the tunable response properties of hydrogels is crucial for their applications in biomedical micro- and nanodevices. Our primary aim in the work reported here was to understand in detail the response properties of tethered, thermo-responsive PNIPAAm hydrogels on gold. Atomic force microscopy (AFM) measurements were completed for direct visualization of the hydrogel phase transitions. The difference in the surface and bulk response was also investigated using AFM analysis. In addition to AFM, quartz crystal microbalance with dissipation (QCM-D) analysis was performed to obtain a fundamental understanding of the effect of crosslinking amount and type on the response kinetics and hydrogel equilibrium stability.

5.3. Experimental methods

5.3.1. Synthesis of temperature responsive hydrogel patterns using μCP and ATRP

The various crosslinked PNIPAAm hydrogel square patterns of controlled thickness were synthesized using μCP followed by ATRP as detailed in a previously published paper [18]. Briefly, 1-octadeacne thiol (ODT; Sigma) was patterned over the gold surface as a

hydrophobic thiol outside the required square patterns (50-25-10µm) via µCP. The PDMS stamp used for patterning is made up of square pits of sizes 50x50, 25x25, 10x10 µm. The square pits are separated from each other by 25 and 10 µm. There are four rows of fifty squares with the respective spaces making a single square size zone. There are six such zones in the PDMS stamp (zone 1: 50x50 µm with 25 µm spacing, zone 2: same squares with 10 µm spacing, zone 3 and 4 for 25x25 µm squares, and zones 5 and 6 for 10x10 µm squares). The hydrophilic initiator bromoisobutyrate undecyl disulfide (Br-Ini; ATRP Solutions) thiol was then backfilled in the non ODT patterned gold squares from which ATRP of the respective hydrogels was carried out under nitrogen atmosphere for different reaction times (12 hours in this work). Poly(ethyleneglycol)n dimethacrylate (n = 400/600; Polyscience. Inc) were used along with PNIPAAm (Sigma) as the different crosslinkers and monomer respectively. A mole ratio of 90:10 mol% and 70:30 mol% (PNIPAAm:PEGnDMA) were used to study the effects of the amount of crosslinker/crosslinking density employed for response studies. For studying the response behavior effects between the bulk versus surface, half coated gold surfaces were first synthesized, then scratched, and finally characterized for thickness along the scratch.

For the scratch sample analysis, half of the gold substrate was stamped with the hydrophobic ODT. To the other non stamped half, hydrophilic Br-Ini was introduced for 24 hours after which ATRP was done for the respective reaction time periods (5, 8, 12 hours). Using a diamond pen, a scratch was done laterally across the sample so that the scratch extends across the two halves of the sample. Non-contact mode AFM imaging was then done across the scratch in both the hydrogel grown initiator attached half and

the ODT coated no hydrogel grown half and subsequent subtraction of the depth of the scratch was done to get the exact thickness of the grown hydrogel.

5.3.2. Synthesis of thermally responsive hydrogel films over gold coated quartz crystals

The various hydrogel thin films were also grown over gold coated QCM-D crystals using ATRP. The crystals were chemically pre-treated using ammonium peroxide solution for 10 minutes followed by UV-ozone treatment for 20 minutes to remove impurities. The resulting clean gold crystals were then used in the QCM-D setup for obtaining its fundamental resonant frequencies. Ethanol was initially passed to obtain the stable frequency and dissipation base line. A 3 mM solution of Br-Ini was then passed through the cells (except the blank cell) at a flow rate of 300 µl/min for about an hour. The crystals were functionalized with Br-Ini for 24 hours equivalent to the patterned samples. A post initiator attachment cleansing was done with ethanol to remove any unattached initiator thiol. A 'no catalyst' ATRP monomer-crosslinker solution devoid of catalyst copper bromide and ligand 2,2'-dipyridyl was then passed through the cells to neutralize the frequency and dissipation baseline shift caused by differences in the ATRP solutions density and viscosity. Once baseline correction was carried out, a nitrogen purged ATRP solution containing the catalyst and ligand was passed through the respective cells for about an hour. ATRP of PEGnDMA crosslinked PNIPAAm hydrogels was allowed to proceed in the respective cells for 12 hours. The reaction was stopped by a DI water purge step, and the hydrogel grown cells were used as such for

thermo-responsive studies. A blank cell with water passed instead of initiator and ATRP solution was also used for comparative reasons.

5.3.3. AFM Imaging

In-situ imaging of the tethered hydrogel patterns in aqueous solution was performed using the liquid cell set up, non contact mode AFM imaging (Agilent Technologies Inc.) with a BS-TAP300 tapping mode cantilever (Budget Sensors; force constant of 40 N/m). The AFM scans delineating the response behavior of the temperature sensitive PEGnDMA crosslinked PNIPAAm hydrogel patterns, was performed at different temperatures using an autotunable temperature controller (Lake Shore). The temperature of water in the chamber was maintained with a measured deviation of $<\pm 0.05^{o}C$. For the temperatures chosen for imaging, the hydrogel pattern was allowed to equilibrate for at least 5 minutes with the water to ensure stability during imaging.

5.3.4. QCM-D Measurements

A commercial Q-Sense E4 system was used for measuring the shifts in frequency (Δf) and dissipation (ΔD). Optically polished, AT-cut gold coated quartz crystal of diameter 1.4 cm and fundamental resonance frequency of 5 MHz was used for all QCM-D measurements (Q-Sense). The Saurbrey constant (C) of the crystal used is 17.8 ng/cm2.Hz. The solution temperature was controlled within $\pm 0.02^{o}C$. All results obtained in this current work were from the measurements of frequency changes in the third overtone (n=3) although higher overtones were also measured. This is because the third

overtone shear wave senses one layer of liquid over the crystal corresponding to the grown hydrogel thickness, unlike the fundamental frequency which senses two layers of liquid. Moreover the third overtone values are reproducible and stable as compared to higher overtones [23]. All data were measured dynamically with changes in temperature to analyze the response kinetics. The crystal as such had very low resonance and dissipation changes with respect to applied temperature changes, but necessary corrections were made for this effect.

5.4. Results and discussion

5.4.1. Effect of the molecular weight and amount of crosslinker on response behavior

The response behavior of temperature sensitive PNIPAAm hydrogels of varying crosslinker molecular weight and amount was studied at different temperatures using AFM and QCM-D. Figure 5.1 (a) shows the 3-dimensional response AFM topography images of a 25 x 25 μm, 12 hour ATRP reacted, 10 mol% PEG400DMA crosslinked PNIPAAm hydrogel pattern at 25^{o}C and 40^{o}C respectively. For the system shown here, we observe that the hydrogel pattern has a higher thickness at 25^{o}C than at 40^{o}C, which is the expected transition behavior of PNIPAAm-based polymers responding to the varying temperatures below and above its LCST. A similar analysis was performed over the 10/30 mol% PEG200DMA/PEG400DMA crosslinked PNIPAAm hydrogel pattern combinations at increasing temperatures of 25, 30, 35, and 40^{o}C, and their thicknesses are plotted as a function of temperature (figure 5.2). The initial dry thickness of the gels was also measured, before performing the response analysis. The dry thickness values for 10

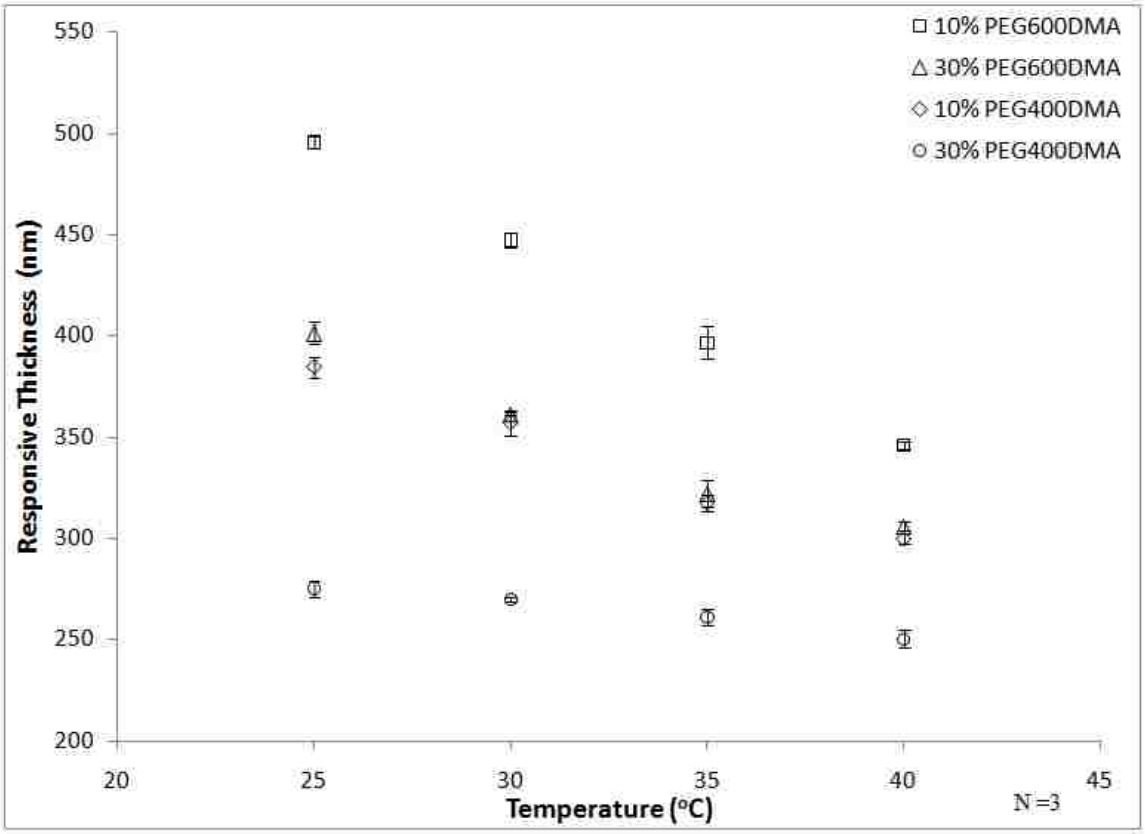

Figure 5.2. Thermo-responsive AFM thickness of the various hydrogel patterns obtained with increase in solution temperature. The effect of the type and the amount of crosslinker employed on the response behavior is clearly observed. (Initial dry thickness data: 10 mol% PEG600DMA – 293nm; 30 mol% PEG600DMA – 268nm; 10 mol% PEG400DMA – 260nm; 30 mol% PEG400DMA – 221nm).

mol% crosslinked PEG600DMA, 30 mol% PEG600DMA, 10 mol% PEG400DMA, and 30 mol% PEG400DMA crosslinked PNIPAAm patterns were 293, 268, 260, and 221 nm, respectively.

The effect of crosslinking density modified by the amount of crosslinker and the molecular weight of crosslinker used on swelling response is observed in figure 5.2. An increase in molecular weight of the PEGnDMA crosslinker from n = 400 to 600 increased the change in swelling greatly (ethylene glycol chain length increased from 9 to 13.5 units). We observe from figure 5.2 that for both the PEG400DMA and PEG600DMA systems, the 10 mol% crosslinked hydrogels swell more than the 30 mol% crosslinked hydrogels at 25^{o}C (room temperature). This is due to the fact that the 10 mol% crosslinked hydrogel has a larger mesh size than the 30 mol% crosslinked hydrogel [24]. As the temperature increased, the polymer - polymer interactions between the hydrogels PNIPAAm backbone increased over the polymer-water interaction, thereby collapsing to a lower thickness state. Although PNIPAAm in solution has a sharp LCST, we observed a broad transition of about 10-13^{o}C along the measured temperatures from figure 5.2. This broadened transition has been reported by Frimpong et al. in the case of PNIPAAm based hydrogels in solution and is commonly observed in crosslinked hydrogel systems (figure 5.1 (b) – transition profile of hydrogel in solution) [24].

The swelling dependence on the type and amount of crosslinker used can be characterized using the volume swelling ratio measured from the change in thickness with respect to dry state thickness (Q_t). The two assumptions used in this calculation are:

1) the swelling and collapse of the surface-tethered hydrogel pattern is spatially confined and therefore the swelling is restricted primarily to the direction perpendicular to the gold surface, and 2) the hydrogels are formed evenly over the entire patterned 25 x 25 μm2 square area. With these assumptions, Q_t is defined as the ratio of the average thickness of the swollen hydrogel pattern at a particular temperature to its average thickness in the dry state. Table 5.1 shows the Q_t values for the different hydrogel patterns of varying crosslinker molecular weight and density at different temperatures. The volume swelling ratio decreases as the amount of crosslinker increases. The Q_t values for the collapsed state at 40^{o}C were observed to be independent of the crosslinking density. At 40^{o}C, all patterns collapse to similar Q_t values (i.e., 1.13-1.18), implying that at higher temperatures all PEGnDMA based PNIPAAm hydrogels behave similarly. Here, tuning the crosslinking parameters/mesh size of the hydrogel was shown to control the extent of swelling change from the swollen to the collapsed state.

5.4.2. Thermally transforming surfaces

There have been several reports to date concerning the structural visualization of the response behavior of PNIPAAm brushes with AFM imaging [12, 13, 25-27]. However, no prior significant work was done to establish a fundamental understanding of the crosslinking effect on the response behavior and the transition temperature of PNIPAAm based hydrogels on gold. We carried out surface roughness analysis over the different hydrogel surfaces by performing non contact mode AFM scans at smaller areas of the patterns as shown in figure 5.3. It shows the non contact mode AFM topography images of the 10 mol% PEG600DMA crosslinked PNIPAAm hydrogel pattern surface in

Table 5.1. Volume swelling ratio (Qt) of the different hydrogel patterns at different temperatures, measured from the change in thickness with respect to dry state respectively.

T (^{o}C)	**Qt (Dry state at 25 ^{o}C = 1)**			
	10% PEG400DMA	*10% PEG600DMA*	*30% PEG400DMA*	*30% PEG600DMA*
25	1.48	1.69	1.25	1.50
30	1.37	1.53	1.23	1.35
35	1.22	1.35	1.18	1.20
40	1.15	1.18	1.13	1.14

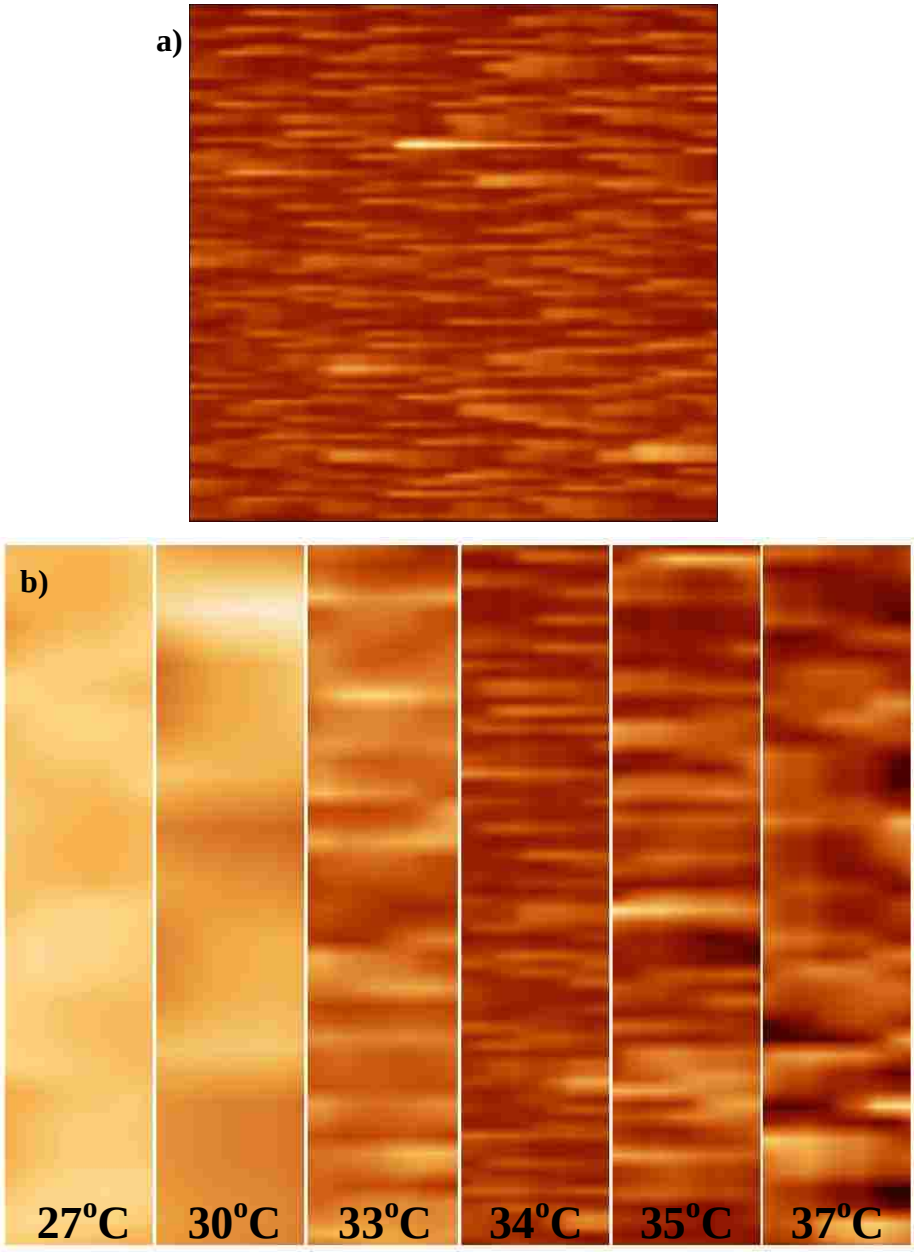

Figure 5.3. a) 2D non contact mode AFM image showing the surface of a 10 mol% PEG600DMA crosslinked PNIPAAm hydrogel square pattern in aqueous conditions at 34°C. b) Sections of the topography images (from original 2 x 2 μm^2) of the same surface at different temperatures in an aqueous media. The features of the surface become significantly evident with temperature, indicating that the hydrogel collapses into a relatively rigid polymer as compared to the swollen state at 25°C.

wet conditions at increasing temperatures (original scan area was 2 x 2 μm^2). At 27^oC, the topography of the hydrogel has only weak structural features, which are a result of the soft swollen gel. At 30^oC and 33^oC the topography images of the hydrogels surface showed the formation of non uniform structural features, which correspond to the partial collapse of the surface with temperature. When the temperature is increased further to 34^oC and beyond, the frequency of non uniformity increased drastically and became clearly visible as sharp features. Biggs et al. also observed similar transformation of a PNIPAAm brush grafted silicon surface with increasing temperatures [25, 26]. They observed from their AFM images that the domain-like structures became sharper with temperature. This is consistent with the continued collapse of the hydrogel as the features became more rigid with temperature.

A better understanding of the different surface transformations to solution temperature changes can be better represented as numerical values of RMS (root-mean-square) roughness. A plot of RMS roughness of the surface with temperature for 10 mol% PEG400DMA, 30 mol% PEG400DMA, 10 mol% PEG600DMA, and 30 mol% PEG600DMA crosslinked PNIPAAm hydrogel is shown in figure 5.4 (a-d). At and near room temperature, the RMS roughness values obtained were usually low due to the flat topography corresponding to the soft swollen state of the hydrogels. As the temperature is increased to and above the critical transition temperature, the RMS value abruptly increases with the formation of sharp features. The RMS roughness flattened out at higher temperatures, indicating the end of the LCST transition. Here, a relatively rigid hydrogel surface is formed by thermo-responsive collapsing.

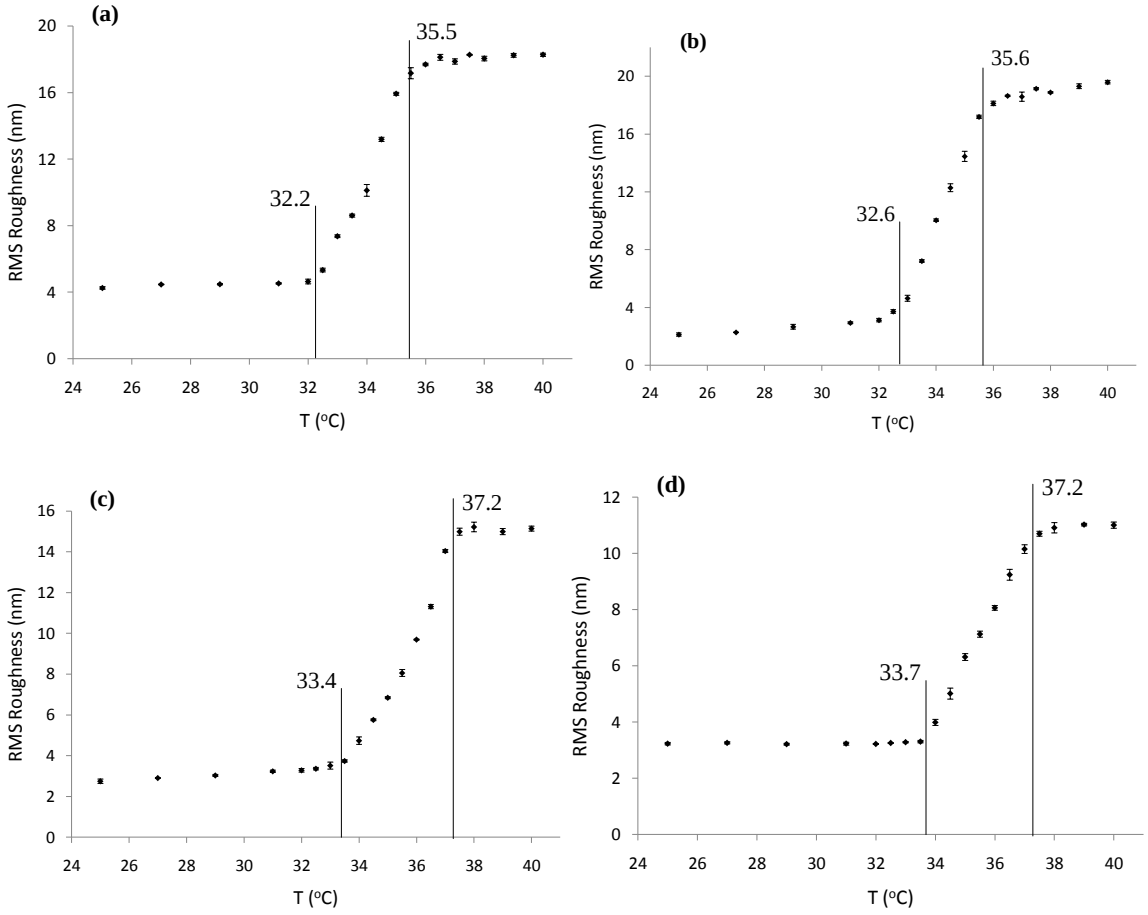

Figure 5.4. Change is RMS roughness of the AFM topography images as a function of temperature for (a) 10 mol% PEG400DMA, (b) 30 mol% PEG400DMA, (c) 10 mol% PEG600DMA, and (d) 30 mol% PEG600DMA crosslinked PNIPAAm hydrogel surfaces. The surface RMS roughness data shows a transition zone for the respective hydrogel systems.

The start and end temperatures of the LCST transitions for the different systems were then determined. The different start and end temperatures are shown in figure 5.4 (a-d). Lutz et al. showed that as the fraction of oligo(ethylene glycol) methacrylate was increased in a copolymer system, it led to the increase of the LCST temperature of the copolymer [28]. We observed a similar but slight shift in the LCST of our systems towards a higher temperature with the increase in the amount of ethylene glycol (EG) units along the crosslinker used (start temperatures: 32.2 to 33.4^{o}C for the 10 mol% and 32.6 to 33.7 ^{o}C for 30 mol%; end temperatures: 35.5 to 37.2 ^{o}C for the 10 mol% and 35.6 to 37.2 ^{o}C for 30 mol%). As the EG molecular weight of PEGnDMA chain increased from 400 to 600, the number of EG units increased from 9 to 13.5 units. This leads to increased stabilizing H-bonds between the ether oxygen of PEG and the surrounding water. Therefore hydrogels synthesized of short PEG400DMA crosslinker is less hydrophilic/more hydrophobic than the longer PEG600DMA crosslinker, which has a higher transition temperature than PEG400DMA.

5.4.3. Surface versus bulk temperature dependent swelling response

The surface response behavior analyzed by the RMS roughness (figure 5.4) is clearly quite different than the response behavior of the entire hydrogel pattern (figure 5.2). The surface or the skin of the hydrogel pattern shows a sharper response transition over about 2.5–3^{o}C. The entire pattern behaves similarly to a macro-scale crosslinked polymer in solution exhibiting a swelling transition of >10^{o}C. This difference between the presence of a transition temperature over the hydrogel surface and a much broader transition in the case of the entirety of the pattern is hypothesized to be a result of

PNIPAAm chains at the surface being only partially crosslinked into the network and, thus, able to respond closer to free PNIPAAm chains or PNIPAAm grafts. This phenomenon poses interesting questions about the dependence of hydrogel response behavior on the thickness of the patterns. For this reason, we synthesized 10 mol% PEG400DMA crosslinked hydrogels over gold surfaces with shorter ATRP reaction periods and studied their response characteristics. The response behavior by thickness change is represented as Qt in figure 5.5. The lines in the plot are only to assist in guiding the eye.

He et al reported a broad transition similar to that of bulk hydrogels in solution for tethered PNIPAAm chains (figure 5.1(b) – transition profile of tethered PNIPAAm) [11]. In figure 5.5, the swelling appears to become sharper around 32.5^{o}C, as the thickness of the tethered hydrogel decreases. The error in the data and the limited data points do not currently enable a conclusion, but a general trend appears to be present. We hypothesize that those portions of the PNIPAAm backbone present at the surface or the 'skin' of the pattern are not fully crosslinked with the adjacent chains and behave similarly to that of tethered polymeric brushes (figure 5.1(b) – zoomed in scheme). The bulk or 'body' of the crosslinked gel matrix lies between the tethered chains at the top of surface ('skin') and the gold substrate at the bottom, and this matrix 'body' is filled with the surrounding fluid. It appears that the swollen matrix behaves closer to that of free solution than to that of the rigid gold surface, and this result in a different transition behavior than the broad transitional behavior of the non-crosslinked surface grafted chains observed by He et al.

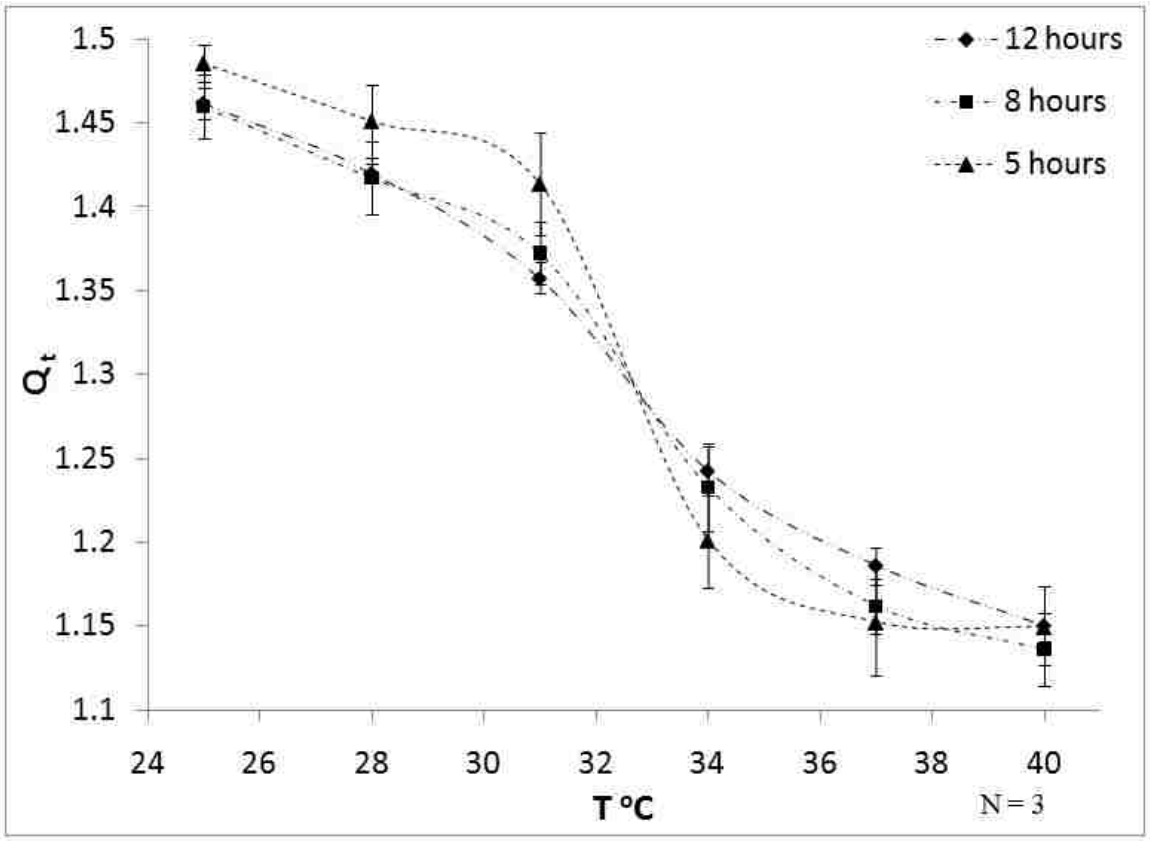

Figure 5.5. The effect of nanoscale on the response behavior of the entire hydrogel similar to that of 'skin' response behavior. Qt for the 10 mol% PEG400DMA crosslinked PNIPAAm systems grown for 5, 8, and 12 hours.

This surface response is similar to that of pure PNIPAAm in solution (figure 5.1(b) – transition profile of free PNIPAAm in solution).

5.4.4. Rapid response behavior of thin film hydrogels

Complimentary QCM-D data was also collected to study the thermo-responsive behavior of PEGnDMA crosslinked PNIPAAm hydrogel thin films. With the gel to be evenly grown over the QCM-D crystal, the change in mass of the hydrogel tethered crystal (Δm) is directly proportional to the negative change in frequency shift of the crystal ($-\Delta f$) as per the Sauerbrey equation [29]. Figure 5.6 (a, b) shows the temperature dependence of frequency and dissipation shift of 10 mol% PEGnDMA crosslinked PNIPAAm hydrogels for three heating and cooling cycles (25-45-25^{o}C; 12 hour ATRP). For all three cycles indicated in figure 5.6 (a) we observed that Δf increased as temperature increased from 25 ^{o}C to 45^{o}C. Δf decreased as temperature decreased from 45^{o}C to 25^{o}C. In terms of Δm, a mass loss with heating and a mass gain with cooling were observed. The mass loss during heating was due to the collapse of the hydrogel, whereas the mass gain was due to the swelling of the hydrogel. The PEG600DMA crosslinked hydrogel showed more mass change than the PEG400DMA system at the two change temperatures. This is due to the decreased crosslinking density of PEG600DMA relative to PEG400DMA complementing the results from figure 5.2.

In recent years, the extended application of using dissipation signal available from the resonance decay has made QCM a more useful tool for real-time measurements of macromolecule adsorption in liquid-phase research applications [30-32]. The dissipation

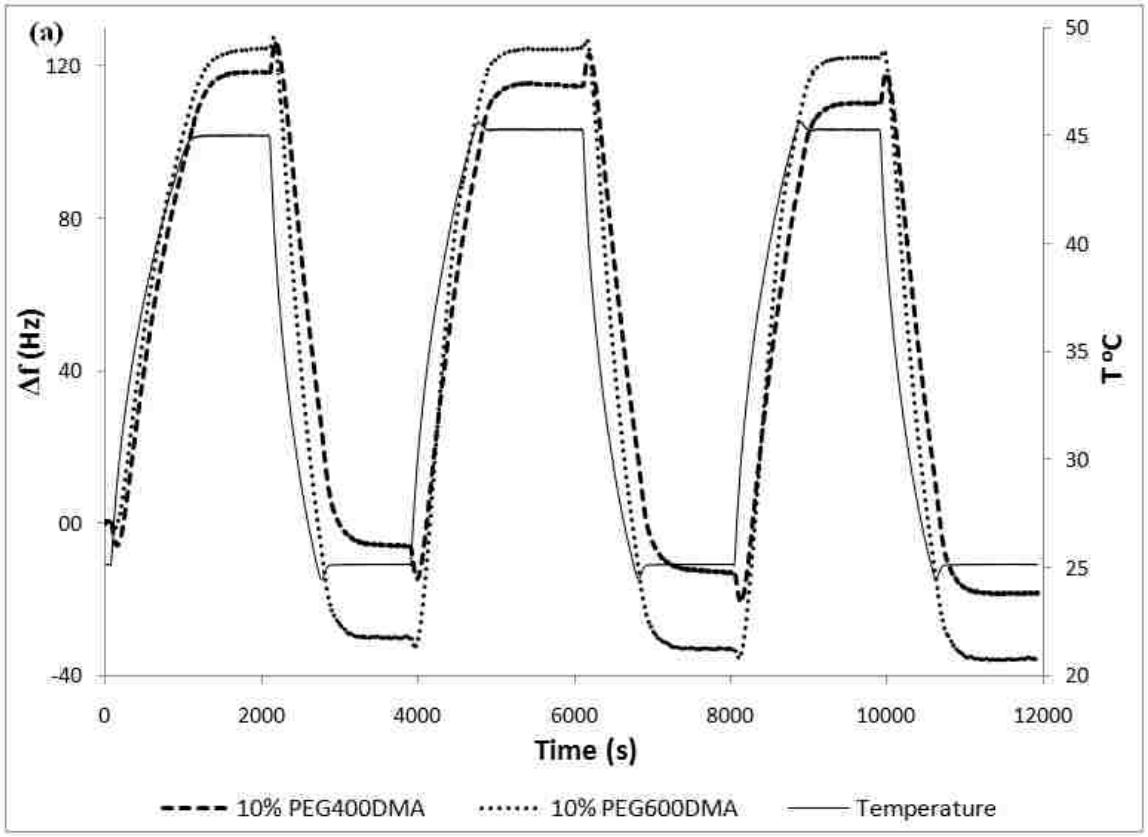

Figure 5.6. Changes in (a) frequency, Δf of 10 mol% PEG400DMA and PEG600DMA crosslinked PNIPAAm hydrogel systems respectively, showing thermo-responsive behavior for three temperature change cycles.

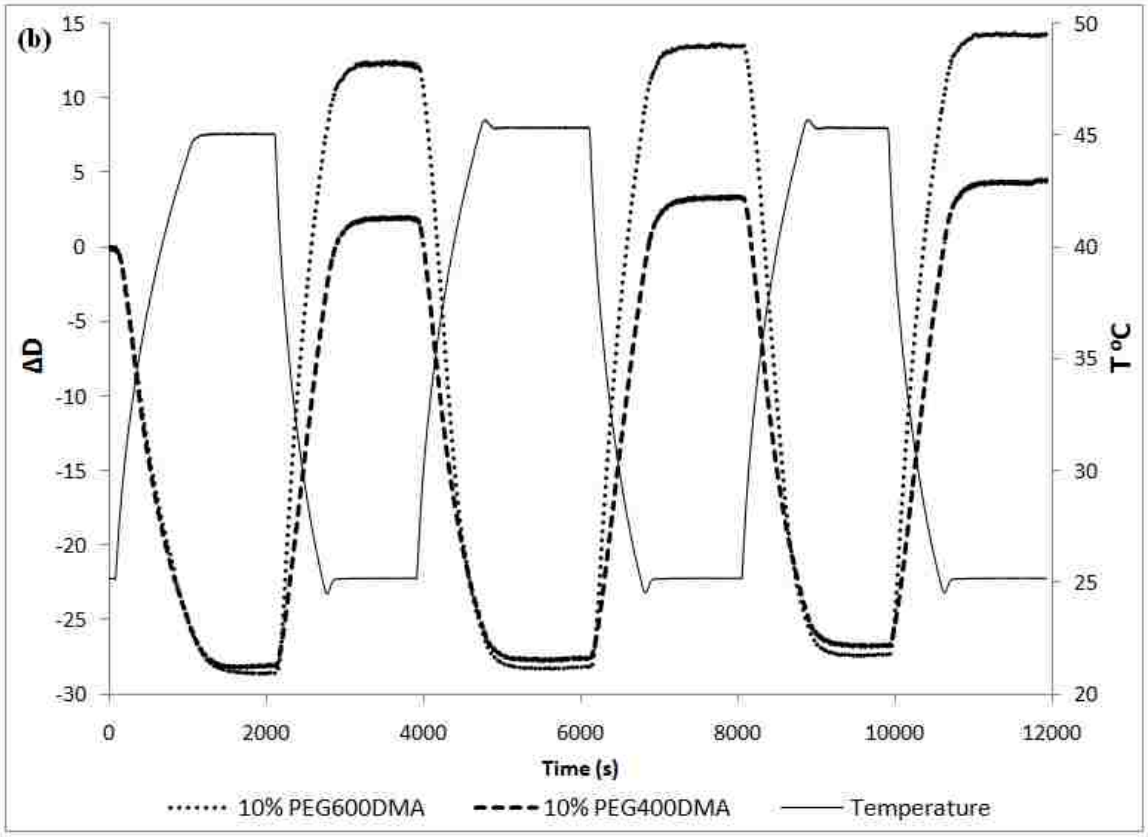

Figure 5.6. Changes in (b) dissipation, ΔD of 10 mol% PEG400DMA and PEG600DMA crosslinked PNIPAAm hydrogel systems respectively, showing thermo-responsive behavior for three temperature change cycles.

factor (D), is defined as the measure of ratio of dissipated energy to stored energy in a material during one oscillation. Rodahl et al. showed that the structure of the visco-elastic polymer layer on a piezoelectric resonator influences the change in dissipation [33]. A collapsed rigid or glassy polymer layer has a small dissipation of energy, whereas a loosely swollen or rubbery polymer layer exhibits a larger dissipation of energy. ΔD in figure 5.6 (b) decreased with temperature increase, and vice versa. This indicates that as heating was introduced, the films collapsed into a more rigid state, whereas under cooling, they became more flexible due to water intake. It is also worth remarking here that while AFM provided insight on the material property of the hydrogel via surface roughness measurements, QCM-D gives information of the hydrogels visco-elastic properties by measuring ΔD. Further, we observed that at 45^{o}C both the PEG400DMA and PEG600DMA crosslinked hydrogels collapsed to an equilibrium rigid state, where both their ΔD measured had similar values. At 25^{o}C, the PEG600DMA hydrogel had more water content than the PEG400DMA hydrogel. This associated increased water content in the PEG600DMA system increased the dissipation energy/ΔD value more than the PEG400DMA system at 25^{o}C.

Figure 5.7 shows the AFM measured Qt data of a 12 hour reacted 10 mol% PEG400DMA crosslinked PNIPAAm pattern at different temperatures and the Δf for the same system on a QCM crystal (Δf of 25-40^{o}C from cycle #2 is normalized and inverted for the sake of comparison). The Δf is monitored continuously as the temperature is ramped over this temperature range. Since the normalized Δf values exhibit the same temperature dependence as the equilibrium Qt values, we can conclude that the Δf values

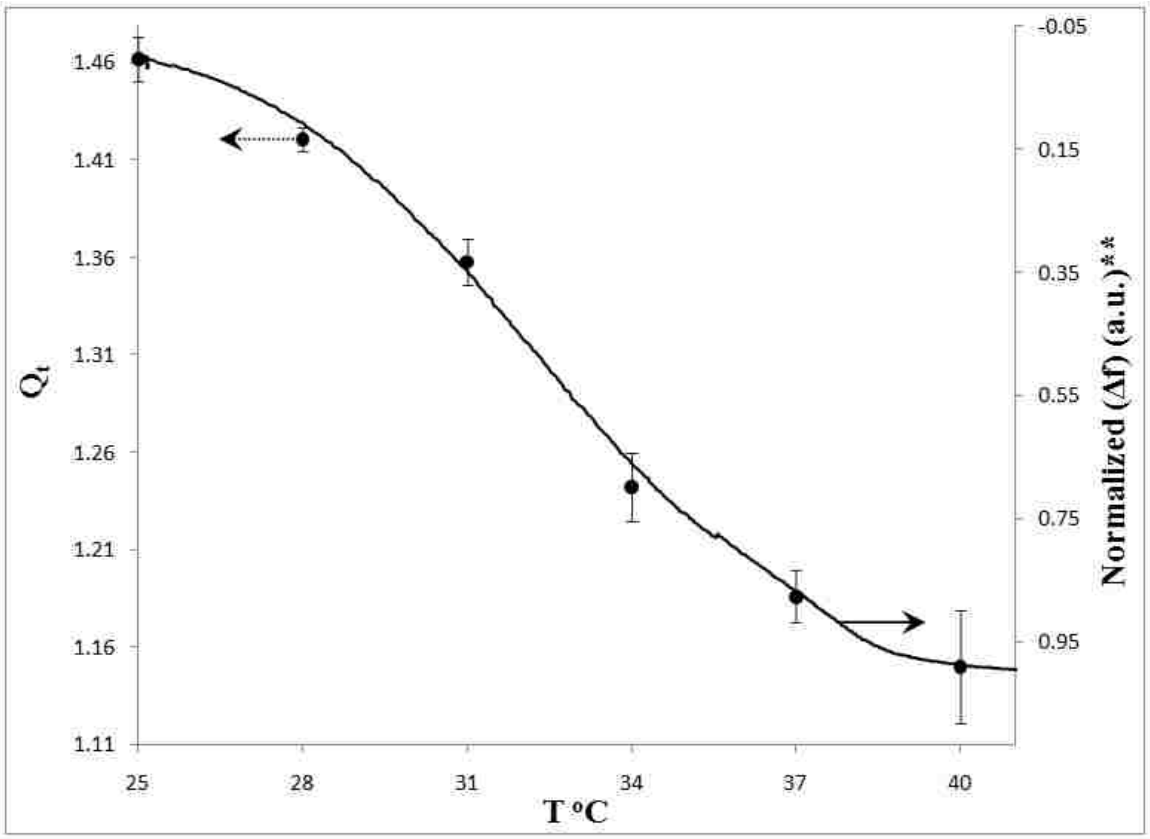

Figure 5.7. AFM analyzed Qt (points) and QCM-D measured Δf (line) of the 10 mol% PEG400DMA crosslinked PNIPAAm hydrogel showing the rapid response to changes in temperature. (** – The frequency change showed here has been inverted and normalized for the sake of comparison)

are also at equilibrium. Thus, the rate at which a responding thin hydrogel pattern achieves equilibrium must be significantly higher than the rate at which the temperature is being ramped in the QCM-D set-up (1.2^{o}C /minute). This equilibrium response with temperature change observed in the kinetic QCM-D analysis demonstrates the rapid response behavior of ATRP grown thin hydrogel patterns. These nanoscale patterns with rapid response behavior are attractive for point of care, rapid/instantaneous diagnosis, and therapeutic applications.

5.4.5. Response equilibrium state of hydrogels

Figure 5.8 (a, b) shows the relation between ΔD and Δf for the three heating-cooling cycles for the 10 mol% PEG400DMA and PEG600DMA crosslinked PNIPAAm hydrogels. We observed from the ΔD versus Δf plot that during the first temperature cycle (heating and cooling), both the hydrogels traced a loop characteristic of water loss and rigidity during the heating stage, followed by water intake and flexibility during the cooling stage. At the end of temperature cycle 1, both the hydrogels had a different ΔD and Δf value as compared to the start of the cycle (origin, in the case of start of cycle 1) indicating an irreversible response transition similar to the hysteresis loop of PNIPAAm brushes [33]. With subsequent temperature cycles (2 and 3), we observed that the loop of the curve extended in area on both directions (area 1-1’ < area 2-2’ < area 3-3’ for PEG400DMA; area a-a’ < area b-b’ < area c-c’ for PEG600DMA). Further, with each temperature cycle, the rate of area increase decreased (noticed by the distances 1-2, 2-3, 1’-2’, 2’-3’ for PEG400DMA; a-b, b-c, a’-b’, b’-c’ for PEG600DMA). The increase in area with each cycle is due to the increased response behavior of the hydrogels. Initially,

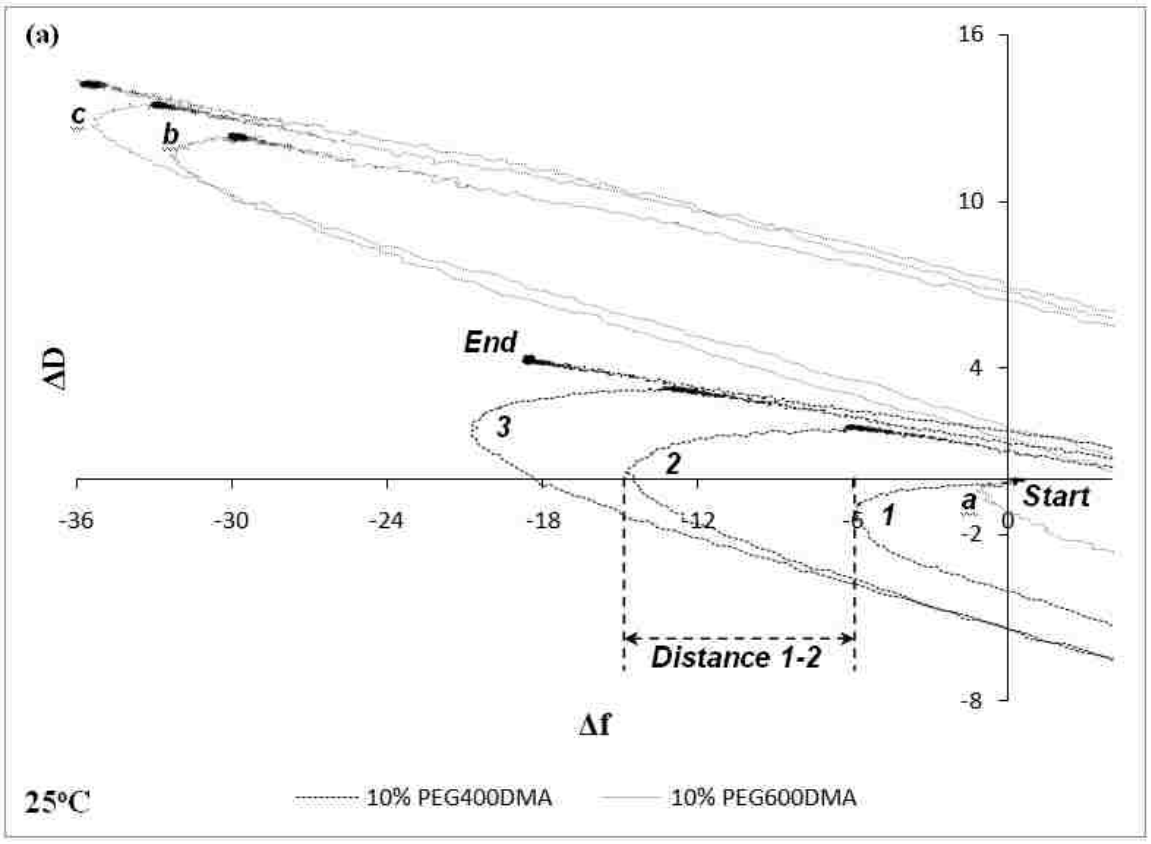

Figure 5.8. ΔD versus Δf plot showing the hysteresis loop ends of the 10 mol% PEGnDMA crosslinked PNIPAAm hydrogel systems at (a) 25°C. The hydrogels try to reach an equilibrium response state at the particular temperatures in subsequent cycles. PEG600DMA crosslinked hydrogel tries to reach equilibrium faster than that of the PEG400DMA system.

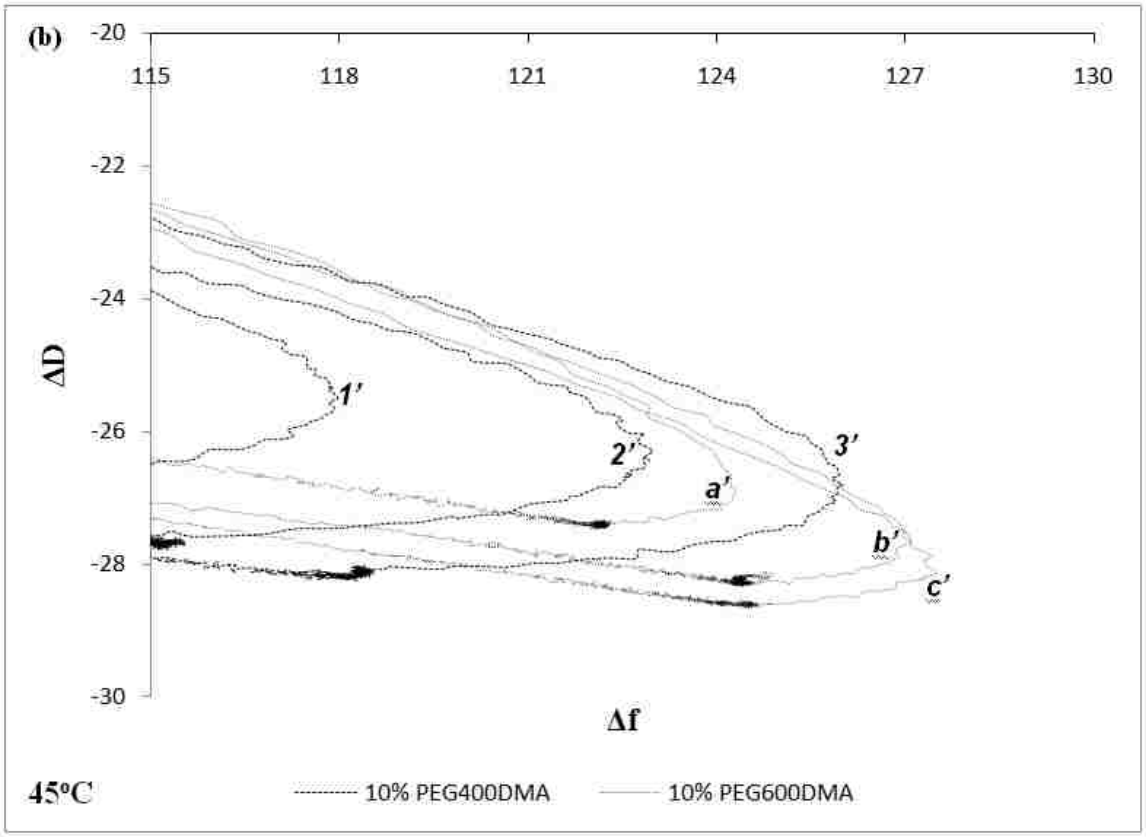

Figure 5.8. ΔD versus Δf plot showing the hysteresis loop ends of the 10 mol% PEGnDMA crosslinked PNIPAAm hydrogel systems at (b) 40°C. The hydrogels try to reach an equilibrium response state at the particular temperatures in subsequent cycles. PEG600DMA crosslinked hydrogel tries to reach equilibrium faster than that of the PEG400DMA system.

the hydrogels are in a thermodynamically stable complex state, where the knotting and entangling of the networked polymer matrix occurs due to the various intrachain and interchain polymeric interactions. With each temperature cycle, the disentanglement of the various polymeric chains continues, thereby contributing to the increasing area along the ΔD-Δf curve. But with subsequent disentanglement over each temperature cycle, the need for further disentanglement/rate of disentanglement decreases thereby decreasing the rate of area increase. This phenomenon of the hydrogels increased response with each temperature cycle continues until the hydrogel reaches the final thermodynamic response equilibrium state, after which there is no significant change in the ΔD-Δf profile. Since PEG600DMA crosslinked hydrogel has his molecular weight polymeric chains, they should exhibit increased mobility and disentangle faster than the PEG400DMA hydrogel for the same temperature cycle number. The difference between distances b-c, b'-c' of PEG600DMA and 2-3, 2'-3' of PEG400DMA confirms this effect. For cycle 3, PEG600DMA crosslinked hydrogel disentangles much closer to its final equilibrium response state than the PEG400DMA crosslinked hydrogel. Once the final response equilibrium state is reached, the hydrogel thin films can be effectively used for precise sensing applications for multiple cycles.

This study confirmed the potential of hydrogel patterns at nanoscale for rapid sensing applications. Functionalized hydrogel thin films at the nanoscale can become the key feature of the future point-of-care biomedical devices because their mesh network have significant advantages over linear polymeric brushes such as entrapping

biomolecules, controlled drug release, tunable response behavior, and better mechanical integrity.

5.5. Conclusion

Herein, we used AFM to visually observe the structural and thickness changes that originated from the thermo-responsive property of the PNIPAAm hydrogels. As the crosslinking density of the hydrogel increased, the mesh size of the hydrogel matrix decreased, thereby decreasing the volume swelling ratio of the hydrogel. The 'bulk' nanoscale patterns were demonstrated to exhibit a broad swelling transition over about 10-13^{o}C. The surface of the nanoscale patterns were observed through RMS roughness analysis to exhibit a sharper swelling transition over about 2-3^{o}C. QCM-D monitoring of the response kinetics of the different hydrogels complemented the results obtained from AFM. PEG600DMA crosslinked hydrogels had more water content than the PEG400DMA crosslinked hydrogels. For the same response cycle, longer PEG600DMA crosslinked hydrogels had a faster equilibrium response state than the shorter PEG400DMA crosslinked hydrogels. The fundamental understanding of the response properties of surface tethered hydrogel thin films is significant and holds promise in augmenting the various biomedical applications that require 'instantaneous' sensing and controlled drug delivery.

5.6. References

[1] Zeng X, Jiang H, Tunable liquid microlens actuated by infrared light-responsive hydrogel. *App. Phys. Lett.* **2008,** 93, 151101.

[2] Agarwal AK, Dong L, Beebe DJ, Jiang H. Autonomously-triggered microfluidic cooling using thermo-responsive hydrogels. *Lab Chip* **2007,** 7, 310-315.

[3] Baldi A, Lei M, Gu Y, Siegel RA, Ziaie B, A microstructured silicon membrane with entrapped hydrogels for environmentally sensitive fluid gating, *Sens. Actuators B* **2006**, 114, 9-18.

[4] Hilt JZ, Gupta AK, Bashir R, Peppas NA. Ultrasensitive biomems sensors based on microcantilevers patterned with environmentally responsive hydrogels. *Biomed. Microdevices* **2003,** 5, 177-184.

[5] Low LM, Seetharaman S, Madou MJ. Microactuators toward microvalves for responsive controlled drug delivery. *Sens. Actuators. B* **2000,** 67, 149-160.

[6] Peppas NA, Khare AR. Preparation, structure and diffusional behavior of hydrogels in controlled release. *Adv. Drug Delivery Rev.* **1993,** 11, 1-35.

[7] Schild HG, Poly(N-isopropylacrylamide): experiment, theory and application. *Progr. Polym. Sci.* **1992,** 17, 163-249.

[8] Huffman AS, Afrassiabi A, Dong LC. Thermally reversible hydrogels: II. Delivery and selective removal of substances from aqueous solutions. *J. Controlled Release* **1986,** 4, (3), 213-222.

[9] Okano T, Bae YH, Jacobs H, Kim SW. Thermally on-off switching polymers for drug permeation and release. *J. Controlled Release* **1990,** 11, (1-3), 255-265.

[10] Matyjaszewski K, Dong H, Jakubowski W, et al. Grafting from Surfaces for "Everyone": ARGET ATRP in the Presence of Air. *Langmuir* **2007**, 23, 4528-4531.

[11] He Q, Kuller A, Grunze M, Li J. Fabrication of Thermosensitive Polymer Nanopatterns through Chemical Lithography and Atom Transfer Radical Polymerization. *Langmuir* **2007,** 23, 3981-3987.

[12] Kaholek M, Lee WK, Ahn SJ, Ma H, Caster KC, LaMattina B, Zauscher S. Stimulus-Responsive Poly(*N*-isopropylacrylamide) Brushes and Nanopatterns Prepared by Surface-Initiated Polymerization. *Chem. Mater.* **2004**, 16, 3688-3692.

[13] Kaholek M, Lee WK, LaMattina B, Caster KC, Zauscher S. Fabrication of Stimulus-Responsive Nanopatterned Polymer Brushes by Scanning-Probe Lithography. *Nano Lett.* **2004**, 4, 373-376.

[14] Tu H, Heitzman CE, Braun PV, Patterned Poly(N-isopropylacrylamide) Brushes on Silica Surfaces by Microcontact Printing Followed by Surface-Initiated Polymerization.*Langmuir* **2004,** 20, 83138320.

[15] Zhou F, Zheng Z, Yu B, Liu W, Huck WTS, Multicomponent Polymer Brushes.*J. Am. Chem. Soc.* **2006,** 128, 16253-16258.

[16] Cushing MC, Anseth KS, Hydrogel Cell Cultures. *Science* **2007,** 316, 1133-1134.

[17] Ali M, Horikawa S, Venkatesh S, Saha J, Hong JW, Byrne ME, Zero-order therapeutic release from imprinted hydrogel contact lenses within *in vitro* physiological ocular tear flow. *J. Controlled Release* **2007,** 124, 154.

[18] Chirra HD, Biswal D, Hilt JZ. Controlled synthesis of responsive hydrogel nanostructures via microcontact printing and ATRP. *Polym. Adv. Technol.* **2009**, DOI:10.1002/pat.1576.

[19] Satarkar NS, Hilt JZ. Hydrogel nanocomposites as remote controlled biomaterials. *Acta Biomater.* **2008,** 4, 11-16.

[20] Tamirisa PA, Hess DW. Water and Moisture Uptake by Plasma Polymerized Thermoresponsive Hydrogel Films. *Macromolecules* **2006,** 39, 7092.

[21] Ritger PL, Peppas NA. A simple equation for description of solute release II. Fickian and anomalous release from swellable devices. *J. Controlled Release* **1987,** 5, 37-42.

[22] Wang J, Chen Z, Mauk M, Hong K-S, Li M, Yang S, Bau HH. Self actuated thermoresponsive hydrogel valves for lan on a chip. *Biomed. Microdevices* **2005**, 7, 313-322.

[23] Zhang G. Study on Conformation Change of Thermally Sensitive Linear Grafted Poly(*N*-isopropylacrylamide) Chains by Quartz Crystal Microbalance. *Macromolecules* **2004,** 37, 6553-6557.

[24] Frimpong RA, Fraser S, Hilt JZ. Synthesis and temperature response analysis of magnetic-hydrogel nanocomposites.. *J. Biomed. Mater. Res., Part A* **2007,** 80A, (1), 1-6.

[25] Ishida N, Biggs S. Direct Observation of the Phase Transition for a Poly(N-isopropylacryamide) Layer Grafted onto a Solid Surface by AFM and QCM-D. *Langmuir* **2007,** 23, 11083-11088.

[26] Ishida, N, Biggs S. Salt-Induced Structural Behavior for Poly(N-isopropylacryamide) Grafted onto Solid Surface Observed Directly by AFM and QCM-D. *Macromolecules* **2007,** 40, 9045-9052.

[27] Bünsow J, Johannsmann D. Electrochemically produced responsive hydrogel films: Influence of added salt on thickness and morphology. *J. Colloid Interface Sci.* **2008,** 326, 61-65.

[28] Lutz J.-F, Hoth, A. Preparation of Ideal PEG Analogues with a Tunable Thermosensitivity by Controlled Radical Copolymerization of 2-(2-Methoxyethoxy)ethyl Methacrylate and Oligo(ethylene glycol) Methacrylate. *Macromolecules* **2006,** 39, 893-896.

[29] Liu G, Zhang G. Collapse and Swelling of Thermally Sensitive Poly(N-isopropylacrylamide) Brushes Monitored with a Quartz Crystal Microbalance. *J. Phys. Chem. B* **2005**, 109, 743-747.

[30] Rodahl M, Kasemo B. A simple setup to simultaneously measure the resonant frequency and the absolute dissipation factor of a quartz crystal microbalance. *Rev. Sci. Instrum.* **1996,** 67, 3238-3241.

[31] Takada K, Diaz DJ. Abruna HD, Cuadrado I, Casado C, Alonso B, Moran M, Losada J. Redox-Active Ferrocenyl Dendrimers; Thermodynamics and Kinetics of Adsorption, In-Situ Electrochemical Quartz Crystal Microbalance Study of the Redox Process and Tapping Mode AFM Imaging. *J. Am. Chem. Soc.* **1997,** 119, 10763-10773.

[32] Hook F, Kasemo B, Nylander T, Fant C, Sott K. Elwing, H., Variations in Coupled Water, Viscoelastic Properties, and Film Thickness of a Mefp-1 Protein Film during Adsorption and Cross-Linking; A Quartz Crystal Microbalance with Dissipation Monitoring, Ellipsometry, and Surface Plasmon Resonance Study. *Anal. Chem.* **2001,** 73, 5796-5804.

[33] Rodahl M, Hook F, Krozer A, Brzezinski P, Kasemo B. Quartz crystal microbalance setup for frequency and Q-factor measurements in gaseous and liquid environments. *Rev. Sci. Instrum.* **1995,** 66, 3924-3930.

CHAPTER 6

Stable hydrogel coated gold nanoparticles using the ISOFURE methodology

6.1. Summary

Polymer coated inorganic nanoparticles are widely studied as carrier systems for various biomedical applications. For their translation into clinical applications, it is critical that they remain in a stable, non-agglomerated state and are also produced at a high yield with ease. In this communication, we introduce a novel methodology called the ISOFURE (ISOlate-Functionalize-RElease) strategy to synthesize stable hydrogel coated nanoparticles in the absence of a stabilizing reagent. As a model platform, we isolated and functionalized gold nanoparticles (GNPs) in a degradable poly(beta amino ester) (PBAE) hydrogel composite. Isolation was done either by adding GNPs to the PBAE hydrogel precursor solution or via in-situ precipitation of GNPs inside the pre-synthesized PBAE hydrogel. Atom transfer radical polymerization (ATRP) was used as the model reaction to grow a temperature responsive poly(ethylene glycol) 600 dimethacrylate crosslinked poly(N-isopropyl acrylamide) hydrogel shell over the GNP core. Release of the temperature responsive hydrogel coated GNPs was done by degrading the PBAE ISOFURE matrix in water. Characterization of the various nanoparticles was done using dynamic light scattering and UV-visible spectroscopy. UV-vis confirmed in-situ precipitation of GNPs as well as ATRP over the GNPs. Light scattering also confirmed the presence of the temperature sensitive hydrogel shell over the GNP surface. Aging studies showed that the ISOFURE method based crosslinked hydrogel coated GNPs showed higher stability and yield than that of the solution-based

functionalized GNPs. The use of ISOFURE strategy shows promise as a simple tool for enhanced functionalization and stabilization over various nanocarriers under flexible experimental conditions.

6.2. Introduction

In the past decade, research on inorganic nanoparticles for the design and development of drug delivery devices and sensors has gained significant attention due to their various optical, electrical, magnetic, heating, and catalytic properties [1, 2]. Noble metal nanoparticles, gold in particular, show relative non-toxicity, easy synthesis and control over size, and the ability to readily conjugate with various reagents and biomolecules through simple gold-thiol chemistry or electrostatic binding, which make them important for biosensing and therapeutic applications [3-5]. In the absence of passivation, the high surface energy of the reduced gold nanoparticles (GNPs) renders them extremely reactive and results in their aggregation [6]. To develop multifunctional nanoparticle systems, it is often necessary to functionalize inorganic nanoparticles with polymer systems for providing both *in vivo* stealth and particle passivation. Of particular interest, polymer brushes or networks that can respond to their environment can allow for the development of advanced nanodevices (e.g., responsive delivery of therapeutic agent).

Environmentally responsive hydrogels with adaptive properties such as surface roughness [7], biocompatibility [8], and optical appearance [9] have been widely used for sensing [10] and controlled drug delivery applications [11]. While the use of drug loaded

hydrogel composites embedded with nanoparticles for biomedical applications is well studied, the use of ultrathin hydrogel coated core-shell nanoparticles for controlled drug release or biosensing is a newer field. Although methods of nanoparticle coating with polymers such as surface initiated polymerization [12, 13] and surfactant free emulsion polymerization [14, 15] are well established, there are often significant limitations in these methods due to agglomeration issues during processing steps. The processing steps often include purification that involves washing, centrifugation, and/or evaporation, and these can result in low yields of stable hydrogel coated nanoparticles [16, 17]. In addition, the nanoparticles can aggregate during the polymerization of a coating when there is interparticle interaction of the growing polymer chains/networks [18].

Herein, we report a novel strategy that increases the stability of hydrogel coated nanoparticles, eradicates the use of additional stabilizing reagents, and eliminates the various purification steps that are usually involved in their synthesis. The strategy called the ISOFURE methodology involves the isolation, functionalization, and release of nanocarriers using a composite of the nanocarrier entrapped in a flexible polymer matrix such as a hydrogel. The hydrogel matrix provides the physical stabilization and isolation of the entrapped nanoparticles, thereby eliminating the need for a stabilizing reagent or the requirement of dilute reaction conditions. Solution-based polymer functionalization of the nanoparticle is done inside the swollen nanocomposite matrix, thereby inhibiting any interactions between the adjacent neighboring particles (figure 6.1). The washing/purification of the functionalized particles at different steps of nanoparticle coating is done by simply soaking the ISOFURE composite in a swelling medium,

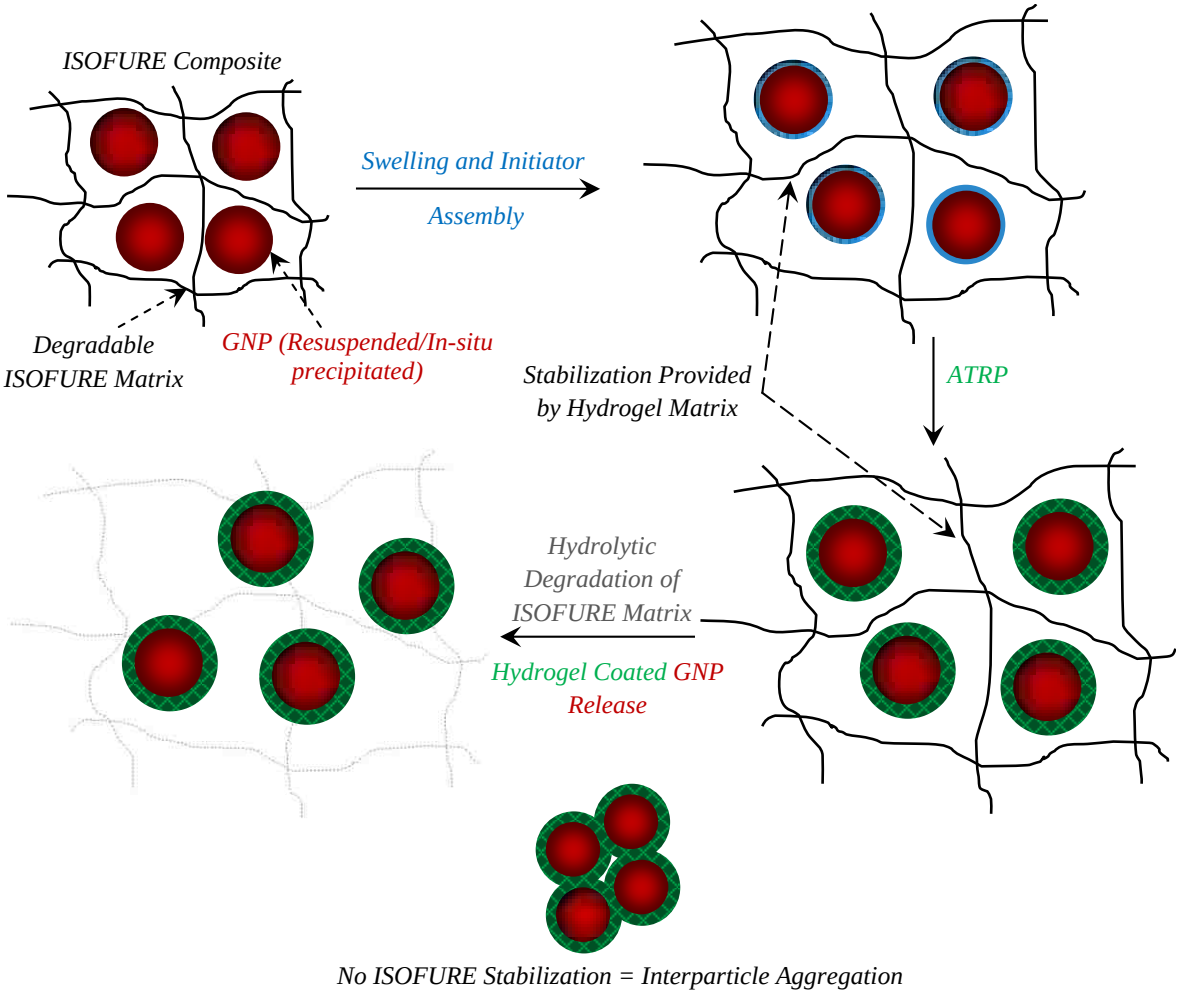

Figure 6.1. Schematic representation of the various steps involved in the novel approach towards increased stabilization of polymer coated nanoparticles in the absence of stabilizing reagents using the degradable ISOFURE system. The system used in this communication consists of ATRP grown crosslinked PNIPAAm responsive hydrogel coated GNPs using the hydrolytically degradable PBAE ISOFURE system.

where-in diffusion of the unreacted components occur. The entrapping ISOFURE hydrogel is chosen in a way that at the end of functionalization, the release of the polymer coated nanoparticle is done by simply degrading or dissolving the matrix. The added advantage of this strategy is that the ISOFURE hydrogels' swelling, matrix mesh size, composition, and degrading properties can be pre-tuned to suit any reaction condition and/or any sized nanoparticle, thereby making them universally applicable to functionalize a multitude of nanocarriers.

As a proof of concept of the ISOFURE strategy, we have used biodegradable poly(β-amino ester) (PBAE) hydrogel matrices entrapping GNPs. Based on prior experience with PBAE hydrogels, hydrolytic degradation of the ester bonds was chosen as the matrix dissolving trigger [19]. Degradable PBAEs were also chosen since they imbibe and transport waste and other fluids similar to that of natural soft tissue, making them applicable for a wide variety of bioconjugation techniques [20]. The main objective of our investigation was to examine whether this novel approach could effectively increase the yield and stability of surface initiated atom transfer radical polymerization (ATRP) grown hydrogel coated GNPs. For this, we have synthesized three different varieties of GNPs coated with temperature sensitive poly (N-isopropyl acrylamide) (PNIPAAm) crosslinked with poly (ethylene glycol) 600 dimethacrylate (PEG600DMA) hydrogels. The first set of samples was a standard approach for the polymerization of hydrogels on GNPs (S-GNPs) that are not entrapped within a polymer matrix. These systems were simply assembled with the initiator followed by ATRP [21]. The second set of samples was the GNP entrapped ISOFURE composite hydrogel (ISOFURE-GNPs)

(figure 6.1). Since the GNPs synthesized are in aqueous medium that degrades the PBAE matrix, they were centrifuged, resuspended in DMSO, and used as such for free radical redox polymerization of the ISOFURE composite. The third set of samples involved the in-situ precipitation of GNPs inside the pre-synthesized degradable PBAE hydrogel matrix (IS-ISOFURE-GNPs). Initiator assembly and ATRP were then carried out on the entrapped nanoparticles. Characterization of the particle size, response behavior of the hydrogel shell, and stability of the particles as compared to solution based GNPs was also carried out.

6.3. Experimental methods

6.3.1. Synthesis of monodispersed gold nanoparticles

Monodispersed gold nanoparticles were prepared using the citrate reduction of gold salts. Briefly, a 1 mM aqueous solution of chloroauric acid ($HAuCl_4$; Sigma) was boiled under stirring. To this solution, 3 mM trisodium citrate (Sigma) in water was added to reduce $HAuCl_4$ to produce GNPs of sub-nanometer size. GNPs were then concentrated by centrifuging at 12,500 rpm for 10 minutes using an Accuspin centrifuge (Fisher Scientific), resuspended in dimethyl sulfoxide (DMSO; Sigma), and used as such for preparing the ISOFURE composite.

6.3.2. Synthesis of H6 macromer

The macromer used for synthesizing the degradable hydrogel matrix was synthesized in accordance to Anderson et al's paper. Based on the time frame of ATRP reaction over GNPs and the swelling ratios of the ISOFURE matrix needed, the system

chosen specifically for this study from the combinatorial library of PBAE degradable materials [22] was the poly(ethylene glycol) 400 diacrylate (Polyscience Inc.; PEG400DA; represented by the letter 'H' from the library) and isobutyl amine (Sigma; IBA; represented by the number '6' from the library) mixed in the molar ratio of 1.2:1 respectively, heated at 85^{o}C for 48 hours, cooled to room temperature, and stored at 4^{o}C.

6.3.3. Synthesis of degradable ISOFURE-GNP and IS-ISOFURE-GNP composite

The hydrolytically degradable GNP entrapped ISOFURE-GNP composite was synthesized using free radical redox polymerization between glass plates separated by 1.5 mm thick Teflon spacers. The vinyl groups of the H6 macromer is reacted to obtain the hydrogel system. For the ISOFURE-GNP composite system, approximately 1 g of the H6 macromer was mixed with 50 wt % of the above prepared GNPs in DMSO. To this, 1 wt % of tetramethyl ethylene diamine (Sigma; TEMED) was added and the solution was vortex mixed. To this solution, 1.5 wt % of ammonium persulfate (Sigma; APS) dissolved in 3 wt % water was added, vortex mixed for approximately 15 s, and then transferred into the glass plate assembly. The plates were allowed to sit at room temperature for 24 hours to ensure complete polymerization. In the case of the IS-ISOFURE-GNP composite, the above mentioned procedure of redox polymerization was performed except that only DMSO was used instead of GNPs in DMSO. After 24 hours, the H6 hydrogel was washed in DMSO for 30 minutes to remove any unreacted macromer and then dried in the vacuum oven overnight. To 1 mM of $HAuCl_4$ in DMSO, the H6 gel was soaked overnight for reduction to occur. Due to the presence of tertiary amines in the H6 gel matrix, reduction of chloroaurate anions occurred and GNPs were

in-situ precipitated inside the H6 hydrogel matrix, thereby making the IS-ISOFURE-GNP composite. Both the composite gels were then washed in DMSO for about 15 minutes to remove loosely bound surface GNPs and then vacuum dried for further usage.

6.3.4. Initiator assembly over GNP surface

To aqueous citrate reduced GNP solution, a 10 mM stock solution of bromoisobutyrate-terminated undecyl disulfide (Br-Ini; Asemblon) in ethanol was added to make the final concentration of Br-Ini to 1.5 mM and then mixed for 24 hours. After 24 hours, the resulting Br-Ini capped GNP solution was dialyzed against water to remove ethanol and excess unreacted initiator. The resulting solution was then centrifuged at 10,000 rpm for 7 minutes, removed of supernatant and concentrated in anhydrous ethanol. This solution was used for the ATRP reaction to produce the ATRP-S-GNPs. In the case of the ISOFURE composites, the GNP entrapped ISOFURE hydrogels were immersed in a 1.5 mM Br-Ini in ethanol solution for 24 hours. They were then washed using ethanol, air dried for an hour, and used as such for ATRP.

6.3.5. Preparation of temperature sensitive hydrogel coated GNPs using ATRP

Surface initiated ATRP was used for the preparation of temperature sensitive hydrogel shells over GNP surfaces. First nitrogen was bubbled to a 20.5 ml methanol and 0.5 ml water mixture for about 30 minutes. To this solvent mixture, a 90:10 molar ratio of hydrogel ingredients made up of 22.5 mM of monomer N-isopropyl acrylamide (NIPAAm; Sigma) and 2.5 mM crosslinker poly(ethylene glycol) 600 dimethacrylate (PEG600DMA; Polyscience Inc.), 0.2 mM copper bromide catalyst (Sigma), 0.6 mM of

ligand 2,2'-dipyridyl (Sigma), and approximately 0.4 mg of copper powder (Sigma) of size less than 425 μm were added. To this mixture, nitrogen was bubbled for another 30 minutes. The initiator coated ISOFURE composite hydrogel was then added to this ATRP solution, and bubbled with nitrogen for another 30 minutes and allowed to undergo polymerization for 12 hours. In the case of S-GNPs, 5 ml of aqueous GNPs was initially added to 16 ml of methanol and used as the initial solvent as mentioned above.

6.3.6. Degradation of ISOFURE composite and release of ATRP-GNPs

The degradation of the ATRP-GNP ISOFURE gel was performed via hydrolytic degradation. The ATRP reacted ISOFURE gel was cut into smaller pieces, and packed inside a 12,000 MWCO dialysis membrane. To this membrane, 2 ml of DI water was added and then immersed in a dialyzing sink of water. Dialysis was done for 72 hours with 12 hour sink change to ensure complete degradation and removal of degraded products. The final ATRP-GNP solution inside the dialysis membrane was used as such for characterization. In the case of the ATRP-S-GNPs, air was bubbled into the mixture to stop ATRP. The solution was then ultra-filtered to about 10 ml volume. This concentrate was then dialyzed against water as mentioned above.

6.4. Results and Discussion

6.4.1. Characterization of ISOFURE composites before and after ATRP

Figure 6.2 shows the UV-vis spectra for the different ISOFURE composite systems and the solution based GNPs. The advantage of using IS-ISOFURE-GNPs over ISOFURE-GNPs is that any aggregation associated with centrifugation and resuspension

in DMSO of the ISOFURE-GNPs and the entrapment of multiple particles by the polymer matrix was eliminated, since they were synthesized directly inside the ISOFURE systems hydrogel matrix. Also, this eliminated any concern associated with the slightest presence of an aqueous phase in the formation of the composite that would partially degrade the surrounding PBAE mesh network, thereby contributing to further aggregation and polydispersity. Further, the mesh size of the polymer network for the IS-ISOFURE-GNPs can be tuned through the synthesis conditions and resultant crosslinking density, which can be used to control the size of the core GNPs.

From UV-vis analysis of the various ISOFURE systems (figure 6.2), we observed that the surface plasmon resonance (SPR) values of both the ISOFURE-GNP (531 nm) and IS-ISOFURE-GNP (524 nm) composites were similar to that of the citrate reduced S-GNPs in water (527 nm). Since, SPR values are characteristics of the identity, thickness of the metal core, and the refractive index of the medium at the interface, it is most likely that all three systems have GNPs of similar size and property. Although it is the same GNPs used from the S-GNPs for the formation of the ISOFURE-GNP composite, a slight red shift in the SPR value is observed from 527 nm to 531 nm indicating slight amount of particle aggregation caused during centrifugation and resuspension in DMSO. It is to be noted that the synthesis of the IS-ISOFURE-GNP composite involved the reduction of the pre-synthesized PBAE hydrogel imbibed chloroauric acid solution ($HAuCl_4$) without the use of any reducing agent such as sodium citrate or sodium borohydride. We hypothesize that the tertiary amine moiety of the crosslinked PBAE hydrogel matrix

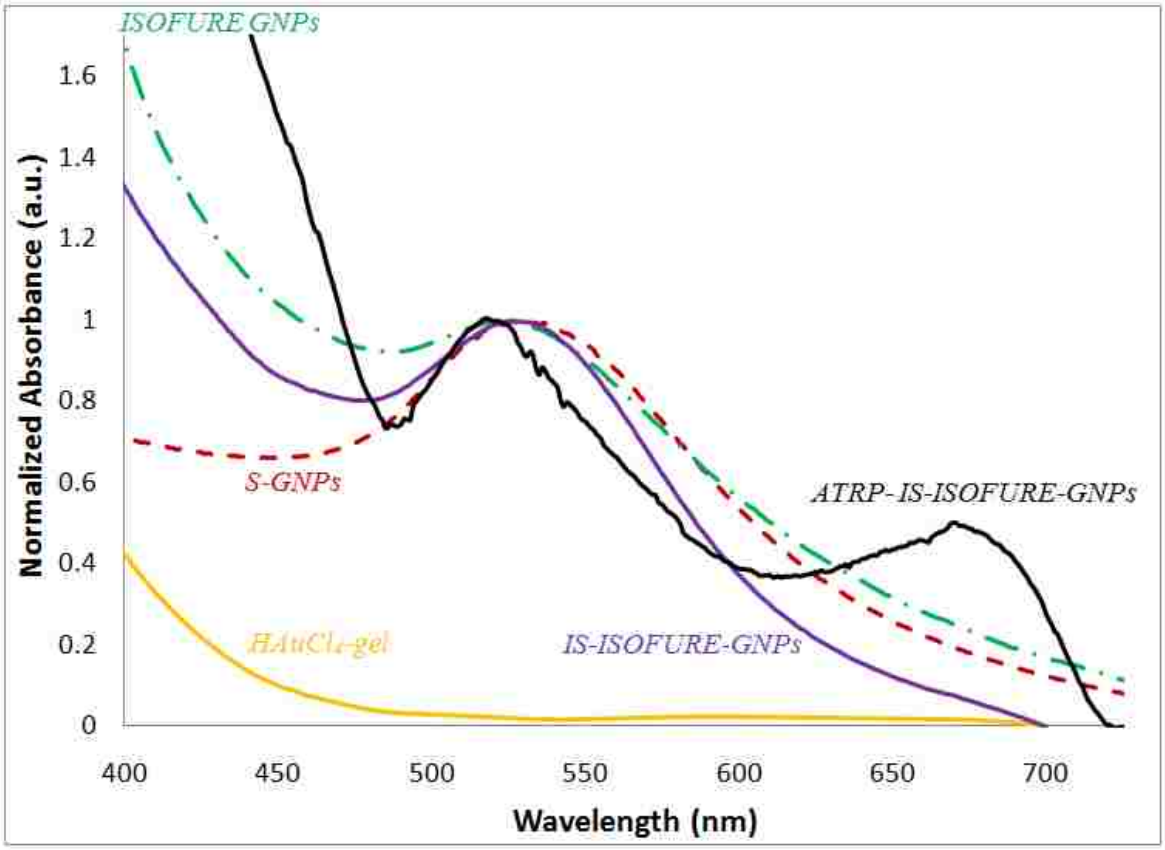

Figure 6.2. UV-vis normalized spectra showing the different kinds of GNP-ISOFURE systems used for the synthesis of ATRP grown crosslinked PNIPAAm hydrogel coated GNPs. All three GNP-ISOFURE systems (S-GNPs in solution, ISOFURE-GNP composite, and IS- ISOFURE-GNP composite) exhibited similar SPR values in the range of 524-531 nm. The presence of the second SPR peak value at 671 nm indicates the increase in size of the entrapped in-situ precipitated GNP via ATRP.

undergoes electron delocalization and resonance hybridization to reduce the chloroaurate anion into neutral metallic gold [23]. Since the gold formed via nucleation is stabilized physically by the surrounding PBAE hydrogel matrix, gold nanoparticles are formed inside the matrix. Since the preparation via in-situ precipitation did not involve any centrifugation, no aggregation occurred and therefore they show lower SPR value of 524 nm as compared to that of the S-GNPs. While a similar strategy for synthesizing in-situ precipitated GNPs using dendrimers was reported by Boisselier et al, release of GNPs from the encapsulated matrix was not carried out [24]. This added advantage of nanoparticle release via degradation of the matrix can be harnessed for enhanced biofunctionalization of particles for biomedical applications. In the absence of any surface passivation, the degradation of the composite still gave stable GNPs of size around 12 nm. This is attributed to the fact that the degradation products (carboxylic acid products from breaking the ester bonds) of the PBAE matrix stabilize the GNPs similar to that of the citrate ions in the case of the S-GNPs. Figure 6.2 also shows the SPR value of ATRP reacted IS-ISOFURE-GNP composite at 671 nm. This red shift in SPR value is due to the local increase in refractive index caused by the growth of the responsive hydrogel by ATRP on the surface of the GNP. Depending on the time of ATRP reaction, this value shifts confirming that the increase in SPR value is indicative of the coating of the particle and not that of aggregation.

6.4.2. Temperature response behavior of the hydrogel coated GNPs

The release of the ATRP reacted hydrogel coated GNPs was done inside a dialysis membrane, where the degradation of the PBAE matrix released the

functionalized nanoparticles while allowing the removal of the smaller degraded products via dialysis in water. The resulting PEG600DMA crosslinked PNIPAAm hydrogel coated GNPs (ATRP-GNPs) in water were analyzed for size, temperature response, and stability. Figure 6.3 shows the temperature response profile of the different GNPs as synthesized using a 12 hour ATRP reaction. Clearly, all three systems of ATRP-GNPs exhibit temperature response behavior indicating the presence of a PNIPAAm-based hydrogel shell. In the case of the ATRP-S-GNPs, functionalized nanoparticle sizes were significantly larger than that of the ISOFURE systems. It was also observed that the nanoparticle sizes were larger for the ATRP-ISOFURE-GNPs in comparison to the ATRP-IS- ISOFURE-GNPs. It is to be noted that particle settling was observed with time during response analysis of the ATRP-S-GNPs, and the yield of the stable ATRP-S-GNPs was relatively low. Thus, the DLS values obtained represent only the stable particle fraction, which still remained suspended in solution.

6.4.3. Enhanced stability of hydrogel coated ISOFURE GNPs than S-GNPs

The effectiveness of using ISOFURE strategy, in terms of preserving the stability of the nanoparticles whose surfaces are modified by polymer coating was observed using the UV-vis spectrophotometer (Figure 6.4). Since the optical density of a nanoparticle solution is proportional to the concentration of same sized nanoparticles in solution, we studied the aging or aggregation of particles with time by normalizing the SPR absorbance values at different time intervals to that of the initial SPR absorbance. As observed in Figure 4, the ATRP-S-GNPs showed a drop in concentration with time, while both the ATRP – IS – ISOFURE - GNPs and ATRP-ISOFURE-GNPs showed higher

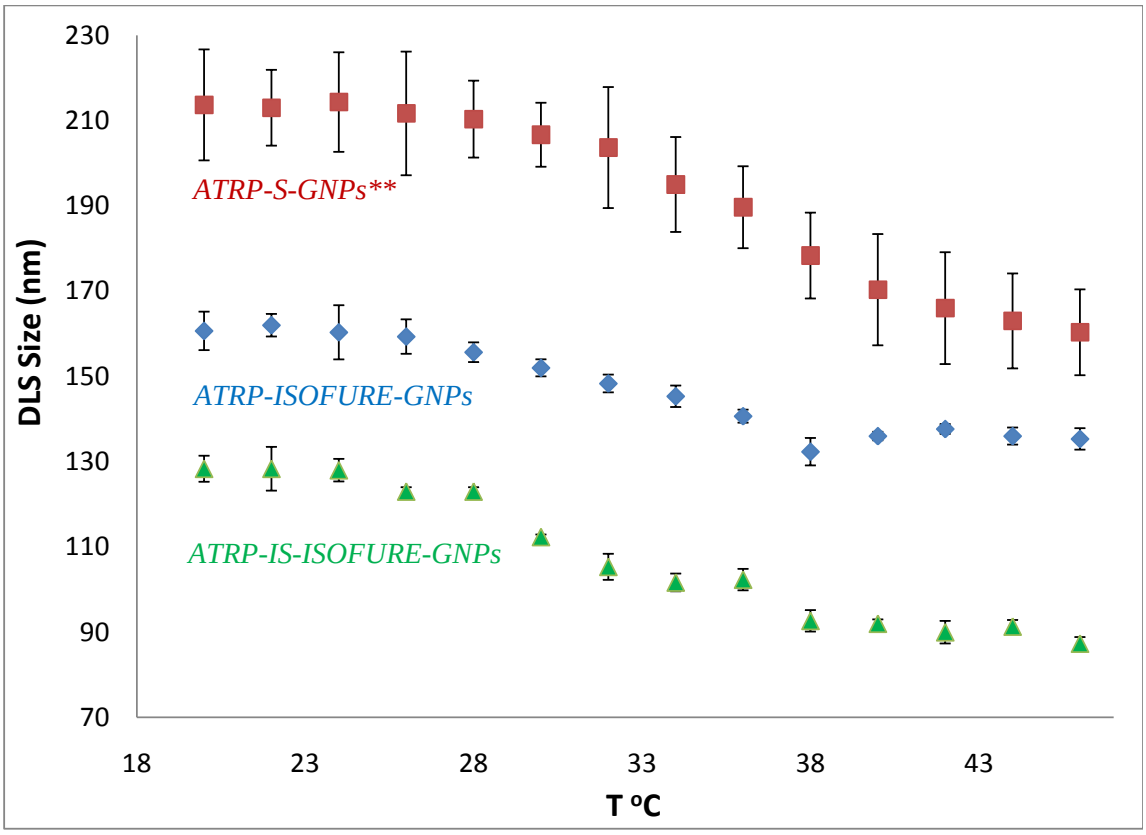

Figure 6.3. Temperature sensitive response behavior of the 12 hour ATRP grown crosslinked PNIPAAm hydrogel coated GNPs for the three different systems (** represents that the DLS size is measured from the peak 1 values of that fraction of straight GNPs which have not settled due to particle aggregation and remain suspended in solution).

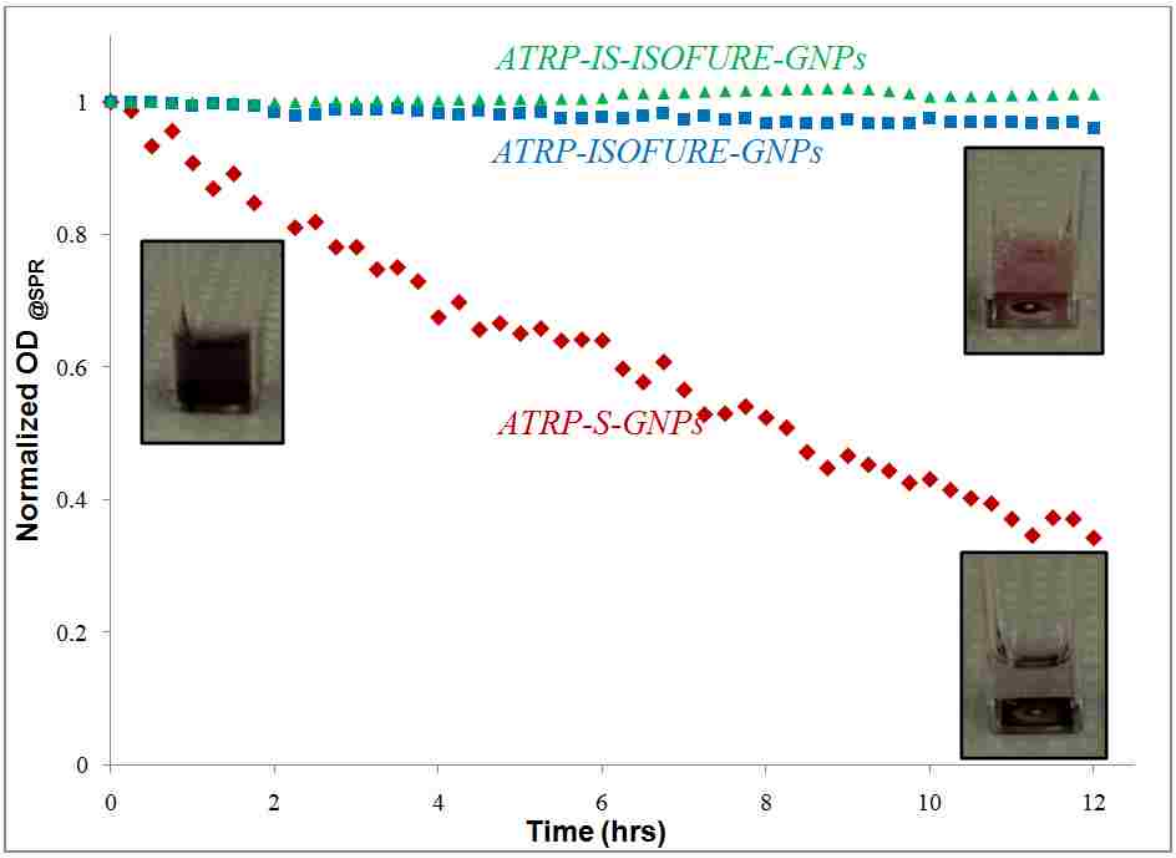

Figure 6.4. Settling kinetics of the ATRP grown crosslinked PNIPAAm hydrogel coated solution based GNPs and ISOFURE-GNPs clearly indicating that the hydrogel coated ISOFURE-GNPs exhibit enhanced stability than the S-GNPs. Insets confirm the settling of the ATRP-S-GNPs as compared to that of the ATRP-ISOFURE-GNPs (same as that of ATRP-IS-ISOFURE-GNPs).

stability. Boisselier et al. observed that the addition of slight amounts of a crosslinker to a surface initiated polymerization reaction over nanoparticles resulted in interparticle crosslinking [24]. We believe that in the presence of PEG600DMA the same interparticle crosslinking is likely to occur resulting in S-GNP aggregation during ATRP. In the case of the ATRP-IS-ISOFURE-GNPS and ATRP-ISOFURE-GNPs, the surrounding matrix physically inhibits the growing PEG600DMA crosslinked PNIPAAm hydrogel shell to interact with the adjacent neighboring GNPs, thereby maintaining the stability of the hydrogel coated GNPs. This added protection during the hydrogel coating step proves vital in maintaining the monodispersity of the modified particle and also in increasing the yield of same sized hydrogel coated nanoparticles as compared to that of the ATRP-S-GNPs. By using the ISOFURE method, stabilization effects can be provided for various particle aggregating reactions such as biomolecular functionalization and polymer coating techniques. The novel idea of using a polymer matrix to provide physical entrapment to nanocarriers is of great interest and can be used universally to functionalize a multitude of polymers or biomolecules to nanocarriers.

6.5. Conclusion

Herein, a proof of concept of enhancing the yield and stability of polymer-coated nanocarriers via a novel isolation, functionalization, and release (ISOFURE) methodology was demonstrated. GNP biodegradable PBAE hydrogel nanocomposites were synthesized either by adding GNPs to the redox polymerizing macromer solution or by carrying out in-situ precipitation of GNPs inside the PBAE matrix. UV-vis analysis showed the formation of stable in-situ precipitated GNPs in the composites. The

polymerization of PEG600DMA crosslinked PNIPAAm hydrogels via ATRP was successfully carried out over the different GNPs. Light scattering analysis of the particles at increasing temperatures showed that the particles exhibited temperature sensitivity. Aging studies using the UV-Vis spectrophotometer showed that the ISOFURE method based hydrogel coated GNPs showed higher stability than that of the solution based GNPs. In addition, the yield of ATRP hydrogel coated GNPs of monodispersed size was higher in the case of the ISOFURE system as compared to that of the S-GNPs. The ISOFURE strategy shows promise for both increasing the stability and enhancing the loading capacity of various polymers and biomolecules to various nanocarriers under flexible experimental conditions.

6.6. References

1. De M, Ghosh PS, Rotello VM. Applications of Nanoparticles in Biology. *Adv. Mater.* **2008**, 20, 4225-4241.
2. Sanvicens N, Marco MP. Multifunctional nanoparticles--properties and prospects for their use in human medicine. *Trends Biotechnol.* **2008**, 26, 425-433.
3. Chirra HD, Biswal D, Hilt JZ. Nanoparticulate Drug Delivery Systems (NPDDS) II: Formulation and Characterization. Pathak, Y.; Thassu, D. eds., *Informa Healthcare USA Inc*. **2009**, pp 90-114.
4. El-Sayed IH, Huang X, El-Sayed M.A. Selective laser photo-thermal therapy of epithelial carcinoma using anti-EGFR antibody conjugated gold nanoparticles. *Cancer Lett.* **2006**, 239, 129-135.

5. Moghimi SM, Hunter AC, Murray JC. Nanomedicine: Current status and future prospects. *FASEB J* **2005,** 19, 311-330.
6. Zhao M, Sun L, Crooks RM. Preparation of Cu Nanoclusters within Dendrimer Templates. *J. Am. Chem. Soc.* **1998**, 120, 4877-4878.
7. Sidorenko A, Krupenkin T, Taylor A, Fratzl P, Aizenberg J. Reversible Switching of Hydrogel-Actuated Nanostructures into Complex Micropatterns. *Science* **2007**, 315, 487-490.
8. Krsko P, Libera M. Biointeractive Hydrogels. *Materials Today* **2005**, 8, 36-44.
9. Houbenov N, Minko S, Stamm M. Mixed Polyelectrolyte Brush from Oppositely Charged Polymers for Switching of Surface Charge and Composition in Aqueous Environment. *Macromolecules* **2003**, 36, 5897-5901.
10. Chirra HD, Biswal D, Hilt JZ. Controlled synthesis of responsive hydrogel nanostructures via microcontact printing and ATRP. *Polym. Adv. Technol.* **2009**, DOI: 10.1002/pat1576.
11. Satarkar NS, Hilt J.Z. Magnetic hydrogel nanocomposites for remote controlled pulsatile drug release. *J. Controlled Release.* **2008**, 3, 246-251.
12. Jordan R, West N, Ulman A, Chou Y-M, Nuyken O. Nanocomposites by surface initiated living cationic polymerization of 2-oxazolines on functionalized gold nanoparticles. *Macromolecules* **2001**, 34, 1606-1611.
13. Ohno K, Koh K-M, Tsuji Y, Fukuda T. Synthesis of gold nanoparticles coated with well-defined, high-density polymer brushes by surface-initiated living radical polymerization. *Macromolecules* **2002**, 35, 8989-8993.

14. Kim JH, Lee TR. Thermo- and pH-responsive hydrogel coated gold nanoparticles. *Chem. Mater.* **2004**, 16, 3647-3651.
15. Kim JH, Lee TR. Discrete thermally responsive hydrogel coated gold nanoparticles for use as drug delivery vehicles. *Drug Dev. Res.* **2006**, 67, 61-69.
16. Chakraborty S, Bishnoi SW, Perez-Luna VH. Gold Nanoparticles with Poly(*N*-isopropylacrylamide) Formed via Surface Initiated Atom Transfer Free Radical Polymerization Exhibit Unusually Slow Aggregation Kinetics. *J. Phys. Chem. C.* **2010**, 114, 5947-5955.
17. Dong H, Zhu M, Yoon JA, Gao H, Jin R, Matyjaszewski K. One-pot synthesis of robust core/shell gold nanoparticles. *J. Am. Chem. Soc.* **2008**, 130, 12852-12853.
18. Li DX, He Q, Cui Y, Li J. Thermosensitive Copolymer Networks Modified Gold Nanoparticles for Nanocomposite Entrapment. *Chem. Eur. J.* **2007**, 13, 2224-2229.
19. Hawkins AM, Satarkar NS, Hilt JZ. Demonstration of remote-controlled drug release from degradable nanocomposite hydrogels. *Pharm. Res.* **2009**, 26, 667-673.
20. Slaughter BV, Khurshid SS, Fisher OZ, Khademhosseini A, Peppas NA. Hydrogels in Regenerative Madicine. *Adv. Mater.* **2009**, 21, 3307-3329.
21. Chirra HD, Hilt JZ. Nanoscale Characterization of the Equilibrium and Kinetic Response of Hydrogel Structures. *Langmuir* **2010**, 26, 11249-11257.
22. Anderson DG, Tweedie CA, Hossain N, Navarro SM, Brey DM, Vliet KJV, Langer R, Burdick JA. A combinatorial library of photocrosslinkable and degradable materials. *Adv Mater* **2006,** 18, 2614-2618.

23. Dzidic I. Relative gas-phase basicities of some amines, anilines, and pyridines. *J. Am. Chem. Soc.* **1972**, 94, 8333-8335.

24. Boisselier E, Diallo AK, Salmon L, Ornelas C, Ruiz J, Astruc D. Encapsulation and Stabilization of Gold Nanoparticles with "Click" Polyethyleneglycol Dendrimers. *J. Am. Chem. Soc.* **2010**, 132, 2729-2742.

CHAPTER 7

Enhanced biofunctionalization of gold nanoparticles using biodegradable ISOFURE Composites

7.1. Summary

The unique chemical and physical properties of inorganic nanoparticles render them as effective carriers for various biosensing and therapeutic applications. For these applications, it is critical that the surface chemistry of the particle is tailored precisely, and in most cases, it becomes difficult to prevent agglomeration in a multistep functionalization process due to changes in surface properties (e.g. charge neutralization and hydrogen bonding). In this work, we introduce a novel methodology called the ISOFURE (isolate-functionalize-release) strategy to synthesize stable functionalized nanoparticles in the absence of a stabilizing reagent, thereby increasing the loading capacity of stable nanoparticles. As a proof of concept, poly(beta amino ester) (PBAE) hydrogels were harnessed to synthesize biotinylated gold nanoparticle (GNP) entrapped ISOFURE hydrogel nanocomposites. Streptavidin was bound to biotinylated GNPs as the GNPs were released via degradation of the PBAE hydrogel matrix. Then, conjugation with enzyme catalase was carried out. Dynamic light scattering and UV-visible spectroscopy results confirmed stabilization of the GNPs during biotinylation inside the PBAE matrix. Bioassaying confirmed enhanced enzymatic activity/biofunctionalization of catalase bound stable ISOFURE GNPs in the absence of an external stabilizing reagent. The use of ISOFURE strategy as the agglomeration inhibiting nanoparticle

stabilizing medium can prove to be a simple yet powerful tool for enhanced biomolecular loading and stabilization over various nanoparticles.

7.2. Introduction

Carrier systems of nanoscale dimensions such as inorganic nanoparticles, liposomes, polymer particles, and viral vectors have gained significant prominence in the design and development of nanoscale drug delivery devices and nanosensors [1]. Over the years, inorganic nanoparticles in particular have been studied due to their unique optical, magnetic, heating, and catalytic properties [2]. In addition to these unique properties, their easy functionalization, high surface to volume ratio, and capability of controlled/targeted delivery make them attractive for biomedical applications. Almost all nanoparticle based bioapplications involves the functionalization of their surface with a targeting agent, drug payload, image contrast agent, and/or a stealth component. Although inorganic nanoparticles can exhibit good stability and dispersion in their initial synthesized form with appropriate surface coatings, agglomeration during biofunctionalization processes via charge neutralization, hydrogen bonding, biomolecular and hydrophobic interactions, etc. is a common issue. In order to avoid agglomeration issues during their functionalization, researchers have employed various nanoparticle stabilizing strategies such as employing covalently attached/physically adsorbed charged capping agents (e.g., anionic carboxylates and sulfates) and neutral steric groups (e.g., polymers/dendrimers, simple carbohydrates, bulky proteins, and DNA) [3-7]. In all of these stabilizing strategies, researchers sacrifice a significant fraction of the valuable nanoparticle surface area to accommodate the stabilizing agent, which leads to lower

drug/biomolecule loading. Also, in spite of the plethora of strategies available for obtaining stabilized nanoparticles, various issues associated with the stabilizing agents (e.g., aggregation in the presence of salts or changes in pH, solubility in aqueous medium, exchange with serum and plasma proteins, lack of *in vivo* suitability and/or stability, etc.) still exist making their translation for bioapplications difficult. These inherent issues present during solution-based biofunctionalization of nanoparticles become amplified when considering a multifunctional nanoparticle for theranostic applications requiring functionalization for stealth, targeting, sensing, and/or delivery.

Herein, we report on a novel strategy to do solution based chemistries in a stabilized matrix to eliminate agglomeration issues during the intermediate steps involved in the biofunctionalization of nanoparticles. This strategy increases the loading capacity of a nanocarrier and also eliminates the use of intermediate stabilizing agents, which eliminates issues that arise in their presence. The methodology in short, deals with the isolation, functionalization, and release (ISOFURE) of nanoparticles/nanocarriers using a composite of the nanoparticle/nanocarrier entrapped in a flexible polymer matrix such as a hydrogel (Figure 7.1A). Stabilization is provided by the entrapment of nanoparticles using the crosslinked hydrogel matrix. The hydrogel swells in the functionalizing medium, allowing for solution-based chemistries to be performed. The polymer matrix physically inhibits interactions between adjacent nanoparticles during functionalization, thereby isolating them and eliminating the need for stabilizing agents. Thus, multiple steps of functionalization at different pH and using different solvents can be then done without concerns associated with agglomeration issues. Once the final step of

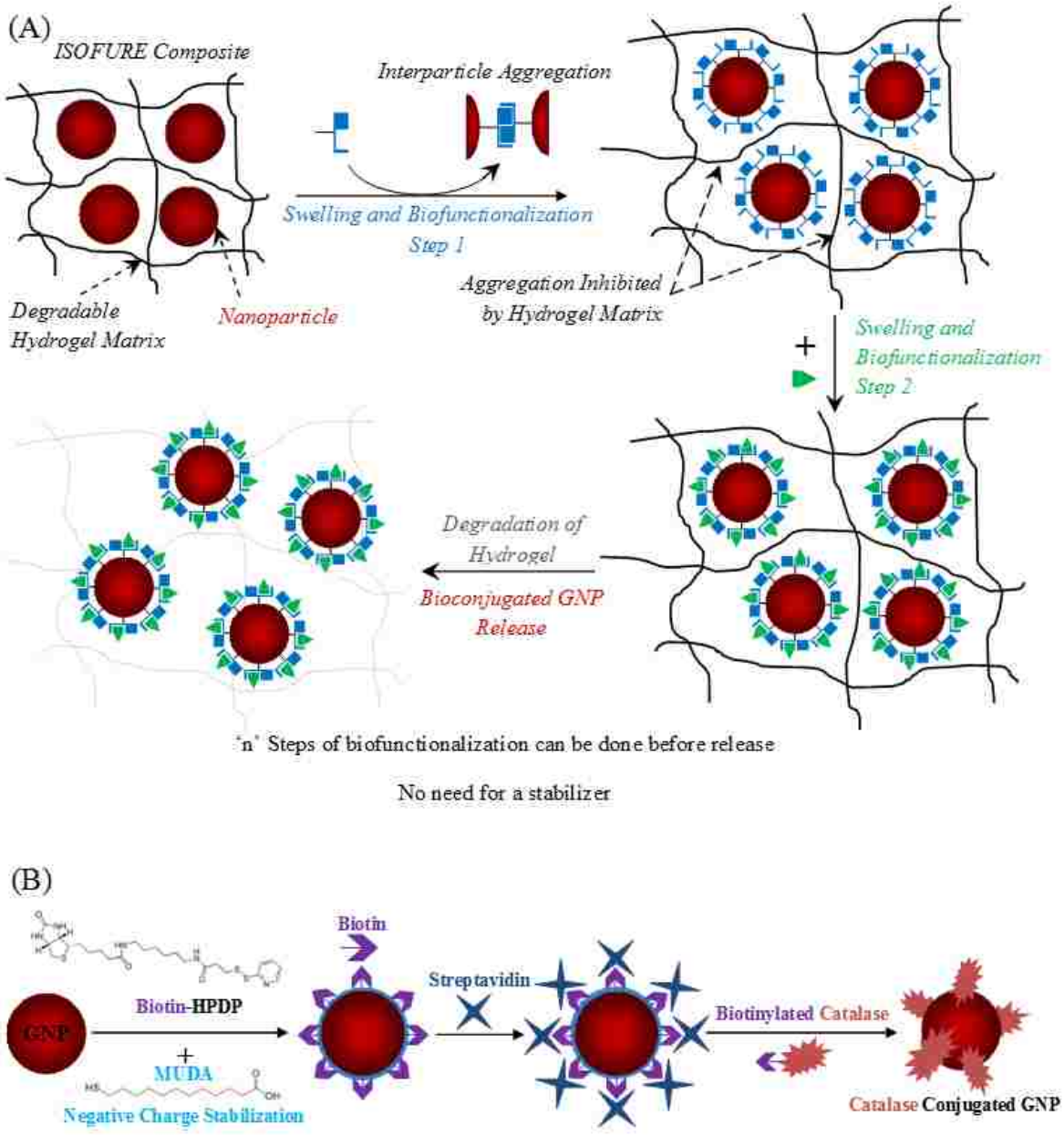

Figure 7.1. Schematic representation of the various steps involved in the novel approach towards enhanced biofunctionalization of nanoparticles in the absence of stabilizing agents using the ISOFURE polymer systems (A), and the bioconjugation of enzyme catalase to GNPs using biotin-streptavidin affinity reactions (B).

functionalization is completed, the stable functionalized nanoparticles are released by simply degrading or dissolving the matrix. This novel ISOFURE strategy is widely applicable due to the inherent ability to choose different polymeric networks, whose properties such as swelling characteristics, mesh size, composition, and degrading trigger, can be tuned to suit various reaction conditions and/or biomolecules.

As a proof of concept, we have initiated our explorations on the ISOFURE strategy using degradable poly(β-amino ester) (PBAE) hydrogel matrices encompassing gold nanoparticles (GNPs). The main objective of our investigation was to examine whether this novel approach can effectively enhance the biomolecular loading of GNPs in the absence of a stabilizing agent. GNPs were used because of their wide applicability and known versatile properties, such as easy synthesis, inertness, and their ability to form functionalized bioconjugates via simple chemistry [8]. They have already been studied extensively for *in vivo* therapeutic applications such as passive targeting [9], active targeting to reduce tumors in mice [10], tumor necrosis factor delivery [11], treatment of colon carcinomas with Paclitaxel grafted gold colloids [12], cellular drug delivery [13-15], gene therapy [16-21], thermoablative therapy [22, 23] and drug release [24-26]. PBAE hydrogels exhibit hydrolytic degradation, allowing for the matrix to be degraded in an aqueous environment. The requirement of fast degradation and significant swelling in solvents governed the selection of the appropriate PBAE system from a combinatorial library of PBAE degradable materials [27]. Herein, the loading of enzyme catalase to GNP surface via biotin-streptavidin affinity interaction was used as the proof of concept model reaction (Figure 7.1B). Other methods of conjugating GNPs with enzyme are also

available (appendix B). Catalase is an antioxidant enzyme that has been studied extensively for potential effectiveness in antioxidative therapy. However, free catalase undergoes rapid elimination from the blood stream and demonstrates poor intracellular delivery [28]. The coupling of catalase to GNPs can potentially increase its half life *in vivo*. Using the PBAE-GNP ISOFURE composites, we have coupled active catalase to GNPs. For comparison, we have also synthesized biotinylated solution-based particles using an acidic thiol as the stabilizing agent. In addition to the elimination of stabilizing agents during functionalization causing an increase in biomolecular loading, the flexibility in choosing an appropriate ISOFURE system for any solution based experimental condition and biomolecule, attracts major interests in the field of nanocarrier functionalization. These methodologies of isolation, functionalization, and release are expected to have a significant impact on future advances in nanocarrier loading for various diagnostic and therapeutic applications.

7.3. Experimental methods

7.3.1. Synthesis of monodispersed gold nanoparticles

Monodispersed gold nanoparticles were prepared using the Turkevich reduction of gold salts [29]. Briefly, a 1 mM aqueous solution of chloroauric acid ($HAuCl_4$; Sigma) was boiled under stirring. To this solution, 3 mM trisodium citrate (Sigma) in water was added to reduce $HAuCl_4$ to produce GNPs of sub-nanometer size. GNPs were then concentrated by centrifuging at 12,500 rpm for 10 minutes using an Accuspin centrifuge (Fisher Scientific), resuspended in dimethyl sulfoxide (Sigma), and used as such for preparing the ISOFURE composite.

7.3.2. Synthesis of H6 macromer

The macromer used for synthesizing the degradable hydrogel matrix was synthesized in accordance to a previous paper (30). The system chosen involved the use of poly(ethylene glycol) 400 diacrylate (Polyscience Inc.; PEG400DA; represented by the letter 'H' from the combinatorial library as represented by Anderson et al [27]) and isobutyl amine (Sigma; IBA; represented by the number '6' from the library) mixed in the molar ratio of 1.2:1 respectively, heated at 85^{o}C for 48 hours, cooled to room temperature, and stored at 4^{o}C.

7.3.3. Synthesis of degradable H6-GNP ISOFURE composite

The hydrolytically degradable GNP entrapped H6 ISOFURE composite was synthesized using free radical redox polymerization between glass plates separated by 1.5 mm thick Teflon spacers. Approximately 1 g of the H6 macromer was mixed with 50 wt % of the above prepared GNPs in DMSO. Then, 1 wt % of tetramethyl ethylene diamine (Sigma; TEMED; 10 mg) was added, and the solution was vortex mixed. To this solution, 1.5 wt % of ammonium persulfate (Sigma; APS; 15 mg) was dissolved in 30 µl of water, added to the above macromer solution, and vortex mixed for approximately 15 s. This solution was then transferred into the glass plate assembly. The plates were allowed to sit at room temperature for 24 hours to ensure complete polymerization. After 24 hours, the removed H6-GNP ISOFURE composite gels were washed in DMSO for about 15 minutes to remove the unreacted components and surface GNPs and then vacuum dried for further usage.

7.3.4. Biotinylation of GNPs in ISOFURE composite

Thiol-gold chemistry was used to incorporate biotin onto the surface of GNPs. For this, a 0.5 mM solution of (*N*-(6-(biotinamido)hexyl)-3'-(2'-pyridyldithio)-propionamide (biotin-HPDP; Soltech Ventures) in dimethyl sulfoxide was made initially. To this, the H6-GNP ISOFURE composite was immersed overnight for biotinylation to occur. The biotinylated composite was then washed with DMSO and vacuum dried for further use. For comparison, GNPs in solution (i.e., not entrapped by the degradable hydrogel; S-GNPs) were treated with biotin-HPDP in DMSO. Since these particles agglomerated with biotinylation, mercaptoundecanoic acid (MUDA; Asemblon) in ethanol was added as a stabilizing agent in ratio to the biotin-HPDP to obtain samples of varying concentrations of surface biotin. For this, the final concentration of MUDA was fixed at 0.5 mM, while biotin-HPDP was added at 50 µM for 1:10 biotin:MUDA S-GNPs, 25 µM for 1:20 S-GNPs and at 5 µM for 1:100 S-GNPs. Both biotin-HPDP and MUDA were added to the stabilized GNPs at the same time, and the reaction was allowed to proceed for approximately 12 hrs. A 100 % MUDA coated GNP was also synthesized as a control sample. All GNPs were dialyzed in 100 mM MES, pH of 5.5 before further use.

7.3.5. Degradation of H6-GNP ISOFURE composite for further biofunctionalization

The degradation of the H6 ISOFURE hydrogel encompassing the biotinylated GNPs (biotin ISOFURE) was performed in an aqueous environment. The biotin ISOFURE gel was cut into smaller pieces and packed inside a 12,000 MWCO dialysis membrane. To this membrane, 2 ml of 100 µM streptavidin in MES was added. The

membrane with its contents of streptavidin and composite gel was immersed in a dialyzing sink of MES. Dialysis was done using three MES buffer changes. Streptavidin (~ 57,000 MW) will not diffuse out of the dialysis membrane. Thus, the biotinylated GNPs were released as the aqueous solution degraded the hydrogel, and they were immediately coated by the surrounding excess streptavidin. The smaller degradation products of the hydrogel were removed via dialysis, leaving only streptavidin coated GNPs. In the case of biotinylated S-GNPs (1:10, 1:20, and 1:100 S-GNPs), 500 µl of the sample was added to 500 µl of 100 µM streptavidin in MES and allowed to react for 4 hours.

7.3.6. Biotinylation of catalase

The biotinylation of catalase was done using succinimide chemistry. Briefly, to a 2 mg/ml catalase (Calbiochem) in 100 mM HEPES buffer of pH 8.0, was added biotin-N-hydroxysuccinimide (BNHS; Vector Labs) at 25 mg/ml in DMSO so that the final concentration of BNHS was 10 wt% of the enzyme to be biotinylated. The mixture was stirred occasionally for 3 hours, after which time 10 µl of 16.4 M ethanolamine was added to stop the reaction by reacting with any free biotin-NHS. The biotinylated catalase was dialyzed against 1 liter of HEPES with three buffer changes.

7.3.7. Coupling of catalase to streptavidin coated GNPs

The streptavidin coated GNPs from both ISOFURE system and solution based particles were centrifuged at 10,000 rpm for 7 minutes and washed with HEPES 3 times to remove any unbound streptavidin. To these particles, biotinylated catalase

(GNP:biotinylated catalase, 3:1 vol%) was added and permitted to bind for 3 hrs at room temperature. The resulting bioconjugated GNPs were centrifuged and washed with HEPES thrice and used for activity assay.

7.3.8. Characterization

Biotinylation, streptavidin coating, and binding of catalase were observed by monitoring the change in the surface plasmon resonance peak using UV-Vis spectroscopy. For the case of the ISOFURE systems, the H6-GNP ISOFURE composite was sandwiched between glass plates, and then scanned for determining the particles surface plasmon resonance peaks. Dynamic light scattering (DLS) and transmission electron microscopy (TEM) were used to observe changes in particle size with conjugation/functionalization. The amount of biotinylation of GNPs was analyzed using the Quant Tag biotin assay kit (Vector Labs). Briefly, 10 µl of biotin standards of varying nmoles of biotin in water and the biotinylated GNP samples (control - non biotinylated MUDA GNPs) were added to a 96 microwell plate. To this a mixture of 100 µl of Quant Tag reagent 1, 100 µl of Quant Tag reagent 2, and 10 µl of reagent 3 are added, and incubated for 45 minutes. The change in absorbance at 535 nm is characteristic of the amount of biotin present in the microwell and can be quantified using the biotin standard microwell absorbance values. The presence of active catalase over the surface of GNPs was determined using the o-phenylene diamine assay (OPD; Sigma). Briefly, the catalase conjugated GNPs were centrifuged, washed, and resuspended in PBS buffer of pH 7.4. To the GNP-catalase, 3 ml of 2 mM H_2O_2 was added. Aliquots of 150 µl were removed at 1 min intervals for 5 min and the reactive oxygen product was assayed using 100 µl of 40

µM OPD and 20 µl of 3 µM horseradish peroxidase (HRP; Calbiochem). The change in absorbance of OPD at 490 nm, characteristic of the quantity of hydrogen peroxide remaining was measured and plotted as a function of time. The rate was calculated from the initial linear phase of the reaction.

7.4. Results and Discussion

7.4.1. Stabilization of biotinylated S-GNPs

The size of monodispersed GNPs used for the synthesis of H6-GNP ISOFURE systems were determined to be around 10 nm using the DLS. The UV-Vis analysis of these particles showed a surface plasmon resonance peak value at 525 nm. Using these parameters, the concentration of GNPs was calculated using the number density relationship equation as described by Haiss et al to about 10 nM [31]. Biotinylation of S-GNPs in suspension (without the presence of an entrapping ISOFURE polymer matrix) was done by adding biotin-HPDP to the GNPs suspended in water. We observed that during biotinylation agglomeration of particles occurred (Figure 7.2A and 7.2B 1:0 S-GNPs). The UV-Vis analysis of biotinylation (result not shown) resulted in a time dependent red shift and subsequent broadening of the GNP SPR peak value from 525 nm to about 683 nm. This is due to the fact that inter-particle hydrogen bonding between the biotin molecules occur leading to their agglomeration and subsequent settling from solution [32].

In order to avoid agglomeration associated with inter-particle hydrogen bonding of biotinylated GNPs, a charge stabilizing organic thiol, MUDA was added in varying

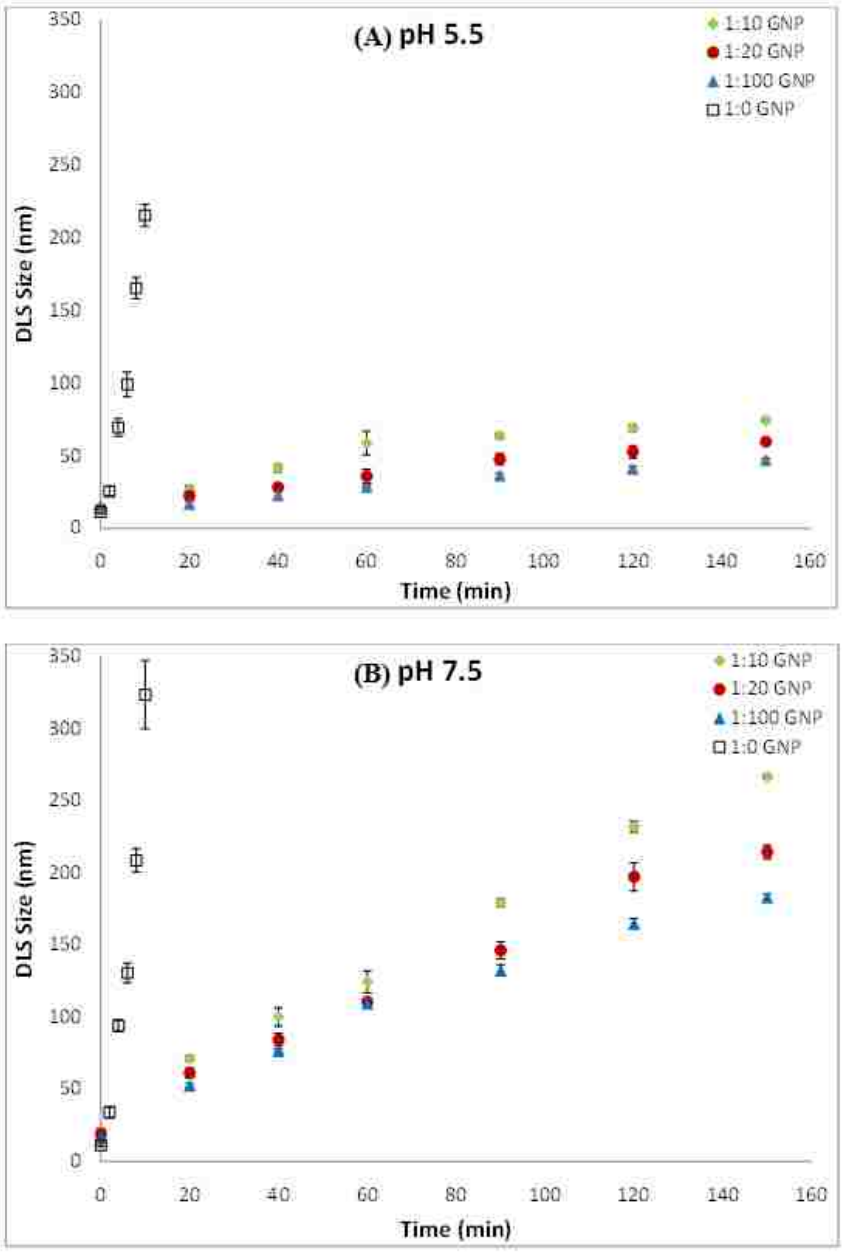

Figure 7.2. Effect of MUDA concentration on stabilizing biotinylated GNPs. DLS data showing the agglomeration of 1:10, 1:20, and 1:100 S-GNPs at pH (A) 5.5 and (B) 7.5 respectively. Also shown is the aggregation data of biotinylated S-GNPs in the absence of MUDA (1:0 S-GNP) for 10 minutes. As the amount of MUDA to biotin increased (1:100 S-GNP>1:20 S-GNP>1:10 S-GNP>1:0 S-GNP), the stability of the particles also increased. *(N=3)*

ratios with respect to biotin-HPDP. We synthesized various S-GNPs containing biotin:MUDA ratios of 1:10, 1:20, and 1:100, along with pure biotinylated S-GNPs. The carboxylic acid group of MUDA provides sufficient repulsion between the nanoparticles at pH greater than its pKa. The stability of biotinylated GNPs with increasing amounts of tethered MUDA was analyzed using the DLS. Figure 7.2 shows the DLS size change of 100 % biotin coated (1:0 S-GNPs for 10 minute period), 1:10, 1:20, and 1:100 biotin:MUDA coated S-GNPs at two different pHs. As observed, the particle size/agglomeration of the GNPs decreased with increasing MUDA or decreasing biotin content. Although a further increase in pH should result in more deprotonation of MUDA molecules and subsequent stabilization of the MUDA stabilized GNPs, we see a reverse effect similar to that as reported by Aslan et al [33]. By comparing the non-MUDA added biotinylated GNPs with that of the 1:10 or 1:20 S-GNPs, the presence of MUDA greatly enhances the stability of biotinylated GNPs. In other words, biotinylated GNPs as such in the absence of any stabilizing agent would agglomerate and result in an increased size change thereby changing their loading properties and applications.

7.4.2. Stabilization and enhanced biotinylation of H6-GNP ISOFURE particles

Biotinylation of GNPs with biotin-HPDP in the H6 ISOFURE system was followed using UV-Vis spectroscopy. As observed from Figure 7.3, the initial H6-GNP ISOFURE composite exhibited a SPR peak value at 530 nm indicating the presence of entrapped particles in the matrix. During biotinylation, biotin-HPDP cleaves at its disulfide bond and yields pyridine-2-thione as a side product. The release of pyridine-2-

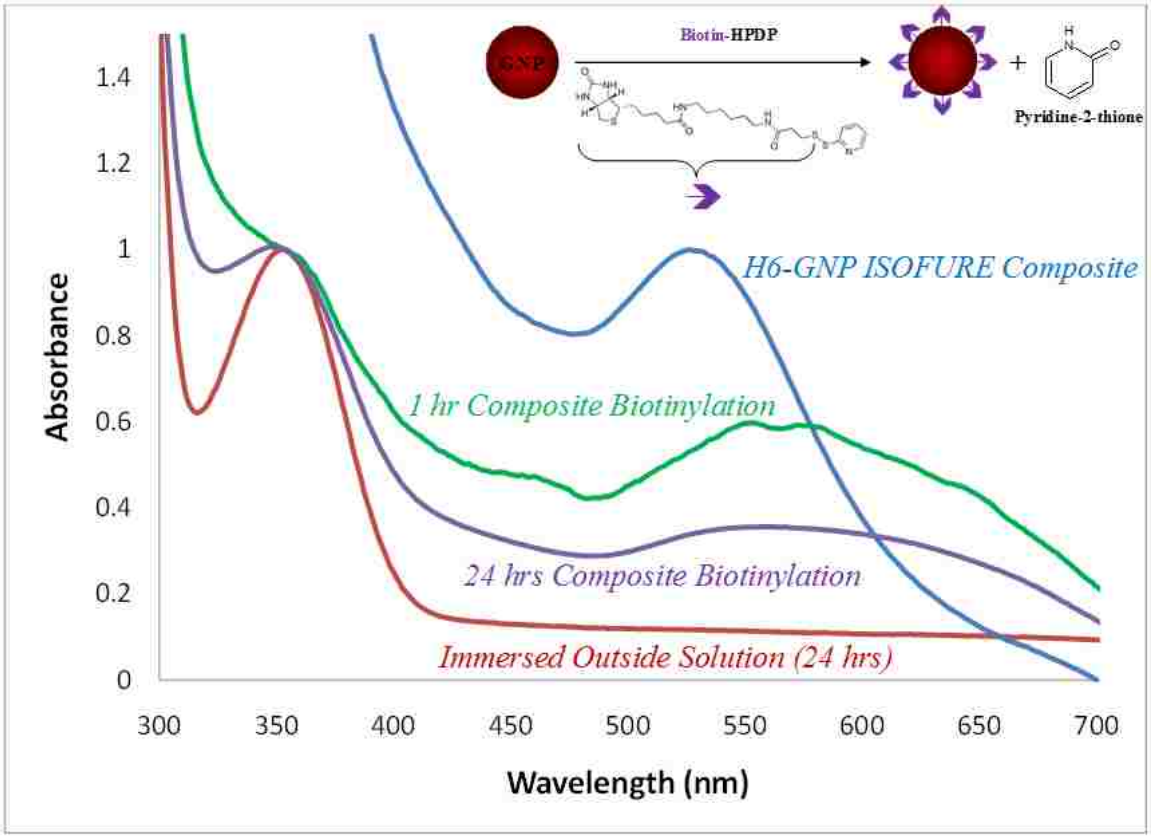

Figure 7.3. UV-Vis spectra showing biotinylation of GNPs in the ISOFURE system as a function of time. The presence of the product pyridine-2-thione peak at 353 nm both in the composite gel and in the solution in which the gel is immersed confirms biotinylation of GNPs.

thione was followed spectrophotometrically at 353 nm to confirm biotinylation. The H6-GNP ISOFURE composite showed the occurrence of 353 nm peak at 1 hour after the addition of biotin-HPDP. A sharper 353 nm absorbance profile at the 24 hour scan period indicated the presence of side product pyridine-2-thione in the gel. This confirmed the cleaving of biotin-HPDP into a thiolated biotin molecule, which readily attached to the GNP surface. Also, most of the pyridine-2-thione was observed to be present in the DMSO solution used for immersing the H6-GNP ISOFURE composite, indicating that they diffused out of the gel with biotinylation time. We observed a slight red shift from 530 nm (H6-GNP ISOFURE) to 542 nm (H6-biotinylated GNP ISOFURE) indicating slight amount of agglomeration in 24 hours similar to that of the S-GNPs. Although this shift shows agglomeration, when compared to the biotinylated S-GNPs, the ISOFURE particles were physically entrapped enough to avoid agglomeration of too many particles, thereby making this system highly capable of functionalizing particles in the absence of any stabilizing agent (e.g., MUDA).

The presence of biotin over the surface of the particles was also confirmed by using the Quant Tag assay kit. Table 7.1 shows the nmoles of biotin attached to the S-GNPs, and also the ISOFURE system GNPs. In the absence of the physically stabilizing hydrogel matrix, the hydrogel degraded biotinylated ISOFURE GNPs agglomerated similar to the zero MUDA added aggregating 1:0 S-GNPs. Both these particles were sonicated prior to Quant Tag assay. It is observed from Table 7.1 that as the stability of particles increased with the addition of MUDA, the amount of biotin also decreased as expected. Also, the amount of biotin coated to the ISOFURE system GNPs is similar to

Table 7.1. Quant tag assay data showing the nmoles of biotin attached to the surface of various GNP samples (both S-GNPs and ISOFURE system GNPs). * indicates that the aggregating particles were sonicated before quant tag assaying and the final values were obtained based on GNP concentration calculations.

Biotinylated GNP Sample	Amount of Biotin over GNP (nmoles)
1:100	0.7
1:20	3
1:10	5
1:0	44*
ISOFURE GNPs	47*

that of the non MUDA stabilized 100 % biotinylated 1:0 S-GNPs indicating that both are coated with biotin in a similar fashion. Also, the amount of biotin over the ISOFURE GNPs are relatively higher than that of the 1:10 S-GNPs, proving that enhanced biotinylation can be achieved using the ISOFURE system protocol. For studying the use of ISOFURE systems for further biofunctionalization, streptavidin was used to coat the biotinylated ISOFURE GNPs devoid of stabilizing agent MUDA. Also, in order to avoid issues of particle aggregation at higher standing periods, streptavidin coating of the MUDA stabilized biotinylated GNPs was carried out.

7.4.3. Demonstration of streptavidin binding to biotinylated GNPs

The high biomolecular affinity between biotin and avidin was harnessed to introduce streptavidin to the surface of biotinylated GNPs. To avoid any issues related with the deactivation of streptavidin in a non-aqueous medium and its slow/non-diffusion through the H6 ISOFURE hydrogel matrix due to its relatively larger molecular size, streptavidin was added along with the degrading medium, water inside the dialyzing membrane. As the hydrogel matrix degraded, the biotinylated GNPs released and were readily available for binding with streptavidin. Also, the degradation of the hydrogel matrix results in the opening/increasing the mesh size, thereby allowing unbound streptavidin to diffuse through the degrading hydrogel and bind with biotinylated GNPs. Streptavidin has four binding sites with a molecular size of 5 nm [34]. Based on the available surface area of a 10 nm sized GNP, a theoretical maximum of ~16 streptavidin molecules can coat a biotinylated GNP. In other words, for a 10 nM concentration of GNP solution that is biotinylated, hypothetically a 160 nM streptavidin concentration is

needed for coating all GNPs. The reactive availability/affinity of biotinylated GNP to undergo biomolecular binding to streptavidin was analyzed using UV-Vis spectroscopy. From Figure 7.4, it was observed that the SPR peak value at H6-ISOFURE biotinylated GNPs shifted from 538 nm (1:20 S-GNPs show and SPR peak value at around 532 nm) before streptavidin attachment to 540 nm after 24 hours of degradation followed by streptavidin binding to the surface biotin. Further, as shown in the bottom inset, the particles remained in suspension similar to that of the 1:10 or 1:20 S-GNPs.

Low concentration of streptavidin (9 nM) was added to the dialyzing membrane containing the H6-ISOFURE biotinylated GNP composite. Since the concentration of available biotin binding sites (36 nM available biotin binding sites) from the added streptavidin concentration (9 nM) is relatively lower than the theoretical total concentration of biotinylated GNPs, it should result in crosslinking between the biotinylated GNPs (with streptavidin being the crosslinker). Figure 7.4 shows a similar result, wherein, crosslinking between the biotinylated particles occurred in the presence of low streptavidin concentration, thereby aggregating to larger sized particles and exhibiting an SPR peak value at 648 nm. Settling of crosslinked aggregated particles occurred leaving a clear solution on the top (top inset). This confirmed the availability of biotin over the surface of GNPs for coupling with biotinylated catalase via intermediate streptavidin binding. However, the agglomeration under these low streptavidin concentrations precluded them for use for catalase coupling. Using excess streptavidin (100 μM), the streptavidin concentration was high enough to coat the entire biotinylated surface of GNPs, thereby minimizing interparticle biotin-streptavidin crosslinking. These

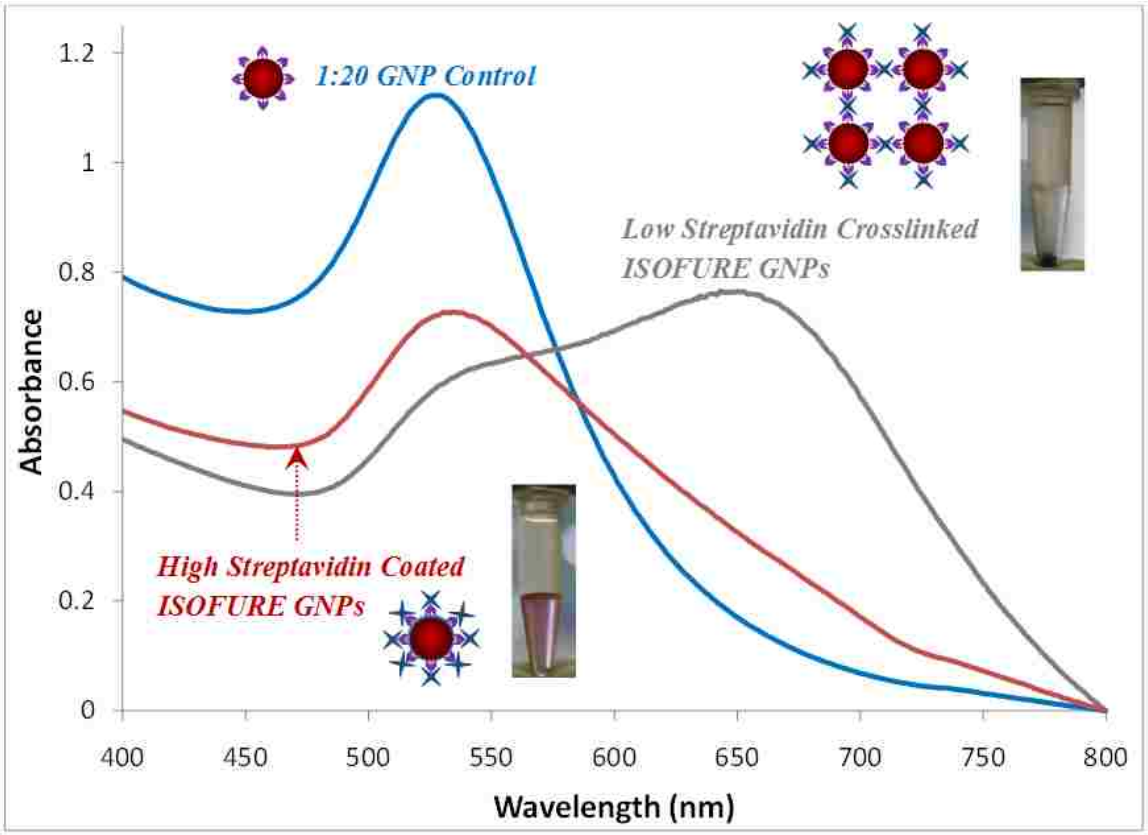

Figure 7.4. UV-Vis spectra showing the crosslinking of biotinylated ISOFURE GNP in the presence of low streptavidin concentration (9 nM) confirming biotin-streptavidin interaction. Also shown is the non-crosslinked high concentration streptavidin (100 µM) coated biotinylated ISOFURE GNP spectrum. Inset images show the dispersed high streptavidin coated biotinylated ISOFURE GNPs and the settled low streptavidin crosslinked biotinylated ISOFURE GNPs.

streptavidin coated GNPs were then dialyzed to remove excess streptavidin and treated with biotinylated catalase (Quant Tag biotin assay gave a value of 128 nmoles of biotin/mg of catalase). Similar to the binding between the biotin of the biotinylated GNP and streptavidin, binding between the binding sites of streptavidin and the biotin in biotinylated catalase was used for introducing the enzyme to the particle surface.

7.4.4. Enhanced biomolecular loading of active catalase over ISOFURE system GNPs

The streptavidin coupled catalase-GNPs (both solution-based and degraded ISOFURE system biotinylated GNPs) were assayed for catalase activity by measuring the oxidation of OPD at 490 nm in the presence of H_2O_2 and horse radish peroxidase. One unit of catalase activity (U) is defined as the amount of enzyme cleaving 1 μmol of H_2O_2 in one minute. The activity of catalase was 44350 U and 41600 U before and after biotinylation, respectively, showing that biotinylation as such did not cause a significant loss in enzymatic activity. Muzykantov and his group observed similar results of no change in activity with biotinylation [35]. Table 7.2 shows the activity data for catalase bound to the surface of streptavidin coated ISOFURE system released GNPs for increasing amounts of biotinylated catalase available for binding. Non-biotinylated catalase was used as control. Negligible non-specific adsorption of catalase to streptavidin coated GNPs was noticed. As the amount of biotinylated catalase increased, more of the biotin binding sites from the coated streptavidin were bound with biotinylated catalase, thereby increasing the activity. This increase in activity subsequently leveled off presumably due to the saturation of GNP surface with catalase.

Table 7.2. Increased activity of the biotin-streptavidin bound catalase to GNPs with increasing amounts of biotinylated catalase added to streptavidin coated ISOFURE system based biotinylated GNPs. Data shown till saturation of the GNPs with catalase.

Concn. of Biotinylated Catalase	**Catalase Activity** (μU/GNP)
8 μM (non-biotinylated; control)	~0.08
0.5 μM	2.3
1 μM	16
2 μM	69
6 μM	322
8 μM	327

Therefore, biomolecular loading of ISOFURE system based particles can be done with ease.

In order to study the effect of using a physical entrapping matrix instead of stabilizing agents on biomolecular loading, biotinylated S-GNPs (1:10, 1:20, and 1:100) were also treated with the same amount of biotinylated catalase. Recent results in another work involving GNPs conjugated catalase showed that the coupling of biotinylated catalase to streptavidin coated GNPs had no loss in activity of the enzyme with binding (36). Briefly, 20 µl of biotinylated catalase (2 mg/ml; 41600 U) was treated to streptavidin coated 1:20 S-GNPs. The activity of the free unbound catalase in the supernatant and bound catalase to the GNP pellet after centrifugation and washing was determined to be 15575 U and 25600 U (16 µU/GNP) respectively. Their combined activity adds to a total of 41175 U, which is close to the enzyme activity of biotinylated catalase. So, the binding of biotinylated catalase to GNPs via biotin-streptavidin binding did not result in any significant loss of enzymatic activity. Table 7.3 shows the activity for the different catalase bound particles with no streptavidin coated 1:10 S-GNP as the control. As expected, the absence of streptavidin resulted in negligible enzymatic binding. With increasing amounts of MUDA, the activity of catalase decreased from 118 µU/GNP for 1:10 S-GNP to12 µU/GNP for 1:100 S-GNP. This can be attributed simply to the fact that there is less biotin with increasing amounts of MUDA. Based on theoretical approximations, the total surface area of a 1:10, 1:20, and 1:100 S-GNPs occupied by biotin is 29 nm^2, 15 nm^2, and 3 nm^2 respectively. By decreasing the MUDA content, one can achieve increased particle bound enzymatic activity, but it is at the

Table 7.3. Increased catalase activity of S-GNPs with increasing amounts of particle surface area occupied by biotin (decreasing amounts of MUDA used). The ISOFURE system based biotinylated GNPs devoid of any MUDA shows maximum catalase activity confirming enhanced biofunctionalization.

Streptavidin GNPs + 8 µM Biotinylated Catalase	**Catalase Activity** (µU/GNP)
1:10 (no streptavidin; control)	~0.05
1:100	12
1:20	64
1:10	109
ISOFURE GNPs	327

expense of particle stability (Figure 7.2). In the case of ISOFURE system entrapped GNPs, the total surface area occupied by biotin is approximately around 315 nm^2. With the particles being stable inside the matrix and readily available for binding with streptavidin on their release with hydrogel degradation, the entire 315 nm^2 surface area is available for binding with excess streptavidin. This further maximizes the number of biotin binding sites from the streptavidin molecule available for loading biotinylated catalase. This effect is observed from table 7.3, where the activity of catalase/GNP of the ISOFURE system based GNPs is comparatively much higher than the 1:10 S-GNPs. Generalizing, the biomolecular loading of a nanocarrier can be enhanced greatly by eradicating the need for a stabilizing agent. The application of a matrix to provide physical stabilization during the functionalization of nanoparticles eliminates the need for stabilizing agents during intermediate steps and increases biomolecular loading. This novel strategy is of great interest and can be widely applied to functionalize nanoparticles with various biomolecules.

7.5. Conclusion

Herein, our novel ISOFURE strategy for enhanced biomolecular loading on nanoparticle systems was demonstrated using a biodegradable hydrogel and gold nanoparticles as model systems. The strong biomolecular binding between biotin and streptavidin was applied to couple catalase to gold nanoparticles as the model reaction. DLS showed that the interparticle aggregation caused by hydrogen bonding between the biotin molecules decreased with increasing concentrations of the stabilizing agent MUDA. The biotinylation of both solution-based S-GNPs and ISOFURE system GNPs

was accomplished using biotin-HPDP. The crosslinking of biotinylated particles in the presence of low streptavidin concentration indirectly confirmed the bioavailability of biotin. The OPD assay confirmed the presence of active catalase over GNPs. Increasing amounts of biotinylated catalase used for binding resulted in increased activity of catalase until saturation was reached. The activity of ISOFURE system GNPs were much higher than that of the MUDA stabilized 1:10 or 1:20 or 1:10 S-GNPs. This method of isolation, functionalization, and release (ISOFURE) shows great promise for loading various biomolecules to nanocarriers under flexible experimental conditions.

7.6. References

1. Yokoyama M, Okano T. Targetable drug carriers: present status and a future perspective. *Adv Drug Delivery Rev* **1996,** 21, 77-80.
2. Xu ZP, Zeng QH, Lu GQ, Yu AB. Inorganic nanoparticles as carriers for efficient cellular delivery. *Chem Engg Sci* **2006,** 61, 1027-1040.
3. Kattumuri V, Katii K, Bhaskaran S, Boote EJ, Casteel SW, Fent GM, Robertson DJ, Chandrasekhar M, Kannan R, Katti KV. Gum Arabic as a phytochemical construct for the stabilization of gold nanoparticle: In vivo pharamacokinetics and X-ray-contrast-imaging studies. *Small* **2007,** 3, 333-341.
4. Zhao W, Lee TMH, Leung SSY, Hsing I-M. Tunable stabilization of gold nanoparticles in aqueous solutions by mononucleotides. *Langmuir* **2007,**23, 7143-7147.
5. Ghosh A, Patra CR, Mukherjee P, Sastry M, Kumar R. Preparation and stabilization of gold nanoparticles formed by in situ reduction of aqueous

chloroaurate ions within surface-modified mesoporous silica. *Microporous and Mesoporous Mater* **2003,** 58, 201-211.

6. Majzik A, Patakfalvi R, Hornok V, Dekany I. Growing and stability of gold nanoparticles and their functionalization by cysteine. *Gold Bulletin* **2009,** 42, 113-123.
7. Stakeborg T, Peeters S, Reekmans G, Laureyn W, Jans H, Borghs G, Imberechts H. Increasing the stability of DNA-functionalized gold nanoparticles using mercaptoalkanes. *J Nanoparticle Res* **2008,** 10, 143-152.
8. Chirra HD, Biswal D, Hilt JZ. in *Nanoparticulate Drug Delivery Systems (NPDDS) II: Formulation and Characterization,* eds Pathak Y, Thassu D (Informa Healthcare USA Inc.) **2009,** pp 90-114.
9. Moghimi SM, Hunter AC, Murray JC. Nanomedicine: Current status and future prospects. *FASEB J* **2005,** 19, 311-330.
10. Dixit V, Bossche J, Sherman DM, Thompson DH, Andres RP. Synthesis and grafting of thioctic acid-PEG-folate conjugates onto Au nanoparticles for selective targeting of cancer cells. *Bioconjugate Chem* **2006,** 17, 603-609.
11. Chen Y-H, Tsai C-Y, Huang P-Y, Chang M-Y, Cheng P-C, Chou C-H, Chen D-H, Wang C-R, Shiau A-L, Wu C-L. Methotrexate conjugated to gold nanoparticles inhibit tumor growth in a synergestic lung tumor model. *Mol Pharmaceutics* **2007,** 4, 713-722.
12. Gibson JD, Khanal BP, Zubarev ER. Paclitaxel functionalized gold nanoparticles. *J Am Chem Soc* **2007,** 129, 11653-11661.

13. Hone DC, Walker PI, Evans-Gowing R, FitzGerald S, Beeby A, Chambrier I, Cook MJ, Russell DA. Generation of cytotoxic singlet oxygen via phthalocyanine stabilized gold nanoparticles: a potential delivery vehicle for photodynamic therapy. *Langmuir* **2002,** 18, 2985-2987.
14. Saito G, Swanson JA, Lee K-D. Drug delivery strategy utilizing conjugation via reversible disulfide linkages: role and site of cellular reducing activities. *Adv Drug Delivery Rev* **2003,** 55, 199-215.
15. Sapsford KE, Berti L, Mendintz IL. Materials for fluorescence energy transfer analysis: beyond traditional donor acceptor combinations. *Angew Chem Int Ed* **2006,** 45, 4562-4589.
16. Lee J-S, Green JJ, Love KT, Sunshine J, Langer R, Anderson DG. Systemic intracellular delivery of siRNA using gold nanoparticles and poly(β-amino ester)s. *Nano Lett* **2009,** 9, 2402-2406.
17. Han G, Martin CT, Rotello VM. Stability of gold nanoparticle bound DNA towards biological, physical, and chemical agents. *Chem Biol Drug Des* **2006,** 67, 78-82.
18. Sandhu KK, McIntosh CM, Simard JM, Smith SW, Rotello VM. Gold nanoparticle mediated transfection of mammalian cells. *Bioconjugate Chem* **2002,** 13, 3-6.
19. Thomas M, Klibanov AM. Conjugation to gold nanoparticles enhances polyethyleneimines transfer of plasmid DNA into mammalian cells. *Proc Natl Acad Sci USA* **2003,** 100, 9138-9143.

20. Rosi NL, Giljohann DA, Thaxton CS, Lytton-Jean AKR, Han MS, Mirkin CA. Oligonucleotide modified gold nanoparticles for intracellular gene regulation. *Science* **2006,** 312, 1027-1030.
21. Verma A, Simard JM, Worrall JWE, Rotello VM. Tunable reactivation of nanoparticle inhibited β galactosidase by glutathione at intracellular concentrations. *J Am Chem Soc* **2004,** 126, 13987-13991.
22. Hirsch LR, Stafford RJ, Bankson JA, Sershen SR, Rivera B, Price RE, Hazle JD, Halas NJ, West JL. Nanoshell mediated near infrared thermal therapy of tumors under magnetic resonance guidance. *Proc Natl Acad Sci USA* **2003,** 100, 13549-13554.
23. Hirsch LR, Jackson JB, Lee A, Halas NJ, West JL. A whole blood immunoassay using gold nanoshells. *Anal Chem* **2003,** 75, 2377-2381.
24. Radt B, Smith A, Caruso F. Optically addressable nanostructured capsules. *Adv Mater* **2004,** 16, 2184-2189.
25. Angelatos AS, Radt B, Caruso F. Light responsive polyelectrolyte/gold nanoparticle microcapsules. *J Phys Chem B* **2005,** 109, 3071-3076.
26. West JL, Halas NJ. Applications of nanotechnology to biotechnology. *Curr Opin Biotechnol* **2000,** 11, 215-217.
27. Anderson DG, Tweedie CA, Hossain N, Navarro SM, Brey DM, Vliet KJV, Langer R, Burdick JA. A combinatorial library of photocrosslinkable and degradable materials. *Adv Mater* **2006,** 18, 2614-2618.
28. Kozower BD, Christopher-Solomidou M, Sweitzer TD, Muro S, Buerk DG, Solomides CC, Albelda SM, Patterson GA, Muzykantov VR. Immunotargeting of

catalase to the pulmonary endothelium alleviates oxidative stress and reduces acute lung transplantation injury. Nat Biotechnol **2003,** 21, 392-398.

29. Turkevich J, Stevenson PC, Hillier J. A study of nucleation and growth process in the synthesis of gold colloids. *Faraday Discuss* **1951,** 11, 55-75.
30. Hawkins AM, Satarkar NS, Hilt JZ. Nanocomposite degradable hydrogels: demonstration of remote controlled degradation and drug release. *Pharm Res* **2009,** 26, 667-673.
31. Haiss W, Thanh NTK, Aveyard J, Fernig DG. Determination of size and concentration of gold nanoparticles from UV-Vis spectra. *Anal Chem* **2007,** 79, 4215-4221.
32. Strzelczyk AA, Dobrowolski JC, Mazurek AP. On the confirmation of biotin molecule. *J Molec Struc (Theochem)* **2001,** 541, 283-290.
33. Aslan K, Perez-Luna PH. Quenched emission of fluorescence by ligand functionalizaed gold nanoparticles. *Langmuir* **2002,** 18, 6059-6065.
34. Scouten WH, Konecny P. Reversible immobilization of antibodies on magnetic beads. *Anal Biochem* **1992,** 205, 313-318.
35. Muzykantov VR, Atochina EN, Ischiropolous H, Danilov VM, Fisher AB. Immunotargeting of antioxidant enzyme to the pulmonary endothelium. *Proc Natl Acad Sci USA* **1996,** 93, 5213-5218.
36. Chirra HD, Sexton T, Biswal D, Hersh LB, Hilt JZ. submitted in *Bioconjug Chem.* **2010.**

CHAPTER 8

Conclusions and future work

8.1. Conclusions

This dissertation was focused on the development of innovative methods for the integration of a wide variety of polymer networks over gold surfaces. Due to the significant advantages associated with the use of crosslinked polymeric networks over linear polymeric brushes such as tunable mesh size, tunable transport of molecular species into and out of the matrix, entrapment and manipulation of cells, and controlled drug delivery applications, crosslinked responsive hydrogels were used as the polymeric systems. Gold was specifically chosen as the model surface since it exhibits properties of relative non-toxicity, inertness, and easy functionalization via thiol-gold chemistry. In addition to polymeric networks, the functionalization of gold surfaces with biomolecules was also studied.

Initially, the development of a flexible platform for the controlled growth of hydrogel nanostructures on planar gold surface was presented. Temperature responsive hydrogel systems composed of poly(N-isopropyl acrylamide) (PNIPAAm) polymer backbone crosslinked using poly(ethylene glycol) n dimethacrylate (PEGnDMA) crosslinkers of varying molecular weight were synthesized. Microcontact printing proved to be a useful soft lithographic tool that provided precise two-dimensional XY planar control at the microscale. Surface-initiated atom transfer radical polymerization (ATRP) was successfully used to produce various PNIPAAm hydrogel structures with controlled

Z thickness at the nanoscale. The ability to synthesize intelligent hydrogel platforms at the nanometer scale holds significant promise for sensing and actuation in diagnostic and therapeutic applications, where hydrogel thin film actuators may manipulate the transportation, diffusion, entrapment, reaction, and detection of a multitude of biomolecules.

Both AFM and quartz crystal microbalance with dissipation were then used to visually observe the structural and thickness changes that originated from the thermo-responsive property of the PNIPAAm backbone in the hydrogel nanostructures. As expected, the hydrogel exhibited a collapsed state at higher temperatures and a swollen state at lower temperatures. An increase in crosslinking density of the hydrogel led to the decrease in volume swelling ratio of the hydrogel. The 'bulk' nanoscale patterns demonstrated a broad transition of about 10-13^{o}C, while the pattern surfaces observed through RMS roughness analysis exhibited a sharper transition of around 2-3^{o}C. For the same response cycle, higher molecular weight PEG600DMA crosslinked hydrogels showed faster equilibrium response than the lower molecular weight PEG400DMA crosslinked hydrogels. The fundamental understanding of the response properties of surface tethered hydrogel thin films is significant and holds promise in augmenting the various biomedical applications that require 'instantaneous' sensing and controlled drug delivery.

Although the use of planar gold as a prime material for devising both implantable drug delivery devices and rapid point of care biosensors is relatively new, the use of gold

nanoparticles (GNPs) for biomedical research is significantly established. But the issues of stability, aggregation during functionalization, and relatively low biomolecular loading hinder its progress into the clinical world. To overcome these barriers, this dissertation also presents the novel ISOFURE methodology, which deals with the ISOlation of nanoparticles using a crosslinked polymer matrix, FUnctionalization of the particulates inside the physically entrapping matrix, and finally the RElease of the functionalized nanocarriers via degradation of the polymer matrix. As a model platform, GNP-poly(β-amino ester) (GNP-PBAE) hydrogel nanocomposites were synthesized to which, biotinylation was carried out in the absence of an anionic carboxylic acid stabilizing agent. Streptavidin coating of the biotinylated GNPs was done by releasing the particles via degradation of the PBAE matrix in an aqueous streptavidin medium. Biotin-streptavidin affinity was successfully used to tether enzyme catalase to the surface of the modified GNPs. Increasing amounts of biotinylated catalase resulted in increased activity of catalase until saturation was reached. Comparison of the activity of ISOFURE-GNP-catalase with the solution based S-GNP-catalase showed that ISOFURE method resulted in enhanced biomolecular loading/functionalization of the GNP surface. This novel ISOFURE technique holds promise for loading various biomolecules to nanocarriers under flexible experimental conditions.

The ISOFURE technique was also used to synthesize ATRP grown responsive PINPAAm hydrogel shells over GNPs. In addition to the standard way of mixing GNPs with PBAE prepolymer solution prior to redox polymerization, an alternate approach of synthesizing GNP-PBAE composites via in-situ precipitation was also presented. This

new approach eliminated issues associated with the agglomeration of GNPs during centrifugation for solvent exchange and partial degradation of the PBAE matrix in the presence of residual water. Light scattering analysis of the particles at increasing temperatures showed that the particles exhibited temperature sensitivity. Aging/stability studies using the UV-Vis spectrophotometer showed that the hydrogel coated GNPs synthesized via ISOFURE technique exhibited higher stability than the S-GNPs. Also, the yield of monodispersed hydrogel coated GNP was higher in the case of the ISOFURE system as compared to that of the S-GNPs. In addition to enhanced particulate loading, the ISOFURE strategy shows promise for increasing the stability of functionalized or polymer coated nanoparticles.

8.2. Future work

The work described in this dissertation covers several studies that are expected to lead to many possible advanced projects. These will hopefully one day prove useful to the clinical community for treating patients who require rapid on-the-go diagnosis and treatment. Potential future work based on this work may include:

- Growing nanopatterns of responsive hydrogels over microdevices such as microcantilevers and microresonators for rapid biosensing applications,
- Growing responsive hydrogel nanopatterns in implantable micropumps and microreservoirs for instantaneous drug delivery applications,
- Functionalization of in-situ precipitated GNPs in responsive, hydrogel microarrays with biomolecules that detect a recognitive agent and subsequently change the microenvironment of the responsive hydrogel for microoptics,

- Use of other hydrogel systems such as molecular imprinted hydrogels and degradable hydrogels for device based applications,
- Study cell-cell and cell-surface interactions by using microcontact printed and ATRP grown responsive hydrogel nanopatterns,
- Use the ISOFURE methodology for the controlled synthesis of in-situ precipitated iron oxide nanoparticles that find applications in variety of treatments including hyperthermia,
- Design and development of novel polymeric systems that degrade to specific external stimuli or in the presence of a specific reagent (e.g. peptidase degradation) so that they can be used for aqueous based chemistries in ISOFURE systems, and
- A prospective study on the use of ISOFURE technique for the entrapment of cellular organisms, observe their characteristics under different microenvironments, functionalize/modify their structure, and release them for use as vaccines.

APPENDIX A

Synthesis of PDMS stamps via replica molding

A.1. Summary

For the fabrication of hydrogel nanopatterns over gold surfaces microcontact printing was employed followed by atom transfer radical polymerization. Microcontact printing uses a poly(dimethoxy silane); PDMS stamp for printing patterns over the surface. Herein, the synthesis of PDMS stamps using replica molding is highlighted. Initial fabrication of a silicon master chip via UV photolithography is also discussed in detail. Characterization of the silicon master chip and the PDMS stamp was done using scanning electron microscopy and atom force microscopy. Both these techniques confirmed that the stamp had features as required for microcontact printing of a thiol over gold surfaces.

A.2. Introduction

In the last couple of decades, hydrogels have attracted a great deal of attention, and significant progress has been made in designing, synthesizing, and using these materials in tissue engineering, drug delivery, and bionanotechnology. Hydrogels have been incorporated as integral components in microdevices, using photolithography, molding, or other approaches. The field of soft lithography has been demonstrated for fabricating high quality micro- and nanostructures, without having the continuous need for the laborious photolithography techniques. Microcontact printing (μCP) is a simple technique for producing well defined self assembled monolayer patterns on different surfaces. μCP utilizes an inked, micropatterned stamp to print/pattern chemicals or

biomolecules onto a substrate [1]. This technique is applicable to several types of inks and substrate, such as chemisorbing molecules onto metal or oxide surface [2, 3], reactants printed onto organic layers [4], and protein transferred to silicon or glass surfaces [5]. Microcontact printing of alkanethiols onto gold is one of the widely studied of soft lithographic techniques. In addition to its potentially high resolution (<100 nm) [6], this ink-substrate system represents a scientifically rich and technologically convenient model system. The reaction between gold and thiol supplied by the stamp causes the covalent assembly of a monolayer of thiols on the metallic substrate.

Super-hydrophobic/super-hydrophilic patterning would be crucial because it is applicable for the control of liquid flow and the immobilization of functional materials into specific areas. Several groups have previously explored the patterning of hydrogels. Sheppard et al. [7] and Yu et al. [8] patterned hydrogels for pH sensitive components and biomedical applications. Tu et al. [9] fabricated patterned polymer brushes on silica surfaces by μCP followed by surface initiated polymerization. Patterned and releasable polymeric microparticles were fabricated for drug delivery applications and as platforms for the construction of multi-functional drug delivery devices by Guan et al. [10]. Most of these methods are gaining much importance in the biomedical fabrication field, for their versatility in achieving specific shapes of hydrogels at the micro- and nanoscale.

By controlling the spatial patterning of the hydrogels, it is possible to synthesize flexible platforms over the surfaces and using the response behavior, these gels can be employed as functional components of various biomedical micro- and nanodevices. Herein, we highlight the synthesis of a poly(dimethoxy silane); PDMS stamp from a

silicon master chip using replica molding. Self assembly of a hydrophobic thiol via microcontact printing using the PDMS stamp and its characterization is also addressed.

A.3. Experimental Procedure

A.3.1. Fabrication of silicon master chips using UV-photolithography

The patterned master chips used for μCP were prepared by UV photolithography using Karl Suss MJB3 Mask Aligner. Silicon wafers (Virginia Semiconductors. Inc.) were cut to the necessary shape and size using a diamond scribe. The samples were then washed with acetone and DI water and subsequently dried. The samples were preheated at 100^{o}C for 2 min. Spin coating of SU-8 (a negative photoresist; Microchem Corp.) was then done for 30 s at 2000 rpm. The thickness of the microstructure can be varied depending on the speed and the type of SU-8 used. The spin coated sample was then soft baked at 70^{o}C for 3 min and at 100^{o}C for 7 min. The hot sample was cooled at ambient conditions for 3 min. It was then exposed to UV light of intensity 17.5mW/cm^{2} and wavelength of 365 nm for 15 s. The photomask used for photolithography was also washed initially with acetone, isopropyl alcohol (IPA), and DI water. Post baking of the exposed sample was carried out for 1 min at 70^{o}C and for 3 min at 100^{o}C. The dried and photopatterned sample was then developed using SU-8 developer for 4 min followed by IPA and DI water wash, each for 1 min. The washed sample was then dried with nitrogen. Figure A.3.1 shows a schematic representation for the fabrication of Si master chips. Patterns of different square sizes and thickness were produced on the Si surface by changing the spin speed and baking time.

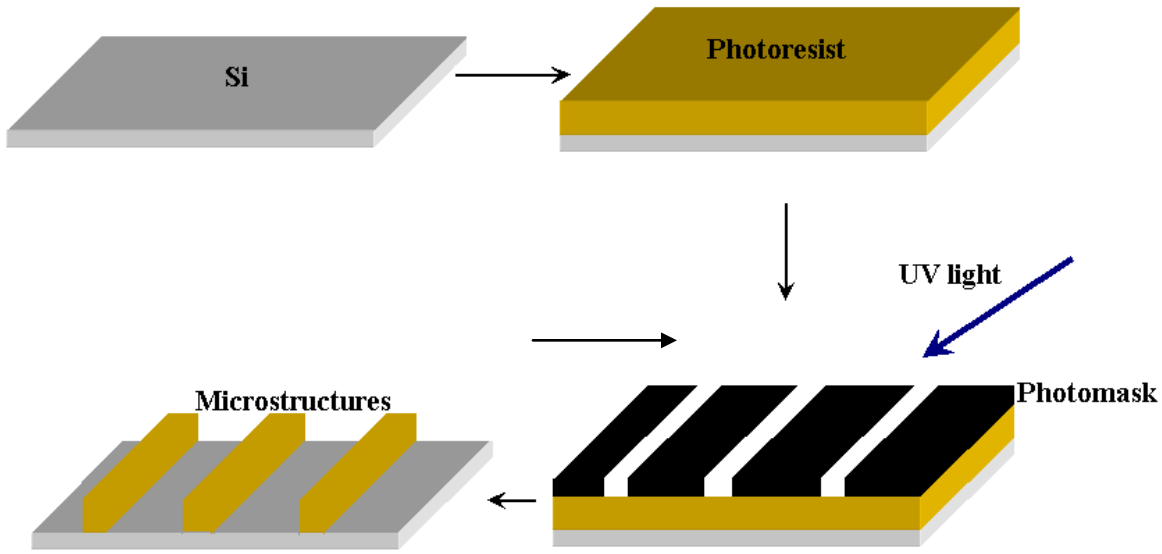

Figure A.3.1. UV Photolithography scheme

A.3.2. Synthesis of PDMS stamps by replica molding

After fabrication of the master, elastomeric poly (dimethylsiloxane) (PDMS) stamps with different square size features were fabricated from the Si master chips. The micropatterned master chip was replicated with 10:1 mixture of Sylgard 184 elastomer/curing agent (Dow Corning, Midland, MI). The PDMS stamp was cured at 100^{o}C for 1h in a circular mold. The PDMS stamp contains the reverse feature of the master chips, from which it was fabricated. A pattern opposite to the microstructures as present on the silicon master stamps is obtained (figure A.3.2).

A.3.3. Microcontact printing over gold and silicon surfaces

The gold surface used for the experiment obtained from Platypus Technology (Madison, WI) was an electron beam deposited gold film (ca. 1000^{o}A) over titanium layer on silicon wafer. Gold samples were cleaned initially with acetone and water to remove any residual dirt over the wafers and were then dried. A 4 mM solution of 1-octadecane thiol (ODT; hydrophobic) in ethanol was prepared. The PDMS stamp containing squares as the microstructures was treated with the ODT solution, and then dried for 2 seconds. The stamp was then brought into contact with the gold surface for 30 seconds (Figure A.3.3). The microcontact printed gold sample was then washed with ethanol and dried.

To show the effectiveness of patterning, the hydrophobicity-hydrophilicity interactions between silanes were utilized. The silicon samples were cleaned using DI water followed by piranha cleaning (piranha solution – a 3:1 volume % of concentrated H_2SO_4 to H_2O_2) for 20 minutes and finally dried. Microcontact printing of a 5 mM

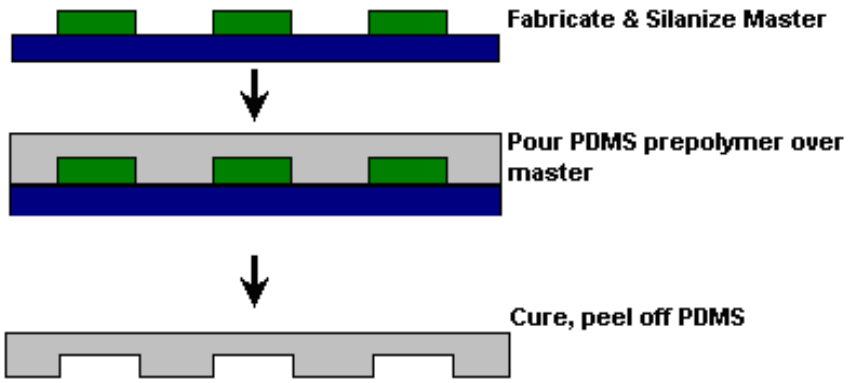

Figure A.3.2. PDMS preparation via replica molding

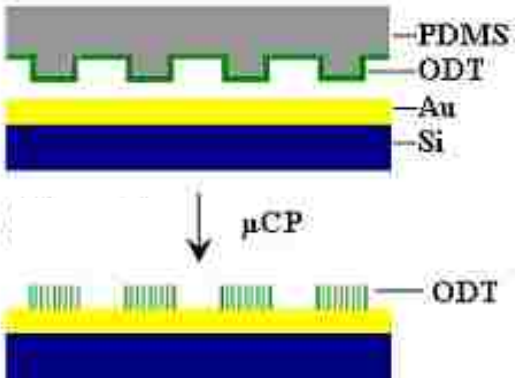

Figure A.3.3. Scheme of microcontact printing

solution of n-octadecyl trichloro silane (OTS; SAM 1, hydrophobic) in toluene was done onto the piranha cleaned Si sample using a similar method as explained in the case of gold. Rinsing was done using toluene. A 2 wt% solution of 2-(4-chloro sulfonyl phenyl)-ehtyl trichloro silane (CTCS; 50% in toluene; SAM 2, hydrophilic) was prepared using toluene as the solvent. The sample containing SAM 1 was immersed in the solution containing CTCS for 24 hours. After 24 hours, the sample was washed with toluene, and DI water, and finally dried.

A scanning electron microscope (SEM, Hitachi S4300) was used to characterize the master chips and PDMS stamp. Height characteristics and aspect ratios of the master stamps were also characterized using a Sloan 1A profilometer. The surface morphology of the patterned SAMs of ODT was observed using an atomic force microscope (AFM) (Micro Imaging Corp.). The microstructures were also imaged using a Nikon Eclipse ME 600 Microscope (Photometrics).

A.4. Results and discussion

A.4.1. Master chips

The silicon master chips produced via UV photolithography were verified for clarity and corner definitions using the microscope and the SEM. From figure A.4.1.1, it is clear that UV photolithography is well suited to fabricate master stamps with precise microscale patterns. Master stamps with 10, 50, 100, 200 and 500 μm squares have been prepared using this method and had been subsequently used for replica molding. The various speeds and SU-8 photoresists produce microstructures of different thickness.

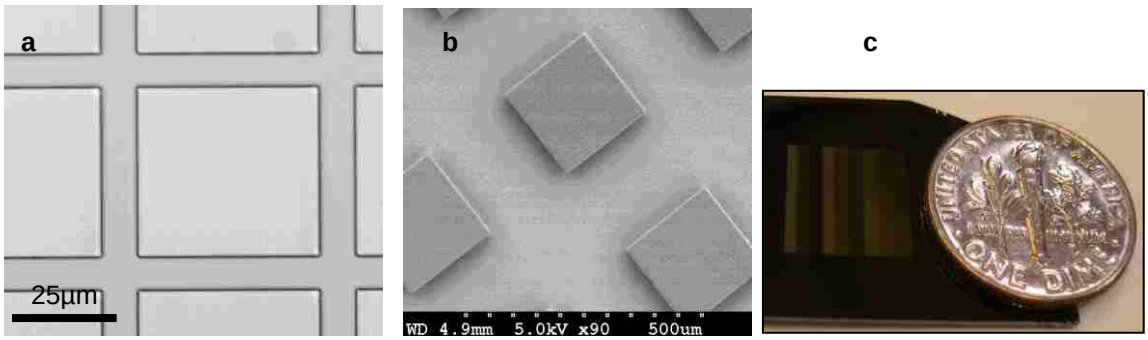

Figure A.4.1.1. Elevated square regions of two different silicon master chip samples, a) Optical microscope image of a 50 µm squares, b) SEM image of a 200 µm elevated square regions of master chips, and c) a representative photograph of the microfabricated silicon master chip.

The master stamps were measured for consistency in height of the microstructures using profilometry and contact mode AFM. Figure A.4.1.2 gives a clear view of how effective UV photolithography can be used for obtaining smooth microstructures.

As expected, an increase in the speed during the spin coating process decreases the height of the microstructure. An AFM image of an SU-8 sample along with the thickness profile is shown in figure A.4.1.3. It is clearly seen from the AFM image that the surface of the square regions and the pits are smooth because of the uniformity created by the spin coating step of UV photolithography.

A.4.2. PDMS stamp

Characterization of the PDMS stamp using the microscope and SEM showed that the microstructures obtained in the PDMS stamp (figures A.4.2.1 a and b) are patterns opposite to the microstructures as present on the silicon master stamps. Non contact mode AFM image (figures A.4.2.1 c) confirmed that the thickness of the PDMS (1.75 μm) was in accordance to that of the master stamp used (master stamp which was spin coated at 3000 rpm). The PDMS stamps showed excellent resistance to wear and tear since it was used multiple times with no issues arising in the case of patterning.

A.4.3. Microcontact printing over gold and silicon surfaces

A.4.3.1. XY control on gold by μCP

The optical microscope was used initially to see the quality of the hydrophobic – hydrophilic SAMs (thiols) patterned over the gold surface. Clear square patterns were

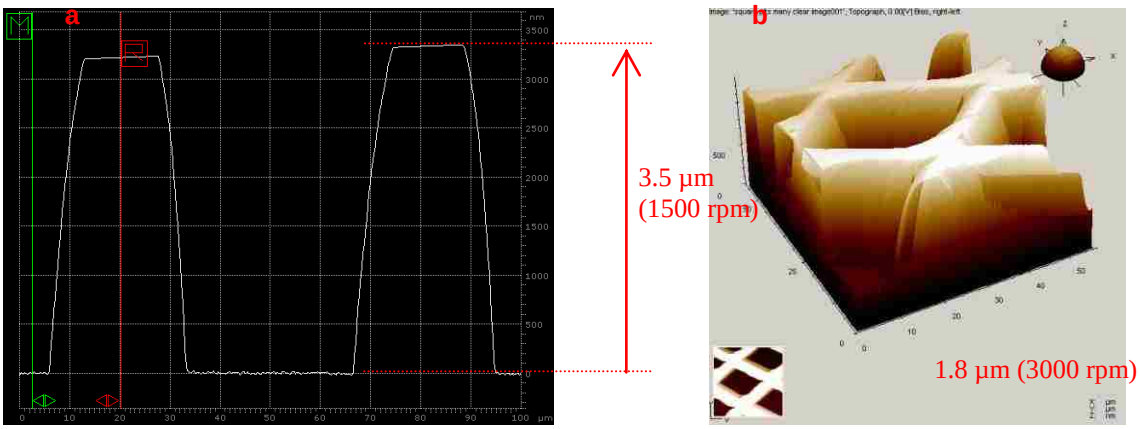

Figure A.4.1.2. a) Profilometry profile of a 1500 rpm and b) AFM image of a 3000 rpm spin coated SU-8 25 square pit samples.

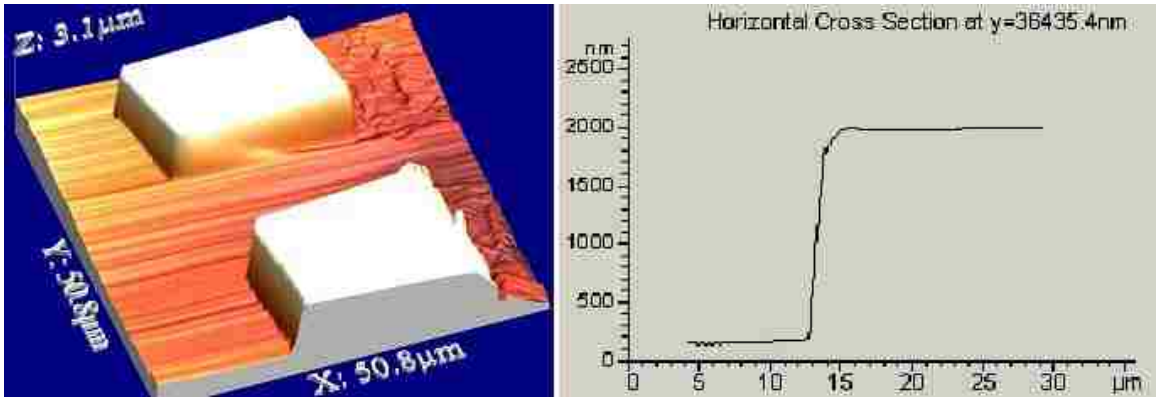

Figure A.4.1.3. AFM image of an elevated square patterned silicon master stamp and its thickness (around 1800 nm) profile along a cross section.

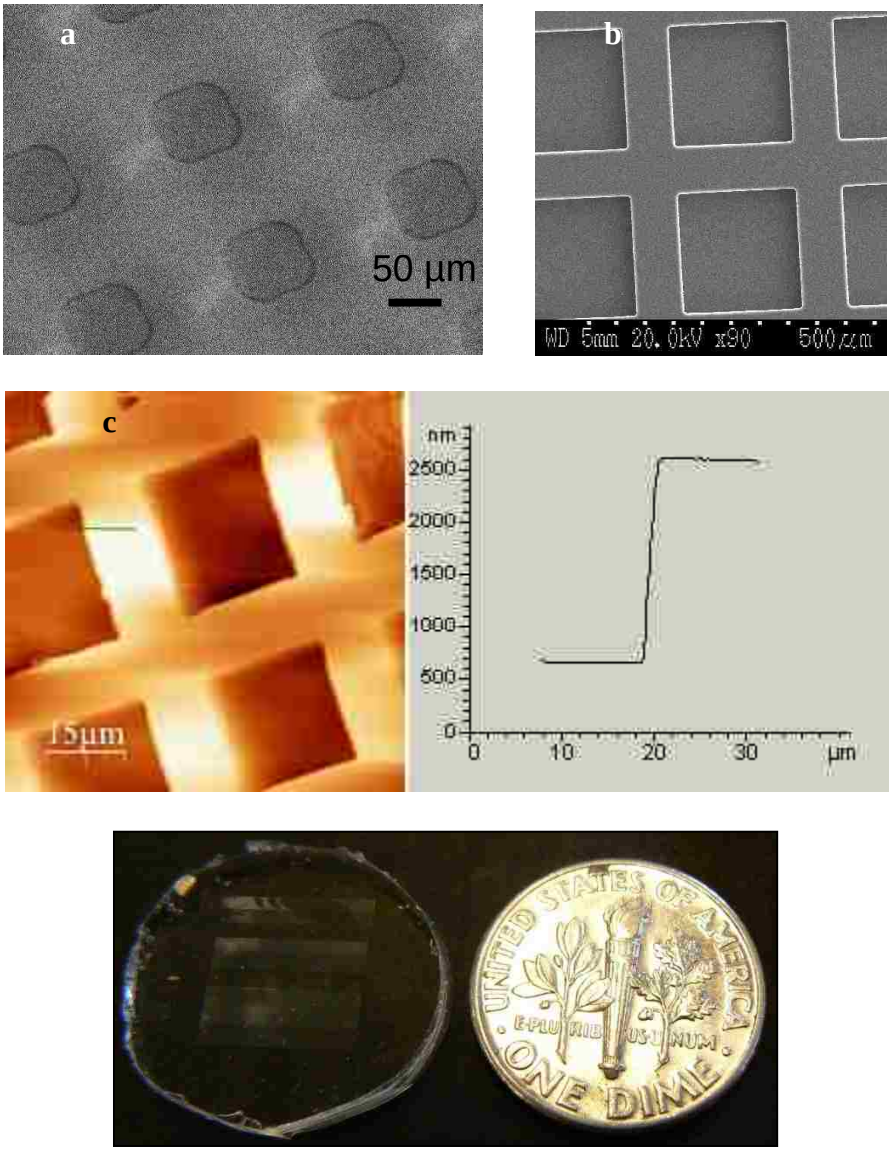

Figure A.4.2.1. a) Optical image, b) SEM image, c) 2-D topography AFM image of the PDMS stamp along with the thickness profile along the green line, and representative photograph showing the size of the PDMS stamp.

visible through the microscope which confirmed the ease with which SAMs can be patterned over gold surface using microcontact printing. The height characteristics of the XY control involved in the stamping of the hydrophobic thiol (ODT) was analyzed using the non contact mode of AFM. The quality of the SAM was found to be good (figure A.4.3.1). The thickness of the hydrophobic SAM, ODT was approximately 2.5 nm illustrated by zooming across the side of the square region represented by the square box in the top left image. As it can be seen from the non zoomed 3D image, a clear pattern of ODT SAM was obtained. Therefore, XY control was achieved over the surface by employing μCP as the patterning technique.

A.4.3.2. XY control on silicon by μCP

The microscopic analysis of the hydrophobic-hydrophilic effect of stamping OTS and CTCS was carried over silicon samples to verify the quality of the patterns formed using microcontact printing. As observed from figure A.4.3.2, the OTS and CTCS patterns obtained by μCP and backfilling subsequently over Si substrates were clearly distinct from each other. While, gold thiol chemistry is easy to carry out, silanes are reactive with atmospheric moisture and may result in non uniformity of pattern formation. This is the reason, why gold was suited over silicon for further hydrogel growth using ATRP.

A.5. Conclusions

In conclusion, replica molding of PDMS stamps from pre synthesized UV-photolithography master chips can be used for effective microcontact printing. Precise

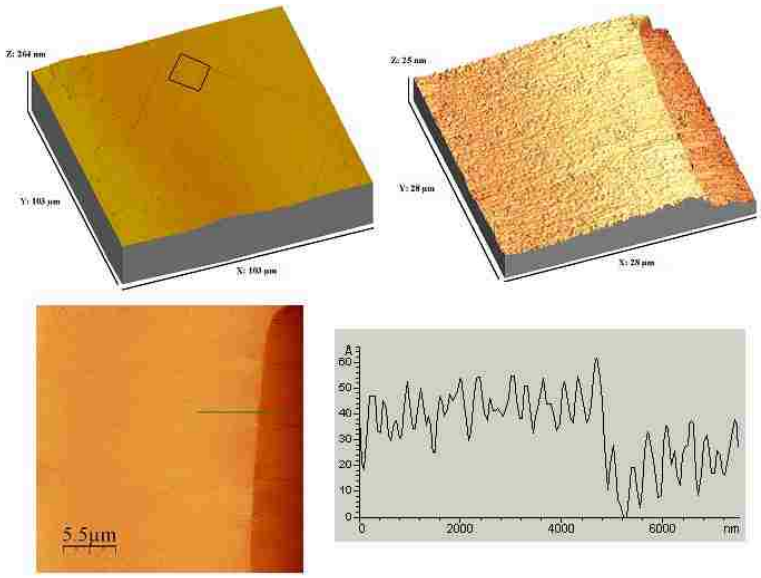

Figure A.4.3.1. Non contact mode AFM image showing XY control over the gold surface. Top images show the 3D profile of the ODT SAM, bottom left is the 2D profile of the zoomed pattern and the graph represents the thickness along the green line.

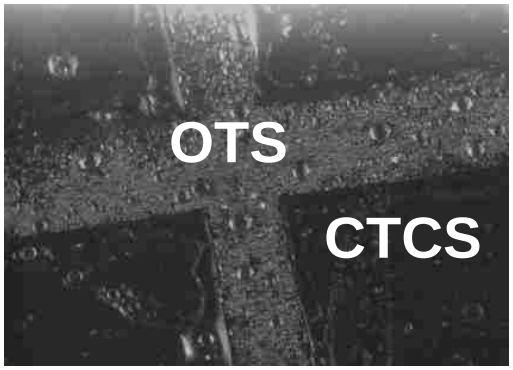

Figure A.4.3.2. Optical image of a patterned sample showing OTS and CTCS regions

XY control of patterning was achieved using microcontact printing and the PDMS stamps can be used multiple times for obtaining the same pattern. μCP is much more versatile, inexpensive and less time consuming than the conventional photolithographic techniques for obtaining patterns over surfaces.

A.6. References

[1] A. Kumar, and G. M. Whitesides, Applied Physics Letter **63**, 2002 (1993).

[2] Y. Xia, M. Mrksich, E. Kim, and G. M. Whitesides, Journal of American Chemical Society **117**, 9576 (1995).

[3] Y. Xia, E. Kim, M. Mrksich, and G. M. Whitesides, Chemistry of Material **8**, 601 (1996).

[4] L. Yan, X. –M. Zhao, and G. M. Whitesides, Journal of American Chemical Society **120**, 6179 (1998).

[5] A. Bernard, E. Delamarche, H. Schmid, B. Michel, H. R. Bosshard, and H. Biebuyck, Langmuir **14**, 2225 (1998).

[6] E. Delamarche, H. Schmid, A. Bietsch, N. B. Larsen, H. Rothuizen, B. Michel, and H. J. Biebuyck, Journal of Physical Chemistry **102**, 3324 (1998).

[7] N. F. Jr. Sheppard, M. J. Lesho, P. McNally and A. S. Francomacaro, Sensor and Actuators B **28**, 95 (1995).

[8] T. Yu, and C. K. Ober, Biomacromolecules **4**, 1126, (2003).

[9] Y. Xia, and G. M. Whitesides, Langmuir **13**, 2059 (1997).

[10] J. Guan, N. Ferrell, L. J. Lee, and D. J. Hansford, Biomaterials **27**, 4034 (2006).

APPENDIX B

Conjugation of enzyme catalase to GNPs: Comparison between carbodiimide and biotin-streptavidin methods

This chapter is modified from the article submitted as

Chirra HD, Sexton T, Biswal D, Hersh LB, Hilt JZ. *Acta Biomaterialia* **2010**

B. 1. Summary

The use of proteins or enzymes for therapeutic applications requires the protein to maintain sufficient activity for the period of *in vivo* treatment. Many proteins exhibit a short half-life *in vivo* and, thus, require delivery systems for them to be applied as therapeutics. The relative biocompatibility and the ability to form functionalized bioconjugates via simple chemistry make gold nanoparticles excellent candidates as protein delivery systems. Herein, two protocols for coupling model enzyme catalase to gold nanoparticles were compared. In the first, the strong biomolecular binding between biotin and streptavidin was used to couple catalase to the surface of gold nanoparticles. In the second protocol, the formation of an amide bond between carboxylic acid coated gold nanoparticles and free surface amines of catalase using carbodiimide chemistry was performed. The stability and kinetics of the different steps involved in these protocols were studied using UV-Visible spectroscopy, dynamic light scattering, and transmission electron microscopy. The addition of mercaptoundecanoic acid in conjugation with (*N*-(6-(biotinamido)hexyl)-3'-(2'-pyridyldithio)-propionamide increased the stability of biotinylated gold nanoparticles. Although the carbodiimide chemistry based bioconjugation approach exhibited a decrease in catalase activity, the carbodiimide

chemistry based bioconjugation approach resulted in more active catalase per gold nanoparticle compared to that of mercaptoundecanoic acid stabilized biotinylated gold nanoparticles. Both coupling protocols resulted in gold nanoparticles loaded with active catalase. Thus, these gold nanoparticle systems and coupling protocols represent promising methods for the application of gold nanoparticles for protein delivery.

B.2. Introduction

Carrier systems of nanoscale dimensions such as liposomes, polymeric particles, and microemulsion droplets are being widely studied for the delivery of various biomolecules [1]. In the case of proteins/enzymes, an important requirement for their immobilization to various carrier systems is that the protein should remain in its active form and be able to carry out necessary functions efficiently [2]. Although physical adsorption of proteins via hydrophobic and electrostatic interactions is experimentally simple, the loss of the protein/enzyme from the carrier once in contact with the *in vivo* environment makes chemically mediated immobilization via covalent bonding attractive for increasing the half life of proteins for *in vivo* therapeutic applications. Additionally, irreversible covalent binding generally leads to high levels of surface coverage. The easy synthesis of inorganic nanoparticles, their high surface to volume ratio, and the ability to control their size prove vital for immobilizing proteins over their surfaces for therapeutic applications [3]. Added advantages of gold nanoparticles (GNPs) include biocompatibility, relative non-toxicity, and the ability to form functionalized bioconjugates via simple chemistry [4]. Some of the *in vivo* therapeutic applications of functionalized GNPs include passive targeting [3], active targeting to reduce tumors in

mice [5], tumor necrosis factor delivery [6], treatment of colon carcinomas with Paclitaxel grafted gold colloids [7], cellular drug delivery [8-10], gene therapy [11-16], thermoablative therapy [17, 18] and drug release [19-21]. With the advent of such successful applications, GNPs can also prove to be suitable carriers for therapeutic protein delivery.

Gold nanoparticles serve as excellent candidates for protein bioconjugation because they readily react with the amino and cysteine thiol groups of proteins. Using this property, proteins such as insulin, pepsin, glucose oxidase, horse radish peroxidase, xanthine oxidase, fungal protease, etc have been directly conjugated to gold nanoparticles [2, 22-26]. In most cases, this strategy alters the conformational structure and active center of the protein similar to that of physical adsorption, thereby causing a reduction in activity [27]. Herein, we report and compare two simple procedures for coupling a model enzyme catalase to GNPs. Catalase catalyzes the conversion of hydrogen peroxide, a harmful oxidizing agent, to water and molecular oxygen. Its antioxidant properties have been studied extensively for potential effectiveness in antioxidative therapy. However, catalase undergoes rapid elimination from the blood stream and demonstrates poor intracellular delivery [28]. Figure B.1 shows a schematic representation of the two approaches utilized in this study for the coupling of catalase to GNPs. The first involves the biotinylation of both the GNP and catalase and then coupling them together using a streptavidin crosslinker. The second method uses carbodiimide chemistry to form amide bonds between carboxylic acid coated GNPs and amino groups of catalase. The first method takes advantage of the high affinity between biotin and streptavidin to form a

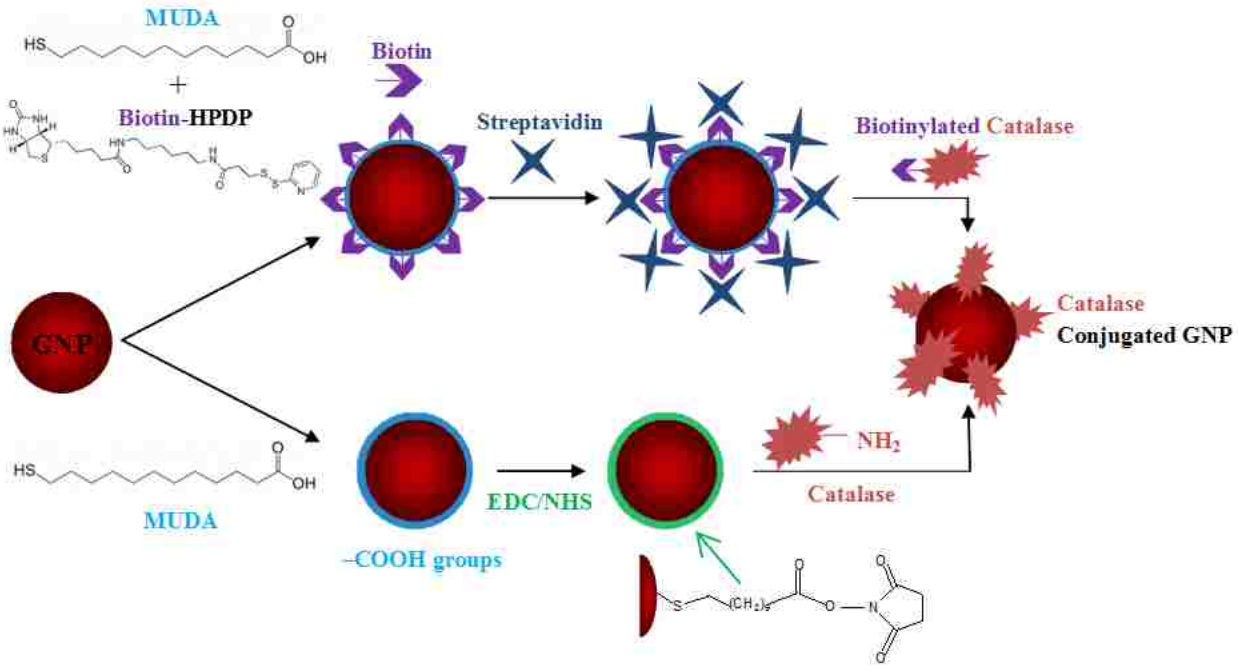

Figure B.1. Schematic representation of the two approaches involved in the coupling of catalase to gold nanoparticles.

biotin-streptavidin complex, which is among the strongest interactions in biology. The advantage of using carbodiimide chemistry is that it employs mild reaction conditions, endowing considerable versatility of bioconjugation for a wide variety of protein and enzyme molecules. The common feature of both procedures is the exploitation of the reaction and attachment of thiol molecules onto the surface of GNPs in the form of thiol-gold chemistry. Characterization of the coupling kinetics, stability of the modified particle, and the activity of catalase bound GNPs were done using UV-Visible spectroscopy, dynamic light scattering, and transmission electron microscopy (TEM). With these simple methods of bioconjugation, protein coupled GNPs can be useful for the delivery of proteins for biomedical applications.

B.3. Experimental section

B.3.1. Synthesis of biotinylated and carboxylic coated GNPs

Monodispersed gold nanoparticles were prepared using the Turkevich reduction of gold salts [29]. Briefly, a 1 mM aqueous solution of chloroauric acid ($HAuCl_4$) was boiled under stirring. To this solution, 3 mM trisodium citrate in water was added to reduce $HAuCl_4$ producing GNPs of sub-nanometer size. Tween 20 at 38 mg/ml was added to a 1 mg/ml final concentration to stabilize the particles for further functionalization. To incorporate biotin into the GNP a 4 mM stock solution of (*N*-(6-(biotinamido)hexyl)-3'-(2'-pyridyldithio)-propionamide (biotin-HPDP; Soltech Ventures) in dimethyl sulfoxide was added to the Tween stabilized GNPs so that the final concentration of biotin-HPDP was 0.5 mM, and the mixture incubated at room

temperature for 4 hr. The biotinylated GNPs were then dialyzed against water to remove excess unreacted biotin-HPDP and stored for further use.

For the carbodiimide chemistry coupling method, carboxylic groups were introduced to the surface of GNPs by adding a 10 mM stock solution of mercaptoundecanoic acid in ethanol (MUDA; Asemblon) to Tween stabilized GNPs to a final concentration of 0.5 mM, followed by stirring the solution for 12 hrs at room temperature. The biotinylated GNPs and MUDA coated GNPs were then dialyzed against water to remove free MUDA. Additionally GNPs containing varying concentrations of surface biotin were synthesized using MUDA as the stabilizing reagent. For this, the final concentration of MUDA was fixed at 0.5 mM, while biotin-HPDP was added at 50 µM for 1:10 biotin:MUDA GNPs and at 25 µM for 1:20 GNPs. Both biotin-HPDP and MUDA were added to the stabilized GNPs at the same time, and the reaction was allowed to proceed for approximately 12 hrs.

B.3.2. Biotinylation of Catalase

Please refer to chapter 7 for the biotinylation of enzyme catalase using biotin-NHS.

B.3.3. Coupling of catalase to the GNP surface via biotin-streptavidin binding

Purified biotinylated GNPs were dialyzed against HEPES prior to catalase coupling. Biotinylated GNPs in HEPES were treated with 100 µM streptavidin (Invitrogen) in 50 mM MES buffer, pH 5.5, for 3 hrs at room temperature. Excess

streptavidin was used to avoid any crosslinking between biotinylated GNP particles. The streptavidin coated GNPs were then centrifuged and washed with HEPES buffer 3 times to remove any unbound streptavidin. To these particles biotinylated catalase (GNP:biotinylated catalase, 3:1 vol%) was added and permitted to bind for 3 hrs at room temperature. The resulting bioconjugated GNPs were centrifuged and washed with HEPES thrice and used as such.

B.3.4. Coupling of catalase to GNPs via carbodiimide chemistry

MUDA coated GNPs were dialyzed against 50 mM MES buffer, pH 5.5. A mixture of 17 µl of 100 mM 1-ethyl-3-(3-dimethylaminopropyl) carbodiimide (EDC; Thermo Scientific) and 63 µl of 50 mM N-hydroxysuccinimide (NHS; Thermo Scientific) in MES buffer was then added to 500 µl of MUDA coated GNPs. The reaction was allowed to proceed for 15-20 min, after which time 0.8 µl of β-mercaptoethanol was added to quench the unreacted excess EDC. The concentration of β-mercaptoethanol was then reduced to less than 5 mM by adding 1.75 ml of HEPES buffer, pH 7.4 containing varying concentrations of catalase. Conjugation via amide linkage was allowed to occur for 3 hrs at room temperature. Catalase conjugated GNPs were then centrifuged at 12,500 rpm for 10 min in an Accuspin centrifuge (Fisher Scientific) and washed thrice with 100 mM HEPES buffer, and used as such for further studies.

B.3.5. Characterization of nanoparticles

Biotinylation, streptavidin coating, binding of catalase, and the various steps of carbodiimide chemistry were followed by the change in the surface plasmon resonance

peak using UV-Vis spectroscopy. Dynamic light scattering (DLS) was also used to observe changes in particle size with conjugation/functionalization. Transmission electron microscopy (TEM; Jeol 2010) was used to confirm the presence of enzyme over the surface of the GNPs. Staining of the particles was carried out using 2% phospho tungstic acid (Sigma), pH 7.4 (neutralized using 1 M potassium hydroxide). The presence of active catalase over the surface of GNPs was determined using the o-phenylene diamine assay (OPD; Sigma). Please refer to chapter 7 for details of assaying.

B.3.6. In vivo injection and characterization of catalase bound GNP activity

To test the feasibility of injecting catalase bound GNPs into a mouse, we first tested the stability of our particles in blood. Both carbodiimide and biotin-streptavidin protocol synthesized GNP-catalase in buffer was added at a 1:40 dilution to blood (approximate dilution of injecting 50 µl of volume into a mouse, which contains approximately 2 ml of blood). The GNP-catalase-blood mixture was incubated at 37°C. Blood samples were taken every 15 minutes for 90 minutes. For each time point, RBCs were spun out and catalase activity in the plasma was measured. For in vivo injection, 50 µl of 1 mg/ml of biotin protocol based GNP-catalase in HEPES buffer was injected into the retro-orbital sinus of mice. At time points of 5, 10, 30, and 60 min following injection 50 µl of blood samples were collected from the opposite retro-orbital sinus into tubes containing 100 units/ml heparin. In order to assay catalase in blood samples, red blood cells (RBCs) were removed from the serum via centrifugation (10000 rpm, 10 min); conditions that are known not to remove GNP-catalase. In triplicate for each mouse and time point, 5 µl of supernatant plasma was exposed to 195 µl of 1.5 mM H_2O_2 for 2

minutes at room temperature. 110 µl of each H_2O_2/plasma solution was then added to an assay well on a 96 well plate containing 75 µl HRP and 15 µl OPD and incubated for 5 min at room temperature. Absorbance was then measured at 590 nm to quantify catalase activity. For these animal studies, we complied with institutional ethical use protocols.

B.4. Results and Discussion

B.4.1. Demonstration of biotinylation of GNPs

Monodispersed GNPs synthesized via the Turkevich method were characterized in terms of size and their surface plasmon resonance (SPR) peak using dynamic light scattering and UV-Vis spectrometry. The size of GNPs was determined to be 9-11 nm showing a SPR peak at 525 nm. Using these parameters, the concentration of GNPs was calculated using the number density relationship equation as described by Haiss et al [30] to be about 10 nM. Biotinylation of GNPs was followed by measuring pyridine-2-thione release at 353 nm. Although preliminary studies of GNP biotinylation with biotin-HPDP showed product formation (result not shown), agglomeration to micron sized particles was observed. This was indicated by a time dependent red shift and subsequent broadening of the GNP SPR peak from 525 nm to about 683 nm. Agglomeration of biotinylated GNPs has been shown to be caused by hydrogen bonding between the inter-particle biotin molecules [31].

In order to avoid agglomeration associated with inter-particle hydrogen bonding, MUDA was added in varying ratios. We synthesized GNPs containing biotin:MUDA ratios of 1:10 and 1:20 (molar ratio). The negative charge on the surface of GNPs caused

by deprotonation of the carboxylic groups provides sufficient repulsion between nanoparticles. For example, figure B.4.1 shows the UV-Vis profiles of a 1:20 biotinylated GNP system at increasing reaction times. As seen in figure B.4.1, the absorbance of pyridine-2-thione at 353 nm increases over time indicating the coupling of biotin to the GNP. Additionally, the GNPs undergo a red shift from 525 nm to 552 nm during the reaction indicating particle size increase (see below) and some minor agglomeration. The biotinylated GNPs were then dialyzed to remove unreacted biotin-HPDP and used for further analyses. The stability of biotinylated GNPs in the presence of tethered MUDA of differing ratios was analyzed to determine the working range of pH for coupling. Please refer to chapter 7 for details of how addition of MUDA effectively increased the stability of solution based biotinylated GNPs. In order to avoid issues of particle aggregation at higher standing periods, we carried out streptavidin coating of the particle suspended buffer solutions immediately, which in turn stabilized the particles from aggregation. We chose 1:20 GNPs as the system for additional studies as it was stable enough for streptavidin binding and subsequent coupling of catalase.

B.4.2. Demonstration of streptavidin binding to biotinylated GNPs

The reactive availability/affinity of biotinylated GNP to undergo biomolecular binding to streptavidin was analyzed using UV-Vis spectroscopy. Streptavidin has four binding sites and a hydrodynamic diameter of 5 nm. Based on the surface area availability from a 10 nm sized GNP, a maximum of ~16 streptavidin molecules can coat a biotinylated GNP. In other words, for a 10 nM concentration of GNP solution that is biotinylated, a 160 nM streptavidin concentration can be estimated as being needed for

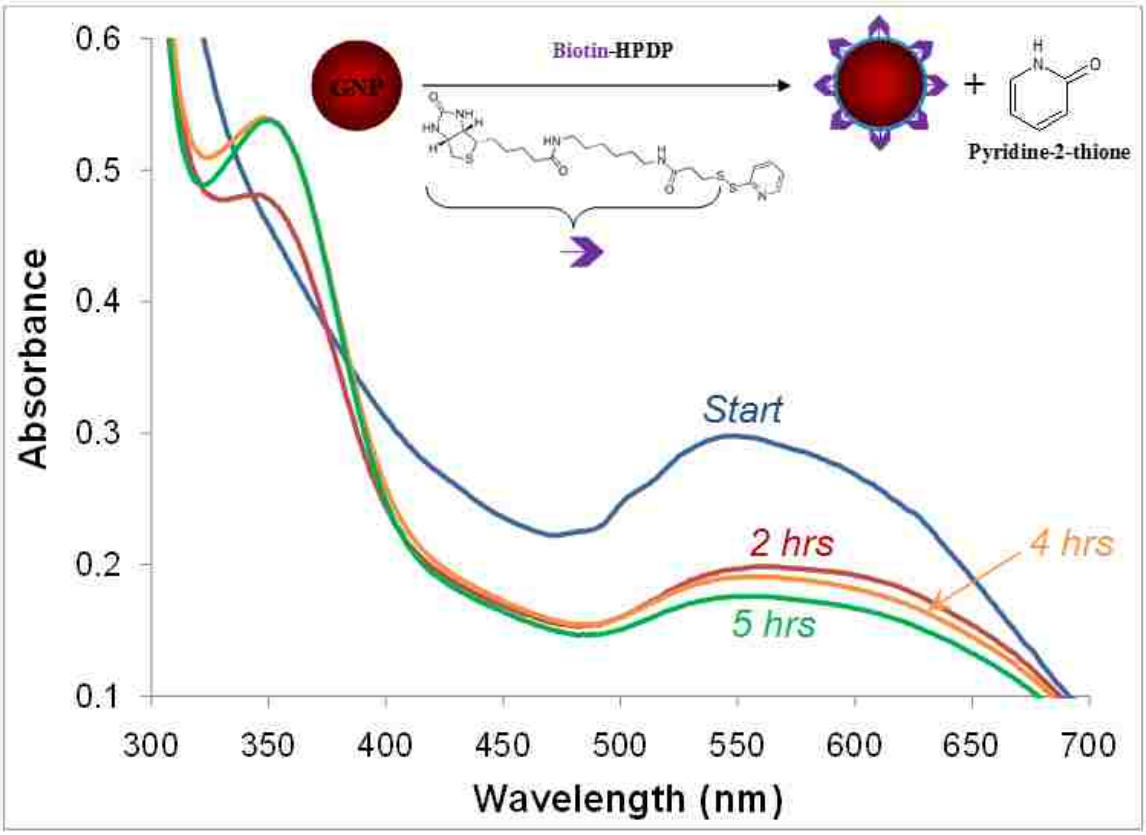

Figure B.4.1. UV-Vis spectra showing biotinylation of GNPs as a function of time. The presence of the product pyridine-2-thione peak at 353 nm confirms biotinylation of GNPs.

coating all GNPs. In order to confirm the binding between biotin and streptavidin, which is also an indirect way to confirm the presence of biotin over the surface of GNPs, a low concentration of 9 nM streptavidin in MES buffer was added to the 1:20 GNPs. This low concentration of available biotin binding sites (36 nM available biotin binding sites) was less than the total amount of biotinylated GNPs and should cause crosslinking between the biotinylated GNPs (with streptavidin being the crosslinker). As observed in figure B.4.2, at the initiation of binding, biotinylated GNPs exhibit their characteristic SPR peak value at 526 nm similar to that of the non-biotinylated GNP control sample (100% MUDA coated GNPs; right image of the inset). With time, biotin-streptavidin binding occurred and led to crosslinking between particles as indicated by the broadening of the spectra (0-2 hours). After 24 and 48 hours, all the streptavidin appeared bound as evidenced by no further crosslinking and the settling of agglomerated crosslinked particles leaving a clear solution on the top (left image of the inset). This confirmed the availability of biotin over the surface of GNPs for coupling with biotinylated catalase via intermediate streptavidin binding. However, the agglomeration under these low streptavidin concentrations precluded them for use for catalase coupling. Instead, using excess streptavidin (100 μM) provides an increased number of available biotin binding sites and results in a decreased probability of adjacent biotinylated particles crosslinking (black dotted absorbance profile). In other words, the streptavidin concentration was high enough to coat the entire biotinylated surface of GNPs, thereby avoiding interparticle biotin-streptavidin crosslinking. These streptavidin coated GNPs were then treated with biotinylated catalase, synthesized as described in methods. An assay of biotinylation (Quant Tag Biotin Kit, Vector Labs) gave a value of 128 nmoles of biotin/mg of catalase.

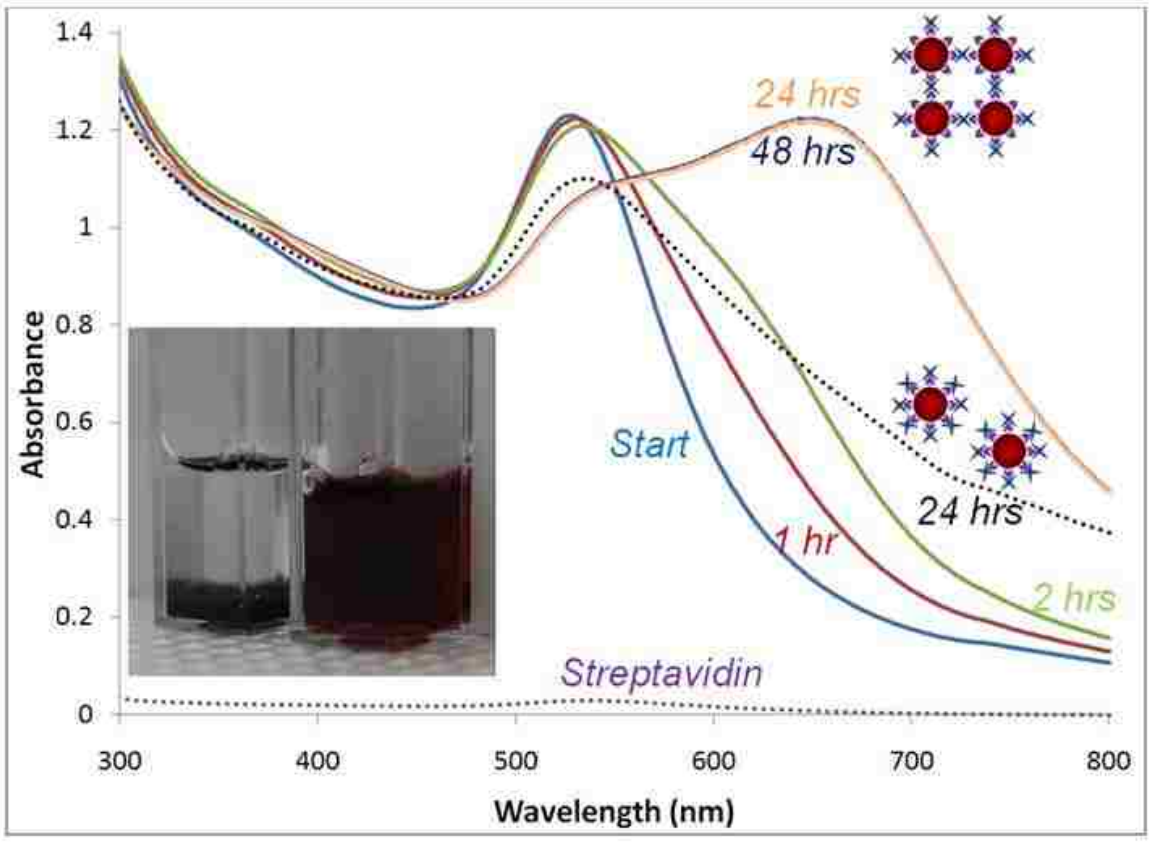

Figure B.4.2. Kinetic study showing the crosslinking of biotinylated GNP in the presence of low streptavidin concentration (9 nM) confirming biotin-streptavidin interaction. Also shown as a dotted line is the non-crosslinked high concentration streptavidin (100 µM) coated GNP profile. Inset shows the initial non-crosslinked dispersed GNPs in the right and the final crosslinked settled GNPs in the left. Also shown in black dotted line is the streptavidin coated biotinylated GNPs (using high streptavidin concentration).

Similar to the binding between the biotin of the biotinylated GNP and streptavidin, binding between the binding sites of streptavidin and the biotin in biotinylated catalase was used for the coupling reaction.

B.4.3. Confirmation of the presence of active catalase over biotin-streptavidin protocol GNPs

Streptavidin coupled catalase-GNPs were assayed for catalase activity by measuring the oxidation of OPD at 490 nm in the presence of H_2O_2 and horse radish peroxidase. One unit of catalase activity (U) is defined as the amount of enzyme cleaving 1 µmol of H_2O_2 in one minute. The activity of catalase was 44,350 U and 41,600 U before and after biotinylation, respectively, showing that biotinylation per se did not significantly affect catalase activity, which is similar to the result obtained by Muzykantov et al. [32]. Table B.4.3 shows the activity for catalase bound to the surface of GNPs via the biotin-streptavidin interaction. Non-biotinylated catalase was used as the control. Very little non-specific adsorption of catalase to streptavidin coated GNPs is observed. As the amount of biotinylated catalase increased, an increase in the activity of catalase-bound GNPs was observed, which leveled off presumably due to the saturation of the GNP surface.

The enzymatic effect of coupling biotinylated catalase to streptavidin coated GNPs was also studied by binding 20 µl of biotinylated catalase (2 mg/ml; 41600 U) to streptavidin coated GNPs. The activity of the free catalase in the supernatant and bound catalase to the GNP pellet after centrifugation and washing was determined to be 15575

Table B.4.3. Increased activity of biotin-streptavidin bound catalase to GNPs with increasing amounts of biotinylated catalase added to streptavidin coated GNPs.

Concn. of Biotinylated Catalase	**Catalase Activity (μU)/GNP**
8 μM (non-biotinylated; control)	~0.05
0.4 μM	1.7
0.8 μM	7
2 μM	41
6 μM	65
8 μM	66

U and 25600 U (16 µU/GNP) respectively. Their combined activity adds to a total of 41175 U, which is within experimental error of the input biotinylated catalase activity. So, the binding of biotinylated catalase to GNPs via biotin-streptavidin binding did not result in any loss of enzymatic activity.

B.4.4. Activation of MUDA coated GNPs to bind catalase via carbodiimide chemistry

In the case of coupling catalase to GNPs using carbodiimide chemistry, catalase was coupled to the GNPs through the reaction of its amino groups with EDC activated esters of MUDA carboxylic acids on the GNP surface. As shown in figure B.4.4, MUDA coated GNPs exhibited a characteristic surface plasmon resonance (SPR) peak value at 530 nm. With the addition of EDC and NHS, carboxyl groups were converted into thioesters that resulted in slight aggregation indicated by the red shift of the SPR peak value to 621 nm. The addition of catalase to the activated particles led to the formation of an amide bond between the amino groups of catalase and the activated carboxyl group of MUDA coated GNPs. The catalase coated particles showed a characteristic Soret iron (III) heme structure absorbance peak at 406 nm confirming the attachment of the enzyme [33]. Shoulder peaks of activated GNPs are also visible in the catalase spectra.

B.4.5. Confirmation of the presence of active carbodiimide coupled catalase on GNPs

The OPD assay was used to determine the amount of active catalase bound to GNPs through carbodiimide chemistry. Table B.4.5 shows the activity for amide bound

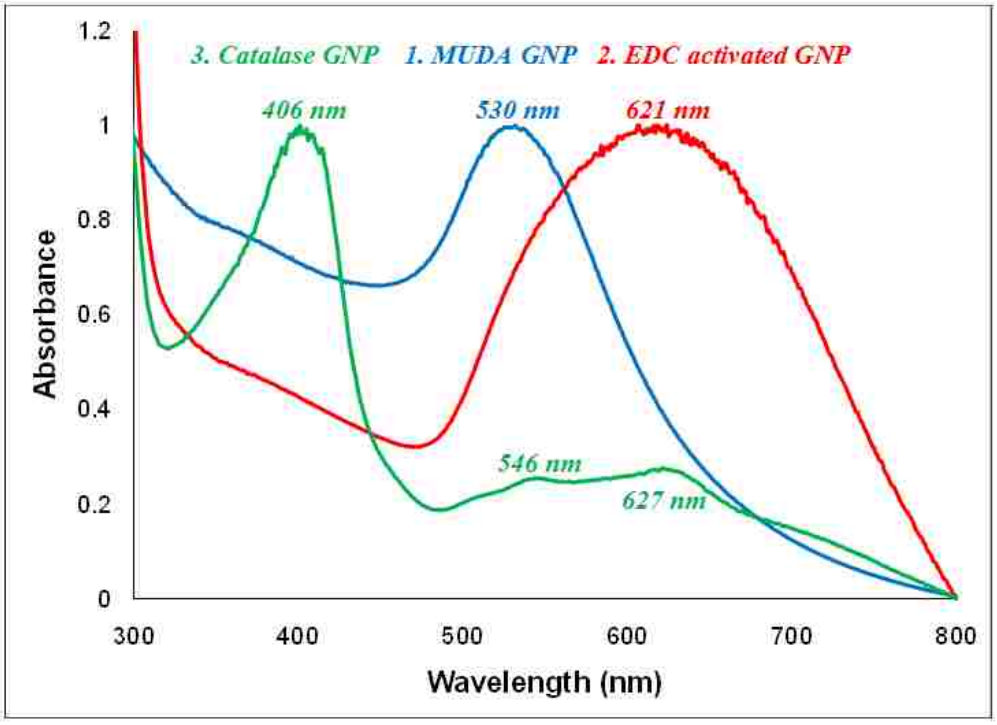

Figure B.4.4. Normalized UV-Vis spectra of the carbodiimide chemistry protocol confirming the activation of MUDA coated GNPs and the subsequent attachment of enzyme catalase.

Table B.4.5. Activity of the carbodiimide coupled catalase to GNPs increases with increasing concentrations of catalase until apparent saturation is reached.

Concn. of Catalase used	Catalase Activity (µU)/GNP
10 µM (no EDC added inactive GNPs; control)	~0.02
0.01 µM	0.4
0.1 µM	7
1 µM	93
5 µM	125
10 µM	131

catalase to the surface of MUDA coated GNPs. Using the carbodiimide chemistry, we achieved catalase coated GNPs, similar to that of the biotinylated GNP protocol with minimal non-specific catalase adsorption onto the particle. As expected, as the concentration of catalase increased, the attachment of catalase via amide linkage to the GNP surface also increased. Saturation of catalase occurred as indicated by a constant activity with increasing added catalase. The enzymatic effect of covalently binding catalase to GNPs via an amide linkage was studied by binding 20 µl of catalase (2 mg/ml; 44,350 U) to MUDA coated GNPs. The activity of free unbound catalase in the supernatant and bound catalase to the GNP pellet was determined to be 8,150 U and 25,075 U (10 µU/GNP) respectively. The combined activity, which comes to a total of 33,225 U, is somewhat less than the activity of the input catalase. Assuming unbound catalase in the supernatant had no activity loss, it is estimated that the bound catalase exhibited minimally 70% activity.

B.4.6. Size and stability analysis of the catalase bound GNPs

TEM analysis of the active particles was compared to that of the Turkevich reduced GNPs. Citrate reduced GNPs (Figure B.4.6.a) showed minimal presence of an amorphous layer over its surface indicative of the charge stabilization of the particle provided by citrate ions. In the case of the biotin-streptavidin affinity based active GNP an amorphous layer of thickness ~ 6.5 nm was observed (Figure B.4.6.b). Although the size of catalase and streptavidin together is > 6.5 nm (hydrodynamic diameter of catalase is around 9 nm [34], while for streptavidin it is 5 nm), the TEM sample of catalase bound via streptavidin to the particle surface is in a dehydrated form. This amorphous layer of

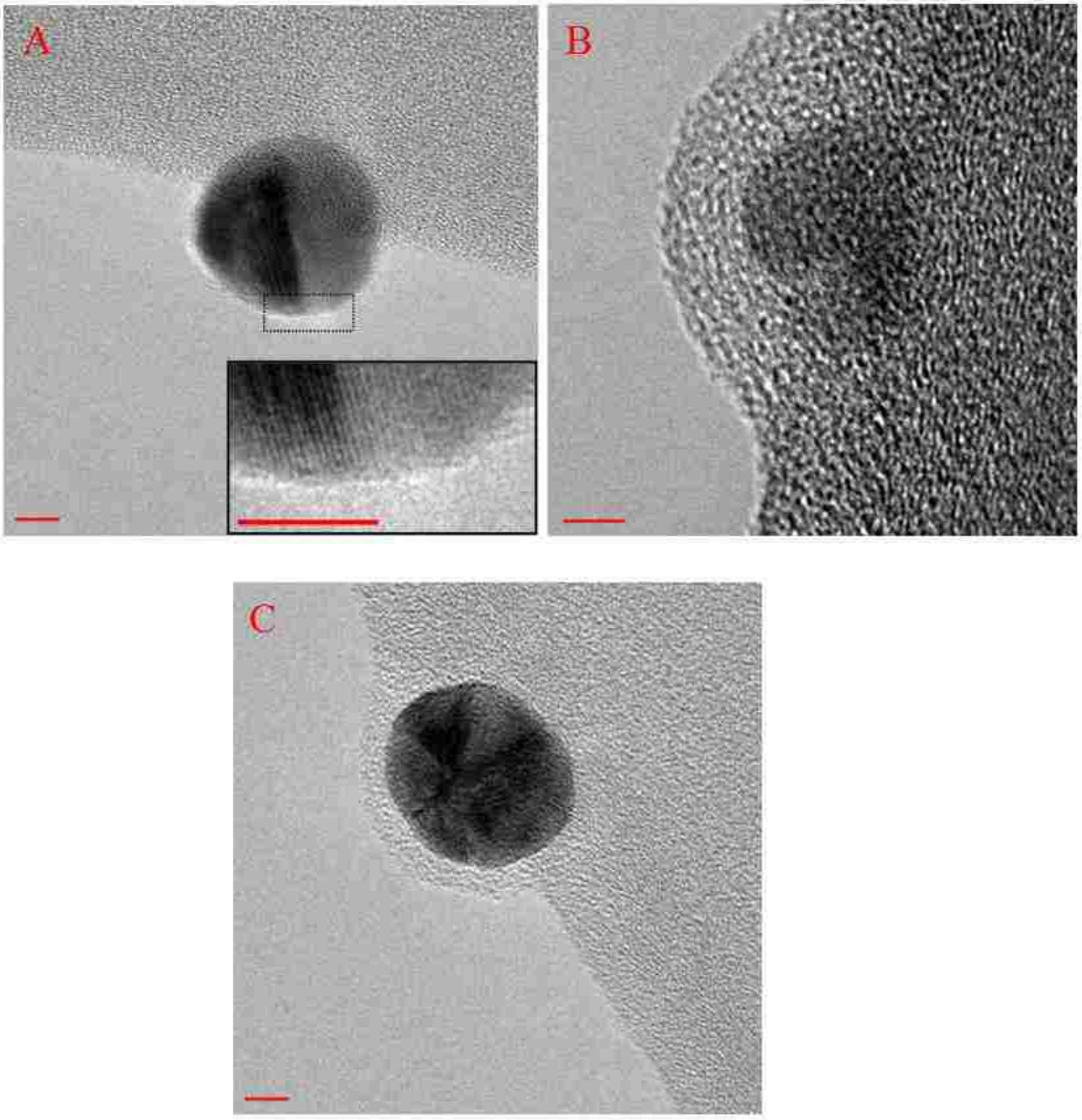

Figure B.4.6. TEM images showing (A) GNP stabilized by citrate ions with the inset showing negligible amorphous layer, (B) carbodiimide chemistry protocol based catalase conjugated GNP (amorphous layer ~ 4 nm), and (C) biotin-streptavidin affinity protocol based catalase conjugated GNP (amorphous layer ~ 6.5 nm). (scale bar is 2 nm)

the enzyme is absent in the case of the initial citrate stabilized GNP. A similar result is observed in the case of catalase bound to GNP via carbodiimide chemistry (Figure B.4.6.c), where the thickness of the amorphous layer is around 4 nm. DLS analysis of the aging/agglomeration with time of catalase bound GNPs were also done over a period of one week. While, the size of biotin-streptavidin protocol based GNP-catalase remained stable in the size range of 65-85 nm over a period of one week, GNP-catalase synthesized using carbodiimide chemistry showed agglomeration to about 400 nm. The agglomeration seen with GNPs containing catalase coupled via carbodiimide chemistry can be attributed to the fact that the surface MUDA groups are modified to amide bonds, thereby leading to charge neutralization and subsequent destabilization. With biotin-streptavidin GNP-catalase, there is free MUDA that can be deprotonated and thus stabilize the particles via charge repulsion.

B.4.7. Clearance of GNP-catalase from blood in vivo

Preliminary studies established that catalase activity on GNPs was stable in plasma. Thus, we injected mice with 50 µl of GNP-catalase for *in vivo* half life studies. We chose the biotin-streptavidin protocol GNP-catalase particles for this purpose, since their size was smaller and more stable than that of the carbodiimide protocol derived GNP-catalase as noted above. Figure B.4.7 shows the activity of GNP-catalase in serum at various times after injection. The activity/µl plasma at the initial injection condition is the theoretical rate measured at *in vitro* conditions assuming the overall volume of blood

in mice is 2 ml. The half life in blood was estimated to be around 6 min, likely reflecting reticuloendothelial system (RES) uptake of the GNPs mostly by liver, spleen, and lung

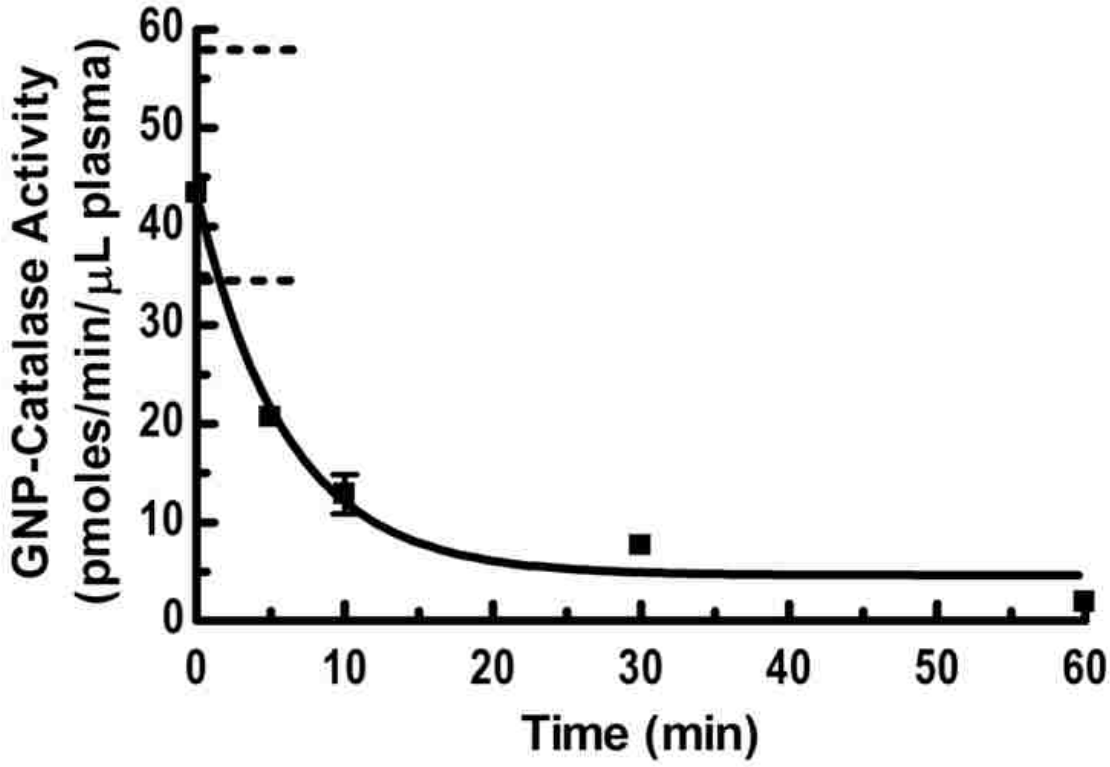

Figure B.4.7. Clearance of GNP-catalase from the plasma of mice showing the half life of GNP-catalase is around 6 minutes (N=3). The zero time value is calculated theoretically at in vitro conditions based on a total blood volume of 2 ml in mice. The dotted lines represent the initial activity range for a 1.5 ml to 2.5 ml total plasma volume range in mice

[35]. As previously noted [36], longer plasma circulation of GNPs with minimum uptake by the RES is possible by coating the particle surface with hydrophilic polymers, such as poly(ethylene glycol) (PEG) derivatives. A detailed study on the effects of PEGylation of enzyme or GNP on *in vivo* half life of GNP bound enzyme/protein will be analyzed, but it was beyond the scope of this study.

B.4.8. Comparison between the biotin-streptavidin and carbodiimide methods

It is clear that both the biotin-streptavidin binding and carbodiimide chemistry methods readily attach catalase to the GNP surface. The carbodiimide chemistry protocol produces a larger amount of active catalase/GNP at saturation than that of the biotin-streptavidin protocol, which could prove useful for those cases of conjugation where higher loading capacity is required. In the case of the carbodiimide chemistry protocol, the entire surface area of MUDA coated GNP (~315 nm^2) is available for binding with catalase. Based on a theoretical approximation, the surface area of 1:20 GNPs occupied by biotin is low (~15 nm^2), and only this area is available for streptavidin and subsequent catalase binding. By increasing the ratio of biotin-HPDP to MUDA, the amount of assembled biotin or available surface for coupling catalase can be increased at the expense of biotinylated particle stability. The carbodiimide chemistry derived GNP-catalase showed increased aggregation with time as compared to biotin-streptavidin derived GNP-catalase which is likely due to absence of free MUDA. Thus, only the streptavidin derived GNP-catalase was utilized for *in vivo* studies. The aggregation could be reduced or eliminated by using sterically hindering carboxylic acid thiols such as

PEGylated MUDA, thereby making them useful for *in vivo* applications. Also, the biotin-streptavidin protocol requires a two step synthesis procedure (synthesis of biotinylated catalase and then conjugation), while the carbodiimide chemistry protocol is carried out in a single step of activation and conjugation. Generalizing, the ideal procedure needed to bind a protein to GNP surface depends on several factors such as the effects of biotinylation on activity of the protein to be bound, size of the protein on binding to the GNP or streptavidin coated GNP, loss of activity with either of the protocols, and the stability of the final protein bound GNP.

B.5. Conclusion

Herein, we used the strong biomolecular interaction between biotin and streptavidin or carbodiimide chemistry to couple catalase to gold nanoparticles. The biotinylation of GNPs was accomplished using biotin-HPDP. Dynamic light scattering showed that the interparticle aggregation caused by hydrogen bonding between biotin molecules decreased with increasing concentrations of the stabilizing reagent MUDA. The stability of the particles decreased with increasing pH. The OPD assay confirmed the presence of streptavidin bound active biotinylated catalase over GNPs. The different surface plasmon resonance peak values obtained via UV-Vis analysis confirmed the individual steps involved in the carbodiimide dependant coupling of catalase to MUDA coated GNPs. The OPD assay confirmed the presence of bound catalase to GNPs in high yields. The saturation values of activity showed that there was more active catalase on carbodiimide chemistry coupled GNPs than on biotin-streptavidin bound GNPs. The enzyme bound particles were stable enough to be used for studies in mice and exhibited a

half life of around 6 min likely reflecting the rate of tissue uptake. Both protocols resulted in the attachment of active catalase to GNPs, and these methods are critical for the development of GNPs as potential carriers for protein delivery.

B.6. References

1. Yokoyama M, Okano T. Targetable drug carriers: present status and a future perspective. *Adv Drug Delivery Rev* **1996**, 21, 77-80.

2. Gole A, Dash C, Soman C, Sainkar SR, Rao M, Sastry M. On the preparation, characterization and enzymatic activity of fungal protease-gold colloid bioconjugates. *Bioconjugate Chem* **2001**, 12, 684-690.

3. Moghimi SM, Hunter AC, Murray JC. Nanomedicine: Current status and future prospects. *FASEB J* **2005**, 19, 311-330.

4. Chirra HD, Biswal D, Hilt JZ. "Gold Nanoparticles and Surfaces: Nanodevices for Diagnostics and Therapeutics", in Nanoparticulate Drug Delivery Systems (NPDDS) II: Formulation and Characterization. Pathak, Y.; Thassu, D. eds., *Informa Healthcare USA Inc.* **2009**, 90-114.

5. Dixit V, Bossche J, Sherman DM, Thompson DH, Andres RP. Synthesis and grafting of thioctic acid-PEG-folate conjugates onto Au nanoparticles for selective targeting of cancer cells. *Bioconjugate Chem* **2006**, 17, 603-609.

6. Chen YH, Tsai CY, Huang PY, Chang MY, Cheng PC, Chou CH, Chen DH, Wang CR, Shiau AL, Wu CL. Methotrexate conjugated to gold nanoparticles inhibit tumor growth in a synergestic lung tumor model. *Mol Pharmaceutics* **2007**, 4, 713-722.

7. Gibson JD, Khanal BP, Zubarev ER. Paclitaxel functionalized gold nanoparticles. *J Am Chem Soc* **2007**, 129, 11653-11661.

8. Hone DC, Walker PI, Evans-Gowing R, FitzGerald S, Beeby A, Chambrier I, Cook MJ, Russell DA. Generation of cytotoxic singlet oxygen via phthalocyanine stabilized gold nanoparticles: a potential delivery vehicle for photodynamic therapy. *Langmuir* **2002**, 18, 2985-2987.

9. Saito G, Swanson JA, Lee KD. Drug delivery strategy utilizing conjugation via reversible disulfide linkages: role and site of cellular reducing activities. *Adv Drug Delivery Rev* **2003**, 55, 199-215.

10. Sapsford KE, Berti L, Mendintz IL. Materials for fluorescence energy transfer analysis: beyond traditional donor acceptor combinations. *Angew Chem Int Ed* **2006**, 45, 4562-4589.

11. McIntosh CM, Eposito EA, Boal AK, Simard JM, Martin CT, Rotello VM. Inhibition of DNA transcription using cationic mixed monolayer protected gold clusters. *J Am Chem Soc* **2001**, 123, 7626-7629.

12. Han G, Martin CT, Rotello VM. Stability of gold nanoparticle bound DNA towards biological, physical, and chemical agents. **Chem Biol Drug Des 2006**, 67, 78-82.

13. Sandhu KK, McIntosh CM, Simard JM, Smith SW, Rotello VM. Gold nanoparticle mediated transfection of mammalian cells. *Bioconjugate Chem* **2002**, 13, 3-6.

14. Thomas M, Klibanov AM. Conjugation to gold nanoparticles enhances polyethyleneimines transfer of plasmid DNA into mammalian cells. *Proc Natl Acad Sci U. S. A.* **2003**, 100, 9138-9143.

15. Rosi NL, Giljohann DA, Thaxton CS, Lytton-Jean AKR, Han MS, Mirkin CA. Oligonucleotide modified gold nanoparticles for intracellular gene regulation. *Science* **2006**, 312, 1027-1030.

16. Verma A, Simard JM, Worrall JWE, Rotello VM. Tunable reactivation of nanoparticle inhibited β galactosidase by glutathione at intracellular concentrations. *J Am Chem Soc* **2004**, 126, 13987-13991.

17. Hirsch LR, Stafford RJ, Bankson JA, Sershen SR, Rivera B, Price RE, Hazle JD, Halas NJ, West JL. Nanoshell mediated near infrared thermal therapy of tumors under magnetic resonance guidance. *Proc Natl Acad Sci U. S. A.* **2003**, 100, 13549-13554.

18. Hirsch LR, Jackson JB, Lee A, Halas NJ, West JL. A whole blood immunoassay using gold nanoshells. *Anal Chem* **2003**, 75, 2377-2381.

19. Radt B, Smith A, Caruso F. Optically addressable nanostructured capsules. *Adv Mater* **2004**, 16, 2184-2189.

20. Angelatos AS, Radt B, Caruso F. Light responsive polyelectrolyte/gold nanoparticle microcapsules. *J Phys Chem B* **2005**, 109, 3071-3076.

21. West JL, Halas NJ. Applications of nanotechnology to biotechnology *Curr Opin Biotechnol* **2000**, 11, 215-217.

22. Bhumkar DR, Joshi HM, Sastry M, Pokharkar VB. Chitosan reduced gold nanoparticles as novel carriers for transmucosal delivery of insulin. *Pharm Res* **2007**, 24, 1415-1426.

23. Phadtare S, Kumar A, Vinod VP, Dash C, Palaskar DV, Rao M, Shukla PG, Sivaram S, Sastry M. Direct assembly of gold nanoparticle shells on polyurethane

microsphere cores and their application as enzyme immobilization templates. *Chem Mater* **2003**, 15, 1944-1949.

24. Xiao Y, Patolsky F, Katz E, Hainfeld JF, Willner I. Plugging into enzymes: nanowiring of redox enzymes by a gold nanoparticle. *Science* **2003**, 299, 1877-1881.

25. Stoneheurner JG, Zhao J, O'Daly JP, Crumbliss AL, Henkens RW. Comparison of colloidal gold electrode fabrication methods: the preparation of a horse radish peroxidase enzyme electrode. *Biosens Bioelectron* **1992**, 7, 421-428.

26. Zhao J, O'Daly JP, Henkens RW, Stoneheurner JG, Crumbliss AL. A xanthine oxidase/colloidal gold enzyme electrode for amperometric biosensor applications. *Biosens Bioelectron* **1996**, 11, 493-502.

27. Patel N, Davies MC, Hartshorne M, Heaton RJ, Roberts CJ, Tendler SJB, Williams PM. Immobilization of protein molecules onto homogenous and mixed carboxylate-terminated self assembled monolayers. *Langmuir* **1997**, 13, 6485-6490.

28. Kozower BD, Christopher-Solomidou M, Sweitzer TD, Muro S, Buerk DG, Solomides CC, Albelda SM, Patterson GA, Muzykantov VR. Immunotargeting of catalase to the pulmonary endothelium alleviates oxidative stress and reduce acute lung transplantation injury. *Nat Biotechnol* **2003**, 21, 392-398.

29. Turkevich J, Stevenson PC, Hillier J. A study of nucleation and growth process in the synthesis of gold colloids. *Faraday Discuss* **1951**, 11, 55-75.

30. Haiss W, Thanh NTK, Aveyard J, Fernig DG. Determination of size and concentration of gold nanoparticles from UV-Vis spectra. *Anal Chem* **2007**, 79, 4215-4221.

31. Strzelczyk AA, Dobrowolski JC, Mazurek AP. On the confirmation of biotin molecule. *J Molec Struc (Theochem)* **2001**, 541, 283-290.

32. Muzykantov VR, Atochina EN, Ischiropolous H, Danilov VM, Fisher AB. Immunotargeting of antioxidant enzyme to the pulmonary endothelium. *Proc Natl Acad Sci U. S. A.* **1996**, 93, 5213-5218.

33. Chen X, Xie H, Kong J, Deng J. Characterization for didodecyldimethylammonium bromide liquid crystal film entrapping catalase with enhanced direct electron transfer rate. *Biosens Bioelectron* **2001**, 16, 115-120.

34. Zhang J, Chi Q, Zhang B, Dong S, Wang E. Molecular characterization of beef liver catalase by scanning tunneling microscopy. *Electroanalysis* **1998**, 10, 738-746.

35. Sonavane G, Tomoda K, Maknio K. Biodistribution of colloidal gold nanoparticles after intravenous administration: effect of particle size. *Colloids Surf B* **2008**, 66, 274-280.

36. Bergen JM, Recum HAV, Goodman TT, Massey AP, Pun SH. Gold nanoparticles as a versatile platform for optimizing physicochemical parameters for targeted drug delivery. *Macromol Biosci* **2006**, 6, 506-516.

Bibliography

Advincula RC. Surface Initiated Polymerization from Nanoparticle Surfaces. *Journal of Dispersion Science and Technology* **2003**, 24, 343 - 361.

Advincula RC, Zhou Q, Park M. Polymer Brushes by Living Anionic Surface Initiated Polymerization on Flat Silicon (SiOx) and Gold Surfaces: Homopolymers and Block Copolymers. *Langmuir* **2002**, 18, 8672-8684.

Agarwal AK, Dong L, Beebe DJ, Jiang H. Autonomously-triggered microfluidic cooling using thermo-responsive hydrogels. *Lab Chip* **2007,** 7, 310-315.

Aili D, Enander K, Rydberg J. Aggregation-Induced Folding of a De Novo Designed Polypeptide Immobilized on Gold Nanoparticles. *J Am Chem Soc* **2006**, 128, 2194-2195.

Ali M, Horikawa S, Venkatesh S, Saha J, Hong JW, Byrne ME. Zero order therapeutic release from imprinted hydrogel contact lenses within an in vitro physiological ocular tear flow. *J. Controlled Release* **2007,** 124, 154-162.

Anderson DG, Akinc A, Langer R. Structure/property studies of polymeric gene delivery using a library of poly(β-amino esters). *Mol. Ther.* **2005,** 26, 4892-4897.

Anderson DG, Tweedie CA, Hossain N, Navarro SM, Brey DM, Vliet KJV, Langer R, Burdick JA. A combinatorial library of photocrosslinkable and degradable materials. *Adv. Mater.* **2006,** 18, 2614-2618.

Andruzzi L, Hexemer A, Li X, Ober CK, Kramer EJ, Galli G, Chiellini E, Fischer DA. Control of surface properties using fluorinated polymer brushes produced by surface initiated controlled radical polymerization. *Langmuir* **2004,** 20, 10498-10506.

Angelatos AS, Radt B, Caruso F. Light-Responsive Polyelectrolyte/Gold Nanoparticle Microcapsules. *J Phys Chem B* **2005**, 109, 3071-3076.

Ashford EJ, Naldi V, O'Dell R, Billingham NC, Armes SP. First example of the atom transfer radical polymerisation of an acidic monomer: direct synthesis of methacrylic acid copolymers in aqueous media. *Chem. Comm.* **1999,** 14, 1285-1286.

Aslan K, Holley P, Davies L. Angular-Ratiometric Plasmon-Resonance Based Light Scattering for Bioaffinity Sensing. *J Am Chem Soc* **2005**, 127, 12115-12121.

Aubin H, Nichol JW, Hutson C, Khademhosseini A. Directed 3D cell alignment and elongation in microengineered hydrogels. *Biomaterials* **2010,** DOI: 10.1016.

Baldi A, Lei M, Gu Y, Siegel RA, Ziaie B. Microstructured silicon membrane with entrapped environmentally sensitive hydrogel for smart flow control. *Sens. Actuators B,* **2006,** 114, 9-18.

Bashir R, Hilt JZ, Elibol O, Gupta AK, Peppas NA. Micromechanical cantilever as an ultrasensitive pH microsensor. *App. Phys. Lett.* **2002,** 81, 3091-3093.

Beebe DJ, Moore JS, Bauer JM, Yu Q, Liu RH, Devadoss C, Jo B. Functional hydrogel structures for autonomous flow control. *Nature* **2000,** 404, 588-590.

Bendayan M. Worth Its Weight in Gold. *Science* **2001**, 291, 1363-1365.

Bergen JM, Archana P, Pun H. Gold Nanoparticles as a Versatile Platform for Optimizing Physicochemical Parameters for Targeted Drug Delivery. *Macromolecular Bioscience* **2006**, 6, 506-516.

Bhumkar D, Joshi H, Sastry M. Chitosan Reduced Gold Nanoparticles as Novel Carriers for Transmucosal Delivery of Insulin. *Pharmaceutical Research* **2007**, 24, 1415-1426.

Biebuyck HA, Whitesides GM. Autophobic Pinning of Drops of Alkanethiols on Gold. *Langmuir* **1994,** 10, 4581-4587.

Biswal D, Chirra H, Hilt JZ, Fabrication of hydrogel microstructures using polymerization controlled by microcontact printing (PCμCP). *Biomed. Microdev.* **2008,** 10, 213-222.

Biswal D, Chirra H, Hilt JZ, Microscale analysis of patterning reactions via FTIR imaging: Application to intelligent hydrogel systems.*Polymer* **2006,** 47, 7355-7360.

Blawas AS, Reichert WM. Protein patterning. *Biomaterials* **1998,** 19, 595-609.

Boisselier E, Diallo AK, Salmon L, Ornelas C, Ruiz J, Astruc D. Encapsulation and Stabilization of Gold Nanoparticles with "Click" Polyethyleneglycol Dendrimers. *J. Am. Chem. Soc.* **2010**, 132, 2729-2742.

Bos GW, Scharenborg NM, Engbers GHM. Proliferation of endothelial cells on surface-immobilized albumin-heparin conjugate loaded with basic fibroblast growth factor. *J. Biomed. Mater. Res*. **1999**, 44, 330-340.

Bowman CN, Carver AL, Kennett SL, Williams MM, Peppas NA, Polymers for information storage systems. *Polymer Bulletin* **1988**, 20, 329-333.

Braun M, Brittain WJ. Synthesis of Polymer Brushes on Silicate Substrates via Reversible Addition Fragmentation Chain Transfer Technique. *Macromolecules* **2002,** 35, 610-615.

Brusatin G, Abbotto A, Innocenzi SP. Poled Sol-Gel Materials With Heterocycle Push-Pull Chromophores that Confer Enhanced Second-Order Optical Nonlinearity. *Advanced Functional Materials* **2004**, 14, 1160-1166.

Brust M, Walker M, Schriffin DJ. Synthesis of thiol-derivatised gold nanoparticles in a two-phase Liquid-Liquid system. *J Chem Soc Commun* **1994**, 801-802.

Bünsow J, Johannsmann D. Electrochemically produced responsive hydrogel films: Influence of added salt on thickness and morphology. *J. Colloid Interface Sci.* **2008,** 326, 61-65.

Cai QY, Kim SH, Choi KS, Kim SY, Byun SJ, Kim KW. Colloidal gold nanoparticles as a blood-pool contrast agent for X-ray computed tomography in mice. *Invest. Radiol.* **2007**, 42, 797–806.

Casadei MA, Pitarresi G. Biodegradable and pH-sensitive hydrogels for potential colon-specific drug delivery: Characterization and in vitro release studies. *Biomacromolecules* **2008,** 9, 43-49.

Cao YC, Jin R, Mirkin CA. Nanoparticles with Raman Spectroscopic Fingerprints for DNA and RNA Detection. *Science* **2002**, 297, 1536-1540.

Cayre OJ, Paunov VN. Fabrication of microlens arrays by gel trapping of self assembled particle monolayers at the decane water interface. *J. Mater. Chem.* **2004,** 14, 3300-3302.

Chakraborty S, Bishnoi SW, Perez-Luna VH. Gold Nanoparticles with Poly(*N*-isopropylacrylamide) Formed via Surface Initiated Atom Transfer Free Radical Polymerization Exhibit Unusually Slow Aggregation Kinetics. *J. Phys. Chem. C.* **2010**, 114, 5947-5955.

Chiellini F, Bizzazrri R, Ober CK, Yu T, Schmaljohann D, Chiellini E. Patterning of polymeric hydrogels for biomedical applications. *Macromol. Rapid Commun.* **2001,** 22, 1284-1287.

Check E. Gene therapy: A tragic setback. *Nature* **2002**, 420, 116-118.

Chen Y-H, Tsai C-Y, Huang P-Y. Methotrexate Conjugated to Gold Nanoparticles Inhibits Tumor Growth in a Syngeneic Lung Tumor Model. *Mol Pharmaceutics* **2007**, 4, 713-22.

Cheng W, Dong S, Wang E. Synthesis and Self-Assembly of Cetyltrimethylammonium Bromide-Capped Gold Nanoparticles. *Langmuir* **2003**, 19, 9434-9439.

Cheng W, Wang E. Size-Dependent Phase Transfer of Gold Nanoparticles from Water into Toluene by Tetraoctylammonium Cations: A Wholly Electrostatic Interaction. *J Phys Chem B* **2004**, 108, 24-26.

Chirra HD, Biswal D, Hilt JZ. in *Nanoparticulate Drug Delivery Systems (NPDDS) II: Formulation and Characterization,* eds Pathak Y, Thassu D (Informa Healthcare USA Inc.) **2009,** pp 90-114.

Chirra HD, Biswal D, Hilt JZ. Controlled synthesis of responsive hydrogel nanostructures via microcontact printing and ATRP. *Polym. Adv. Technol.* **2009**, DOI:10.1002/pat.1576.

Chirra HD, Hilt JZ. Nanoscale Characterization of the Equilibrium and Kinetic Response of Hydrogel Structures. *Langmuir* **2010**, 26, 11249-11257.

Chirra HD, Sexton T, Biswal D, Hersh LB, Hilt JZ. submitted in *Bioconjug Chem.* **2010.**

Chun YW, Webster TJ. The role of nanomedicine in growing tissues. *Ann. Biomed. Eng.* **2009**, 37, 2034–2047.

Clark LA, Ye GT, Snurr RQ. Molecular Traffic Control in a Nanoscale System. *Phys. Rev. Let.* **2000,** 84, 2893-2895.

Cortie MB. The Weird World of Nanoscale Gold. *Gold Bulletin* **2004**, 37, 12-19.

Crespilho FN, Emilia Ghica M, Florescu M. A strategy for enzyme immobilization on layer-by-layer dendrimer-gold nanoparticle electrocatalytic membrane incorporating redox mediator. *Electrochemistry Communications* **2006**, 8, 1665-1670.

Croutxe-Baghorn C, Soppera O, Lougnot DJ, Chemically tunable lensing of stimuli responsive hydrogel microdomes *Eur. Phys. J. Appl. Phys.* **2001**, 13, 31-36.

Cushing MC, Anseth KS. Hydrogel cell cultures. *Science* **2007,** 316, 1133-1134.

Daniel MC, Astruc D. Gold Nanoparticles: Assembly, Supramolecular Chemistry, Quantum-Size-Related Properties, and Applications toward Biology, Catalysis, and Nanotechnology. *Chem Rev* **2004**, 104, 293-346.

De M, Ghosh PS, Rotello VM. Applications of Nanoparticles in Biology. *Adv. Mater.* **2008**, 20, 4225-4241.

Dingenouts N, Norhausen C, Ballauff M, Observation of the Volume Transition in Thermosensitive Core−Shell Latex Particles by Small-Angle X-ray Scattering. *Macromolecules* **1998,** 31, 8912-8916.

Dixit V, Bossche J, Sherman DM. Synthesis and Grafting of Thioctic Acid-PEG-Folate Conjugates onto Au Nanoparticles for Selective Targeting of Folate Receptor-Positive Tumor Cells. *Bioconjugate Chem* **2006**, 17, 603-609.

Dong H, Zhu M, Yoon JA, Gao H, Jin R, Matyjaszewski K. One-pot synthesis of robust core/shell gold nanoparticles. *J. Am. Chem. Soc.* **2008**, 130, 12852-12853.

Dong L, Jiang H, Autonomous microfluidics with stimuli-responsive hydrogels. *Soft Matter* **2007,** 3, 1223-1239.

DosSantos DS, Goulet PJG, Pieczonka NPW. Gold Nanoparticle Embedded, Self-Sustained Chitosan Films as Substrates for Surface-Enhanced Raman Scattering. *Langmuir* **2004**, 20, 10273-10277.

Du L, Jiang H, Liu X. Biosynthesis of gold nanoparticles assisted by Escherichia coli DH5[α] and its application on direct electrochemistry of hemoglobin. *Electrochemistry Communications* **2007**, 9, 1165-1170.

Duan H, Nie S. Etching Colloidal Gold Nanocrystals with Hyperbranched and Multivalent Polymers: A New Route to Fluorescent and Water-Soluble Atomic Clusters. *J Am Chem So*c **2007**, 129, 2412-2413.

Dune X, Henrik A, Teodor A. Surface-Confined Photopolymerization of pH-Responsive Acrylamide/Acrylate Brushes on Polymer Thin Films. *Langmuir* **2008**, 24, 7559-7564.

Dupont J, Fonseca GS, Umpierre AP. Transition-Metal Nanoparticles in Imidazolium Ionic Liquids: Recycable Catalysts for Biphasic Hydrogenation Reactions. *J Am Chem Soc* **2002**, 124, 4228-4229.

Dzidic I. Relative gas-phase basicities of some amines, anilines, and pyridines. *J. Am. Chem. Soc.* **1972**, 94, 8333-8335.

Edmondson S, Osborne VL, Huck WTS. Polymer brushes via surface-initiated polymerizations. *Chemical Society Reviews* **2004**, 33, 14-22.

Ehrick JD, Deo SK, Browning TW, Bachas LG, Madou MJ, Daunert S. Genetically engineered protein in hydrogels tailors stimuli-responsive characteristics. *Nature Materials* **2005,** 4, 298-302.

Elghanian R, Storhoff JJ, Mirkin CA. Selective Colorimetric Detection of Polynucleotides Based on the Distance-Dependent Optical Properties of Gold Nanoparticles. *Science* **1997**, 277, 1078-1081.

El-Sayed IH, Huang X, El-Sayed M.A. Selective laser photo-thermal therapy of epithelial carcinoma using anti-EGFR antibody conjugated gold nanoparticles. *Cancer Lett.* **2006**, 239, 129-135.

Engel E, Michiardi A, Navarro M, Lacroix D, Planell JA. Nanotechnology in regenerative medicine: the materials side. *Trends. Biotechnol.* **2008**, 26, 39–47.

Esumi K, Hosoya T, Suzuki A. Spontaneous Formation of Gold Nanoparticles in Aqueous Solution of Sugar-Persubstituted Poly(amidoamine)dendrimers. *Langmuir* **2000**, 16, 2978-2980.

Fortina P, Kricka LJ, Surrey S. Nanobiotechnology: the promise and reality of new approaches to molecular recognition. *Trends in Biotechnology* **2005**, 23, 168-173.

Frimpong RA, Fraser S, Hilt JZ. Synthesis and temperature response analysis of magnetic-hydrogel nanocomposites. *J. Biomed. Mater. Res., Part A* **2007,** 80A, 1-6.

Frens G. Controlled nucleation for the regulation of the particle size in monodisperse gold suspensions. *Nature (London) Physical Science* **1973**, 241, 20.

Gang Han, You C-C, Rotello VM. Light-Regulated Release of DNA and Its Delivery to Nuclei by Means of Photolabile Gold Nanoparticles13. *Angewandte Chemie International Edition* **2006**, 45, 3165-3169.

Gao F, Yuan R, Chai Y. Amperometric hydrogen peroxide biosensor based on the immobilization of HRP on nano-Au/Thi/poly (p-aminobenzene sulfonic acid)-modified

glassy carbon electrode. *Journal of Biochemical and Biophysical Methods* **2007**, 70, 407-413.

Garcia ME, Baker LA, Crooks RM. Preparation and Characterization of Dendrimer-Gold Colloid Nanocomposites. *Anal Chem* **1999**, 71, 256-258.

Ghosh A, Patra CR, Mukherjee P, Sastry M, Kumar R. Preparation and stabilization of gold nanoparticles formed by in situ reduction of aqueous chloroaurate ions within surface-modified mesoporous silica. *Microporous and Mesoporous Mater* **2003,** 58, 201-211.

Gibson JD, Khanal BP, Zubarev ER. Paclitaxel-Functionalized Gold Nanoparticles. *J Am Chem Soc* **2007**, 129, 11653-11661.

Gole A, Dash C, Soman C, Sainkar SR, Rao M, Sastry M. On the preparation, characterization and enzymatic activity of fungal protease-gold colloid bioconjugates. *Bioconjugate Chem* **2001**, 12, 684-690.

Guo K, Chu CC. Controlled release of paclitaxel from biodegradable unsaturated poly(ester amide)s/poly(ethylene glycol) diacrylate hydrogels. *J. Biomaterials Sci. Polym. Ed.* **2007**, 18, 489-504.

Haba Y, Kojima C, Harada A. Preparation of Poly(ethylene glycol)-Modified Poly(amido amine) Dendrimers Encapsulating Gold Nanoparticles and Their Heat-Generating Ability. *Langmuir* **2007,** 23, 5243-5246.

Haiss W, Thanh NTK, Aveyard J, Fernig DG. Determination of size and concentration of gold nanoparticles from UV-Vis spectra. *Anal Chem* **2007,** 79, 4215-4221.

Hammond P, Whitesides GM. Formation of Polymer Microstructures by selective deposition of Polyion Multilayers Using self-assembled monolayers as a Template, *Macromolecules* **1995**, 28, 7569-7571.

Han G, Chari NS, Rotello VM. Controlled Recovery of the Transcription of Nanoparticle-Bound DNA by Intracellular Concentrations of Glutathione. *Bioconjugate Chem* **2005**, 16, 1356-1359.

Han G, Martin CT, Rotello VM. Stability of Gold Nanoparticle-Bound DNA toward Biological, Physical, and Chemical Agents. *Chemical Biology & Drug Design* **2006**, 67, 78-82.

Hawkins AM, Satarkar NS, Hilt JZ. Nanocomposite degradable hydrogels: demonstration of remote controlled degradation and drug release. *Pharm Res* **2009,** 26, 667-673.

Hayes RA, Feenstra BJ. Video-speed electronic paper based on electrowetting. *Nature* **2003,** 425, 383-385.

He L, Musick MD, Nicewarner SR. Colloidal Au-Enhanced Surface Plasmon Resonance for Ultrasensitive Detection of DNA Hybridization. *J Am Chem Soc* **2000**, 122, 9071-9077.

He P, Urban MW. Phospholipid-Stabilized Au-Nanoparticles. *Biomacromolecules* **2005**, 6, 1224-1225.

He P, Zhu X. Phospholipid-assisted synthesis of size-controlled gold nanoparticles. *Materials Research Bulletin* **2007**, 42, 1310-1315.

He Q, Kuller A, Grunze M. Fabrication of Thermosensitive Polymer Nanopatterns through Chemical Lithography and Atom Transfer Radical Polymerization. *Langmuir* **2007**, 23, 3981-3987.

Hilt JZ, Gupta AK, Bashir R, Peppas NA. Ultrasensitive bioMEMs sensors based on microcantilevers patterned with environmentally responsive hydrogels. *Biomed. Microdev.* **2003**, 5, 177-184.

Hirsch LR, Halas NJ, West JL. A Whole Blood Immunoassay Using Gold Nanoshells. *Anal Chem* **2003**, 75, 2377-2381.

Hirsch LR, Stafford RJ, Bankson JA. Nanoshell-mediated near-infrared thermal therapy of tumors under magnetic resonance guidance. *Proceedings of the National Academy of Sciences of the United States of America* **2003**, 100, 13549-13554.

Hirotsu S, Hirokawa Y, Tanaka T, Volume-phase transitions of ionized N-isopropyl acrylamide. *J. Chem Phys* **1987,** 87, 1392-1395.

Hoffman AS. Hydrogels in biomedical applications. *Adv. Drug Deliver. Rev.* **2002**, 43, 3-12.

Hoffman AS. Intelligent polymers. In: Controlled Drug Delivery: Challenges and Strategies, Park, K. (Ed.), *American Chemical Society **1997***, Washington, DC, pp 485-497.

Hoffman AS, Afrassiabi A, Dong LC. Thermally reversible hydrogels: II. Delivery and selective removal of substances from aqueous solutions. *J. Controlled Release* **1986,** 4, (3), 213-222.

Hone DC, Walker PI, Evans-Gowing R. Generation of Cytotoxic Singlet Oxygen via Phthalocyanine-Stabilized Gold Nanoparticles: A Potential Delivery Vehicle for Photodynamic Therapy. *Langmuir* **2002**, 18, 2985-2987.

Hong R, Forbes NS, Rotello VM. Glutathione-Mediated Delivery and Release Using Monolayer Protected Nanoparticle Carriers. *J Am Chem Soc* **2006**, 128, 1078-1079.

Hook F, Kasemo B, Nylander T, Fant C, Sott K. Elwing, H., Variations in Coupled Water, Viscoelastic Properties, and Film Thickness of a Mefp-1 Protein Film during Adsorption and Cross-Linking; A Quartz Crystal Microbalance with Dissipation Monitoring, Ellipsometry, and Surface Plasmon Resonance Study. *Anal. Chem.* **2001,** 73, 5796-5804.

Houbenov N, Minko S, Stamm M. Mixed Polyelectrolyte Brush from Oppositely Charged Polymers for Switching of Surface Charge and Composition in Aqueous Environment. *Macromolecules* **2003**, 36, 5897-5901.

Huang H, Yang X. Synthesis of Chitosan-Stabilized Gold Nanoparticles in the Absence/Presence of Tripolyphosphate. *Biomacromolecules* **2004**, 5, 2340-2346.

Hsu H-Y, Huang Y-Y. RCA combined nanoparticle-based optical detection technique for protein microarray: a novel approach. *Biosensors and Bioelectronics* **2004**, 20, 123-126.

Huang W, Baker GL, Bruening ML, Controlled Synthesis of Cross-Linked Ultrathin Polymer Films by Using Surface-Initiated Atom Transfer Radical Polymerization*Angew. Chem. Int. Ed.* **2001,** 40, 1510-1512.

Huang W, Baker GL, Bruening ML. Surface-Initiated Thermal Radical Polymerization on Gold. *Langmuir* **2001**, 17, 1731-1736.

Huang X, Qian W, El-Sayed IH. The potential use of the enhanced nonlinear properties of gold nanospheres in photothermal cancer therapy. *Lasers in Surgery and Medicine* **2007**, 39, 747-753.

Hussain I, Graham S, Wang Z. Size-Controlled Synthesis of Near-Monodisperse Gold Nanoparticles in the 1-4 nm Range Using Polymeric Stabilizers. *J Am Chem Soc* **2005**, 127, 16398-16399.

Husseman M, Malmstrom EE, McNamara M, Mate M, Mecerreyes D, Benoit DG, Hedrick JL, Mansky P, Huang E, Russell TP, Hawker CJ. Controlled Synthesis of Polymer Brushes by Living Free Radical Polymerization Techniques. *Macromolecules* **1999 ,** 32, 1424-1431.

Hüther A, Maurer M, Swelling of *N*-isopropyl acrylamide hydrogels in aqueous solutions of poly(ethylene glycol). *Fluid Phase Equil.* **2004,** 226, 321.

Isaacs SR, Cutler EC, Park JS. Synthesis of Tetraoctylammonium-Protected Gold Nanoparticles with Improved Stability. *Langmuir* **2005**, 21, 5689-5692.

Ishida N, Biggs S. Direct Observation of the Phase Transition for a Poly(N-isopropylacryamide) Layer Grafted onto a Solid Surface by AFM and QCM-D. *Langmuir* **2007,** 23, 11083-11088.

Ishida, N, Biggs S. Salt-Induced Structural Behavior for Poly(N-isopropylacryamide) Grafted onto Solid Surface Observed Directly by AFM and QCM-D. *Macromolecules* **2007,** 40, 9045-9052.

Ishii T, Otsuka H, Kataoka K. Preparation of Functionally PEGylated Gold Nanoparticles with Narrow Distribution through Autoreduction of Auric Cation by α-Biotinyl-PEG-block-[poly(2-(N,N-dimethylamino)ethyl methacrylate)]. *Langmuir* **2004**, 20, 561-564.

Itoh H, Naka K, Chujo Y. Synthesis of Gold Nanoparticles Modified with Ionic Liquid Based on the Imidazolium Cation. *J Am Chem Soc* **2004**, 126, 3026-3027.

Jena BK, Raj CR. Electrochemical Biosensor Based on Integrated Assembly of Dehydrogenase Enzymes and Gold Nanoparticles. *Anal Chem* **2006**, 78, 6332-6339.

Jenekhe SA, Zhang X, Chen XL, Choong V-E, Gao Y, Hsieh BR. Finite Size Effects on Electroluminescence of Nanoscale Semiconducting Polymer Heterojunctions. *Chem. Mater.* **1997**, 9, 409–412.

Jeong B, Kim SW, Bae YH. Thermosensitive sol-gel reversible hydrogels, *Adv. Drug Deliv. Revs.* **2002,** 54, 37-51.

Jian Li, He W, Sun X. Preparation of poly(styrene-co-N-isopropylacrylamide) micelles surface-linked with gold nanoparticles and thermo-responsive ultraviolet-visible absorbance. *Journal of Polymer Science Part A: Polymer Chemistry* **2007**, 45, 5156-5163.

Jin R, Wu G, Mirkin CA. What Controls the Melting Properties of DNA-Linked Gold Nanoparticle Assemblies? *J Am Chem Soc* **2003**, 125, 1643-1654.

Jones CD, Serpe MJ, Schroeder L, Lyon LA, Microlens formation of microgel/gold colloid composite materials via photothermal patterning. *J. Am. Chem. Soc.* **2003**, 125, 5292-5293.

Jones DM, Huck WTS. Controlled Surface-Initiated Polymerizations in Aqueous Media. *Advanced Materials* **2001**, 13, 1256-1259.

Jordan R, Ulman A. Surface Initiated Living Cationic Polymerization of 2-Oxazolines. *J Am Chem Soc* **1998**, 120, 243-247.

Jordan R, Ulman A, Kang JF. Surface-Initiated Anionic Polymerization of Styrene by Means of Self-Assembled Monolayers. *J Am Chem Soc* **1999**, 121, 1016-1022.

Jordan R, West N, Ulman A, Chou Y-M, Nuyken O. Nanocomposites by surface initiated living cationic polymerization of 2-oxazolines on functionalized gold nanoparticles. *Macromolecules* **2001**, 34, 1606-1611.

Jones DM, Huck WTS, Controlled Surface-Initiated Polymerizations in Aqueous Media. *Adv. Mater.* **2001,** 13, 1256-1259.

Jones DM, Smith JR, Huck WTS, Variable Adhesion of Micropatterned Thermoresponsive Polymer Brushes: AFM Investigations of Poly(N-isopropylacrylamide) Brushes Prepared by Surface-Initiated Polymerizations. *Adv. Mater.* **2002,** 14, 1130-1134.

Kaholek M, Lee WK, Ahn SJ, Ma H, Caster KC, LaMattina B, Zauscher S. Stimulus-Responsive Poly(*N*-isopropylacrylamide) Brushes and Nanopatterns Prepared by Surface-Initiated Polymerization. *Chem. Mater.* **2004**, 16, 3688-3692.

Kaholek M, Lee WK, LaMattina B, Caster KC, Zauscher S. Fabrication of Stimulus-Responsive Nanopatterned Polymer Brushes by Scanning-Probe Lithography. *Nano Lett.* **2004**, 4, 373-376.

Kang Y, Taton TA. Core/Shell Gold Nanoparticles by Self-Assembly and Crosslinking of Micellar, Block-Copolymer Shells. *Angewandte Chemie International Edition* **2005**, 44, 409-412.

Kattumuri V, Katii K, Bhaskaran S, Boote EJ, Casteel SW, Fent GM, Robertson DJ, Chandrasekhar M, Kannan R, Katti KV. Gum Arabic as a phytochemical construct for the stabilization of gold nanoparticle: In vivo pharamacokinetics and X-ray-contrast-imaging studies. *Small* **2007,** 3, 333-341.

Kerman K, Morita Y, Takamura Y. Modification of Escherichia coli single-stranded DNA binding protein with gold nanoparticles for electrochemical detection of DNA hybridization. *Analytica Chimica Acta* **2004**, 510, 169-174.

Kerman K, Saito M, Morita Y. Electrochemical Coding of Single-Nucleotide Polymorphisms By Monobase-Modified Gold Nanoparticles. *Anal Chem* **2004**, 76, 1877-1884.

Khare AR, Peppas NA. Release Behavior of Bioactive Agents from pH-Sensitive Hydrogels, *J. Biomat. Sci., Polym. Ed.* **1993,** 4, 275-289.

Kim JB, Bruening ML, Baker GL. Surface-Initiated Atom Transfer Radical Polymerization on Gold at Ambient Temperature. *J Am Chem Soc* **2000**, 122, 7616-7617.

Kim JH, Lee TR. Thermo- and pH-Responsive Hydrogel-Coated Gold Nanoparticles. *Chem Mater* **2004**, 16, 3647-3651.

Kim JH, Lee TR. Discrete thermally responsive hydrogel coated gold nanoparticles for use as drug delivery vehicles. *Drug Dev. Res.* **2006**, 67, 61-69.

Kim KS, Demberelnyamba D, Lee H. Size-Selective Synthesis of Gold and Platinum Nanoparticles Using Novel Thiol-Functionalized Ionic Liquids. *Langmuir* **2004**, 20, 556-560.

Kim M-K, Jeon Y-M, Jeon WS. Novel dendron-stabilized gold nanoparticles with high stability and narrow size distribution. *Chemical Communications* **2001**, 667-668.

Kim SY, Shin HS, Lee YM, Jeong CN. Properties of electroresponsive poly(vinyl) alcohol/poly(acrylic acid) IPN hydrogels under an electric stimulus. *J. App. Polym. Sci.* **1999,** 73, 1675-1683.

Kim YG, Oh SK, Crooks RM. Preparation and Characterization of 1-2 nm Dendrimer-Encapsulated Gold Nanoparticles Having Very Narrow Size Distributions. *Chem Mater* **2004**, 16, 167-172.

Kozower BD, Christopher-Solomidou M, Sweitzer TD, Muro S, Buerk DG, Solomides CC, Albelda SM, Patterson GA, Muzykantov VR. Immunotargeting of catalase to the pulmonary endothelium alleviates oxidative stress and reduces acute lung transplantation injury. Nat Biotechnol **2003,** 21, 392-398.

Kuiper S, Hendriks BHW. Variable-focus liquid lens for miniature cameras. *Appl. Phys. Lett.* **2004,** 85, 1128-1130.

Kumar A, Whitesides GM. Features of gold having micrometer to centimeter dimensions can be formed through a combination of stamping with an elastomeric stamp and an alkanethiol "ink" followed by chemical etching, *Appl. Phys. Lett.* **1993,** 63, 2002-2004.

LaVan DA, McGuire T, Langer R. Small-scale systems for in vivo drug delivery. *Nat. Biotech.* **2003**, 21, 1184–1191.

Langer R, Peppas NA. Advances in Biomaterials, Drug Delivery, and Bionanotechnology. *AICHE J.* **2003,** 49, 2990-3006.

Lee J-S, Green JJ, Love KT, Sunshine J, Langer R, Anderson DG. Systemic intracellular delivery of siRNA using gold nanoparticles and poly(β-amino ester)s. *Nano Lett* **2009,** 9, 2402-2406.

Lindner JR. Contrast ultrasound molecular imaging: harnessing the power of bubbles. *Cardiovasc. Res.* **2009**, 83, 615–616.

Li DX, He Q, Cui Y, Li J. Thermosensitive Copolymer Networks Modified Gold Nanoparticles for Nanocomposite Entrapment. *Chem. Eur. J.* **2007**, 13, 2224-2229.

Liu G, Zhang G. Collapse and Swelling of Thermally Sensitive Poly(N-isopropylacrylamide) Brushes Monitored with a Quartz Crystal Microbalance. *J. Phys. Chem. B* **2005**, 109, 743-747.

Liu S, Ju H. Reagentless glucose biosensor based on direct electron transfer of glucose oxidase immobilized on colloidal gold modified carbon paste electrode. *Biosensors and Bioelectronics* **2003**, 19, 177-183.

Loo C, Lin A, Hirsch L. Nanoshell-Enabled Photonics Based Imaging and Therapy of Cancer. *Technology in Cancer Research and Treatment* **2004**, 3, 33-40.

Loo L, Guenther RH, Basnayake VR. Controlled Encapsidation of Gold Nanoparticles by a Viral Protein Shell. *J Am Chem Soc* **2006**, 128, 4502-4503.

Lopez CA, Lee CC, Hirsa AH. Electrochemically activated adaptive liquid lens *Appl. Phys. Lett.* **2005,** 87, 134102-134105.

Love JC, Estroff LA, Whitesides GM. Self-Assembled Monolayers of Thiolates on Metals as a Form of Nanotechnology. *Chem Rev* **2005**, 105, 1103-1170.

Low LM, Seetharaman S, Madou MJ. Microactuators towards microvalves for responsive controlled drug delivery. *Sens. Actuators B*, **2000,** 67, 149-160.

Lowman AM, Peppas NA. Hydrogels. in: E. Mathiowitz (Ed.), Encyclopedia of Controlled Drug Delivery, Vol. 1, *Wiley*, New York, **1999**, pp. 397-418.

Luo X-L, Xu J-J A glucose biosensor based on chitosan-glucose oxidase-gold nanoparticles biocomposite formed by one-step electrodeposition. *Analytical Biochemistry* **2004**, 334, 284-289.

Luo X-L, Xu J-J, Zhang Q. Electrochemically deposited chitosan hydrogel for horseradish peroxidase immobilization through gold nanoparticles self-assembly. *Biosensors and Bioelectronics* **2005**, 21, 190-196.

Lutz JF, Hoth A. Preparation of ideal PEG analogues with a tunable thermosensitivity by controlled radical copolymerization of 2-(2-methoxyethoxy)ethyl methacrylate and oligo(ethylene glycol) methacrylate. *Macromolecules* **2006,** 39, 893-896.

Lyon LA, Musick MD, Natan MJ. Colloidal Au-Enhanced Surface Plasmon Resonance Immunosensing. *Anal Chem* **1998**, 70, 5177-5183.

Majzik A, Patakfalvi R, Hornok V, Dekany I. Growing and stability of gold nanoparticles and their functionalization by cysteine. *Gold Bulletin* **2009,** 42, 113-123.

Manandhar P, Jang J, Schatz GC, Ratner MA, Hong S. Anomalous Surface Diffusion in Nanoscale Direct Deposition Processes. *Phys. Rev. Let.* **2003**, 90, 115505-115507.

Manso J, Mena ML, Pingarrón J. Electrochemical biosensors based on colloidal gold-carbon nanotubes composite electrodes. *Journal of Electroanalytical Chemistry* **2007**, 603, 1-7.

Marchetti M, Prager S, Cussler EL. Thermodynamic predictions of volume changes in temperature-sensitive gels. 1. Theory. *Macromolecules* **1990,** 23, 1760-1765.

Matyjaszewski K, Beers KL, Woodworth B, Metzner Z, Controlled/Living Radical Polymerization in the Undergraduate Laboratories. 2. Using ATRP in Limited Amounts of Air to Prepare Block and Statistical Copolymers of n-Butyl Acrylate and Styrene. *J. Chem. Edu.* **2001,** 78, 547-550.

Matyjasewski K, Davis TP. Handbook of Radical Polymerization. First ed. Hoboken: John Wiley & Sons; **2002,** 28-143.

Matyjaszewski K, Dong H, Jakubowski W. Grafting from Surfaces for "Everyone": ARGET ATRP in the Presence of Air. *Langmuir* **2007**, 23, 4528-4531.

Matyjaszewski K, Miller PJ, Shukla N. Polymers at Interfaces: Using Atom Transfer Radical Polymerization in the Controlled Growth of Homopolymers and Block Copolymers from Silicon Surfaces in the Absence of Untethered Sacrificial Initiator. *Macromolecules* **1999**, 32, 8716-8724.

Maxwell DJ, Taylor JR, Nie S. Self-Assembled Nanoparticle Probes for Recognition and Detection of Biomolecules. *J Am Chem Soc* **2002**, 124, 9606-9612.

Mayadunne RTA, Rizzardo E, Chiefari J. Living Radical Polymerization with Reversible Addition-Fragmentation Chain Transfer (RAFT Polymerization) Using Dithiocarbamates as Chain Transfer Agents. *Macromolecules* **1999**, 32, 6977-6980.

McIntosh CM, Martin CT, Rotello VM. Inhibition of DNA Transcription Using Cationic Mixed Monolayer Protected Gold Clusters. *J Am Chem Soc* **2001**, 123, 7626-7629.

Meenach SA, Hilt JZ, Anderson KW, Poly(ethylene glycol) based magnetic hydrogel nanocomposites for hyperthermia cancer therapy. *Acta Biomaterialia* **2010**, 6, 1039-1046.

Mena ML, Yáñez-Sedeño P, Pingarrón JM. A comparison of different strategies for the construction of amperometric enzyme biosensors using gold nanoparticle-modified electrodes. *Analytical Biochemistry* **2005**, 336, 20-27.

Mirkin CA, Letsinger RL, Mucic RC. A DNA-based method for rationally assembling nanoparticles into macroscopic materials. *Nature* **1996**, 382, 607-609.

Miyama T, Yonezawa Y. Aggregation of Photolytic Gold Nanoparticles at the Surface of Chitosan Films. *Langmuir* **2004**, 20, 5918-5923.

Miyata T, Uragami T, Nakamae K. Biomolecule-sensitive hydrogels, *Adv. Drug Delivery Revs.* **2002**, 54, 79-98.

Moghimi SM, Hunter AC, Murray JC. Nanomedicine: current status and future prospects. *FASEB J* **2005**, 19, 311-330.

Mocellin S, Bronte V, Nitti D. Nitric oxide, a double edged sword in cancer biology: Searching for therapeutic opportunities. *Medicinal Research Reviews* **2007**, 27, 317-352.

Mulvaney SP, Musick MD, Keating CD. Glass-Coated, Analyte-Tagged Nanoparticles: A New Tagging System Based on Detection with Surface-Enhanced Raman Scattering. *Langmuir* **2003**, 19, 4784-4790.

Muzykantov VR, Atochina EN, Ischiropolous H, Danilov VM, Fisher AB. Immunotargeting of antioxidant enzyme to the pulmonary endothelium. *Proc Natl Acad Sci USA* **1996,** 93, 5213-5218.

Nakao S, Torigoe K, Kon-No K. Self-Assembled One-Dimensional Arrays of Gold-Dendron Nanocomposites. *J Phys Chem B* **2002**, 106, 12097-12100.

Nam JM, Stoeva SI, Mirkin CA. Bio-Bar-Code-Based DNA Detection with PCR-like Sensitivity. *J Am Chem Soc* **2004**, 126, 5932-5933.

Nath N, Chilkoti A, Creating "Smart" Surfaces Using Stimuli Responsive Polymers.*Adv. Mater.* **2002,** 14, 1243-1247.

Odian G. Principles of Polymerization, Wiley Intersceince, 4th ed., **2004**.

Ohno K, Koh Km, Tsujii Y. Synthesis of Gold Nanoparticles Coated with Well-Defined, High-Density Polymer Brushes by Surface-Initiated Living Radical Polymerization. *Macromolecules* **2002**, 35, 8989-8993.

Oishi M, Nakaogami J, Ishii T. Smart PEGylated Gold Nanoparticles for the Cytoplasmic Delivery of siRNA to Induce Enhanced Gene Silencing. *Chemistry Letters* **2006**, 35, 1046-1047.

Okamoto T, Mori M, Karasawa T, Hayakawa S, Seo I, Sato H, Ultraviolet cured polymer microlens arrays. *Appl. Opt.* **1999**, 38, 2991-2996.

Okano T, Bae YH, Jacobs H, Kim SW. Thermally on-off switching polymers for drug permeation and release. *J. Controlled Release* **1990,** 11, (1-3), 255-265.

Okano T, Yamada N, Sakai H, Sakurai Y. A novel recovery system for cultured cells using plasma-treated polystyrene dishes grafted with poly(N-isopropylacrylamide). *J. Biomed. Mater. Res.* **1993,** 27, 1243-1251.

Oldenburg SJ, Averitt RD, Westcott SL. Nanoengineering of optical resonances. *Chemical Physics Letters* **1998**, 288, 243-247.

Olivier J-C, Huertas R, Lee HJ. Synthesis of Pegylated Immunonanoparticles. *Pharmaceutical Research* **2002**, 19, 1137-1143.

Orosco MM, Pacholski C, Sailor MJ. Real-time monitoring of enzyme activity in a mesoporous silicon double layer. *Nat. Nanotech.* **2009**, 4, 255–258.

Otsuka H, Akiyama Y, Nagasaki Y. Quantitative and Reversible Lectin-Induced Association of Gold Nanoparticles Modified with α-Lactosyl-ω-mercapto-poly(ethylene glycol). *J Am Chem Soc* **2001**, 123, 8226-8230.

Otsuka H, Nagasaki Y, Kataoka K. PEGylated nanoparticles for biological and pharmaceutical applications. *Advanced Drug Delivery Reviews* **2003**, 55, 403-419.

Ozsoz M, Erdem A, Kerman K. Electrochemical Genosensor Based on Colloidal Gold Nanoparticles for the Detection of Factor V Leiden Mutation Using Disposable Pencil Graphite Electrodes. *Anal Chem* **2003**, 75, 2181-2187.

O'Neal DP, Hirsch LR, West JL. Photo-thermal tumor ablation in mice using near infrared-absorbing nanoparticles. *Cancer Letters* **2004**, 209, 171-176.

Paciotti GF, David GI, Tamarkin KL. Colloidal gold nanoparticles: a novel nanoparticle platform for developing multifunctional tumor-targeted drug delivery vectors. *Drug Development Research* **2006**, 67, 47-54.

Papavasiliou G, Songprawat P, Perez-Luna V, Hammes E, Morris M, Chiu YC, Brey E. Three Dimensional Patterning in Poly(ethylene glycol) Hydrogels Through Surface Initiated Photopolymerization. *Tissue Eng. C* 2008, 14, 129-140.

Park S-J, Taton TA, Mirkin CA. Array-Based Electrical Detection of DNA with Nanoparticle Probes. *Science* **2002**, 295, 1503-1506.

Patel N, Davies MC, Hartshorne M, Heaton RJ, Roberts CJ, Tendler SJB, Williams PM. Immobilization of protein molecules onto homogenous and mixed carboxylate-terminated self assembled monolayers. *Langmuir* **1997**, 13, 6485-6490.

Pekka P. Theoretical Chemistry of Gold. *Angewandte Chemie International Edition* **2004**, 43, 4412-4456.

Peppas NA, Bures P, Leobandung W, Ichikawa H. Hydrogels in pharmaceutical formulations. European *J. Pharm Biopharm* **2000**, 50, 27-46.

Peppas NA, Hilt JZ, Khademhosseini A, Langer R. Hydrogels in biology and medicine: from fundamentals to bionanotechnolgoy. *Adv. Mater.* **2006,** 18, 1345-1350.

Peppas NA, Huang Y, Torres-Lugo M, Ward JH, Zhang J. Physiochemical foundations and structural design of hydrogels in medicine and biology. *Ann. Revs. Biomed. Eng.* **2000,** 2, 9-29.

Peppas NA, Khare AR. Preparation, structure and diffusional behavior of hydrogels in controlled release. *Adv. Drug Delivery Rev.* **1993,** 11, 1-35.

Perignon N, Marty JD, Mingotaud AF. Hyperbranched Polymers Analogous to PAMAM Dendrimers for the Formation and Stabilization of Gold Nanoparticles. *Macromolecules* **2007**, 40, 3034-3041.

Phadtare S, Kumar A, Vinod VP, Dash C, Palaskar DV, Rao M, Shukla PG, Sivaram S, Sastry M. Direct assembly of gold nanoparticle shells on polyurethane microsphere cores and their application as enzyme immobilization templates. *Chem Mater* **2003**, 15, 1944-1949.

Pingarrón JM, Yáñez-Sedeño P, González-Cortés A. Gold nanoparticle-based electrochemical biosensors. *Electrochimica Acta* **2008**, 53, 5848-5466.

Place ES, George JH, Williams CK, Stevens MM. Synthetic polymer scaffolds for tissue engineering. *Chem. Soc. Rev.* **2009**, 38, 1139–1151.

Polizzi MA, Stasko NA, Schoenfisch MH. Water-Soluble Nitric Oxide-Releasing Gold Nanoparticles. *Langmuir* **2007**, 23, 4938-4943.

Popovic ZD, Sprague RA, Connell GAN. Technique for monolithic fabrication of microarrays lens. *Appl. Opt.* **1988,** 27, 1281-1284.

Prucker O, Ruhe J. Synthesis of Poly(styrene) Monolayers Attached to High Surface Area Silica Gels through Self-Assembled Monolayers of Azo Initiators, *Macromolecules,* **1998,** 31, 592-597.

Qi Z, Zhou H, Matsuda N. Characterization of Gold Nanoparticles Synthesized Using Sucrose by Seeding Formation in the Solid Phase and Seeding Growth in Aqueous Solution. *J Phys Chem B* **2004**, 108, 7006-7011.

Radt B, Smith A, Caruso F. Optically Addressable Nanostructured Capsules. *Advanced Materials* **2004**, 16, 2184-2189.

Ren H, Wu ST. Variable-focus liquid lens by changing aperture. *Appl. Phys. Lett.* **2005,** 86, 211107-211110.

Revzin A, Russell RJ, Yadavalli VK, Koh W, Deister C, Hile DD, Mellott MB, Pishko MV, Fabrication of poly(ethylene glycol) hydrogel microstructrues using photolithography. *Langmuir* **2001**, 17, 5440-5447.

Ritger PL, Peppas NA. A simple equation for description of solute release: Fickian and non Fickian release. *J. Control. Rel.* **1987**, 5, 23-30.

Rodahl M, Hook F, Krozer A, Brzezinski P, Kasemo B. Quartz crystal microbalance setup for frequency and Q-factor measurements in gaseous and liquid environments. *Rev. Sci. Instrum.* **1995,** 66, 3924-3930.

Rodahl M, Kasemo B. A simple setup to simultaneously measure the resonant frequency and the absolute dissipation factor of a quartz crystal microbalance. *Rev. Sci. Instrum.* **1996,** 67, 3238-3241.

Rosi NL, Giljohann DA, Thaxton CS. Oligonucleotide-Modified Gold Nanoparticles for Intracellular Gene Regulation. *Science* **2006**, 312, 1027-1030.

Saito G, Swanson JA, Lee K-D. Drug delivery strategy utilizing conjugation via reversible disulfide linkages: role and site of cellular reducing activities. *Advanced Drug Delivery Reviews* **2003**, 55, 199-215.

Saitoh A, Tanaka K. Self-developing aspherical chalcogenide-glass microlenses for semiconductor lasers. *Appl. Phys. Lett.* **2003,**83, 1725-1727.

Sakellariou G, Advincula R, Mays J. Homopolymer and block copolymer brushes on gold by living anionic surface-initiated polymerization in a polar solvent. *Journal of Polymer Science Part A: Polymer Chemistry* **2006**, 44, 769-782.

Sandhu KK, McIntosh CM, Rotello VM. Gold Nanoparticle-Mediated Transfection of Mammalian Cells. *Bioconjugate Chem* **2002**, 13, 3-6.

Sanders LM, McRae GI, Vitale KM, Kell BA. Controlled delivery of an LHRH analogue from biodegradable injectable microspheres. *J. Controlled Rel.* **1985,** 2, 187-195.

Santini JT, Richards AC, Scheidt R, Cima MJ, Langer R. Microchips as controlled drug-delivery devices. *Angew. Chem. Int. Ed.* **2000**, 39, 2396–2407.

Sapsford KE, Berti L, Mendintz IL. Materials for Fluorescence Resonance Energy Transfer Analysis: Beyond Traditional Donor-Acceptor Combinations. *Angewandte Chemie International Edition* **2006**, 45, 4562-4589.

Sanvicens N, Marco MP. Multifunctional nanoparticles--properties and prospects for their use in human medicine. *Trends Biotechnol.* **2008**, 26, 425-433.

Satarkar NS, Hilt JZ. Hydrogel nanocomposites as remote controlled biomaterials. *Acta Biomater.* **2008,** 4, 11-16.

Satarkar NS, Hilt J.Z. Magnetic hydrogel nanocomposites for remote controlled pulsatile drug *release. J. Controlled Release.* **2008**, 3, 246-251.

Scheeren CW, Machado G, Dupont J. Nanoscale Pt(0) Particles Prepared in Imidazolium Room Temperature Ionic Liquids: Synthesis from an Organometallic Precursor, Characterization, and Catalytic Properties in Hydrogenation Reactions. *Inorg Chem* **2003**, 42, 4738-4742.

Schild HG. Poly(n-isopropylacrylamide): Experiment, theory and application. *Progress in Polymer Science* **1992,** 17, 163-249.

Schmaljohann D, Oswald J, Jorgensen B, Nitschke M, Beyerlein D, Werner C. Thermo responsive PINPAAm-g-PEG films for controlled cell detachment. *Biomacromolecules* **2003,** 4, 1733-1739.

Schmid G. Large Clusters and Colloids. Metals in Embryotic State. *Chem Rev* **1992**, 12. 92, 1709-1727.

Schmid, G, Baumle M, Geerkens M, Heim, I, Osemann C, Sawitowski T. Current and future applications of nanoclusters. *Chem. Soc. Rev.* **1999,** 28, 179-185.

Schmidt R, Zhao T, Green JB. Photoinitiated Polymerization of Styrene from Self-Assembled Monolayers on Gold. *Langmuir* **2002**, 18, 1281-1287.

Schneider GB, English A, Abraham M, Zaharias R, Stanford C, Keller J. The effect of charge density on cellular detachment. *Biomaterials* **2004,** 25, 3023-3028.

Scouten WH, Konecny P. Reversible immobilization of antibodies on magnetic beads. *Anal Biochem* **1992,** 205, 313-318.

Sershen S, Mensing G, Beebe D, West J. Independent optical control of microfluidic valves formed from optomechanically responsive nanocomoposite hydrogels. *Adv. Mater.* **2005,** 17, 1366-1372.

Shah RR, Merreceyes DM, Hedrick JL. Using Atom Transfer Radical Polymerization to Amplify Patterned Monolayers of Initiator into Polymeric Barriers for Wet Chemical Etchants. *Macromolecules* **2000,** 33, 597-605.

Shan J, Nuopponen M, Jiang H. Preparation of Poly(N-isopropylacrylamide)-Monolayer-Protected Gold Clusters: Synthesis Methods, Core Size, and Thickness of Monolayer. *Macromolecules* **2003**, 36, 4526-4533.

Shibayama M, Tanaka T, Volume phase transition and related phenomena of polymer gels. In *Responsive Gels: Volume Transitions I* **1993,** pp 1-92.

Shimmin RG, Schoch AB, Braun PV. Polymer Size and Concentration Effects on the Size of Gold Nanoparticles Capped by Polymeric Thiols. *Langmuir* **2004**, 20, 5613-5620.

Sidorenko A, Krupenkin T, Taylor A, Fratzl P, Aizenberg J. Reversible Switching of Hydrogel-Actuated Nanostructures into Complex Micropatterns. *Science* **2007**, 315, 487-490.

Sirkar K, Pishko MV. Amperometric biosensors based on oxidoredictases immobilized in photopolymerized poly(ethylene glycol) redox polymer hydrogels. *Anal. Chem.* **1998,** 70, 2888-2894.

Skirtach AG, Oliver J, Karen K. Laser-Induced Release of Encapsulated Materials inside Living Cells. *Angewandte Chemie International Edition* **2006**, 45, 4612-4617.

Slaughter BV, Khurshid SS, Fisher OZ, Khademhosseini A, Peppas NA. Hydrogels in Regenerative Madicine. *Adv. Mater.* **2009**, 21, 3307-3329.

Slocik JM, Morley OS, Rajesh RN. Synthesis of Gold Nanoparticles Using Multifunctional Peptides13. *Small* **2005**, 1, 1048-1052.

Slocik JM, Naik RR, Stone MO. Viral templates for gold nanoparticle synthesis. *Journal of Materials Chemistry* **2005**, 15, 749-753.

Sokuler M, Gheber LA, Nano fountain pen manufacture of polymer lens for nano biochip applications. *Nano Lett.* **2006**, 6, 848-853.

Son SJ, Bai X, Lee SB. Inorganic hollow nanoparticles and nanotubes in nanomedicine part 2: imaging, diagnostic and therapeutic applications. *Drug. Discov. Today.* **2007,** 12, 657-663.

Soppimath KS, Aminabhavi TM, Dave AM, Kumbar SG, Rudzinski WE. Stimulus-responsive “smart” hydrogels as novel drug delivery systems. *Drug Development and Industrial Pharmacy* **2002,** 28, 957-974.

Sonavane G, Tomoda K, Maknio K. Biodistribution of colloidal gold nanoparticles after intravenous administration: effect of particle size. *Colloids Surf B* **2008**, 66, 274-280.

Stakeborg T, Peeters S, Reekmans G, Laureyn W, Jans H, Borghs G, Imberechts H. Increasing the stability of DNA-functionalized gold nanoparticles using mercaptoalkanes. *J Nanoparticle Res* **2008,** 10, 143-152.

Stoneheurner JG, Zhao J, O'Daly JP, Crumbliss AL, Henkens RW. Comparison of colloidal gold electrode fabrication methods: the preparation of a horse radish peroxidase enzyme electrode. *Biosens Bioelectron* **1992**, 7, 421-428.

Storhoff JJ, Elghanian R, Mirkin CA. One-Pot Colorimetric Differentiation of Polynucleotides with Single Base Imperfections Using Gold Nanoparticle Probes. *J Am Chem Soc* **1998**, 120, 1959-1964.

Strzelczyk AA, Dobrowolski JC, Mazurek AP. On the confirmation of biotin molecule. *J Molec Struc (Theochem)* **2001,** 541, 283-290.

Takada K, Diaz DJ. Abruna, H. D.; Cuadrado, I.; Casado, C.; Alonso, B.; Moran, M.; Losada, J., Redox-Active Ferrocenyl Dendrimers; Thermodynamics and Kinetics of Adsorption, In-Situ Electrochemical Quartz Crystal Microbalance Study of the Redox Process and Tapping Mode AFM Imaging. *J. Am. Chem. Soc.* **1997,** 119, 10763-10773.

Takae S, Akiyama Y, Otsuka H. Ligand Density Effect on Biorecognition by PEGylated Gold Nanoparticles: Regulated Interaction of RCA Lectin with Lactose Installed to the Distal End of Tethered PEG Strands on Gold Surface. *Biomacromolecules* **2005**, 6, 818-824.

Takei YG, Aoki T, Sanui K. Okano T. Dynamic Contact Angle Measurement of Temperature-Responsive Surface Properties for Poly(N-isopropylacrylamide) Grafted Surfaces. *Macromolecules* **1994**, 27, 6163-6166.

Tamirisa PA, Hess DW. Water and Moisture Uptake by Plasma Polymerized Thermoresponsive Hydrogel Films. *Macromolecules* **2006,** 39, 7092.

Tan J, Tien J, Chen C. Microcontact printing of proteins on mixed self-assembled monolayers. *Langmuir* **2002,** 18, 519-523.

Tang DP, Yuan R, Chai YQ. Novel potentiometric immunosensor for hepatitis B surface antigen using a gold nanoparticle-based biomolecular immobilization method. *Analytical Biochemistry* **2004**, 333, 345-350.

Tang DP, Yuan R, Chai YQ. Preparation and application on a kind of immobilization method of anti-diphtheria for potentiometric immunosensor modified colloidal Au and polyvinyl butyral as matrixes. *Sensors and Actuators B: Chemical* **2005**, 104, 199-206.

Tang DP, Yuan R, Chai YQ. Electrochemical immuno-bioanalysis for carcinoma antigen 125 based on thionine and gold nanoparticles-modified carbon paste interface. *Analytica Chimica Acta* **2006**, 564, 158-165.

Tansil NC, Gao Z. Nanoparticles in biomolecular detection. Nano Today 2006, 1, 28-37.

Taton TA, Mirkin CA, Letsinger RL. Scanometric DNA Array Detection with Nanoparticle Probes. *Science* **2000**, 289, 1757-1760.

Taton TA, Mucic RC, Mirkin CA. The DNA-Mediated Formation of Supramolecular Mono- and Multilayered Nanoparticle Structures. *J Am Chem Soc* **2000**, 122, 6305-636.

Templeton AC, Wuelfing WP, Murray RW. Monolayer-Protected Cluster Molecules. *Acc Chem Res* **2000**, 33, 27-36.

Teranishi T, Kiyokawa I, Miyake M. Synthesis of Monodisperse Gold Nanoparticles Using Linear Polymers as Protective Agents. *Advanced Materials* **1998**, 10, 596-599.

Theis T, Parr D, Binks P, Ying J, Drexler KE, Schepers E, Mullis K, Bai C, Boland JJ, nan'o.tech.nol'o.gy n. *Nat. Nanotech.* **2006**, 1, 8-10.

Thomas M, Klibanov AM. Conjugation to gold nanoparticles enhances polyethylenimine's transfer of plasmid DNA into mammalian cells. *Proceedings of the National Academy of Sciences of the United States of America* **2003**, 100, 9138-9143.

Treat ND, Ayres N, Boyes SG. A Facile Route to Poly(acrylic acid) Brushes Using Atom Transfer Radical Polymerization. *Macromolecules* **2006**, 39, 26-29.

Truskett VN, Watts MPC. Trends in imprint lithography for biological applications. *Trends Biotech.* **2006**, 24, 312-317.

Tu H, Heitzman CE, Braun PV. Patterned Poly(N-isopropylacrylamide) Brushes on Silica Sufaces by Microcontact Printing Followed by Surface-Initiated Polymerization, *Langmuir* **2004,** 20, 8313-8320.

Tugulu S, Barbey R, Harms M. Synthesis of Poly(methacrylic acid) Brushes via Surface-Initiated Atom Transfer Radical Polymerization of Sodium Methacrylate and Their Use as Substrates for the Mineralization of Calcium Carbonate. *Macromolecules* **2007**, 40, 168-177.

Turkevich J, Stevenson PC, Hillier J. A study of the nucleation and growth processes in the synthesis of colloidal gold. *Discussions of the Faraday Society* **1951**, 11, 55-75.

Veiseh O, Sun C, Gunn J, Kohler N, Gabikian P, Lee D, Bhattarai N, Ellenbogen R, Sze R, Hallahan A, Olson J, Zhang M. Optical and MRI multifunctional nanoprobe for targeting gliomas. *Nano Letters* **2005,** 5, 1003-1008.

Verma A, Simard JM, Rotello VM. Tunable Reactivation of Nanoparticle-Inhibited β-Galactosidase by Glutathione at Intracellular Concentrations. *J Am Chem Soc* **2004**, 126, 13987-1399.

Wan D, Fu Q, Huan J. Synthesis of amphiphilic hyperbranched polyglycerol polymers and their application as template for size control of gold nanoparticles. *Journal of Applied Polymer Science* **2006**, 101, 509-514.

Wang B, Chen K, Jiang S. Chitosan-Mediated Synthesis of Gold Nanoparticles on Patterned Poly(dimethylsiloxane) Surfaces. *Biomacromolecules* **2006,** 7, 1203-1209.

Wang H, Chen Y, Li XY. Synthesis of Oligo(ethylenediamino)-β-Cyclodextrin Modified Gold Nanoparticle as a DNA Concentrator. *Mol Pharmaceutics* **2007**, 4, 189-198.

Wang J, Chen Z, Mauk M, Hong K-S, Li M, Yang S, Bau HH. Self actuated thermoresponsive hydrogel valves for lan on a chip. *Biomed. Microdevices* **2005**, 7, 313-322.

Wang M, Wang L, Wang G. Application of impedance spectroscopy for monitoring colloid Au-enhanced antibody immobilization and antibody-antigen reactions. *Biosensors and Bioelectronics* **2004**, 19, 575-582.

Wang R, Yang J, Seraphin S. Dendron-Controlled Nucleation and Growth of Gold Nanoparticles. *Angewandte Chemie International Edition* **2001**, 40, 549-552.

Wang W, Zhang C, Wang S, Zhao J, Diffusion of Single Polyelectrolytes on the Surface of Poly(*N*-isopropylacrylamide) Brushes. *Macromolecules* **2007,** 40, 9564.

Wang YX, Hussain SM, Krestin GP. Superparamagnetic iron oxide contrast agents: physicochemical characteristics and applications in MR imaging. *Eur. Radiol.* **2001**, 11, 2319–2331.

Ward JH, Bashir R, Peppas NA. Micropatterning of Biomedical Polymer Surfaces by Novel UV Polymerization Techniques, *J. Biomed. Mater. Res.* **2001**, 56, 351-360.

Ware M. Photographic Printing in Colloidal Gold. *The Journal of Photographic Science* **1994**, 42, 157-161.

Weibel DB, Garstecki P, Whitesides GM. Combining microscience and neurobiology, *Current Opinions in Neurobiology* **2005,** 15, 560-567.

Weller H. Colloidal semiconductor Q- particles: chemistry in the transition region between solid state and molecules. *Angew. Chem. Int. Ed.* **1993,** 32, 41-53.

West JL, Halas NJ. Applications of nanotechnology to biotechnology: Commentary. *Current Opinion in Biotechnology* **2000**, 11, 215-217.

Whitesides GM. The right size in nanobiotechnology. *Nat. Biotechnol.* **2003**, 21, 1161-1165.

Whitesides GM, Labinis PE. Wet chemical approaches to the characterization of organic surfaces: self-assembled monolayers, wetting, and the physical-organic chemistry of the solid-liquid interface, *Langmuir* **1990,** 6, 87-96.

Whitesides GM, Ostuni E, Takayama S, Jiang XY, Ingber DE. Soft lithography in biology and biochemistry. *Ann. Rev. Biomed. Eng.* **2001**, 3, 335–373.

Willner I, Baron R, Willner B. Integrated nanoparticle–biomolecules systems for biosensing and bioelectronics, *Biosens. Bioelectronics*. **2006**, Paper presented as a plenary lecture at Biosensors 2006, Toronto, Canada.

Wu B-Y, Hou S-H, Yin F. Amperometric glucose biosensor based on layer-by-layer assembly of multilayer films composed of chitosan, gold nanoparticles and glucose oxidase modified Pt electrode. *Biosensors and Bioelectronics* **2007**, 22, 838-844.

Wu HK, Odom TM, Whitesides GM, Connectivity of features in microlens array reduction photolithography: generation of various patterns using a single photomask. *J. Am. Chem. Soc.* **2002**, 124, 7288-7289.

Wu MH, Whitesides GM, Fabrication of diffractive and micro- optical instruments using microlens projection lithography. *Adv. Mater.* **2002**, 14, 1502-1507.

Wuelfing WP, Gross SM, Murray RW. Nanometer Gold Clusters Protected by Surface-Bound Monolayers of Thiolated Poly(ethylene glycol) Polymer Electrolyte. *J Am Chem Soc* **1998**, 120, 12696-12697.

Zhan J, Bando Y, Hu J, Liu Z, Yin L, Goldberg D. Fabrication of metal-semiconductor nanowire heterojunctions. *Angew. Chem. Int. Ed.* **2005,** 44, 2140-2144.

Xia Y, Whitesides GM. Soft Lithography. *Annu. Rev. Mater. Sci.* **1998,** 28, 153-184.

Xia Y, Whitesides GM**.** Extending Microcontact Printing as a Microlithographic Technique, *Langmuir* **1997**, 13, 2059-2067.

Xian Y, Hu Y, Liu F. Glucose biosensor based on Au nanoparticles-conductive polyaniline nanocomposite. *Biosensors and Bioelectronics* **2006**, 21, 1996-2000.

Xiao Y, Patolsky F, Katz E, Hainfeld JF, Willner I. Plugging into enzymes: nanowiring of redox enzymes by a gold nanoparticle. *Science* **2003**, 299, 1877-1881.

Xu FJ, Zhong SP, Yung LYL, Kang ET, Neoh KG, Surface-Active and Stimuli-Responsive Polymer-Si(100) Hybrids from Surface-Initiated Atom Transfer Radical Polymerization for Control of Cell Adhesion. *Biomacromolecules* **2004,** 5, 2392-2403.

Xu ZP, Zeng QH, Lu GQ, Yu AB. Inorganic nanoparticles as carriers for efficient cellular delivery. *Chem Engg Sci* **2006,** 61, 1027-1040.

Xuping Sun. One-Step Synthesis and Size Control of Dendrimer-Protected Gold Nanoparticles: A Heat-Treatment-Based Strategy. *Macromolecular Rapid Communications* **2003**, 24, 1024-1028.

Yamato M, Konno C, Utsumi M, Kikichi A. Thermally responsive polymer-grafted surfaces facilitate patterned cell seeding and co-culture. *Biomaterials* **2003,** 23, 561-567.

Yang R, Wang WJ, Soper SA. Out-of-plane microlens array fabricated using ultraviolet lithography. *Appl. Phys. Lett.* **2005** 86, 161110-161113.

Yang S, Chen G, Aizenberg J. Functional Biomimetic Microlens Arrays with Integrated Pores. *Adv. Mater.* **2005,** 17, 435-439.

Yean S, Cong L, Yavuz CT, Mayo JT, Yu WW, Kan AT, Colvin VL, Tomson MB. Effect of magnetite particle size on adsorption and desorption of arsenite and arsenate. *J. Mater. Res.* **2005** 20, 3255-3264.

Yeh P, Perricaudet M. Advances in adenoviral vectors: from genetic engineering to their biology. *FASEB J* **1997**, 11, 615-623.

Yildiz Y, Uyanik N, Erbil C. Compressive elastic moduli of PNIPAAm hydrogels crosslinked with PDMS. *J. Macromolecular Sci. A* **2006,** 43, 1091-1106.

Yokoyama M, Okano T. Targetable drug carriers: present status and a future perspective. *Adv Drug Delivery Rev* **1996,** 21, 77-80.

Yoshida R, Sakai K, Okano T, Sakurai Y, *J. Biomaterial Sci. Polymer Ed.* Comb-type grafted hydrogels with rapid deswelling response to temperature changes. **1995,** 6, 585-591.

Zeng X, Jiang H, Tunable liquid microlens actuated by infrared light-responsive hydrogel. *App. Phys. Lett.* **2008,** 93, 151101.

Zhang DY, Lien V, Berdichevsky Y, Choi J, Lo YH. Fluidic adaptive lens with high focal length tenability. *Appl. Phys. Lett.* **2003,** 82, 3171-3172.

Zhang G. Study on Conformation Change of Thermally Sensitive Linear Grafted Poly(*N*-isopropylacrylamide) Chains by Quartz Crystal Microbalance. *Macromolecules* **2004,** 37, 6553-6557.

Zhang L, Gu FX, Chan JM, Wang AZ, Langer R, Farokhzad OC. Nanoparticles in medicine: therapeutic, applications and developments. *Clini. Pharmaco. Thera.* **2008,** 83, 761-769.

Zhang L, Sun X, Song Y. Didodecyldimethylammonium Bromide Lipid Bilayer-Protected Gold Nanoparticles: Synthesis, Characterization, and Self-Assembly. *Langmuir* **2006**, 22, 2838-2843.

Zhao M, Sun L, Crooks RM. *Preparation of Cu Nanoclusters within Dendrimer* Templates. *J. Am. Chem. Soc.* **1998**, 120, 4877-4878.

Zhang X, Jenekhe SA, Perlstein J. Nanoscale Size Effects on Photoconductivity of Semiconducting Polymer Thin Films. *Chem. Mater.* **1996,** 8, 1571–1574.

Zhao B, Moore JS. Fast pH and ionic strength responsive hydrogels in microchannels, *Langmuir* **2001,** 17, 4758-4763.

Zhao QQ, Boxmann A, Chowdhry U. Nanotechnology in the chemical industry – opportunities and challenges. *J. Nanoparticle Res.* **2003,** 5, 567-572.

Zhao W, Lee TMH, Leung SSY, Hsing I-M. Tunable stabilization of gold nanoparticles in aqueous solutions by mononucleotides. *Langmuir* **2007,**23, 7143-7147.

Zheng P, Jiang X, Zhang X. Formation of Gold at Polymer Core-Shell Particles and Gold Particle Clusters on a Template of Thermoresponsive and pH-Responsive Coordination Triblock Copolymer. *Langmuir* **2006**, 22, 9393-9396.

Zhou F, Zheng Z, Yu B, Liu W, Huck WTS, Multicomponent Polymer Brushes.*J. Am. Chem. Soc.* **2006,** 128, 16253-16258.

Zhuo Y, Yuan R, Chai Y. A reagentless amperometric immunosensor based on gold nanoparticles/thionine/Nafion-membrane-modified gold electrode for determination of [α]-1-fetoprotein. *Electrochemistry Communications* **2005**, 7, 355-360.

Zourob M, Gough JE, Ulijn RV. A Micropatterned Hydrogel Platform for Chemical Synthesis and Biological Analysis. *Adv. Mater.* **2006**, 18, 655-659.

Zubarev ER, Xu J, Sayyad A. Amphiphilic Gold Nanoparticles with V-Shaped Arms. *J Am Chem Soc* **2006**, 128, 4958-4959.

The United States National Nanotechnology Initiative website. Retrieved on September 1, 2010. "Nanotechnology - Big things from a tiny world" document. http://www.nano.gov.

Vita

Hariharasudhan Chirra Dinakar was born on November 30th, 1983 in Tuticorin, Tamil Nadu, India. He attended the Alagappa College of Technology at Anna University, Guindy, India where he graduated among the top of the class with a Bachelor of Technology in Chemical Engineering, in May 2005. He had the distinguished privilege of pursuing research at the Indian Institute of Technology, Madras, India during his senior year of B. Tech. before joining the University of Kentucky in August 2005 to pursue a doctoral degree in Chemical Engineering.

Hari has published three peer-reviewed journal papers and has already submitted three more manuscripts for publication from his doctoral work. He also holds a published book chapter on his name. He has had the opportunity to present his research work annually since 2005 in the form of presentations and posters at several national and regional meetings including American Institute of Chemical Engineers (AIChE), Society for Biomaterials (SFB), and Materials Research Society (MRS). He has won two AIChE Nanotechnology Science and Engineering Forum awards and has mentored David Spencer in winning the AIChE Kentucky Chapter Freshman Recognition Award.